

eman ta zabal zazu



Universidad
del País Vasco

Euskal Herriko
Unibertsitatea

DEVELOPMENT AND APPLICATION OF THERMAL DESORPTION TECHNIQUES FOR THE MEASUREMENT OF PAHs IN AMBIENT AIR

A thesis submitted to the University of the Basque Country
for the degree of
Doctor of Philosophy

by

Iñaki Elorduy Escobio

Directed by: Dra. M^a Nieves Durana Jimeno

Chemical and Environmental Engineering Department
Faculty of Engineering
University of the Basque Country

Bilbao, 2017

*“La verdadera ciencia enseña, por encima
de todo, a dudar y a ser ignorante”*

Miguel de Unamuno 1864-1936

*“Da igual. Prueba otra vez. Fracasa
otra vez. Fracasa mejor”*

Samuel Beckett 1906-1989

ACKNOWLEDGEMENTS

Bueno, parece que el escribir una tesis es un proceso más complejo de lo que esperaba y que ha llevado más tiempo del que tenía previsto, pero al final el trabajo está terminado. No sería muy humilde, ni justo por mi parte, atribuirme el mérito completo de la realización de este trabajo olvidándome de las personas que han colaborado y hecho posible que esta tesis salga adelante. Por eso quisiera aprovechar este pequeño espacio para agradecer esas colaboraciones y apoyos.

En primer lugar, tengo que dar las gracias a mi directora de tesis, la Dra. M^a Nieves Durana Jimeno por su dedicación, disposición y guía para sacar adelante este trabajo a pesar de las dificultades con las que nos hemos encontrado.

También me gustaría agradecer al resto de miembros del “Grupo de Investigación Ambiental” del Departamento de Ingeniería Química y del Medio Ambiente de la Escuela Técnica Superior de Ingeniería de Bilbao la ayuda y consejos prestados durante esta tesis.

Tengo que dar las gracias también al Servicio Central de Análisis de la Universidad del País Vasco, concretamente a la unidad de Álava y a una de sus responsables, la Dra. M^a Carmen Sampedro Yanguela cuya ayuda fue esencial para el desarrollo de una parte de esta tesis.

Quisiera también agradecer al Ministerio de Ciencia e Innovación del Gobierno de España por la beca FPI disfrutada durante la realización de esta tesis.

I am also grateful to Professor Roy Harrison, my supervisor at the University of Birmingham where I did my stay of three months, for his hospitality and guidance. I cannot forget Eunhwa Jang who was amazingly helpful and kind and helped me with PMF modeling.

Gracias a mi compañeros de trabajo: Iratxe, Jarol, Tamara, Urko, David por la ayuda, el apoyo recibido y los buenos momentos que me han hecho pasar durante todo este tiempo. No me puedo olvidar tampoco de Saioa, en muchos momentos cotutora “en las sombras” de esta tesis, y apoyo y compañera incondicional durante todo esta

aventura. Espero que su nueva etapa le de muchas alegrías y le permita seguir haciendo lo que le más le gusta, investigar.

Por último, pero no menos importante, tengo que dar las gracias a mi familia, por el apoyo y sobre todo la enorme paciencia que han demostrado aguantándome todo este tiempo mientras escribía la tesis.

SUMMARY

The present Ph.D. thesis started in September 2011 with the support of the Spanish Ministry of Science and Innovation (MICINN) through FPI (“Formación de Personal Investigador”) grant associated with the project PROMESHAP (CTM 2010-20607). The work has been developed in the Atmospheric Research Group (GIA) at the Chemical and Environmental Engineering Department in the Faculty of Engineering of Bilbao (University of the Basque Country, UPV/EHU). Part of the work was also performed in the Division of Environmental Health and Risk Management at the School of Geography, Earth and Environmental Sciences of the University of Birmingham (United Kingdom), during a 3-month period (September-December 2014).

Among all air pollutants, polycyclic aromatic hydrocarbons (PAHs) have become an issue of increasing concern in recent decades. Due to their features (persistent organic pollutants possessing carcinogenic, mutagenic, and immunotoxic properties) and high atmospheric persistence, these components have been listed in international protocols for emission reductions.

Environmental samples usually contain only a small fraction of PAHs with respect to total organic matter. In addition, depending on the source that originates them, the environmental samples that contain this type of compounds can be very complex and difficult to analyse. Due to this, the conventional methods for the determination of PAHs in air demand a large and laborious sample preparation in order to increase the sensitivity and selectivity of the analysis. These extraction methods are performed by using organic solvents, which significantly prolongs the analysis time and implicates a high manipulation of the sample, generating losses of PAHs during the procedure. Furthermore, the use of organic solvents generates large amounts of solvent waste, which is costly and causes environmental problems. Therefore, alternative methods based on solvent-free extraction techniques have been developed in recent years to overcome these limitations.

This thesis aims at the development of a field-applicable and semicontinuous measurement method to determine polycyclic aromatic hydrocarbons (PAHs) in ambient air, based on a thermal desorption technique coupled to gas chromatography-mass spectrometry (GC-MS). As a consequence, a scientific article has been published

in a peer-reviewed journal (Atmospheric Environment); furthermore, several scientific contributions have been presented at international conferences.

Regarding the structure of this memory, first, a **table of contents** indicating the starting page number of each chapter is shown. Next, a **summary**, written both in English and Spanish, is included providing the reader with an overall idea of the research work carried out. Afterwards, the memory has been divided into the following seven chapters:

Chapter 1 is a general introduction that describes the main properties and the significance of the PAHs in atmospheric pollution. This chapter reviews the formation, the physicochemical properties, the sources, the toxicology, the legislation and the emission levels (in Spain and Europe) of these pollutants. In addition, it provides information on the state-of-the-art of the methods for the determination of PAHs in air, focusing mainly on extraction techniques, especially on thermal desorption. Finally, it describes the main diagnostic ratios and receptor models (UNMIX and positive matrix factorization (PMF) models) for the identification and quantitative source apportionment of PAHs.

Chapter 2 presents the methodological approach used in this study and its justification. The main objective and the specific objectives of this Ph.D. work are also indicated herein.

Chapter 3 describes the experimental methodology applied during the study. Firstly, it explains the measurement methodology in detail (including the sampling equipment, sample preparation and analysis method by TD-GC/MS). The study used filters and solid adsorbents as sampling media of particulate and gas PAHs, respectively. Subsequently, the chapter presents the methodology used in the TD-GC/MS software (TurboMass) for the acquisition, identification and quantification of the results. Finally, it describes the Büchi extraction system B-811, as the study compares the conventional method for analysis of PAHs (Soxhlet extraction-GC/MS) to the TD-GC/MS.

The development of the PAHs analysis technique (TD-GC/MS) for the determination of both phases (gas and particle) is presented in **Chapter 4**. In more detail, the chapter includes:

In **Section 4.1**, different methods and times for the conditioning of PAH sampling media (filter and solid adsorbent) are studied.

The most significant parameters in the two-stage thermal desorption process (sampling tube and cryogenic trap desorption) are tested with different values in **Section 4.2** for both PAH phases. It analyses the efficiency in the two-stage thermal desorption process under optimized conditions.

In **Section 4.3** the analytical method is evaluated, calculating parameters such as linearity, precision, and detection and quantification limits. The TD-GC/MS detection limits are compared with those obtained by other authors using the same technique, and with analytical methods based on solvent extraction.

Before the application of the method, its validation is necessary. In **Section 4.4** the TD-GC/MS method is validated for the determination of particulate PAHs with standard reference material (urban dust). The same validation is performed with the conventional method for analysis of PAHs (Soxhlet extraction-GC/MS) in order to compare both methods.

Section 4.5 includes the estimation of measurement uncertainty of particulate PAHs that is associated with the TD-GC/MS method. This section follows the four stages proposed by ISO normative references to calculate the uncertainty: the specification of the measurement process, and the identification, quantification and combination of the uncertainty sources involved in the analytical process. In addition, the uncertainty related to Soxhlet-GC/MS method is determined to compare both methods.

Because the reference material used to validate the method contains other PAHs besides the target compounds (the 16 PAHs prioritized by the U.S. Environmental Protection Agency), it was considered to increase the number of PAHs determined by the technique. **Section 4.6** describes the identification and quantification of these compounds by relative response factors.

After the development and validation, **Chapter 5** analyses the application of the TD-GC/MS method for the characterization of particulate PAHs in an urban area (Bilbao city) during some months (between July 2013 and June 2014). In this chapter:

Section 5.1 describes the sampling area (Bilbao city) and details the campaign measurement periods.

Section 5.2 shows and analyses the meteorological conditions (wind speed and direction, temperature, atmospheric pressure, solar irradiation, rainfall and relative humidity) and other conventional pollutant concentrations (NO, NO₂, NO_x, SO₂, O₃, benzene, toluene y o-xylene) measured in the sampling area during the campaign.

The particulate PAH concentrations obtained during the sampling campaign are shown in **Section 5.3**, which displays a descriptive statistic of the results. Moreover, their diurnal variability is studied.

The identification and apportionment of PAH sources present in the Bilbao urban area is developed in **Section 5.4**. This section details the application of diagnostic ratios and receptor models (UNMIX and PMF), and the interpretation of their results for the identification of potential PAH sources.

The effect of meteorological conditions and their influence on the variability of particulate PAH concentrations is analysed in **Section 5.5**.

The last section of this chapter (**Section 5.6**) studies the carcinogenic potency associated with the measured PAHs during the sampling campaign.

Chapter 6 summarizes the main conclusions achieved throughout this study.

Chapter 7 features the bibliography used for this study.

Finally, the appendix contains a table with mean PAH concentrations during the sampling campaign (**Appendix A**), the published article and the list of scientific contributions to international conferences (**Appendix B**).

RESUMEN

El proyecto de tesis actual se inició en septiembre de 2011 gracias al Ministerio de Ciencia e Innovación de España (MICINN) a través de una beca FPI (formación de personal investigador) asociada al proyecto PROMESHAP (CTM 2010-20607). El trabajo ha sido desarrollado en el Grupo de Investigación Atmosférica (GIA) del Departamento de Ingeniería Química y del Medio Ambiente de la Escuela Técnica Superior de Ingeniería de Bilbao (Universidad del País Vasco, UPV/EHU). Parte del trabajo fue llevado a cabo también en la División de Salud Ambiental y Gestión de Riesgos de la Universidad de Birmingham (Reino Unido), durante un periodo de 3 meses, de septiembre a diciembre de 2014.

Entre todos los contaminantes, los hidrocarburos aromáticos policíclicos (HAPs) han sido objeto de un interés creciente en los últimos años. Debido a sus características (propiedades carcinogénicas, mutagénicas e inmunotóxicas) y alta persistencia en la atmosfera, estos compuestos aparecen como contaminantes objetivo en los protocolos internacionales para la reducción de emisiones.

Las muestras ambientales suelen contener sólo una pequeña fracción de HAPs respecto de la materia orgánica total. Además, dependiendo de la fuente que los origine, las muestras ambientales que contienen este tipo de compuestos pueden ser muy complejas y difíciles de analizar. Debido a esto los métodos convencionales para el análisis de HAPs requieren largos y laboriosos procesos de preparación de la muestra para lograr la separación de estos contaminantes de otras sustancias interferentes. En estos métodos la extracción se realiza mediante disolventes orgánicos lo que prolonga significativamente el tiempo de análisis y genera pérdidas de los HAPs debido a la alta manipulación de las muestras durante el proceso. Además el uso de disolventes orgánicos de carácter tóxico, supone un problema ambiental y elevan los costes del proceso por el tratamiento de los residuos. Como resultado, en los últimos años, los métodos alternativos basados en extracciones sin disolventes han sido desarrollados para superar estas limitaciones.

Este trabajo de investigación tiene por objetivo: el desarrollo, la puesta a punto y la aplicación en condiciones de campo de un método de medida semicontinua de HAPs en aire ambiente, basándose en la técnica de desorción térmica (TD) acoplada a un cromatografía de gases- espectrometría de masas (GC-MS). Como resultado, se ha

publicado un artículo científico en una revista indexada (Atmospheric Environment), y se han presentado también diversas contribuciones en conferencias internacionales.

En cuanto a la estructura de esta memoria, se presenta en primer lugar un **índice general** indicando la numeración de cada capítulo. Seguidamente, se incluye un **resumen**, escrito tanto en inglés como en castellano, que proporciona al lector una idea general de la labor realizada. Posteriormente, la memoria se estructura en los siguientes siete capítulos:

El **Capítulo 1** es una introducción general donde se describen las principales características de los HAPs y la relevancia que estos tienen en la contaminación atmosférica. En el capítulo se repasan la formación, las propiedades físico-químicas, las fuentes, la toxicología, la normativa y los niveles de emisión (en Europa y España) de estos contaminantes. También se presenta un estado del arte sobre las técnicas de determinación de HAPs en aire, centrándose sobre todo en los métodos de extracción, especialmente en la desorción térmica. Finalmente, se describen los principales ratios de diagnóstico y modelos receptores (modelos UNMIX y PMF) habitualmente usados para la identificación de las fuentes de emisión de HAPs.

El **Capítulo 2** presenta el enfoque metodológico utilizado así como su justificación. Además, se indica el objetivo principal y los objetivos específicos de este proyecto de tesis doctoral.

En el **Capítulo 3** se describe la metodología experimental aplicada durante el estudio. Primero, se detalla la metodología asociada a la medida (incluyendo el equipo de muestreo, la preparación de muestras y el método de análisis mediante TD-GC/MS). En este estudio se usaron filtros y adsorbente sólido (Tenax GR y Tenax TA) como medios de captación de HAPs para la fase particulada y gas, respectivamente. Después, se describe la metodología empleada en el software del TD-GC/MS (TurboMass) para la adquisición, identificación y cuantificación de los resultados. Finalmente se describe el sistema de extracción sólida-líquida Büchi extraction system B-811, ya que el método de análisis convencional de HAPs (extracción Soxhlet-GC/MS) fue comparado con el TD-GC/MS en el estudio.

La puesta punto de la técnica de análisis de HAPs (TD-GC/MS) para la determinación de ambas fases (gas y partícula) es desarrollada en el **Capítulo 4**. En este capítulo:

En la **Sección 4.1**, diferentes métodos y tiempos para el acondicionamiento del medio de captación de HAPs (filtro o adsorbente sólido) son estudiados.

En las dos etapas de la desorción térmica (desorción desde el tubo de muestreo y desde la trampa criogénica), los parámetros más significativos (temperatura en el tubo de muestreo y en la trampa criogénica, tiempo de desorción, flujo de desorción, y los flujos de división en la entrada y salida de la trampa) son testados con diferentes valores en la **Sección 4.2** para ambas fases de HAPs. Con las condiciones optimizadas se analiza la eficacia en las dos etapas de la desorción térmica (desorción en el tubo de muestreo y desorción en la trampa criogénica).

En la **Sección 4.3**, se evalúa el método analítico, calculando parámetros como la linealidad, la precisión y los límites de detección y cuantificación. Los límites de detección del método se compararon con los obtenidos por otros autores mediante la misma técnica y con métodos de análisis basados en la extracción con disolventes.

Para la aplicación de una técnica, previamente, es necesaria la validación de la misma. En la **Sección 4.4** se valida el método TD-GC/MS para la determinación de la fase particulada con material de referencia certificado (polvo). La misma validación se realiza para el método de determinación convencional de HAPs (extracción Soxhlet-GC/MS) con el fin de comparar ambos métodos.

La **Sección 4.5** engloba el cálculo de la incertidumbre de la medida de la fase particulada de HAPs asociada al método TD-GC/MS. En esta sección se siguieron las cuatro etapas propuestas por la normativa ISO para calcular la incertidumbre: la especificación del proceso de medida y la identificación, cuantificación y combinación de las fuentes de incertidumbre implicadas en el proceso analítico. También se determina la incertidumbre asociada al método Soxhlet-GC/MS para comparar ambos métodos.

Debido a que en el material de referencia empleado en la validación del método contenía otros HAPs, aparte de los compuestos objetivos del análisis (los 16 HAPs considerados prioritarios por la Agencia de Protección del Medio Ambiente de Estados Unidos), se decidió ampliar el número de HAPs determinados mediante la técnica. La **Sección 4.6** describe la identificación y cuantificación mediante factores de respuesta de estos compuestos.

Después de la puesta a punto y la validación, el **Capítulo 5** explora la aplicación del método TD-CG/MS para la caracterización de los HAPs en fase particulada en un área urbana (la ciudad de Bilbao) durante varios meses (entre julio de 2013 y junio de 2014). En este capítulo:

La **Sección 5.1** describe la zona de muestreo (la ciudad de Bilbao) y se detallan los periodos de muestreo de la campaña de medida de los HAPs.

La **Sección 5.2** se presentan y analizan las condiciones meteorológicas (velocidad y dirección del viento, temperatura, presión atmosférica, irradiación solar, precipitación y humedad relativa) y las concentraciones de otros contaminantes convencionales (NO, NO₂, NO_x, SO₂, O₃, benceno, tolueno y orto-xileno) medidas en la zona de muestro durante la campaña de medida.

Las concentraciones de HAPs en fase particulada obtenidas durante la campaña de medida son presentadas en la **Sección 5.3** donde se lleva a cabo una descripción estadística de los resultados y se estudia su variabilidad diurna.

La identificación y asignación de las fuentes de HAPs presentes en el área urbana Bilbao se desarrolla en la **Sección 5.4**. En esta sección se detalla la aplicación de los ratios de diagnóstico y los modelos receptores UNMIX y PMF y la interpretación de sus resultados para la identificación de las fuentes de HAPs potenciales.

El efecto de las condiciones meteorológicas y su influencia en la variabilidad de las concentraciones de HAP en fase particulada es analizado en la **Sección 5.5**.

En la última sección del capítulo (**Sección 5.6**) se estudia el potencial carcinogénico asociado a los HAPs medidos durante la campaña.

El **Capítulo 6** presenta las conclusiones alcanzadas a lo largo de este trabajo de investigación.

El **Capítulo 7** recoge la bibliografía utilizada en esta memoria.

Finalmente, se adjuntan una tabla con las concentraciones medias de los HAPs obtenidas durante la campaña de medida (**Anexo A**), el artículo publicado y la lista de

contribuciones científicas presentadas en conferencias internacionales, derivadas del trabajo realizado (**Anexo B**).

TABLE OF CONTENTS

Chapter 1: Introduction	1
1.1 Physical and chemical characteristics of PAHs.....	3
1.2 Formation of PAHs	6
1.3 Sources of PAHs	8
1.4 Atmospheric transport and fate of PAHs.....	10
1.5 Emissions and ambient concentrations of PAHs.....	13
1.5.1 Europe.....	13
1.5.2 Spain	17
1.6 Toxicity and regulation of PAHs.....	19
1.7 Determination of PAHs in air	23
1.7.1 Collection of PAHs.....	23
1.7.2 Extraction methods for PAHs.....	26
1.7.3 Analytical methods for PAHs	38
1.7.4 Application of TD-GC/MS.....	40
1.8 Source apportionment of PAHs	42
1.8.1 Diagnostic ratios	42
1.8.2 Receptor models	43
Chapter 2: Approach and objectives	47
Chapter 3: Experimental	51
3.1 Measuring methodology	53
3.1.1 Sampling methods.....	53
3.1.2 Sample preparation	55
3.1.3 Analysis method	59
3.1.4 Auxiliary equipment and gases.....	72
3.2 Setting and use of TD-GC/MS software	73
3.2.1 MS Tuning.....	73
3.2.2 Data acquisition	75
3.2.3 Qualitative and quantitative analysis.....	79
3.2.4 Data quality control.....	82
3.3 Soxhlet extraction	82

Chapter 4: Development of TD-GC/MS method 85

4.1 Conditioning	87
4.1.1 Particulate phase.....	87
4.1.2 Gas phase.....	89
4.2 Desorption stage	92
4.2.1 Primary desorption (tube desorption).....	92
4.2.2 Secondary desorption (trap desorption).....	103
4.2.3 Desorption efficiency	106
4.3 Evaluation of analytical method	108
4.3.1 Linearity.....	108
4.3.2 Precision.....	111
4.3.3 Limit of detection, limit of quantification and method detection limit. ...	112
4.4 Method Validation.....	117
4.5 Uncertainty of the method.....	121
4.5.1 Uncertainty derived calibration curves $(u(\text{Cal})/C)^2$	123
4.5.2 Uncertainty derived from sample volume and from air flow $(u(V_s)/V_s)^2$ and $(u(V_{\text{air}})/V_{\text{air}})^2$	132
4.5.3 Uncertainty derived from recovery $(u(R)/R)^2$	133
4.5.4 Combined uncertainty $(u_{\text{comb}}/C)^2$	135
4.6 Determination of other PAHs in the particulate phase.....	136

Chapter 5: Determination of particle-bound PAHs in urban area by TD-CG/MS method..... 143

5.1 Sampling site.....	145
5.2 Meteorological conditions and conventional pollutant concentrations	148
5.3 Results of the sampling campaign	155
5.3.1 Temporal evolution: diurnal variability.....	160
5.4 PAH source assessment	164
5.4.1 Diagnostic ratio analysis.....	164
5.4.2 UNMIX.....	168
5.4.3 Positive matrix factorization (PMF)	171
5.5 Effect of meteorology.....	178
5.6 Carcinogenic potential assessment	182

Chapter 6: Conclusions	187
Chapter 7: Bibliography.....	193
Appendix A	217
Appendix B	229

LIST OF FIGURES

Figure 1.1. Reaction flux diagram for formation of PAHs from ethylene (blue arrows highlight those reactions contributing to the synergistic effects on PAHs) (adapted from Wang et al., 2013). A1: benzene, A2: naphthalene, A3: phenanthrene, A4: pyrene, A5: benzo[e]pyrene, A6: benzo[ghi]pyrene, A7: coronene	7
Figure 1.2. Conceptual representation of processes influencing the atmospheric transport and fate of POPs (among them the PAHs) (source: Van Drooge and Grimalti, 2012). (1) Primary emissions of POPs to the atmosphere, (2) atmospheric deposition and photochemical degradation/transformation, (3) re-volatilisation from secondary sources in the different environmental compartments and burial in sediments, (4) bioaccumulation and biotic transport, (5) accumulation in glaciers and ice caps, with probable releases due to melting ...	13
Figure 1.3. EU-28 emission trends for total PAHs and the four indicators of PAHs considered in the 1979 Convention on Long-range Transboundary Air Pollution, from 1990 to 2014 (source: EEA, 2016)	14
Figure 1.4. Main sources of total PAHs in the EU and their contributions (%) in 2014 (source: EEA, 2016).....	16
Figure 1.5. Spain vs EU-28 emission trends for total PAHs from 1990 to 2014 (sources: Spanish Ministry of Agriculture, Food and Environment, 2016).....	18
Figure 1.6. Main sources of total PAHs in Spain and their contributions (%) in 2014 (source: Spanish Ministry of Agriculture, Food and Environment, 2016).	18
Figure 1.7. Short and long term health effects of exposure to PAHs (source: Kim et al., 2013).	20
Figure 1.8. Schematic diagram active (left) vs. passive (right) sampler (sources: Queensland Government, 2016; MonAirNet project, 2016).....	24
Figure 1.9. Schematic diagram of conventional Soxhlet extraction method (source: de Castro and Priego-Capote, 2010)	27
Figure 1.10. Schematic diagram of ultrasonic-assisted extraction (UAE) (source: Kadam et al., 2013)	28
Figure 1.11. Schematic diagram of accelerated solvent extraction (ASE) (source: Björklund et al., 2000).....	29
Figure 1.12. Schematic diagram of microwave-assisted extraction (MAE) (source: Zhang et al., 2011).....	30
Figure 1.13. Two-stage thermal desorption incorporating capillary cryofocusing (source: Woolfenden, 2012).....	35

Figure 1.14. Two-stage thermal desorption incorporating sorbent focusing trap and heated valve (source: Woolfenden, 2012).....	36
Figure 3.1. TD-GC/MS system	53
Figure 3.2. High-volume sampler Digital DHA-80 (left) and its block diagram (right) (source: Digital Elektronik AG, 2010)	55
Figure 3.3. Configuration of the sampling tube in the determination of the particulate phase (adapted from PerkinElmer, 2007).....	56
Figure 3.4. Configuration of the sampling tube in the determination of the gas phase (adapted from PerkinElmer, 2007)	57
Figure 3.5. The Gauze-Loading Ring (source: PerkinElmer, 2007)	57
Figure 3.6. The Adsorbent Tube Injector System (ATIS) (source: Sigma-Aldrich, 2016).	58
Figure 3.7. First desorption stage (source: Agilent Technologies, 2016).	59
Figure 3.8. Second desorption stage (source: Agilent Technologies, 2016).	60
Figure 3.9. Temperature program of the chromatographic oven.....	62
Figure 3.10. SCAN vs. SIM mode. Identification of fluoranthene and pyrene in reference material certificate (NIST 1649b urban dust).	63
Figure 3.11. Identification of 16 EPA and deuterated PAHs in SCAN mode, from 0 to 15 min: 1) Naph-d8, 2) Naph, 3) Bph-d10, 4) Acy, 5) Ace, 6) FL.....	67
Figure 3.12. Identification of 16 EPA and deuterated PAHs in SCAN mode, from 15 to 20.5 min: 7) Phe-d10, 8) Phe, 9) Ant, 10) Ft, 11) Pyr-d10, 12) Pyr.....	67
Figure 3.13. Identification of 16 EPA and deuterated PAHs in SCAN mode, from 22.5 to 35.5 min: 13) BaA-d12, 14) BaA, 15) Chry, 16) BbFt, 17) BkFt, 18) BaP-d10, 19) BaP, 20) IP, 21) DBahA, 22) BghiP-d12, 23) BghiP.	68
Figure 3.14. Identification of group 1 in SIM mode.	68
Figure 3.15. Identification of group 2 in SIM mode	69
Figure 3.16. Identification of group 3 in SIM mode	69
Figure 3.17. Identification of group 4 in SIM mode	70
Figure 3.18. Identification of group 5 in SIM mode	70
Figure 3.19. Identification of group 6 in SIM mode	71
Figure 3.20. Identification of group 7 in SIM mode	71
Figure 3.21. Flowchart of zero air system.....	72
Figure 3.22. Instrument tune parameters in TurboMass software.....	74
Figure 3.23. Example of SCAN and SIM window configuration for 21 functions (function 1: SCAN; functions 2 – 21: SIM) by TurboMass software.	76
Figure 3.24. SCAN mode parameters for MS in TurboMass software	76
Figure 3.25. SIM mode parameters for MS in TurboMass software.....	78

Figure 3.26. Sample list screen in TurboMass software	79
Figure 3.27. Quantitative method editor in TurboMass software.....	80
Figure 3.28. Peak detect options in quantitative method editor in TurboMass software..	
.....	81
Figure 3.29. Calibration curve settings in quantitative method editor in TurboMass software.....	81
Figure 3.30. Büchi extraction system B-811(source: Büchi, 2016a).....	82
Figure 3.31. Operation of Büchi extraction system B-811 (source: Büchi, 2016b).	83
Figure 4.1. 16 EPA PAHs amount in the filter (ng) obtained from different conditioning methods, including the unconditioned samples.....	88
Figure 4.2. Area (in %) for each of the 16 EPA PAHs obtained in the study of the desorption temperature with tubes (n=5) loaded with filter	93
Figure 4.3. Area (in %) for each of the 16 EPA PAHs obtained in the study of the desorption temperature with tubes (n=5) packed with Tenax GR.....	94
Figure 4.4. Area (in %) for each of the 16 EPA PAHs obtained in the study of the desorption temperature with tubes (n=5) packed with Tenax TA.....	94
Figure 4.5. Area (in %) for each of the 16 EPA PAHs obtained in the study of desorption time with tubes (n=5) loaded with filter.....	96
Figure 4.6. Area (in %) for each of the 16 EPA PAHs obtained in the study of desorption time with tubes (n=5) packed with Tenax GR.	97
Figure 4.7. Area (in %) for each of the 16 EPA PAHs obtained in the study of desorption time with tubes (n=5) packed with Tenax TA	97
Figure 4.8. Area (in %) for LMW (low molecular weight), MMW (middle molecular weight) and HMW (high molecular weight) PAHs obtained with desorption flow of 120 and 150 mL min ⁻¹	99
Figure 4.9. Area (in %) for LMW (low molecular weight), MMW (middle molecular weight) and HMW (high molecular weight) PAHs obtained in the study of desorption flow with tubes (n=5) packed with Tenax GR	100
Figure 4.10. Area (in %) for LMW (low molecular weight), MMW (middle molecular weight) and HMW (high molecular weight) PAHs obtained in the study of desorption flow with tubes (n=5) packed with Tenax TA.....	100
Figure 4.11. Area (in %) for each of the 16 EPA PAHs obtained in the study of the low trap temperature with tubes (n=5) loaded with filter.....	104
Figure 4.12. Area (in %) for LMW (low molecular weight), MMW (middle molecular weight) and HMW (high molecular weight) PAHs obtained in the study of the trap time with tubes (n=5) loaded with filter.....	105

Figure 4.13. Area (in %) for each of the 16 EPA PAHs obtained in the study of the outlet split flow with tubes (n=5) loaded with filter.....	106
Figure 4.14. Recovery (in %) of the 16 EPA PAHs in the tube (particulate and gas phase) and in the trap.....	108
Figure 4.15. Calibration curve of BaP for particulate phase (filter).....	110
Figure 4.16. Calibration curve of BaP for gas phase (Tenax GR).....	110
Figure 4.17. Calibration curve of BaP for gas phase (Tenax TA).....	111
Figure 4.18. Calibration curve of BaP in TD-GC/MS used in the determination of $(u(C_x)/C_x)^2$	124
Figure 4.19. PAHs and deuterated PAHs in SIM windows (m/z 226, 240, 228 and 234) in the analysis of NIST SRM 1694b dust.....	138
Figure 4.20. PAHs and deuterated PAHs in SIM windows (m/z 252 and 264) in the analysis of NIST SRM 1694b dust	139
Figure 4.21. PAHs and deuterated PAHs in SIM windows (m/z 276, 288 and 278) in the analysis of NIST SRM 1694b dust.	139
Figure 4.22. PAHs and deuterated PAHs in m/z 300 SIM window in the analysis of NIST SRM 1694b dust.	140
Figure 5.1. Geographical location of the sampling site in Bilbao city (Spain), and meteorological (Feria) and air pollution (Mazarredo) sampling stations (sources: Google Earth and GeoEuskadi)	146
Figure 5.2. Industrial emissions of PAHs in the metropolitan area of Bilbao (years 2013 and 2014). Sampling site (yellow star), steel industry (red factory), waste treatment industry (green factory) (sources: Google Earth and Basque E-PRTR).....	147
Figure 5.3. Wind rose showing the wind speed and direction frequencies at Bilbao city for the sampling periods of the campaign (based on hourly data)	154
Figure 5.4. Average diurnal NO ₂ concentration ($\mu\text{g m}^{-3}$) in Bilbao city during sampling campaign	155
Figure 5.5. Cross plots for the ratios Ft/(Ft+Pyr) vs Ant/(Ant+Phe) according to the (A) month and (C) diurnal period, and IP/(IP+BghiP) vs BaA/(BaA+Chry) according to the (B) month and (D) diurnal period.....	167
Figure 5.6. Measured vs. predicted total PAH concentration (ng m^{-3}) in UNMIX model ..	170
Figure 5.7. Measured vs. predicted total PAH concentration (ng m^{-3}) in PMF model	174
Figure 5.8. PMF factor profiles.	175
Figure 5.9. Total PAH source contribution (ng m^{-3} ; %) by PMF model in Bilbao city	176

Figure 5.10. Bivariate polar plot of PMF factor concentrations (ng m^{-3}) and of NOx concentrations ($\mu\text{g m}^{-3}$) at Bilbao city..... 177

Figure 5.11. Average diurnal wind speed (m s^{-1}) in Bilbao city. Seasonal comparison 182

Figure 5.12. Average diurnal NO₂ concentration ($\mu\text{g m}^{-3}$) in Bilbao city. Seasonal comparison..... 182

LIST OF TABLES

Table 1.1. Physicochemical properties of some relevant PAHs (source: Gustafsson et al., 2001).....	4
Table 1.2. Total PAH emissions (in Mg) in each member state and their contribution (%). Comparison between 1990 and 2014 (source: EEA, 2016)	15
Table 1.3. Summary of recent (not older than 1990) typical European PAH concentrations in ng m ⁻³ as annual mean value (source: European Commission, 2001).	17
Table 1.4. US-EPA's 16 priority-pollutant PAHs. Classification for carcinogenicity.....	21
Table 1.5. TEFs proposed for individual PAHs according to different authors.....	22
Table 1.6. Some studies reported in the literature where the solvent-based extraction-GC/MS methods were used to determine PAHs in air.....	32
Table 1.7. Standard methods for the determination of PAHs in air.....	39
Table 1.8. Studies reported in the literature where the TD-GC/MS method was used to determine PAHs in air (last ten years).....	41
Table 1.9. Diagnostic PAH ratios for source identification.....	42
Table 3.1. Quantification ions of 16 EPA PAHs	64
Table 3.2. Quantification ions of deuterated PAHs	65
Table 3.3. Quantification groups of 16 EPA PAHs with their deuterated compound....	66
Table 3.4. Configuration of the extraction system B-811 used in the study.	84
Table 4.1. Mean amount of 16 EPA PAHs (in ng) in new Tenax GR samples (n=5) after conditioning at 350°C for 60 and 90 min. Comparison with unconditioned Tenax GR samples (n=3). Standard deviation in brackets	89
Table 4.2. Mean amount of 16 EPA PAHs (in ng) in new Tenax TA samples (n=3) after conditioning at 350°C for 60 and 90 min. Comparison with unconditioned Tenax TA samples (n=4). Standard deviation in brackets	90
Table 4.3. Mean amount of 16 EPA PAHs (in ng) in tubes packed with used Tenax GR (n=4) and TA (n=4) after re-conditioning at 350°C for 15 and 30 min. Standard deviation in brackets.	91
Table 4.4. Area of chromatographic peak (in %) for each 16 EPA PAHs obtained in the study of the inlet split flow with tubes (n=5) loaded with filter.	102
Table 4.5. Optimized conditions for thermal desorption system	107

Table 4.6. Coefficients of determination (R^2) of 16 EPA PAHs obtained in the linearity study for PAH particulate (filter) and gas phase (Tenax GR and TA)	109
Table 4.7. Relative standard deviation (RSD) in % of 16 EPA PAHs obtained in the precision study for the particulate (filter) and gas phase (Tenax GR and TA).....	112
Table 4.8. Results of detection limit analysis of 16 EPA PAHs obtained by TD-GC/MS with sample tubes loaded with quartz filters	114
Table 4.9. Results of detection limit analysis of 16 EPA PAHs obtained by TD-GC/MS with sample tubes packed with Tenax GR and Tenax TA.	115
Table 4.10. LODs (in ng) obtained in this and other studies by the TD-GC/MS method (only for PAHs in the particulate phase).....	116
Table 4.11. Comparison of MDLs (in ng m ⁻³) obtained in this study by TD-GC/MS to those obtained in other studies by the solvent-based extraction-GC/MS method (only for PAHs in the particulate phase). A sampling volume of 240 m ³ was assumed in all studies.....	117
Table 4.12. TD-GC/MS method validation parameters for the 16 EPA PAHs in NIST-SRM 1649b urban dust (n=10).....	118
Table 4.13. Timed events and oven program used in direct injector mode.	120
Table 4.14. Soxhlet extraction-GC/MS method validation parameters for the 16 EPA PAHs in SRM 1649b (n=7).....	121
Table 4.15. Relative ($u(C_x)/C_x$) for each PAH in TD-GC/MS and Soxhlet extraction-GC/MS method	126
Table 4.16. The manufacturer's specification data of lab tools, PAH standard and solvents	128
Table 4.17. Uncertainty associated with syringe and volumetric flask during the standard solution preparation for each dilution stage (TD-GC/MS method).....	129
Table 4.18. Uncertainties associated with dilution and standard solution preparation for each calibration solution (TD-GC/MS method).....	129
Table 4.19. Uncertainties associated with syringe and volumetric flask during the standard solution preparation for each dilution stage (Soxhlet extraction-GC/MS method)..	130
Table 4.20. Relative ($u(Cal)/C$) for each PAH in the TD-GC/MS and Soxhlet extraction-GC/MS methods	132
Table 4.21. Value of R and relative uncertainty associated with recovery obtained in TD-GC/MS and Soxhlet extraction-GC/MS for each PAH.	135
Table 4.22. u_{comb}/C and u_{expan}/C for 16 EPA PAHs in both methods.....	136

Table 4.23. Quantification ions of 16 EPA PAHs and deuterated PAHs determined by the TD-GC/MS method (extra PAHs included).....	137
Table 4.24. Reference PAH, RRFs and the coefficients of variation for each extra PAH	141
Table 5.1. Meteorological conditions during the sampling campaign. Standard deviations in brackets	150
Table 5.2. Air regulated pollutant concentrations during the sampling campaign. Standard deviations in brackets	152
Table 5.3. Descriptive statistics of the individual and total particle-bound PAH concentrations (diurnal and sampling period-averaged data).....	156
Table 5.4. Diurnal period (n=7) and weekly (n=21) mean concentrations (ng m ⁻³) of total PAHs (Σ 25PAHs) and contribution (in %) of PAH-ring groups to the PM ₁₀ fraction during the sampling period. Standard deviation in brackets	161
Table 5.5. Diurnal period (n=7) and weekly (n=21) mean diagnostic ratios of PAHs over the sampling period (n=182). Standard deviation in brackets.....	165
Table 5.6. Number of acceptable data, data below the MDL, and missing data for each PAH in the database.....	169
Table 5.7. Source profiles (in ng m ⁻³) obtained from UNMIX.....	170
Table 5.8. Pearson correlation coefficients of PAHs with meteorological parameters depending on the diurnal period (n=61 per diurnal period).....	179
Table 5.9. Diurnal period (n=7) and weekly (n=21) mean BaP _{eq} concentrations (ng m ⁻³) over the sampling period. Standard deviation in brackets	183
Table 5.10. Mean contribution of individual PAHs to BaP _{eq} (in %) during the sampling campaign	184
Table 5.11. Diurnal period (n=7) and weekly (n=21) mean ICR during the sampling campaign (based on the IUR _{BaP} of the WHO).....	185
Table A.1. Diurnal period (n=7) and weekly (n=21) mean concentrations (ng m ⁻³) of individual PAHs during the sampling period. Standard deviation in brackets.....	219

Chapter 1:

Introduction

1.1 Physical and chemical characteristics of PAHs

Polycyclic aromatic hydrocarbons (PAHs) are a class of persistent organic pollutants (POPs) comprised of hundreds of individual substances. These compounds contain two or more fused aromatic rings (made up of carbon and hydrogen atoms) in linear, angular or cluster arrangements. They are semi-volatile organic compounds (SVOC), thus, they are present in the atmosphere in both the gas and the particulate phases as well as dissolved or suspended in precipitation (fog or rain).

The general characteristics common to PAHs are high melting and boiling points, and low vapour pressures. Table 1.1 lists the physical and chemical properties of some PAHs.

Table 1.1. Physicochemical properties of some relevant PAHs (source: Gustafsson et al., 2001).

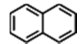
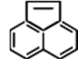
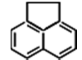
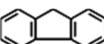
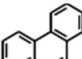
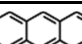
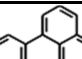
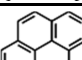
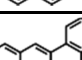
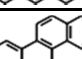
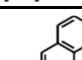
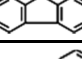
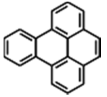
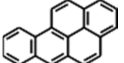
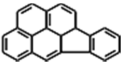
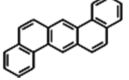
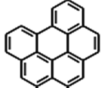

Name	Ring no.	Molecular formula	Chemical structure	Exact mono-isotopic molecular weight (Da)	Boiling point at 1013 hPa (°C)	Vapour pressure at 25°C (Pa)	Water solubility at 25°C (mg L ⁻¹)	Henry's constant K _{aw} at 25°C	Log K _{ow}
Naphthalene	2	C ₁₀ H ₈		128.06	218	11.30	31.00	0.02	3.35
Acenaphthylene	3	C ₁₂ H ₈		152.06	280	0.89	16.10	4.66 · 10 ⁻³	3.94
Acenaphthene	3	C ₁₂ H ₁₀		154.08	279	0.29	3.90	7.53 · 10 ⁻³	3.92
Fluorene	3	C ₁₃ H ₁₀		166.08	295	0.08	1.69	3.93 · 10 ⁻³	4.18
Phenanthrene	3	C ₁₄ H ₁₀		178.08	340	0.02	1.15	1.73 · 10 ⁻³	4.46
Anthracene	3	C ₁₄ H ₁₀		178.08	340	1.07 · 10 ⁻³	0.04	2.27 · 10 ⁻³	4.45
Fluoranthene	4	C ₁₆ H ₁₀		202.08	384	1.23 · 10 ⁻³	0.26	3.62 · 10 ⁻⁴	5.16
Pyrene	4	C ₁₆ H ₁₀		202.08	404	6.00 · 10 ⁻⁴	0.14	4.87 · 10 ⁻⁴	4.88
Benzo[a]anthracene	4	C ₁₈ H ₁₂		228.09	438	2.80 · 10 ⁻⁵	9.40 · 10 ⁻³	4.91 · 10 ⁻⁴	5.76
Chrysene	4	C ₁₈ H ₁₂		228.09	448	8.30 · 10 ⁻⁷	2.00 · 10 ⁻³	2.14 · 10 ⁻⁴	5.81
Benzo[b]fluoranthene	5	C ₂₀ H ₁₂		252.09	443	6.67 · 10 ⁻⁵	1.50 · 10 ⁻³	2.69 · 10 ⁻⁵	5.78
Benzo[k]fluoranthene	5	C ₂₀ H ₁₂		252.09	480	1.05 · 10 ⁻⁷	8.00 · 10 ⁻⁴	2.39 · 10 ⁻⁵	6.11

Table 1.1. (continued) Physicochemical properties of some relevant PAHs (source: Gustafsson et al., 2001).

Name	Ring no.	Molecular formula	Chemical structure	Exact mono-isotopic molecular weight (Da)	Boiling point at 1013 hPa (°C)	Vapour pressure at 25°C (Pa)	Water solubility at 25°C (mg L ⁻¹)	Henry's constant K _{aw} at 25°C	Log K _{ow}
Benzo[e]pyrene	5	C ₂₀ H ₁₂		252.09	443	2.59 · 10 ⁻⁶	6.30 · 10 ⁻³	1.23 · 10 ⁻⁵	6.44
Benzo[a]pyrene	5	C ₂₀ H ₁₂		252.09	496	1.03 · 10 ⁻⁴	1.62 · 10 ⁻³	1.87 · 10 ⁻⁵	6.13
Indeno[1,2,3-cd]pyrene	6	C ₂₂ H ₁₂		276.09	536	1.67 · 10 ⁻⁸	1.90 · 10 ⁻⁴	1.42 · 10 ⁻⁵	6.70
Dibenzo[a,h]anthracene	5	C ₂₂ H ₁₄		278.11	524	1.33 · 10 ⁻⁸	2.19 · 10 ⁻³	5.03 · 10 ⁻⁶	6.75
Benzo[ghi]perylene	6	C ₂₂ H ₁₂		276.09	>500	1.33 · 10 ⁻⁸	2.60 · 10 ⁻⁴	1.35 · 10 ⁻⁵	6.63
Coronene	7	C ₂₄ H ₁₂		300.36	525	5.87 · 10 ⁻⁸	1.40 · 10 ⁻⁴	8.67 · 10 ⁻⁷	7.64

The solubility of PAHs in water is low and decreases with the molecular weight, thus, these compounds are considered sparingly soluble in water. Nevertheless, in many organic solvents such as benzene, acetone, methanol or hexane, PAHs present a good solubility (Rajput and Lakhani, 2010). The log octanol-water partition coefficients of PAHs show values between 2 and 6.5, this identifies them as lipophilic compounds; the lipophilicity increases with increasing complexity (Connell, 2005).

Vapour pressure plays an essential role in the distribution of PAHs in the air-water-soil environment. This property is inversely related to molecular weight, thus, low molecular weight PAHs (2-3 rings) are more volatile than high molecular weight PAHs (>3 rings), which are primarily associated with particles.

PAHs have characteristic UV absorbance spectra; each ring structure and isomer presents its own spectra. Most PAHs are also fluorescent, emitting characteristic wavelengths of light when they are excited (when the molecules absorb light, generally in the 200-400 nm range) (Santana Rodríguez and Padron Sanz, 2000; Rivera-Figueroa et al., 2004)

1.2 Formation of PAHs

Polycyclic aromatic hydrocarbons (PAHs) are formed by incomplete combustion high-temperature pyrolytic processes involving fossil fuels or biomass. Pyrolysis and pyrosynthesis are two mechanisms that can explain the formation of PAHs.

In temperatures higher than 500°C, the organic matter is cracked (pyrolysis) to form unstable and smaller fragments (radicals). These radicals, which present high reactivity and a very short average lifetime, lead to more stable PAH formation through recombination reactions (pyrosynthesis). This process can also be referred to as “waterfall mechanism”, in which complex-structure compounds with high molecular weight are formed through the combination of small fragments during combustion (Figure 1.1) (Mastral and Callén, 2000).

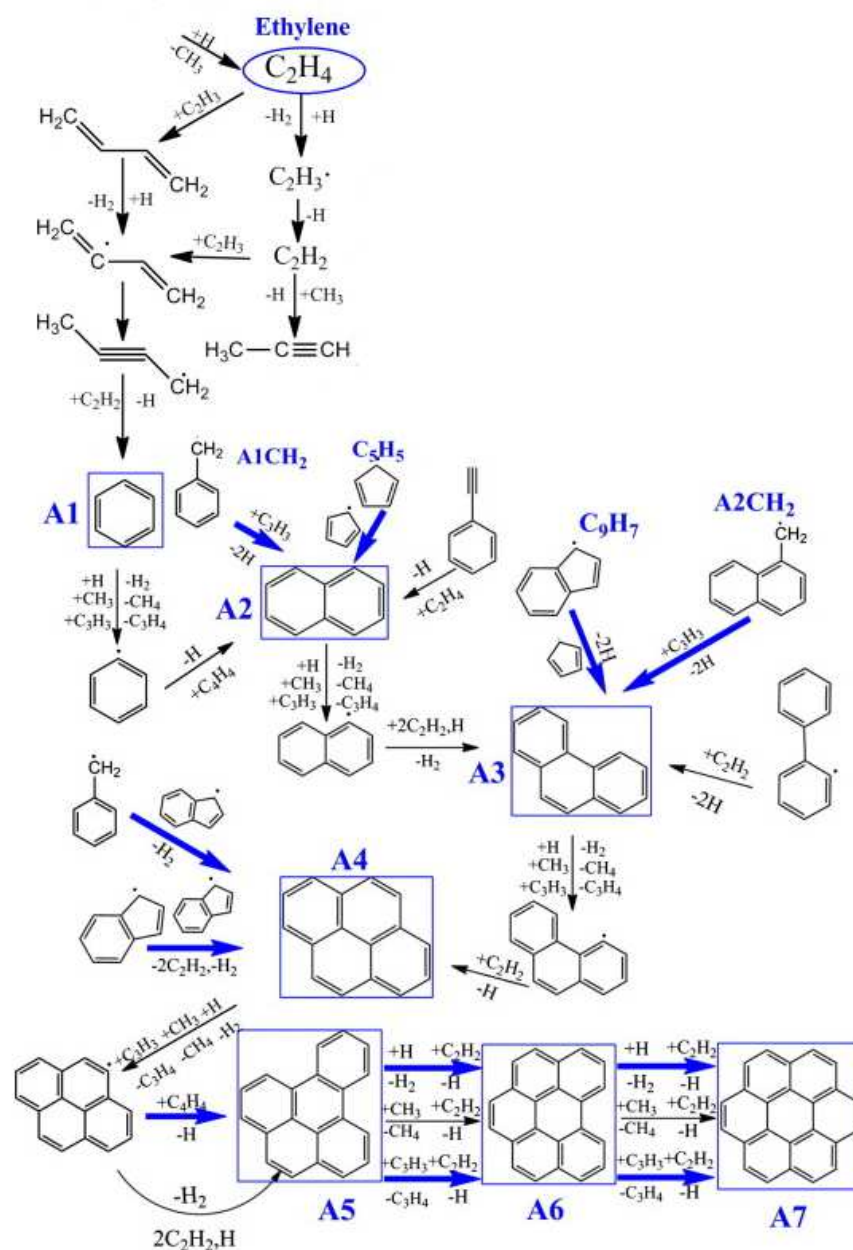


Figure 1.1. Reaction flux diagram for formation of PAHs from ethylene (blue arrows highlight those reactions contributing to the synergistic effects on PAHs) (adapted from Wang et al., 2013). A1: benzene, A2: naphthalene, A3: phenanthrene, A4: pyrene, A5: benzo[e]pyrene, A6: benzo[ghi]pyrene, A7: coronene.

The tendency of hydrocarbons to form PAHs by pyrosynthesis increases in the following order: aromatics > cycloolefins > olefins > paraffins (Manahan, 1994). Haynes (1991) suggests that PAHs are formed during combustion by mechanisms involving slow Diels-Alder condensations, rapid radical reactions and ionic reactions.

In the case of internal combustion engines, the formation of PAHs is affected by factors such as type of fuel, amount of oxygen and temperature (Lima et al., 2005).

In spite of the previous studies, the underlying chemistry of the formation of PAHs is still not completely understood.

1.3 Sources of PAHs

PAHs are mainly derived from anthropogenic activities related to pyrolysis and incomplete combustion of organic matter. Emission sources of PAHs affect their characterization and distribution, as well as their toxicity (Lee, 2010). These sources can be divided into the following categories (Ravindra et al., 2008):

- Natural.
- Domestic.
- Mobile.
- Industrial.
- Agricultural.

The relative importance of these sources is expected to change with time as a result of regulations and economic development.

Natural sources

Accidental burning of forests, woodland, and moorland due to lightning strikes are natural sources of PAHs (Baumard et al., 1999). Furthermore, volcanic eruptions and decaying organic matter are also important natural sources, contributing to the levels of PAHs in the atmosphere (Wild et al., 1995). Meteorological conditions (such as wind, temperature, and humidity) and fuel type (such as moisture content, and green vs. seasoned wood) may play an important role in the degree of natural PAH production. Natural sources have not been investigated in great detail, but may contribute significantly to local PAH levels.

Domestic sources

Heating and cooking are dominant domestic sources of PAHs. The burning and pyrolysis of coal, oil, gas, garbage, wood, or other organic substances are the main domestic sources. The production of PAHs from these sources presents a big geographic variation due to the differences in climate patterns and domestic heating systems. It was estimated that 65 % of global emissions of PAHs in 2007 were derived from the use of solid fuels in homes (Shen et al., 2013). Furthermore, these emissions may be a major health concern because of the prevalence of PAHs in indoor environments (Ravindra et al., 2006).

Mobile sources

Mobile sources are major causes of PAH emissions in urban areas. The exhaust fumes of vehicles, including automobiles, railways, ships, aircrafts, and other motor vehicles, are the main sources of PAH emissions. These may be caused by three distinct mechanisms:

- Synthesis from simpler molecules in fuel, particularly from aromatic compounds (Mitchell et al., 1994).
- Storage in engine deposits and subsequent emission of PAHs already present in fuel (Lin et al., 2006).
- Pyrolysis of lubricants (Westerholm and Lin, 1994).

Factors such as engine type, fuel composition, load and age, millage, the PAH accumulation in lubricant oil, the lubricant oil combustion and the driving mode determine the emission of these pollutants (Cheruiyot et al., 2015).

Industrial sources

Burning of fuels such as gas, oil, and coal is the major cause of PAH emissions in the industry. Sources of PAHs include emissions from industrial activities, such as primary aluminium and coke production, petrochemical industries, rubber tire and cement manufacturing, bitumen and asphalt industries, wood preservation, commercial heat and power generation, and waste incineration.

Agricultural sources

All agricultural activities that involve the burning of organic materials under sub-optimum combustion conditions (such as stubble burning, the open burning of moorland heather for regeneration purposes or the open burning of brushwood and straw) are sources of atmospheric PAHs.

The uncertainty in emission factors and the occurrence of these activities complicate the quantification of the sources (Ravindra et al., 2008).

1.4 Atmospheric transport and fate of PAHs

The gas/particle partitioning of PAHs plays an important role in the transport, deposition, and chemical transformation of these compounds. The partition of PAHs depends on the molecular weight of the compounds, temperature, humidity and precipitation (Van Jaarsveld et al., 1997; Lee and Jones, 1999). Low-volatile PAHs with >5 rings, characterized by relatively high condensation temperatures, are adsorbed on airborne particles. They are classified in the low mobility category of PAHs subject to rapid deposition and retention close to the source (Wania and Mackay, 1996). In general, between the 70% and 90 % of the PAHs at ambient temperature are in the particulate phase (Ravindra et al., 2008). The lower-molecular weight compounds with 2-3 rings, exhibiting low temperatures of condensation, are more abundant in the gas phase (Lee and Jones, 1999). These PAHs can undergo worldwide atmospheric dispersion, accumulating preferentially in Polar Regions (Wania and Mackay, 1996; Van Jaarsveld et al., 1997).

There is general agreement on the seasonal variability of PAH concentration; for the particulate phase the higher concentrations are usually registered in winter while in summer the PAHs in gas phase are predominant. Changes in the vertical dispersion (due to thermal inversion), in the mixing layer height, in the temperature (affecting the sorption of PAHs to particles) and in the emissions (domestic heating and power plants increase their emissions during winter) explain this seasonal variation (Subramanyam et al., 1994; Lee et al., 2005; Ravindra et al., 2006).

The atmosphere is an important pathway for the transport of PAHs. The pollutants in the atmosphere are not only transported to remote sites, but can also be transferred to a different matrix via wet and dry deposition (Ortiz et al., 2012; Inomata et al., 2012;

Karaca et al., 2014). The PAHs present in the atmosphere can mainly be removed from it by three mechanisms: wet/dry deposition, photochemical transformation and reactions with other pollutants. The physical mechanism of PAH loss from the atmosphere is the deposition. The particulate compounds are mainly subject to this removal mechanism, which depends on the next factors: the physicochemical properties of the PAHs, their gas/particle partitioning, and the meteorological parameters. In general, the gaseous PAHs dissolve within clouds into the raindrops, whereas PAHs bound to particles are washed out by precipitation (Golomb et al., 2001; Ravindra et al., 2003). In case of the PAHs which are hydrophobic, dry deposition dominates (Golomb et al., 1997). Due to the fact that the lifetime of PAHs in the aqueous phase is higher than in the dry air, the PAHs obtained from wet depositions could be from farther sources (hundreds to thousands kilometres from their original source) (Mackay et al., 1992).

After dry and wet deposition, the photo-induced reaction is considered to be the next most important mechanism in removing PAHs from the atmosphere (Reisen and Arey, 2005). Many PAHs are susceptible to photochemical and chemical oxidation under atmospheric conditions.

Keyte et al. (2013) reviewed the reactivity of PAHs (gas and particle phases) with hydroxyl radical ($\cdot\text{OH}$), ozone (O_3), nitrate radical ($\text{NO}_3\cdot$) and nitrogen dioxide (NO_2). They reported:

Gas phase

- The reactions with the OH radical could be the main sink for gas phase PAHs. The rate coefficients for these reactions were considerably (up to 5 orders of magnitude) higher than the corresponding reactions with NO_3 for most 3-4 ring PAHs.
- NO_3 reactions appeared to be less significant than OH reactions as a PAH degradation process. During night-time, the higher nitro-PAH yields suggested that reactions of PAHs with NO_3 may be significant contributors to these compounds in the atmosphere, in addition to daytime OH reactions.
- Reactions of PAHs with O_3 were considered to be of negligible importance in the atmosphere due to the slow reaction with the aromatic ring.

Particle phase

- The reactivity of PAHs with atmospheric oxidants involves complex processes that demonstrated the influence of a number of factors, including the nature (chemical composition, surface area, porosity) of the matrix, presence of other species (e.g. nitric acid, water or other organic species), oxidant concentration, PAH molecule involved, and PAH surface concentration.
- The wide diversity in particle properties, including their chemical composition (organic, mineral, biogenic), sources (combustion, erosion, gas phase condensation), origin (natural, anthropogenic), the method of particle formation (temperature, pressure), physical properties (size, porosity, specific surface area), surface coatings (water, nitric acid, organic molecules), means that gaining a full understanding of this reactivity will be extremely difficult as the relative importance of these different factors is highly variable across reaction systems.
- Reaction with OH radicals was the dominant pathway for degradation of PAHs compared with reactions with NO₂ and O₃, with second order rate coefficients 1-7 orders of magnitude higher on carbonaceous particles.
- Particles exhibited a potential 'inhibiting factor' on the reactivity of PAHs due to slow diffusion of the oxidant or inaccessibility of PAHs in the bulk particle. This may turn PAHs to persistent compounds in air.
- Reactions of particle-bound PAHs with O₃ proceeded more quickly than the corresponding reactions in the gas phase.

Finally, the reaction of the PAHs with other atmospheric chemicals generates derivatives. Transformations of PAHs on particles can affect the toxicity of particles through the formation of species that are more toxic than the original species, for example nitro-PAHs and oxy-PAHs (Sasaki et al., 1997; Lundstedt et al., 2003).

Figure 1.2 shows the main inputs and outputs of the persistent organic pollutants (POPs), among them the PAHs, in the environment.

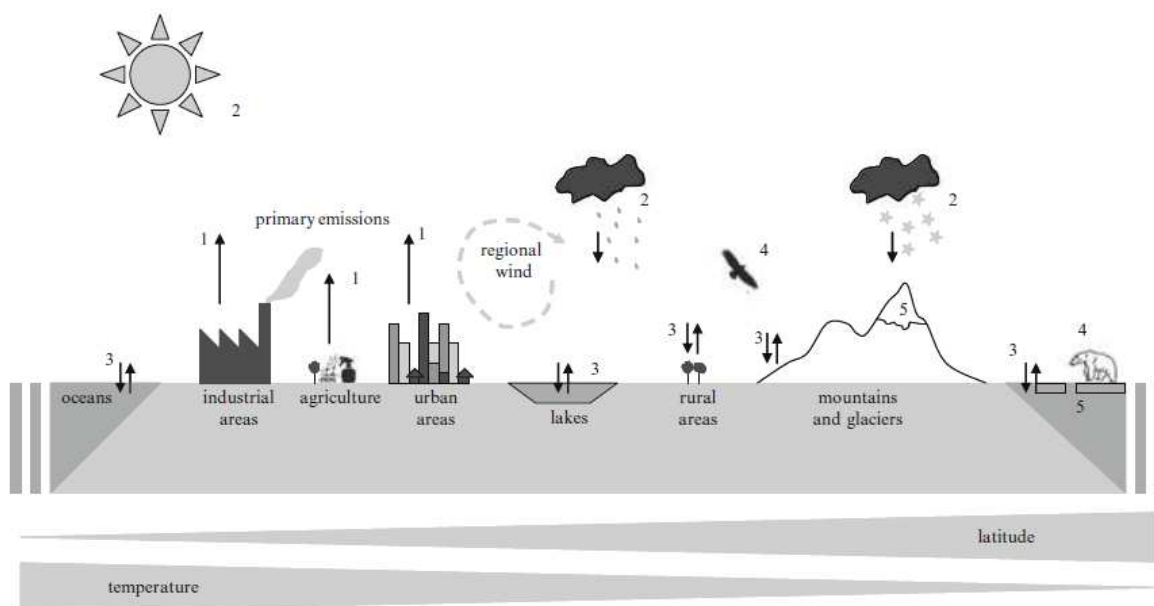


Figure 1.2. Conceptual representation of processes influencing the atmospheric transport and fate of POPs (among them the PAHs) (source: Van Drooge and Grimalti, 2012). (1) Primary emissions of POPs to the atmosphere, (2) atmospheric deposition and photochemical degradation/transformation, (3) re-volatilisation from secondary sources in the different environmental compartments and burial in sediments, (4) bioaccumulation and biotic transport, (5) accumulation in glaciers and ice caps, with probable releases due to melting.

1.5 Emissions and ambient concentrations of PAHs

Emission inventories are important tools in the management of air quality. Current inventories have a high level of uncertainty, and further work is required to improve the reliability of the estimates. Nevertheless, these PAH inventories have allowed the identification and prioritization of the likely main emission sources.

1.5.1 Europe

The application of environmental policies and emission mitigation technologies has significantly reduced the PAH emissions in Europe since 1990. In spite of the clear decreases over the last 25 years, the emissions have remained broadly stable since 2002 (Figure 1.3).

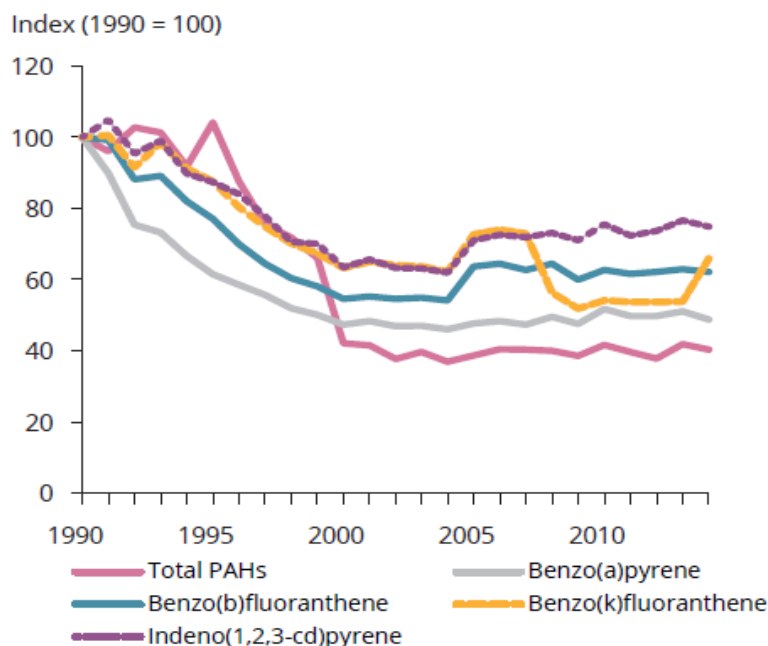


Figure 1.3. EU-28 emission trends for total PAHs and the four indicators of PAHs considered in the 1979 Convention on Long-range Transboundary Air Pollution, from 1990 to 2014 (source: EEA, 2016).

According to the last European emission inventory (EEA, 2016), the total PAH emission in 2014 was 1116 Mg, which includes 186 Mg of benzo[a]pyrene. Furthermore, the countries that contributed most to these emissions in 2014 (with values more than 10%) were Germany, Spain, Poland and Portugal. Compared with 1990 levels, total PAH emissions have dropped in the EU-28 by 60% (Table 1.2).

Table 1.2. Total PAH emissions (in Mg) in each member state and their contribution (%). Comparison between 1990 and 2014 (source: EEA, 2016)

Member State	Total PAHs (Mg)		Change (%)	Share in EU-28 (%)	
	1990	2014	1990-2014	1990	2014
Austria	16	4.9	- 70	0.6	0.4
Belgium	79	23	- 71	2.9	2.0
Bulgaria	50	28	- 44	1.8	2.5
Croatia	16	8.0	- 49	0.6	0.7
Cyprus	1.7	0.5	- 73	0.1	0.0
Czech Republic	752	20	- 97	27.2	1.8
Denmark	5.2	6.4	22	0.2	0.6
Estonia	9.0	7.0	- 22	0.3	0.6
Finland	15	9.7	- 37	0.6	0.9
France	45	19	- 57	1.6	1.7
Germany	378	158	- 58	13.6	14.2
Greece	n/a	n/a			
Hungary	85	15	- 83	3.1	1.3
Ireland	49	16	- 66	1.8	1.5
Italy	99	77	- 22	3.6	6.9
Latvia	17	9.6	- 45	0.6	0.9
Lithuania	18	10	- 42	0.6	0.9
Luxembourg	4.8	0.5	- 89	0.2	0.0
Malta	0.0	32	> 100	0.0	2.9
Netherlands	20	4.7	- 77	0.7	0.4
Poland	147	143	- 3	5.3	12.9
Portugal	154	116	- 25	5.6	10.4
Romania	274	80	- 71	9.9	7.2
Slovakia	29	19	- 34	1.0	1.7
Slovenia	8.7	5.6	- 36	0.3	0.5
Spain	273	266	- 3	9.8	23.8
Sweden	18	12	- 33	0.7	1.1
United Kingdom	205	24	- 88	7.4	2.1
EU-28	2776	1116	- 60	100	100

Dark-grey shaded cells indicate that no emission values are available.

Light-grey shaded cells denote graph-filled data.

Finally, regarding the sources of PAHs, in 2014 the main contribution of PAH emissions in the European Union (EU) came from the “commercial, institutional and household” sector with a value of 54% (Figure 1.4).

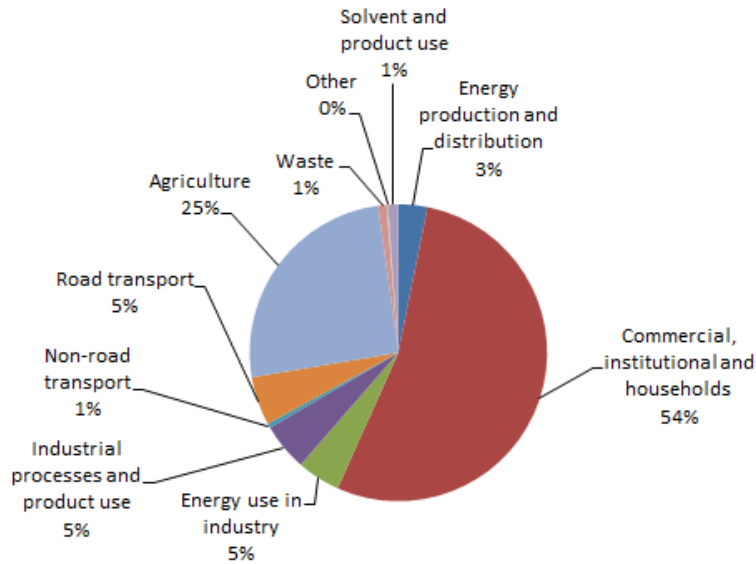


Figure 1.4. Main sources of total PAHs in the EU and their contributions (%) in 2014 (source: EEA, 2016).

In general, the data on PAH levels in ambient air are sparse compared to those of classical pollutants like SO₂. This can be explained by the fact that (a) a rather complex and expensive sampling and analytical procedure is needed to measure the ambient air concentration of PAH and (b) there are only few countries with a legal basis requiring the measurements of PAH (European Commission, 2001).

PAHs are ubiquitous; concentrations are lower at remote background sites than at rural sites. Higher concentrations are found in urban areas, with peak concentrations measured at urban sites with both traffic and nearby industrial installations (Table 1.3).

Table 1.3. Summary of recent (not older than 1990) typical European PAH concentrations in ng/m³ as annual mean value (source: European Commission, 2001).

PAH	Remote site	Rural site	Urban	Traffic	Industrial
Acenaphthylene	0.01				
Acenaphthene	0.01	0.3 – 2.6			98
Fluorene	0.2 – 0.4	0.3 – 46			
Phenanthrene	0.1 – 0.3	0.42 – 150			
Anthracene	n.d. ¹	0.04 – 15		0.2 – 0.6	1.1
Fluoranthene	0.14	202			42
Pyrene	0.08	202	0.24 – 1.2	9.2 – 15	75
Benzo[a]anthracene	0.00 – 0.02	0.01 – 0.9	0.2 – 1.3	0.6 – 4.2	0.37 – 42
Chrysene		0.02 – 4.4	0.3 – 2.2		0.3 – 37
Benzo[b]fluoranthene	0.00 – 0.01	0.04 – 0.6			0.3 – 34
Benzo[k]fluoranthene		0.04 – 0.32	0.2 – 1		0.3 – 17
Benzo[a]pyrene	0.02	0.02 – 1.6	0.4 – 2	0.7 – 3.1	0.5 – 39
Benzo[e]pyrene	0.01 – 0.02	0.18 – 1.1	0.2 – 2.1	0.9 – 3.7	0.65 – 80
Indeno[1,2,3-cd]pyrene	0.02 – 0.04	0.04 – 0.21	0.3 – 2.1	1.3 – 2.6	0.4 – 37
Dibenzo[ah]anthracene	n.d. ¹	0.02 – 1.1	0.06 – 0.3	0.1 – 0.4	0.05 – 7.5
Benzo[ghi]perylene	0.01	0.15 – 1.0	0.5 – 2.8	1 – 4.7	0.7 – 52
Coronene	0.00 – 0.01	0.02 – 0.5	0.1 – 0.6	0.4 – 2.5	0.26 – 5.2

¹ Not detected

1.5.2 Spain

In Spain the total PAH emissions have dropped in the last 25 years, following the European trend. Nevertheless, since 2001 the emissions in Spain have been more unstable, with significant rises and falls. In 2014, the drop in Spanish emissions was significantly less than the European average (- 3% vs. - 60%) (Figure 1.5).

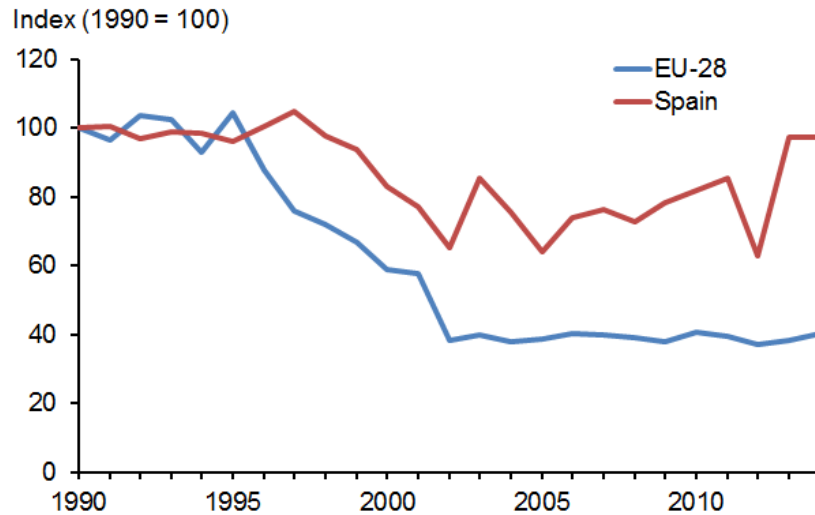


Figure 1.5. Spain vs EU-28 emission trends for total PAHs from 1990 to 2014 (sources: Spanish Ministry of Agriculture, Food and Environment, 2016).

The PAH sources in 2014 have also showed a different profile in Spain, with the “Agriculture” sector being the main source with a contribution of 67% in the total PAH emissions (Figure 1.6). The totality of the PAH emissions in this sector came from the burning of agricultural field residues (177.72 t in 2014) (Spanish Ministry of Agriculture, Food and Environment, 2016).

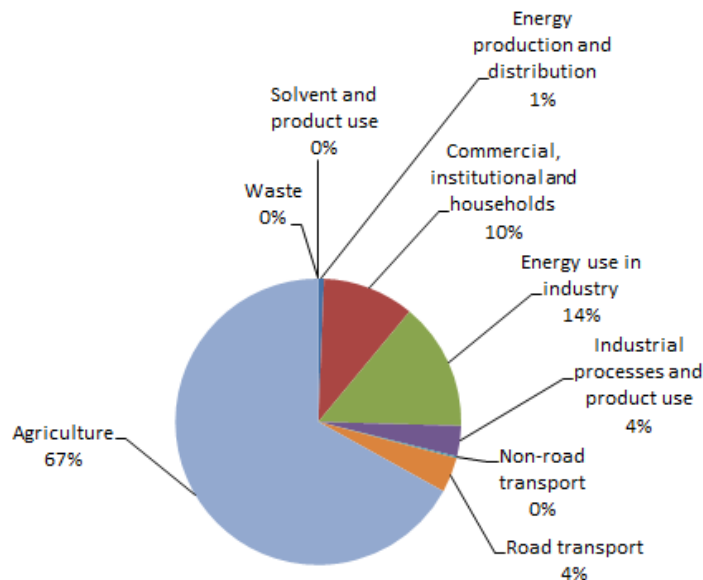


Figure 1.6. Main sources of total PAHs in Spain and their contributions (%) in 2014 (source: Spanish Ministry of Agriculture, Food and Environment, 2016).

1.6 Toxicity and regulation of PAHs

As previously mentioned, the majority of the PAHs are adsorbed on suspended particles at ambient temperature. Although particulate matter (PM) can be defined or classified in a number of ways, aerodynamic diameter is one of the main criteria to describe its transport ability in the atmosphere and/or inhaling ability through a respiratory organism (Esworthy, 2013):

- PM₁₀ refers to particles with a diameter less than 10 microns. These particles are called coarse particulate matter and can lodge in the trachea (upper throat) or in the bronchi (Atkinson et al., 2010).
- PM_{2.5} refers to particles with a diameter of less than 2.5 microns. These are usually called fine particles and can reach all the way down to the alveoli in the lungs (Löndahl et al., 2007).
- PM_{0.1} refers to particles with a diameter less than 0.1 microns, and they are called ultra-fine particles. These particles are usually exhaled but can penetrate into the bloodstream (Valavanidis et al., 2008).

Therefore, these particles can generate adverse effects in animals and humans. Reactive metabolites of some PAHs have become one of the major health concerns because of their potential to bind to cellular proteins and DNA with toxic effects (Armstrong et al., 2004). The resulting biochemical disruption and cell damage can lead to mutations, developmental malformations, tumours, and cancer (Bach et al., 2003).

Yuan et al. (2013) suggested that PAHs may be also teratogenic. Because PAHs are lipophilic, they readily penetrate cellular membranes (including the placenta). During the PAH metabolism, enzymatic activity can result in the formation of reactive intermediates, which affect the DNA, generating cellular mutations (Rice and Baker, 2007; Wells et al., 2010).

Figure 1.7 shows a simple flow chart that recollects the main health effects associated with short and long term exposure to PAHs.

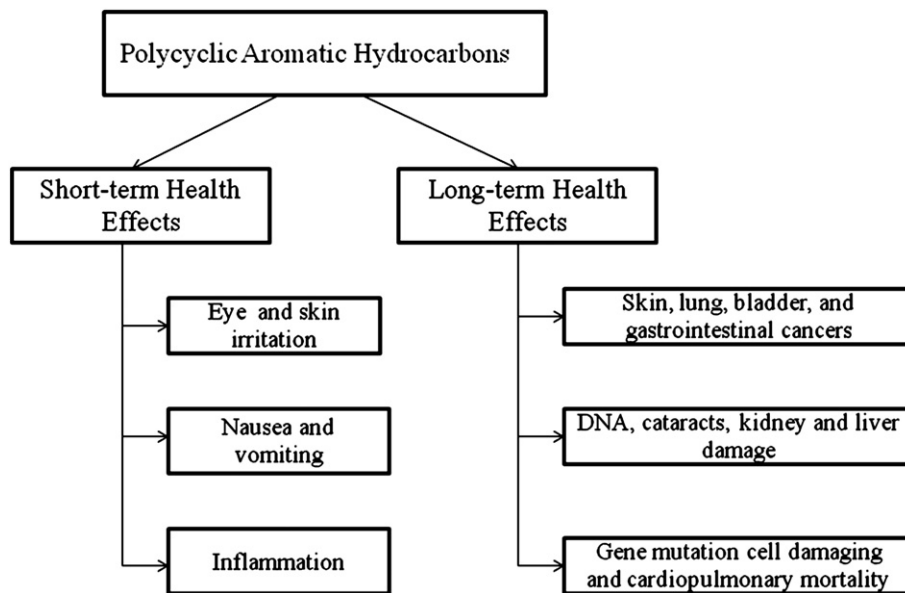


Figure 1.7. Short and long term health effects of exposure to PAHs (source: Kim et al., 2013).

The harmful health effects of PAHs and their persistence pose an environmental concern. These compounds were among the first atmospheric pollutants identified as suspected carcinogens (Boström et al., 2002). Moreover, PAHs belong to the group of POPs included in the list of 16 POPs specified by the UNECE Convention on Long-range Transboundary Air Pollution Protocol on Persistent Organic Pollutants (UNECE, 1979; Council Decision 2004/259/EC, 2004). Due to these features, the United States Environmental Protection Agency (US-EPA) has listed 16 of them as priority pollutants (16 EPA PAHs) (OFR, 1982). Furthermore, the same organization and the Agency for Research on Cancer (IARC) have classified the 16 EPA PAHs according to their carcinogenicity (Table 1.4).

Table 1.4. US-EPA's 16 priority-pollutant PAHs. Classification for carcinogenicity.

PAH	Abbreviation	Carcinogenicity	
		IARC ^a	US-EPA ^b
Naphthalene	Naph	2B	C
Acenaphthylene	Acy	Not available	D
Acenaphthene	Ace	3	Not available
Fluorene	FL	3	D
Phenanthrene	Phe	3	D
Anthracene	Ant	3	D
Fluoranthene	Ft	3	D
Pyrene	Pyr	3	D
Benzo[a]anthracene	BaA	2A	B ₂
Chrysene	Chry	2B	B ₂
Benzo[b]fluoranthene	BbFt	2B	B ₂
Benzo[k]fluoranthene	BkFt	2B	B ₂
Benzo[a]pyrene	BaP	1	B ₂
Indeno[1,2,3-cd]pyrene	IP	2B	B ₂
Dibenzo[ah]anthracene	DBahA	2A	Not available
Benzo[ghi]perylene	BghiP	3	D

^a (IARC, 2016): Group 1 - carcinogenic to humans; Group 2A - probably carcinogenic to humans; Group 2B - possibly carcinogenic to humans; Group 3 - unclassifiable as to carcinogenicity in humans; Group 4 - probably not carcinogenic to humans.

^b (US- EPA, 2016): Group A - human carcinogens; Group B - probable human carcinogens (B1: based on limited evidence of carcinogenicity in humans and sufficient evidence in animals; B2: based on sufficient evidence of carcinogenicity in animals); Group C - possible human carcinogens; Group D - not classifiable as to human carcinogens; Group E - evidence of non-carcinogenicity for humans

The carcinogenic potency associated with exposure to a given PAH compound can be obtained by calculating its BaP equivalent concentration (BaP_{eq}). The toxicity equivalency factor (TEF) method described by Nisbet and Lagoy (1992) is used to calculate the BaP_{eq} for each individual PAH. The carcinogenic potency associated with the total PAH content is evaluated by the sum of each individual BaP_{eq} (Eq.1.1)

$$BaP_{eq} = \sum_{i=1}^N (PAH)_i \cdot TEF_i \quad (1.1)$$

where BaP_{eq} is the benzo[a]pyrene equivalent concentration, TEF is toxic equivalent factor for each individual PAH, $(PAH)_i$ is the concentration for each individual PAH, and N is the number of individual PAHs.

TEFs of individual PAHs have been reported by many researchers (Table 1.5).

Table 1.5. TEFs proposed for individual PAHs according to different authors

PAH	Nisbet and Lagoy, 1992	Malcom and Dobson, 1994	Kalberlah et al., 1995	Muller et al., 1997	Liao et al., 2006
Naph	0.001	0.001			0.001
Acy	0.001	0.001	0.01		0.001
Ace	0.001	0.001	0.001		0.001
FL	0.001	0.001	0		0.001
Phe	0.001	0.001	0	0.00064	0.001
Ant	0.01	0.01	0.01		0.01
Ft	0.001	0.001	0.01		0.001
Pyr	0.001	0.001	0.001	0	0.001
BaA	0.1	0.1	0.1	0.014	0.1
Chry	0.01	0.01	0.01	0.026	0.01
BbFt	0.1	0.1	0.1	0.11	0.1
BkFt	0.1	0.1	0.1	0.037	0.1
BeP		0.01		0	0.01
BaP	1	1	1	1	1
IP	0.1	0.1	0.1	0.067	0.1
DBahA	1	1	1	0.89	1
BghiP	0.01	0.01	0.01	0.026	0.01

Finally, the cancer risk from PAH exposure can be calculated using Eq.1.2

$$ICR = BaP_{eq} \cdot IUR_{BaP} \quad (1.2)$$

where ICR is the inhalation cancer risk, BaP_{eq} is the benzo[a]pyrene equivalent concentration, IUR_{BaP} is inhalation unit risk of exposure to BaP (specifically, “the calculated, theoretical upper limit possibility of contracting cancer when exposed to BaP at a concentration of one microgram per cubic meter of air for a 70-year lifetime”).

In order to protect public health, the European Union (EU), has established and implemented different directives to lay down limits to specific pollutants in ambient air in recent years:

- Directive 1999/30/EC: Sulphur dioxide, nitrogen dioxide and oxides of nitrogen, particulate matter and lead.
- Directive 2000/69/EC: Carbon monoxide and benzene.
- Directive 2002/3/EC: Ozone.
- Directive 2004/107/EC: Polycyclic aromatic hydrocarbons, arsenic, nickel, cadmium and mercury.

The Ambient Air Quality and Cleaner Air for Europe (CAFE) Directive (2008/50/EC), published in 2008, replaced the previous directives except the last one (2004/107/CE), which will be included in CAFE at a later stage.

For PAHs in ambient air, the Directive 2004/107/CE settles the target value considering benzo[a]pyrene as the marker of carcinogenic PAH risk. The target values is 1 ng m^{-3} , and it is estimated as annual average of the total content in PM_{10} with a minimum number of measurements adequately distributed along the weeks and years. To fully assess the contribution of benzo[a]pyrene in ambient air, EU also recommended monitoring of other relevant PAHs (e.g. benzo[a]anthracene, benzo[b]fluoranthene, benzo[j]fluoranthene, benzo[k]fluoranthene, indeno[1,2,3-cd]pyrene, and dibenzo[a,h]anthracene), but the target values of these compounds have not been settled yet.

The CAFE Directive was transposed into Spanish legislation by Real Decreto 102/2011 relating to air quality improvement. This regulation replaced the previous Real Decreto 1072/2002, 1796/2003 and 812/2007 which transposed the European Directives 1999/30/EC, 2000/69/EC, 2002/3/EC and 2004/107/EC, respectively.

1.7 Determination of PAHs in air

1.7.1 Collection of PAHs

The particle-gas partitioning of PAHs is the main factor that determines the selection of sampling equipment. PAHs in the atmosphere are mainly collected by two sampling models: active and passive sampling.

Active sampling involves the use of an air sampling pump to actively pull air through a collection device such as a filter or sorbent material where target PAHs compounds are accumulated. Active samplers include high-volume, low-volume and cascade samplers.

Passive sampling, however, does not require active air movement from a pump. Airborne gases and vapours are collected by a physical process such as diffusion through a static air layer or permeation through a membrane (Figure 1.8). The passive samplers are classified based on diffusion direction (axial or radial).

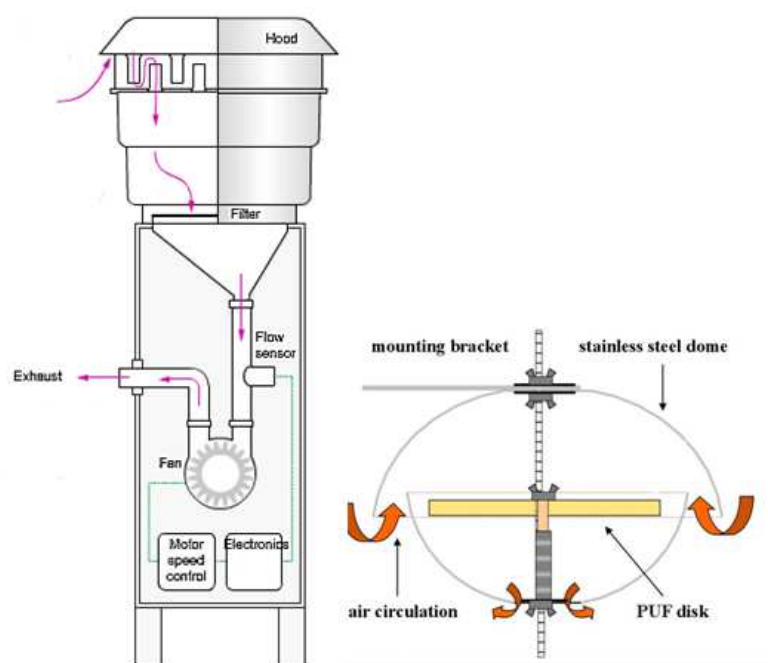


Figure 1.8. Schematic diagram active (left) vs. passive (right) sampler (sources: Queensland Government, 2016; MonAirNet project, 2016)

Particulate PAHs sampling devices

The glass fibre and the quartz fibre filters are the sampling media commonly used to collect the particle-bound and particle plus gaseous PAHs in air (Mandalakis et al., 2002; Omar et al., 2002; Lottmann et al., 2007; Chantara and Sangchan, 2009). However, in some studies, Teflon has been used as coating material for glass fibre filters (Marr et al., 2006) or as sampling media (Pleil et al., 2004).

Glass fibre filters (GFFs) are the most frequently employed collection devices for particle phase PAHs. They have been used for the sampling of PAHs (mainly 16 EPA

PAHs and their derivatives and occasionally additional PAHs) in diverse locations from rural to industrial areas (Mandalakis et al., 2002; Omar et al., 2002; Tsapakis and Stephanou, 2005). On rare occasions, modifications of GFFs have also been used for the collection of particle-bound PAHs. Marr et al. (2006) used Teflon-coated GFFs to collect particle phase PAHs from urban atmospheres in Mexico city.

Quartz fibre filters (QFFs) are another preferred medium for the collection of particle-bound PAHs. Just as in the case of GFFs, these filters have been used in the sampling in different locations, with high (Park et al., 2002; Lottmann et al., 2007) and low (Chaspoul et al., 2005; Chantara and Sangchan 2009) air sampling volumes. Due to their higher thermal resistance, the QFF are recommended as collection media for solvent-free methods (e.g. thermal desorption (TD)).

Finally, Teflon filters have been employed in some studies as a medium to collect particle PAHs (Lung et al., 2004a; Re-Poppi et al., 2005).

After the sampling, the particulate-bound PAHs collected on the filters are susceptible to degradation from oxidizing compounds, particularly ozone, but also NO₂, present in the sampled air. This may result in substantial underestimation of the concentrations of PAHs present in ambient air. The European normative (Directive 2004/107/CE) mandates Member States to use sampling periods of 24h, as longer sampling periods could ease the degradation of these compounds from oxidation reactions.

Gaseous PAHs sampling devices

Collection of gaseous PAHs from the atmosphere onto solid adsorbents is the most widely used methodology.

Polyurethane Foam (PUF) has been utilized as the most common means of enriching gas phase PAHs. Numerous studies have used this adsorbent to collect a wide range of PAHs (including 16 EPA PAHs) in urban, industrial and rural sites (Ravindra et al. 2006; Vasilakos et al. 2007; Li et al., 2014). The applicability of PUF samplers has also been demonstrated in the determination of diverse PAH derivatives (e.g. nitro-PAHs and oxy-PAHs) in the vapour phase (Albinet et al., 2007; Wei et al., 2015).

Like PUF, XAD resins have been widely used in the sampling of gaseous PAHs (Motelay-Massei et al., 2006; Zhu et al., 2009; Liu et al., 2015). In general, XAD

provides a better collection of volatile PAHs than PUF because of its higher collection and retention efficiency, whereas PUF cartridges are easier to handle in the field and maintain better flow characteristics during sampling (US-EPA, 1999a).

Besides XAD resins, other porous polymeric adsorbents are used to collect gaseous PAHs. Tenax TA is the most thermally stable of them and has low affinity for water (hydrophobic). Moreover, this adsorbent can be used at high temperatures, generating low artefacts. Tenax GR presents similar characteristics to TA but its composition contains graphitized carbon (23%). This means that this adsorbent shows lower adsorption of water vapours and higher packing density than Tenax TA.

Wauters et al. (2008) and subsequently Lazarov et al. (2013) studied the application of a mixed bed of polydimethylsiloxane (PDM) and Tenax TA as sampling method to collect PAHs in urban and indoor environments. The results obtained in both studies showed a better collection of low molecular weight PAHs (higher concentrations), in comparison with the sampling by PUF. This was also registered by Martins et al. (2013), using Tenax TA sorption tubes as sampling method.

1.7.2 Extraction methods for PAHs

Once the PAHs have been collected and concentrated on suitable filters or sorbent materials, they have to be extracted for the final determination. The extraction of PAHs from the multiple matrices is a difficult step. PAHs are found in the environment in very low concentrations, consequently an effective extraction method, able to quantitatively separate the analytes from the matrix, is required. The extraction methods of PAHs can be divided into two groups: solvent-based and free-solvent extraction methods.

Solvent-based extraction methods

PAHs collected on filters or solid adsorbents are extracted with organic solvents (in the liquid phase) to be finally determined, preferably by Gas Chromatography/Mass Spectrometry (GC/MS). Microwave-assisted extraction (MAE), accelerated solvent extraction (ASE), ultrasonic-assisted extraction (UAE), and Soxhlet extraction (SE) are the most used solvent-based extraction techniques for PAHs. These conventional methods have been employed successfully to describe the levels, source apportionment, and phase distribution (gas or liquid) of PAHs from diverse environmental settings (rural, urban, industrial and indoor conditions).

Soxhlet extraction

Solvent extraction, which is commonly known as “solid–liquid extraction”, is the classic method for organic contaminant extraction, among others for PAHs, from solid matrices. It not only serves to remove and separate compounds of interest from insoluble high molecular weight fractions, but also from other compounds that could interfere with subsequent steps of the analytical process. This method works in a manner analogous to continuous liquid-liquid extraction, except the sample is solid instead of liquid. The sample is placed in a thimble-holder that is gradually filled with condensed fresh extractant (term used to refer to the solvent used for extraction) from a distillation flask (Figure 1.9). When the liquid reaches the overflow level, a siphon aspirates the solute from the thimble-holder and unloads it back into the distillation flask, thus carrying the extracted analytes into the bulk liquid. This operation is repeated until the extraction is complete.

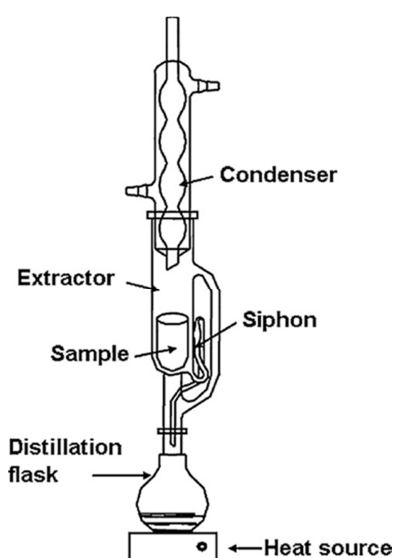


Figure 1.9. Schematic diagram of conventional Soxhlet extraction method (source: Luque de Castro and Priego-Capote, 2010).

Soxhlet extraction is widely used due to its advantages: it is a very simple methodology that requires basic equipment and training, the sample is repeatedly brought into contact with the fresh portions of the solvent and the temperature of the system remains relatively high. Thus, several authors have applied the method to diverse sample matrices, such as contaminated soil (Guerin, 1999; Hawthorne et al., 2000), waste water sludge (Ahmad et al., 2004), soils and sediments (Kronholm et al., 2004),

fly ash (Joa et al., 2009), filters (Rynö et al., 2006; Leung et al., 2014) and PUF (Cheng et al., 2013).

The most significant drawbacks of Soxhlet extraction compared to other conventional techniques for extraction are the time required for the extraction and the large amount of solvent waste. Over the last years, automated versions of Soxhlet extraction have been developed to overcome these drawbacks. The modifications in these methods, based on the direct contact between the sample and solvent at the solvents' boiling point, significantly reduce the extraction times (Blachnik, 2002).

Ultrasonic-assisted extraction (UAE).

The ultrasonic agitation, also known as sonication, is a technique that engages the acoustic energy of ultrasonic waves in fluid, causing rapid compression and rarefaction of fluid movement which results in the cavitation phenomenon, that is, the reoccurring formation and collapse of microbubbles (Lau et al., 2010). This technique (Figure 1.10) is a good option for extraction processes, because the cavitational effect provides efficient contact between solid and solvent due to an increase of pressure (which favours penetration and transport) and temperature (which improves solubility and diffusivity). Furthermore, the ultrasonic extraction consumes less solvent and is faster than the classic Soxhlet process.

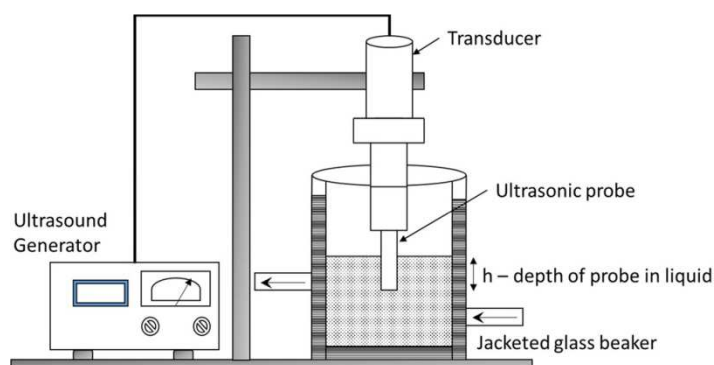


Figure 1.10. Schematic diagram of ultrasonic-assisted extraction (UAE) (source: Kadam et al., 2013).

In terms of efficiency, Sun et al. (1998) evaluated the efficiency of extraction for the 16 U.S. EPA PAHs in soil samples by ultrasonic and Soxhlet extraction. Their results showed higher extraction efficiencies for sonication extraction. Contrary to these

observations, other studies have indicated that sonication was less efficient than the Soxhlet with relatively low recoveries, particularly for lower molecular weight PAHs (44 -76%) (Stephens Jr. et al., 1994; Smith et al., 2006).

In the determination of 16 EPA PAHs in airborne particulates, several authors such as Park et al. (2002), Duan et al. (2005) and Wiriya et al. (2013) have applied the sonication as extraction method, obtaining good recoveries for these compounds (81 -90%, 70 - 124%, and 80 - 104%, respectively)

Accelerated solvent extraction (ASE)

The accelerated solvent extraction (ASE), also known as pressurized fluid extraction (PFE), is a technique where the solid sample is submitted to extraction at high pressure and temperature (Figure 1.11). Raising the temperature increases the diffusion rates, the solubility of the analytes and the mass transfer, and decreases the viscosity and surface tension of the solvents. These changes improve the contact of the analytes with the solvent and enhance the extraction, reducing the extraction time and solvent consumption (Ramos L. et al., 2002).

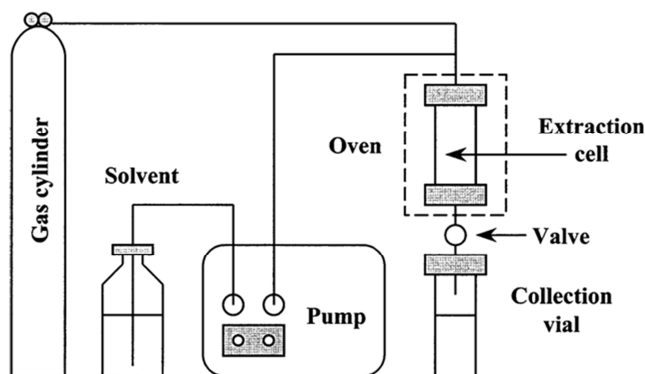


Figure 1.11. Schematic diagram of accelerated solvent extraction (ASE) (source: Björklund et al., 2000).

In comparison with more conventional extraction techniques such as Soxhlet extraction and sonication, the ASE has shown a higher efficacy (She and Shao, 2005; Sporning et al., 2005; García et al., 2008).

Balasubramanian and He (2010) validated (recoveries between 82 and 126%) and applied this extraction method in an urban area (Singapore city) to determine the 16

EPA PAHs in the air. Furthermore, Wu et al. (2006) measured the airborne particle-bound PAHs in urban and rural sites, applying the ASE as extraction technique with good results (recoveries between 66 and 104%).

Microwave-assisted extraction.

Microwave-assisted extraction (MAE) is basically ASE, but the heat source comes from microwave energy (Portet-Koltalo et al., 2007) (Figure 1.12). The main advantage of this method to ASE is the possibility of extracting large numbers of samples (more than 10) simultaneously (Karthikeyan et al., 2006).

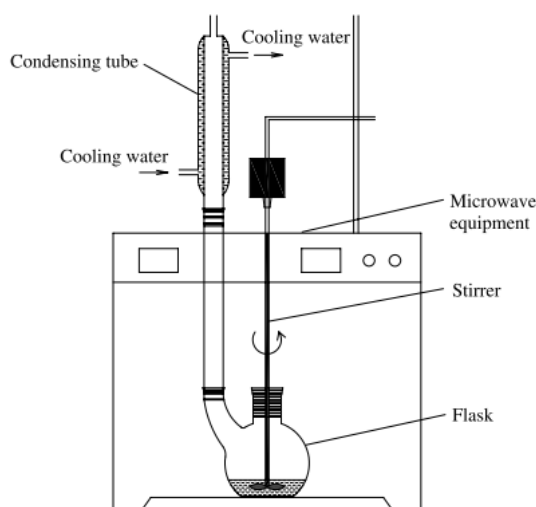


Figure 1.12. Schematic diagram of microwave-assisted extraction (MAE) (source: Zhang et al., 2011).

Like ASE, MAE allows rapid extraction of solutes from solid matrices, with higher extraction efficiencies than the classical Soxhlet extraction (Balasubramanian and He, 2010; Itoh et al., 2008).

Several studies have selected MAE as the method to extract PAHs from particulate matter (PM). Piñero-Iglesias et al. (2000) evaluated the applicability of MAE for extracting PAHs from airborne particles and validated the method using standard reference material (NIST SRM 1648 urban particulates). The results showed 70-103% recovery of PAHs for urban particulates. The MAE was also applied by Slezakova et al. (2013) in their study of the impact of traffic emissions on particulate-bound PAHs. In this case recovery values between 81 and 112% were obtained for most PAHs.

Table 1.6 summarizes some studies reported in the literature in the last years, in which the solvent-based extraction-GC/MS methods were used to determine PAHs.

Table 1.6. Some studies reported in the literature where the solvent-based extraction-GC/MS methods were used to determine PAHs in air.

Target PAHs	Environmental condition	Location	Period	Sampling period(h)/ Number of samples	Mean total PAHs Concentration (ng/m ³)	Reference
SE-GC/MS						
C (PM10 + gas)	Urban	Various Japanese cities	2011-2012	23 h / 44	7.3 (s) 8.3 (w)	Yagishita et al., 2015
B (PM10)	Urban	Various Brazilian cities	2010	24 h / -	1.51 (s) 2.08 (w)	Teixeira et al., 2013
C (PM10)	Urban	Zaragoza (Spain)	2010-2011	24 h / 84	1.78	Callén et al., 2013a
A (PM10 + gas)	Urban	Beijing (Chine)	2008	24 h / 40	104.1 (PM10) 118.7 (g)	Ma et al., 2011
UAE-GC/MS						
A (PM10)	Semi-urban	Dourados (Brazil)	2010	24 h / 22	1.52	Ré et al., 2015
A (PM10)	Urban	Chiang Mai (Thailand)	2010-2011	24 h / 94	3.12 - 25.87	Wiriya et al., 2013
C (PM10)	Urban	Mexico city (Mexico)	1999-2002	48 - 72 h / 310	0.69 - 0.93 (light PAHs) 4.64 - 6.21 (heavy PAHs)	Amador-Muñoz et al., 2013
A (PM10)	Urban and semi-urban	Changsha (Chine)	2008	8 h / 27	24.74 (s) 19.34 (a)	Yang et al., 2010

Notes: A = 16 EPA PAHs, B = some of 16 EPA PAHs, C = some of 16 EPA PAHs + some extra, D = 16 EPA PAHs+ some extra, s =summer, a = autumn, w = winter, r = rural, u = urban, g = gas, SE = Soxhlet extraction, UAE = Ultrasonic-assisted extraction, ASE = accelerated solvent extraction, MAE = Microwave-assisted extraction

Table 1.6. (continued) Some studies reported in the literature where the solvent-based extraction-GC/MS methods were used to determine PAHs in air.

Target PAHs	Environmental condition	Location	Period	Sampling period(h)/ Number of samples	Mean PAHs Concentration (ng/m ³)	Reference
ASE- GC/MS						
A (PM10)	Urban	Chiang Mai (Thailand)	2011	24 h / 72	3.4	Walgraeve et al., 2015
D (PM10+ gas)	Urban and Industrial	Alexandria (Egypt)	2010-2011	48 – 72 h / 82 (PM10) 68 (g)	330 - 1770 (s) 170 - 1290 (w)	Khairy et al., 2013
B (PM from 0.03 to 10)	Urban	Rome (Italy)	2007-2008	15 days / 12	32.39 (PM10)	Di Filippo et al., 2010
A (PM10 + gas)	Urban	Singapore	2006	24 h / -	13.62 - 52.26	Balasubramanian et al., 2010
MAE-GC/MS						
C (PM10+ PM2.5)	Urban	Porto (Portugal)	2007 - 2008	24 h / 54	0.24 – 3.21 (PM10) 1.56 – 21.3 (PM2.5)	Slezakova et al., 2013
B (PM10)	Urban and rural	Pamplona (Spain)	2009	24 h / 58 (u) 60 (r)	1.20 (u) 0.63 (r)	Aldabe et al., 2012

Notes: A = 16 EPA PAHs, B = some of 16 EPA PAHs, C= some of 16 PAHs EPA PAHs + some extra, D = 16 EPA PAHs+ some extra, s =summer, a = autumn, w = winter, r = rural, u = urban, g = gas, SE = Soxhlet extraction, UAE = Ultrasonic-assisted extraction, ASE = accelerated solvent extraction, MAE = Microwave-assisted extraction

Solvent-free extraction methods

The use of toxic organic solvents in the solvent-based extraction methods causes added difficulties with sample handling and generates large amounts of solvent waste, which is costly and can generate additional environmental problems. To overcome such limitations, in recent years, alternative analytical procedures for PAHs based on the use of solvent-free extraction methods have been studied.

Thermal desorption involves heating sample materials or sorbents in a flow of inert carrier gas, so that retained organic volatiles and semivolatiles are released and transferred or injected into the analytical system (e.g. into the carrier gas stream of the GC column). The key method parameters for this technique include temperature, carrier gas flow rate, desorption time, and sorbent (stationary phase selection).

The power and potential of TD allow configuring the technique in multiple stages so that analytes are repeatedly desorbed into increasingly small volumes of gas, thus concentrating the compounds of interest and enhancing detection limits. Another benefit of TD is that it is often possible to quantitatively retain target compounds during one or more of the trapping stages, while unwanted, e.g. water and / or permanent gases, are selectively purged to vent. This avoids the entrance of unwanted compounds into the analytical system that could generate interferences during the analysis and / or damage to the equipment.

The evolution of TD Technology

Due to the limitations of conventional GC sample preparation and extraction techniques in the mid-1970s, the experimental packing of conventional GC injector liners with sorbent material was started. These primitive adaptations of conventional GC injectors were not exempt from numerous limitations (air ingress, volatile losses, variability, contamination from the outer surfaces of the liner, single stage, etc.). In the late 1970s, the US-EPA developed and integrated the purge-and-trap technology in thermal desorption and applied it in the analysis of VOCs in drinking water.

The first early commercial configurations of TD technology were based around desorption of a single tube or badge. These early desorbers offered only single-stage desorption without any current functions, such as leak testing or prepurging of air from the tube (Coker, 1979).

The most important early technical breakthroughs came from Working Group 5 (WG5) of the UK Health and Safety Executive (HSE) in the late 1970s. They saw the advantages of TD and in subsequent years improved the technology by developing and integrating two-stage desorption and predesorption checks (stringent leak testing and prepurging of air to vent).

As regards two-stage desorption, WG5 realized that the process with single-stage desorption was limited, as tens of millilitres of gas are required for complete extraction of a standard tube. Volumes like these are not compatible with capillary chromatography and compromise analytical resolution even with packed columns. Initial attempts of two-stage desorption utilized capillary cryofocusing positioned between the sample tube and analytical system (Figure 1.13). In this case, analytes desorbed from the primary sample tube were concentrated in a short length of capillary or narrow-bore tubing cooled with liquid cryogen. Heat was then applied to release the compounds into the analytical system in a small volume of carrier gas.

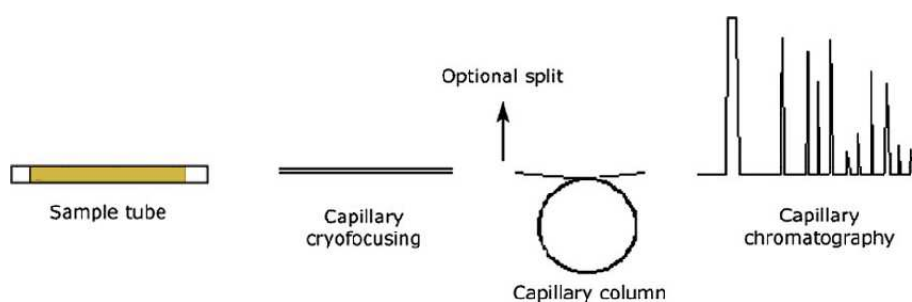


Figure 1.13. Two-stage thermal desorption incorporating capillary cryofocusing (source: Woolfenden, 2012).

Nevertheless, the capillary cryofocusing showed several limitations such as ice blockage, incomplete retention of very volatile compounds (Manura, 1999), loss of high-boilers due to aerosol formation (Kolb, 1999), and high running costs (high N₂ consumption) (Holdren and Smith, 1991). Furthermore, the direct connection between capillary cryofocusing devices and the GC column complicated the implementation of the predesorption checks specified by WG5.

In 1981 the PerkinElmer ATD 50 unit was introduced. This equipment, designed by Dr Peter Higham, incorporated a small, Peltier-(electrically) cooled, sorbent-packed focusing trap and a rotary valve (Figure 1.14). The combination of sorbent packing and modest focusing temperatures (minimum: -30°C) was a genuine breakthrough. This

change offered quantitative retention of a wide range of compounds including very volatile species (Coker et al., 1989), without the cost and inconvenience of liquid cryogen. The trap design avoiding ice plug formation and allowed for rapid desorption with minimal split and good sensitivity. Moreover, the inclusion of a rotary valve isolated the sample tube from the GC, allowing both “stop-flow” leak testing and prepurging of air to vent prior to desorption of every tube.

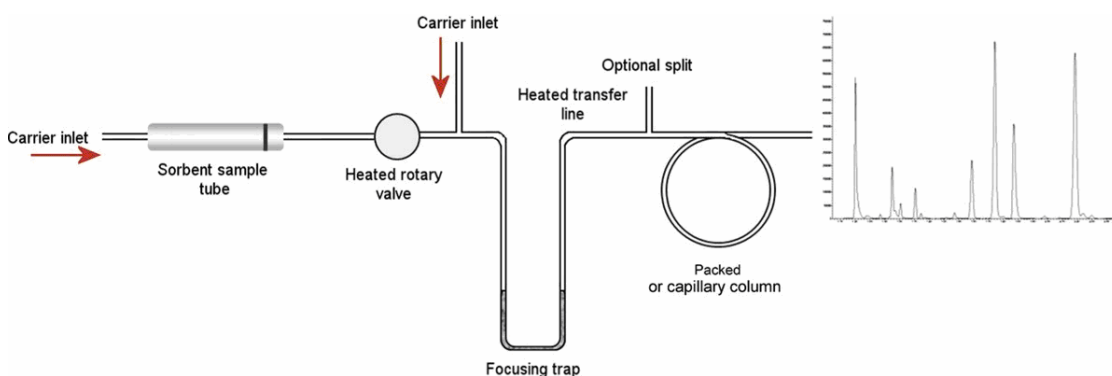


Figure 1.14. Two-stage thermal desorption incorporating sorbent focusing trap and heated valve (source: Woolfenden, 2012).

Although double splitting was not in the original WG5 specifications, this enhancement was incorporated into the ATD 50 in 1985. Now both desorption stages could be carried out either in split or splitless modes. This new incorporation brought some significant benefits in terms of technique versatility, allowing the successful analysis of a wide range of analyte concentrations (from trace levels to high levels).

In addition to the versatility, double splitting also enhanced the two-stage desorption process itself. The implementation of a split during primary desorption (known as inlet split) allows the application of a high carrier gas flow through the hot sample tube during desorption. At the same time it maintains a low flow through the trap, aiding analyte retention. The second split (known as outlet split) applied during trap desorption guarantees the release of the retained analytes, increasing the flow through the trap.

In recent years TD technology has been considerably refined. Nowadays inert materials are used in the construction of the trap and rotary valve. The traps are also configured in “blackflush mode” (the analytes enter and leave the trap from the same end). This mode allows packing the trap with a series of sorbents of increasing

strength, extending the analyte volatility range (Woolfenden, 2010). Finally, the one-shot limitation of traditional TD technology has been overcome by the implementation of the re-collection of split flow on several different commercial systems. This modification allows repeating the analysis, also with the lowest concentration (ppt level) samples.

Thermal desorption vs. solvent extraction

The main advantages of TD versus solvent-based extraction are:

- Enhanced sensitivity. The TD technique allows transferring 100% of retained analytes to the analytical system, whereas solvent-based extraction only transfers the analytes from microliter injections of millilitre extracts. This means that TD offers enhancement in sensitivity versus equivalent solvent-based extraction procedures.
- Enhanced desorption efficiency. TD is a dynamic process (the gas is continually purging compounds from the sorbent or sample matrix as soon as they are released into the vapour phase). In contrast, solvent-based extraction is a static process where there is analyte partitioning between the solvent, sorbent and vapour phases, limiting desorption efficiency. Due to this, the TD method shows higher desorption efficiency (> 95%) than solvent-based extraction (around 75%).
- Reliable extraction efficiency. Static analyte partitioning in the solvent-based methods is subject to increased variability of analyte recovery depending on the nature of the target compounds and the presence of interferences. This uncertainty could generate problems in the measurements of compounds when the analyst is not aware of field conditions (e.g. high water content); moreover, poor recovery may lead to significant under-reporting.
- Enhanced automation. TD requires less manual sample manipulation than solvent-based extraction; hence this technique can be easily automated.
- Reduced analytical interference. The use of solvents has a tendency to generate interferences in the analysis, including the masking of target peaks, signal quenching and baseline disturbances. These problems make integration difficult and prone to error. TD is inherently free of solvent interference.
- Selective elimination of interferences. TD is a more selective technique, facilitating selective purging of sample interferences such as water prior to

analysis. In contrast, solvent-based methods require significant volatility between target compounds and the interferences to show a good selectivity.

- Reduced exposure risk. The toxicity of common solvent extraction presents a significant potential health and safety hazard. The systems with TD, where wet chemistry procedures are only confined to preparation of liquid standards, do not require additional extraction equipment (e.g. fume hoods).
- Reusable samplers and lower cost per analysis. In general, the sampling costs associated with the TD technique are lower than for solvent-based extractions. The possibility to reuse the sorbent sampler (e.g. a limit of hundred uses of packed TD tubes), the option of automatic sample cleaning by the TD process, the minimal use of solvents, and the low amount of generated residuals are main reasons for this difference.

1.7.3 Analytical methods for PAHs

Determination of PAHs in environmental samples can be difficult due to the physicochemical properties of these compounds (a multi-component mixture with a wide range of volatilities, solubilities and molecular weights). Chromatographic techniques can resolve this problem, and they are the best option to separate, identify and measure the individual PAHs. High-performance liquid and/or gas chromatography (HPLC and CG, respectively) are the main techniques used in the standard methods reported by several international agencies for determination of PAHs in air (Porter et al., 2006). Table 1.7 summarizes these standard methods.

Table 1.7. Standard methods for the determination of PAHs in air.

Method	Title	Analytical technique	Reference
US-EPA TO-13A	Determination of PAHs in ambient air using GC-MS	GC-MS	US-EPA, 1999b
NIOSH 5506	PAHs by HPLC	HPLC-FLD/UV	NIOSH, 1998
NIOSH 5515	PAHs GC	GC-FID	NIOSH, 1994
UNE-ISO 16362:2005	Ambient air. Determination of particle-phase PAHs by HPLC	HPLC-FLD or HPLC-DAD	ISO, 2005
UNE-EN 15549:2008	Standard method for the measurement of the concentration of BaP in ambient air	HPLC-FLD or GC-MS	ISO, 2008
ISO 11338:2003	Stationary source emissions. Determination of gas and particle-phase PAHs	HPLC or GC-MS	ISO, 2003
ISO 12884:2000	Ambient air. Determination of total (gas and particle-phase) PAHs. Collection on sorbent-backed filters with GC-MS analyses.	GC-MS	ISO, 2000
ASTM D6209-98:2004	Standard Test Method for Determination of Gaseous and Particulate PAHs in Ambient Air (Collection on Sorbent-Backed Filters with GC-MS Analysis)	GC-MS	ASTM, 2004

DAD: diode array detector; GC-MS: gas chromatography-mass spectrometry; HPLC: high-performance liquid chromatography; FID: flame ionization detector; FLD: fluorescence detection and UV: ultraviolet detection.

Both techniques, HPLC and GC, offer unique information or have unique aspects. For example, HPLC can analyse the compounds without considering volatility and molecular weight, moreover, it shows good selectivity and high sensitivity (Liu et al., 2007). Nevertheless, LC columns show a low peak capacity (number of resolvable peaks), limiting the analysis to only a few dozen compounds. In contrast, the use of capillary columns in GC shows a greater selectivity, resolution and sensitivity to resolve hundreds of compounds in complex samples (Poster et al., 2006). Therefore, GC is usually the chromatographic technique used in the standard methods to determine PAHs in air.

Following GC separation, flame ionization detection (FID) and mass spectrometry (MS) are the most commonly used techniques for the detection of PAHs. Although GC-FID has been successfully used to measure PAHs in air (Lung et al., 2004b; Sharma et al., 2007), compared with GC/MS it is less accurate, because the number of interferences from co-eluting compounds is often higher (Poster et al., 2006). Besides the accuracy, the ease of operation, the low costs and the use of quadrupole mass spectrometer detectors have made GC/MS the most used method for the determination of PAHs.

1.7.4 Application of TD-GC/MS.

The advantages of TD extraction that were discussed in previous sections made this technique a good option to quantify PAHs in ambient air, where these compounds are generally present in trace levels. During the past ten years, several authors have applied the TD-GC/MS method to determine PAHs in different environmental conditions (Table 1.8). Few of the studies achieved temporal resolution measurements higher than 24h. This time resolution seems insufficient to comprehend the variability, fate and behaviour of PAHs in the atmosphere (Ringuet et al., 2012), as their concentrations may be subject to diurnal variations due to changes over the course of the day in sources, meteorological factors (Williams, 1996) and atmospheric reactivity (Keyte et al., 2013).

Table 1.8. Studies reported in the literature where the TD-GC/MS method was used to determine PAHs in air (last ten years).

Target PAHs	Environmental condition	Location	Period	Sampling period(h)/ Number of samples	Mean total PAHs Concentration (ng/m ³)	Reference
C (TSPM)	Urban	Srinagar (India)	2008 - 2009	24 h / -	4 - 768	Huma et al., 2016
A (PM10 + gas)	Urban	Seoul (Korea)	2014	12 h / 5	78.8	Kim and Kim, 2015
A (PM10)	Urban	Beijing, Ningbo, Chongqing (China)	--	- / -	0 - 0.81	Hu et al., 2014
C (PM2.5)	Rural	Ispra (Italy)	2010	24 h / 12	For BaP : 1.40·10 ⁻⁴ - 1.54·10 ⁻³	Grandesso and Pérez Ballesta, 2014
A (gas)	Urban	Antwerp (Belgium)	2012	24 h / 26	For BaP : 0.32	Lazarov et al., 2013
C (PM2.5)	Urban	Beijing (China)	2006	24 h / 38	125	Li et al., 2013
D (PM10)	Urban	New Delhi (India)	2006 - 2009	24 h / -	287 - 536	Yadav et al., 2013
B (PM10)	Indoor	France	2010 - 2011	- / 6	For BaP : 36 - 228	Mercier et al., 2012
C (PM2.5)	Urban	Hong Kong (China)	2006 and 2010	24 h / 51 (2006); 40 (2010)	2.94 (2006) 4.36 (2010)	Yu et al., 2011
C (PM2.5)	Urban	Augsburg (Germany)	2007 - 2008	24 h / 66	1.34(s) 11 (w)	Pietrogrande et al., 2011
B (PM2.5)	Urban	Golden (Canada)	2005 - 2007	24 h / 115	0.02 - 1.83	Ding et al., 2009
B (PM2.5 and PM10)	Urban	Elche (Spain)	2007	24 h / 3	For BaP : 0.17 (PM2.5) 0.18 (PM10)	Gil-Molto et al., 2009
C (PM10)	Rural	Ispra (Italy)	2007 - 2008	3 h / 56	For BaP : 3·10 ⁻² - 2.36	Van Drooge et al., 2009
D (gas)	Urban	Gent (Belgium)	2005 - 2006	24 h / 52	170.44	Wauters et al., 2008
A (TSPM)	Roadside	Hong Kong (China)	2001	12 - 24 h / 16	5·10 ⁻³ - 0.14	Ho et al., 2004

Notes: A = 16 EPA PAHs, B = some of 16 EPA PAHs, C = some of 16 PAHs EPA PAHs + some extra, D = 16 EPA PAHs+ some extra, s =summer, w = winter,

TSPM = total suspended particulate matter

1.8 Source apportionment of PAHs.

1.8.1 Diagnostic ratios.

Specific PAHs have been suggested as markers for certain processes of PAH release, for which PAH concentration profiles and ratios could be used as diagnostic tools to identify PAH sources (Tobiszewski and Namiesnik, 2012 ; Galarneau, 2008). Table 1.9 lists the typical diagnostic ratios taken from literature with their reported values for particular processes.

Table 1.9. Diagnostic PAH ratios for source identification.

Ratios	Value range	Source	Reference
Ant/(Ant+Phe)	< 0.1	Petrogenic	Yunker et al., 2002
	> 0.1	Pyrogenic	
Ft/(Ft+Pyr)	< 0.4	Petrogenic	Yunker et al., 2002; Varea et al., 2011
	0.4 - 0.5	Petroleum combustion (mixed sources)	
	> 0.5	Biomass and coal combustion	
BaA/(BaA+Chry)	< 0.2	Petrogenic	Yunker et al., 2002; Varea et al., 2011
	0.2 - 0.35	Petroleum combustion (mixed sources)	
	> 0.35	Biomass and coal combustion	
IP/(IP+BghiP)	< 0.2	Petrogenic	Yunker et al., 2002; Varea et al., 2011
	0.2 - 0.5	Petroleum combustion (mixed sources)	
	> 0.5	Biomass and coal combustion	
BaA/BaP	0.5	Gasoline exhaust	Callén et al., 2011
	1	Diesel exhaust	
	1	Wood combustion	
BbFt/BkFt	> 0.5	Diesel exhaust	Oliveira et al., 2011
BaP/BghiP	0.3-0.4	Gasoline exhaust	Callén et al., 2011, Sisovic et al., 2012
	0.46-0.81	Diesel exhaust	
BghiP/IP	3.5-3.8	Gasoline exhaust	Slezakova et al., 2010
	1.1-1.2	Diesel exhaust	

The information provided for diagnostic ratios should be processed with caution due to the difficulty of discriminating PAH sources, and the possible processes that could influence PAH concentrations (photolysis, photo-oxidation or deposition) from their sources to the receptor site (Galarneau, 2008).

1.8.2 Receptor models.

The application of receptor modelling is another technique commonly used in the field of atmospheric sciences to infer the source-types and estimate their contributions to the measured site concentrations. Receptor modelling is based on the mass balance equation (Eq. 1.3):

$$x_{ij} = \sum_{k=1}^p g_{ik} \cdot f_{kj} + e_{ij} \quad (1.3)$$

where x_{ij} is the concentration of species j measured on sample i ; p is the number of factors contributing to the samples; g_{ik} is the relative contribution of factor k to sample i ; f_{kj} is the concentration of species j in factor profile k ; and e_{ij} is error of the model for the species j measured on sample i .

This equation can be written in matrix form:

$$X = G \cdot F + E \quad (1.4)$$

where X is an m by n data matrix with measurements and n number of species; G is an m by p source contribution matrix with p sources; and F is a p by n source profile matrix; and E is an m by n matrix of residuals, which contains the variance not explained by the model.

The main assumption for the mass balance in Eq.1.3 is that the composition of particulate matter (PM) remains constant and chemical species do not react with each other. The source apportionment is accomplished by solving the mass balance equations expressing the measured ambient elemental concentrations as the sum of products between the source contributions and the elemental abundances in the source emissions, e.g. the source profiles. There are different receptor models that differ in the mathematical approaches used to solve the mass balance equations, as well as in the different degrees of knowledge about source profiles required for source apportionment analysis. Among the receptor models, the factor analysis methods (e.g. principal component analysis or PCA, positive matrix factorization or PMF, UNMIX) are commonly used tools, because software to perform this type of analysis is widely available and detailed prior knowledge of the sources and source profiles is not required.

UNMIX model

The UNMIX model solves the mass balance (Eq.1.3) by using a factor analysis followed by an “edge” detection technique to reduce the dimensionality of the dataset without centring the original data (Henry, 2003). Edges are hyperplanes determined by points in which a source profile is absent or has a very low relative contribution. These edges are used as constraints to define a region of the real solution where source contributions are greater than or equal to zero. Once the edges are found, the appropriate number of sources is estimated by the NUMFACT algorithm, which also reports the signal-to-noise (S/N) ratio associated with the factors in the data matrix. The number of quantifiable factors corresponds to the number of principal components (PCs) with a S/N ratio greater than two (Henry, 2003).

Although UNMIX is a useful tool to apportion the potential sources and their contributions, the model does not always find a mathematical solution to the mass balance and to the characteristic of UNMIX that is able to resolve the most intense sources, while the weakest sources often show poor agreement between the expected and estimated source contributions (Henry, 2003).

UNMIX has been successfully applied to the apportionment of PAHs in urban area by numerous authors (Larsen and Baker, 2003; Callén et al., 2013b; Khairy et al., 2013).

PMF model.

The PMF model has been widely used for source apportionment of ambient particulate matter (PM), where the goal is to identify the mixture of sources that contributes to PM samples (Paatero and Tapper, 1994; Malinowski, 2002). This receptor model incorporates the variable uncertainties associated with measurements of environmental samples and avoids obtaining negative results (forces the values in the solution profiles and contributions to be nonnegative). Due to this, PMF provides more realistic results than solutions obtained by other methods, e.g. by principal component analysis (PCA) (Reff et al., 2007).

The mathematical approach of this model for resolving the mass balance equation (Eq.1.3) is based on finding a solution that minimizes an object function Q (Eq. 1.5). This function is determined based on the uncertainties associated with individual

measured data, subject to nonnegative constraints (Paatero et al., 2014). Q is defined as:

$$Q = \sum_{i=1}^n \sum_{j=1}^m \left(\frac{x_{ij} - \sum_{k=1}^p g_{ik} \times f_{kj}}{u_{ij}} \right)^2 \quad (1.5)$$

where u_{ij} is the uncertainty of the j th species concentration in sample i , n is the number of samples, and m is the number of species.

Two programs have been developed to implement different algorithms for solving Eq. 1.3, the PMF2 (Paatero, 1997) and the Multilinear Engine (ME-2) (Paatero, 1999). ME-2 is a more flexible program than PMF2, and permits the incorporation of any *a priori* information such as chemical properties or linear constraints into the model as a target to be fit to some specification.

In order to provide a widely applicable PMF with a user-friendly and graphic user interface (GUI)-based program, the US Environmental Protection Agency (EPA) developed a version of PMF in 2005 (Hopke et al., 2006; Eberly, 2005).

In its last version, EPA PMF 5.0 (Norris et al., 2014), the user interface feeds the data and user specifications to the ME-2 program, which then performs the interactions. The input data include the species concentrations and the uncertainties associated with each measurement. This version allows the user to automatically replace missing data and their respective uncertainty. This is particularly important when a limited number of samples is available. To obtain physically realistic solutions, the user can add an additional constraint to the non-negativity one: the sum of the predicted elemental mass contributions for each source must be less than or equal to the total measured mass for each element. The main outputs consist of a source profile matrix (F) and source contribution (G). Secondary output includes various model diagnostics to assist in the interpretation of the results. The uncertainty in the solution is estimated using a bootstrapping technique.

PMF has been widely applied for source apportionment of PAHs by numerous authors in different areas, e.g. urban area (Ma et al., 2010; Gupta et al., 2011; Callén et al.,

2013a), industrial area (Park et al., 2011; Aydin et al., 2014), and rural area (Vestenius et al., 2011).

Chapter 2:

Approach and objectives

2.1 Approach

Air pollution is recognized as one of the leading contributors to the global environmental burden of disease. There is extensive scientific evidence of adverse health effects even in countries with relatively low concentrations of air pollution. Among all the air pollutants, PAHs (persistent organic pollutants possessing carcinogenic, mutagenic, and immunotoxic properties) have become an issue of increasing concern in recent decades. Due to their features and high atmospheric persistence, these components have been listed in international protocols for emission reductions (UNECE, 1979).

Despite their environmental and health impact, the environmental data available for PAHs are scarce in comparison to other pollutants. The low PAH concentrations, the presence of other interfering organic compounds in ambient air, and the complex sampling and analytical procedure are the main factors that can hamper the monitoring of these pollutants. In the atmosphere, PAHs are distributed between gas and particle phases. This partitioning is a key factor to determine the transport processes and to design ambient air sampling, monitoring and controlling systems. The analysis of the particle phase in general has always aroused greater toxicological interest, because the highest contributors in the total carcinogenicity of the PAHs are the 5-6 ring PAHs (species mainly associated with airborne particles). Therefore, studies focused on the analysis of particle-bound PAHs are the most common in the bibliography.

In PAH monitoring, high temporal sampling resolutions enable a better knowledge of the variability, fate and behaviour of PAHs in the atmosphere (Ringuet et al., 2012), as the PAH composition of aerosols can vary according to the diurnal changes in source, meteorological conditions and atmospheric reactivity (Alam et al., 2014). Hence, short time PAH monitoring studies (< 24h) are more conducive. At present, some studies have investigated the diurnal variation of particle-bound PAHs, but most studies have been conducted at time resolutions of 12h (Ringuet et al., 2012; Liu et al., 2013; Wu et al., 2014), while there are still few studies performed at higher temporal sampling resolutions in urban areas (Guzman-Torres et al., 2009; Morville et al., 2011; Delhomme et al., 2012). This is most likely due to the limits of detection of the currently used analytical procedures, which limit the temporal resolution of PAHs in ambient air.

The conventional methods for the determination of PAHs in air demand a large and laborious sample preparation in order to increase the sensitivity and selectivity of the PAH analysis. These methods usually include stages such as extraction by organic solvents, drying, concentration and purification of the sample. These stages significantly prolong the analysis time and implicate a high manipulation of the sample, generating PAH losses during the procedure. Furthermore, the use of organic solvents generates large amounts of solvent waste, which is costly and causes environmental problems. Therefore, in recent years, alternative methods have been developed to overcome these limitations.

Thermal desorption (TD) is a solvent-free extraction method where the analytes are extracted from the sample matrix by heat and a flow of inert gas. This method is becoming more popular and readily available, but has not been thoroughly tested. The features of this technique (the absence of sample manipulation, high desorption efficiency, good sensitivity and reproducibility, elimination of interferences, and lower extraction times and costs) provide a faster, simpler, and more sensitive and accurate method to determine trace level PAHs in ambient air.

The general objective of this Ph.D. thesis was to develop and validate an analytical method based on thermal desorption-gas chromatography-mass spectrometry (TD-GC-MS) for the determination of PAHs (gas + particle) in ambient air. To achieve this objective the following partial objectives need to be fulfilled:

- Setting up of TD-GC/MS instrumental parameters.
- Validation of the method for the determination of PAHs in aerosol samples by certified urban dust, and comparison with the conventional method based on solvent extraction and GC/MS analysis.
- Estimation of the associated uncertainty of the PAH analysis by TD-GC/MS and comparison with the conventional method (solvent-based extraction and GC/MS analysis).
- Application of TD-GC/MS method to characterize the particle-bound PAHs obtained by high temporal resolution samples in an urban area: study of PAH concentrations and trends, source identification and apportionment, and estimation of the carcinogenic potential.

Chapter 3:

Experimental

3.1 Measuring methodology

The determination of PAHs has been performed using an automatic thermal desorption unit (PerkinElmer Turbomatrix 150 ATD) coupled by a fused-silica capillary transfer line (0.32 mm i.d.) to GC/MS (PerkinElmer Clarus 500). Figure 3.1 shows the main equipment components in the determination of these compounds.

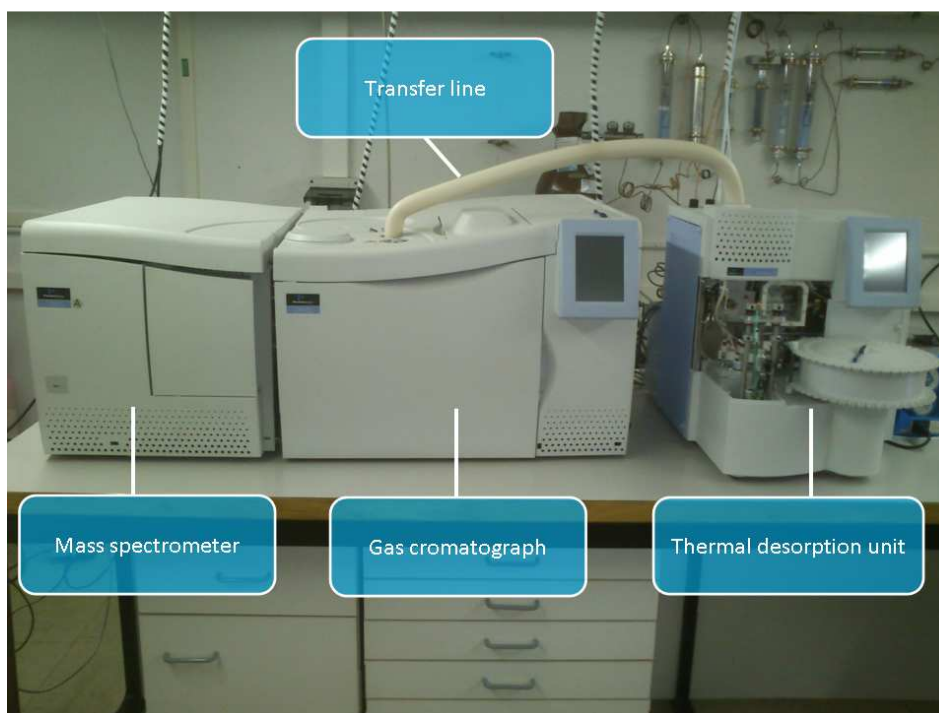


Figure 3.1. TD-GC/MS system

3.1.1 Sampling methods

In this study, the TD-GC/MS method has been applied only for the determination of particle-bound PAHs in PM₁₀, therefore, only the sampling methodology associated with this phase is described in this section.

Particulate phase

As previously mentioned (section 1.6), glass, quartz and Teflon filters have commonly been used in the sampling of airborne particle bounded PAHs. In this study, the sampling and subsequent analysis of particulate PAHs were based on the TO-13A method (US-EPA, 1999b), hence, quartz filters were used to collect the particulate

phase. These filters show a good thermal stability and are usually used in solvent-free techniques such as thermal desorption (Pandey et. al., 2011).

A high-volume sampler (Digitel DHA-80) with a sampling flow of $30\text{m}^3 \text{h}^{-1}$ and time periods of 8 hours were used to collect particle PAHs in 150 mm quartz fibre filters (Whatman International Ltd). DHA-80 stores 15 filters stretched in filter holders. The filters are changed automatically to the flow position at the pre-set time. The air is sampled via a sampling probe, using a sampling tube, vertically from the top to the bottom through the filter placed in the flow chamber. After the filter, the transported air quantity is measured using a flow meter with a floater. Its double photo-sensor optically senses the floater position. In connection with the control electronics the capacity of the blower is adapted to the rpm control, so that the air quantity maintains the set-point value.

Air pressure and temperature are measured upstream the flow meter and continuously averaged by the controller. A real-time protocol states sampling volumes yielding from the sampling time and controlled volume flow as core information.

Digitel DHA-80 has integrated temperature control in the filter storage section, in this way the used filters can be stored at low temperatures (in this study at 4°C) after the sampling. The image and block diagram of the high-volume sampler are shown in Figure 3.2.

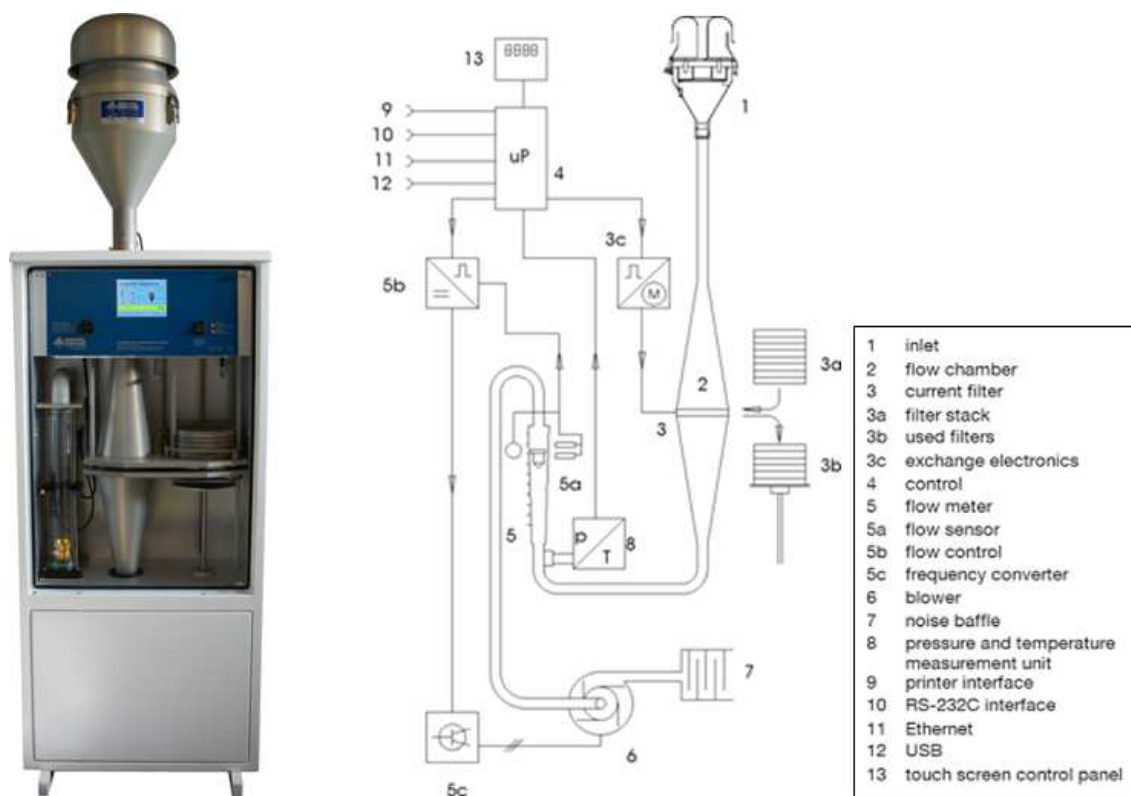


Figure 3.2. High-volume sampler Digital DHA-80 (left) and its block diagram (right) (source: Digital Elektronik AG, 2010).

3.1.2 Sample preparation

Packed sampling tubes with filter or adsorbent were analysed by TD-GC/MS. The material of these tubes can be stainless steel, glass or a mixture of both. In this study, stainless steel tubes were selected (5 mm outer diameter x 90 mm in length) because they are more resistant and protect the PAHs from photodegradation. The internal packing of these tubes showed different configurations according to the analysed PAH phase.

In the particulate phase, 8 discs of 1 cm² each were cut from each original sampled filter with a steel round punch. These portions, suitably folded, were introduced in the sampling tubes. In order to retain the filters in the tubes, a gauze disk was placed at one end and a retaining spring at the other (Figure 3.3).

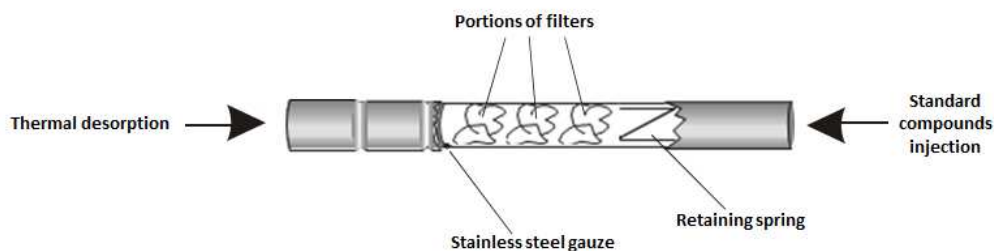


Figure 3.3. Configuration of the sampling tube in the determination of the particulate phase (adapted from PerkinElmer, 2007).

For the gas phase, the tubes were packed with an adsorbent bed. The adsorbents used in this study were Tenax TA 35/60 mesh and Tenax GR 35/60 mesh (both Chromatography Research Supplies Inc.). These adsorbents, porous polymer resins based on 2,6-diphenyl-phenylene oxide, are strongly recommended to collect and determine PAHs because their high thermal stability, hydrophobic character and low inherent artefacts. For this reason, they are the best option for analysis by solvent-free techniques (such as thermal desorption). Both adsorbents show similar properties, however, the composition of Tenax GR contains graphitized carbon (23%). This means that this adsorbent shows lower adsorption of water vapours and higher packing density than Tenax TA. In Chapter 4, the optimized desorption conditions with both adsorbents is studied.

The sampling tubes to collect the gas phase (Figure 3.4) were packed with the next configuration:

- Initially, a retaining gauze disk was inserted into the sampling tube with a gauze-loading accessory (Figure 3.5).
- Then 1 cm³ of adsorbent (250 mg for Tenax TA or 400 mg for Tenax GR) was packed into the tube.
- Finally, a small plug of glass wool, a retaining gauze disk and a spring were inserted in order to hold the adsorbent bed in the correct position.

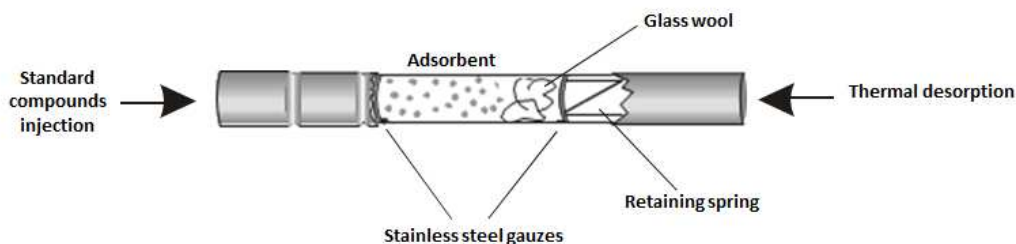


Figure 3.4. Configuration of the sampling tube in the determination of the gas phase (adapted from PerkinElmer, 2007).

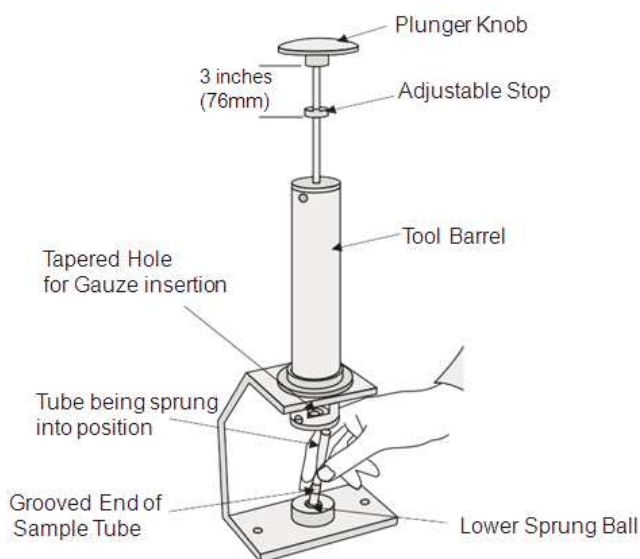


Figure 3.5. The Gauze-Loading Ring (source: PerkinElmer, 2007).

Regarding the mesh size of the adsorbent, this cannot be higher than 60/80 mesh in order to avoid losses during tube desorption, which could cause blockages in the sampling system. For this reason, Tenax TA and GR 35/60 mesh were used in the study.

During the calibration stage, in order to introduce the gas phase PAHs into the sampling tube, an Adsorbent Tube Injector System (Supelco ATIS) was used (Figure 3.6). The system employs the technique of flash vapourization to vapourize the standard compounds into a continuous flow of an inert gas (in this study, a helium flow of 100 mL min^{-1} at 100°C), which carries the compounds to the adsorbent tube. After

approximately 5 minutes, the tube is removed from the ATIS and analysed using the appropriate technique.

In order to guarantee the collection of PAHs into the adsorbent it was necessary to determine the breakthrough volume (BV) and the safe sampling volume (SSV). The BV is defined as volume of air containing a constant concentration of analyte which may be passed through a sorbent tube before a detectable level (typically 5%) of the analyte concentration elutes from the sampling tube (US-EPA, 1999a). Although this parameter can be estimate by tests, this study took as reference the BV for different compounds in Tenax GR and TA published on the Scientific Instrument Services website (SIS, 2016). The values of BV for naphthalene in Tenax GR and TA at 100°C (temperature of the ATIS during the preparation) were 1.8 and 40 L g⁻¹, respectively. The SSV sets a volume limit to avoid the purge of the analyte during the sampling. US-EPA method TO-17 suggested that the SSV should not be greater than two-thirds of BV. Thus, in this study, during the introduction of PAHs in the sampling tubes by ATIS, the naphthalene showed SSV of 0.48 L for Tenax GR (considering 250 mg of adsorbent) and 6.7 L for TA (considering 400 mg of adsorbent), guaranteeing the collection of PAHs on the adsorbents. Although for Tenax GR, the SSV of naphthalene was lower than the sampled helium volume (0.5 L), the purge losses of this compound were considered negligible (< 5% of the analyte concentration).



Figure 3.6. The Adsorbent Tube Injector System (ATIS) (source: Sigma-Aldrich, 2016).

3.1.3 Analysis method

Both phases of PAHs (gas and particulate) were determined by a TD-GC/MS system. Initially the samples underwent a thermal desorption process in order to concentrate PAHs. This thermal desorption was performed in two stages:

- First stage (Tube desorption). The sampling tube is placed in desorption position, sealed and leak tested. When the sampling tube has passed the leak test, this is purged with carrier gas in order to reduce the risk of adsorbent oxidation during desorption. Upon finishing the purge, the tube oven is brought into contact with the sampling tube and the desorb time begins. Analytes, released from the tube, are transferred to the cold trap. After desorption, the sampling tube is allowed to cool for 2 minutes (Figure 3.7).

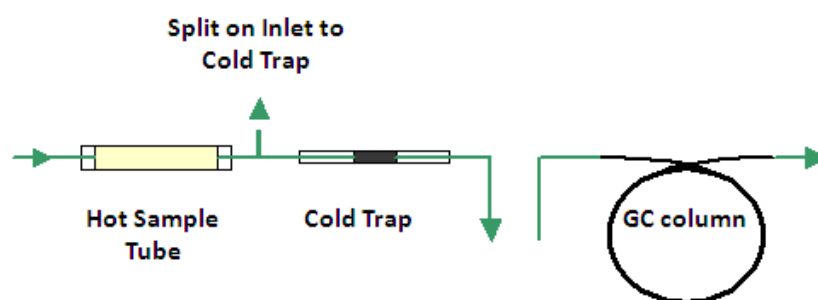


Figure 3.7. First desorption stage (source: Agilent Technologies, 2016).

- Second stage (Trap desorption). After completing the primary desorption, the equipment diverts the carrier gas flow through the cold trap. This is quickly heated to its highest temperature. The trapped volatiles are released and swept through the heated transfer line to the GC column (Figure 3.8).

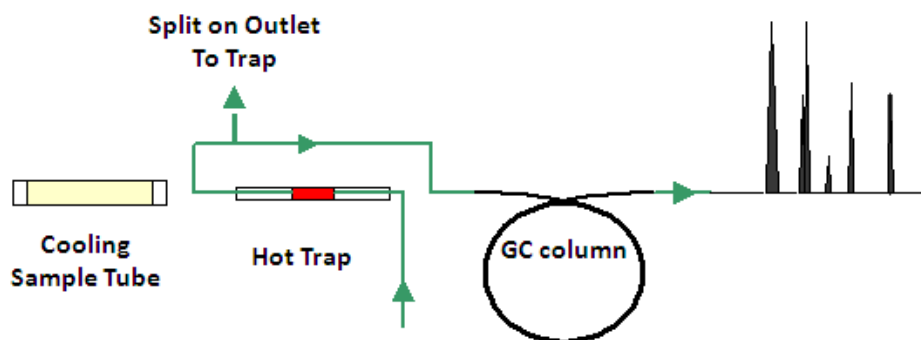


Figure 3.8. Second desorption stage (source: Agilent Technologies, 2016).

Turbomatrix 150 ATD also allows to perform a tube conditioning, the process is similar to first stage desorption but in this mode the cold trap is isolated from the sampling tube at all times.

Sample split points on both the inlet and outlet of the cold trap simplify the analysis of samples containing relatively large amounts of water. They also enable the ATD to perform both trace level environmental monitoring and the determination of percent levels of volatiles in solids. In order to enhance the process of two-stage thermal desorption, the double split mode was used.

With the double split mode it possible to achieve the next objectives at each desorption stage:

- To ensure complete recovery from the sampling tube.
- To establish a reasonably low flow through the cold trap during primary desorption in order to enhance component retention on the trap.
- To establish a reasonably high flow through the heated cold trap during secondary desorption in order to enhance component elution from the trap.

In the double split mode, during the primary desorption:

$$\text{sampling tube flow} = \text{desorb flow} + \text{inlet split flow} \quad (3.1)$$

$$\text{flow through the cold trap tube} = \text{desorb flow} \quad (3.2)$$

From the inlet split the fraction of sample reaching the cold trap from the tube is:

$$\frac{\text{cold trap flow}}{\text{tube flow}} = \frac{\text{desorb flow}}{\text{desorb flow} + \text{inlet split flow}} \quad (3.3)$$

During the secondary desorption:

$$\text{flow through the heated trap} = \text{column flow} + \text{outlet split flow} \quad (3.4)$$

From the outlet split the fraction of sample reaching the analytical column from the trap is:

$$\frac{\text{column flow}}{\text{heated trap flow}} = \frac{\text{column flow}}{\text{column flow} + \text{outlet split flow}} \quad (3.5)$$

Finally, combining the primary and secondary desorption, the percentage of compounds from the sampling tube that reach the analytical column (total analyte transfer) is:

$$\frac{\text{column flow} \cdot \text{desorb flow} \cdot 100}{(\text{outlet split flow} + \text{column flow}) \cdot (\text{desorb flow} + \text{inlet split flow})} \quad (3.6)$$

This configuration ensures that only between 20 and 0.001% of the components from the sampling tube reach the GC/MS.

The chromatographic separation of PAHs was conducted on a Meta.X5 silphenylene phase capillary column (Teknokroma) 30 m x 0.25 mm i.d. x 0.25 µm film thickness. This column shows a good thermal stability, low bleeding level and provides optimal resolution for aromatic compounds (Teknokroma, 2015).

The temperature program of the oven (Figure 3.9) was optimized for the operation of the ATD-GC/MS system. Initially the oven is at 100°C for the initial 3 minutes. Afterwards the temperature reaches 250°C with an increase of 10°C min⁻¹. From this value the rate drops to 5°C min⁻¹ and maintains it up to 320°C. When the temperature reaches this value the oven holds it for 10 min. The total analysis time was 42 min per sample.

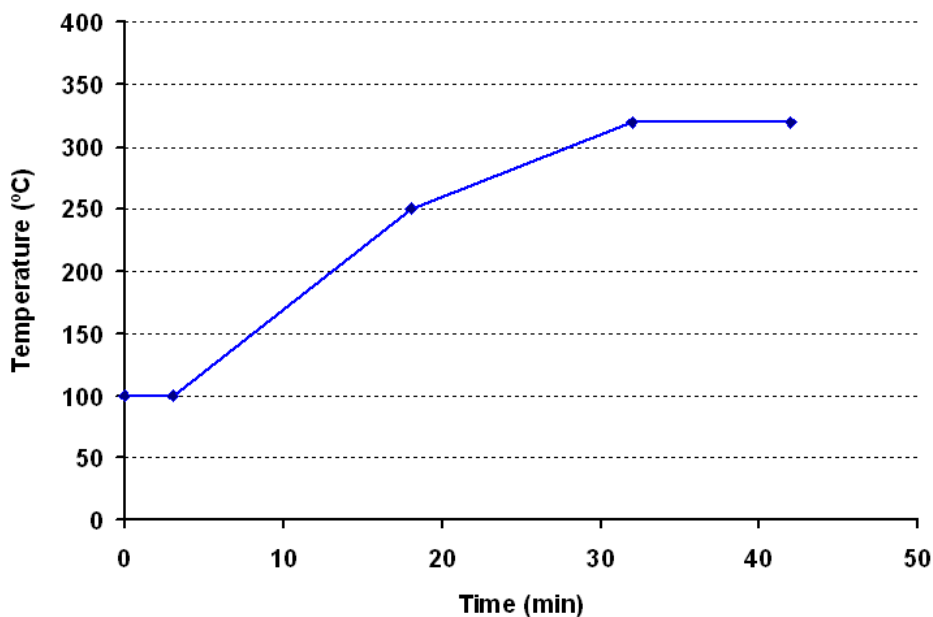


Figure 3.9. Temperature program of the chromatographic oven

After the separation of PAHs by gas chromatography, the chromatographic peaks were detected by a quadrupole mass spectrometer. This detector uses electric ionization to transform the components of the sample into gaseous ions which separate according to their mass-to-charge ratio (m/z).

For the identification and quantification of the PAHs, the used MS allows the simultaneous acquisition of the mass spectrum by full scan (SCAN) and single ion monitoring (SIM). The SCAN monitors a range of mass-to-charge ratio (m/z) between two pre-established limits, while the SIM mode only monitors pre-selected individual masses, weeding out or ignoring unwanted or irrelevant masses. The simultaneous application of both modes allows obtaining the SCAN and SIM mode information in one chromatographic run, receiving more information in less time.

It is necessary that MS works under vacuum in order to maintain stable working conditions and protect the most sensitive parts (the source, the optical components and the detector). For this reason, a vacuum of $2 \cdot 10^{-5}$ Torr was applied to the MS by a vacuum pump.

Identification and quantification

The SCAN mode shows good characteristics in the scanning of unknown samples, due to the complete mass spectrum it obtains. It can also use parameters such as the retention time of the different compounds (amount of time between the injection of a sample and its elution from the column) to help in their identification. Furthermore, the mass spectra search programs that are usually installed in GC/MS instruments guarantee a correct identification of the analytes by comparison with well-known databases (NIST or Wiley mass spectral libraries).

However, the selective scanning, and thus the reduction in the number of scanned m/z ratios, results in the SIM mode showing a higher sensitivity than the SCAN mode. Due to this, the SIM mode is usually applied to quantitative analyses (Figure 3.10).

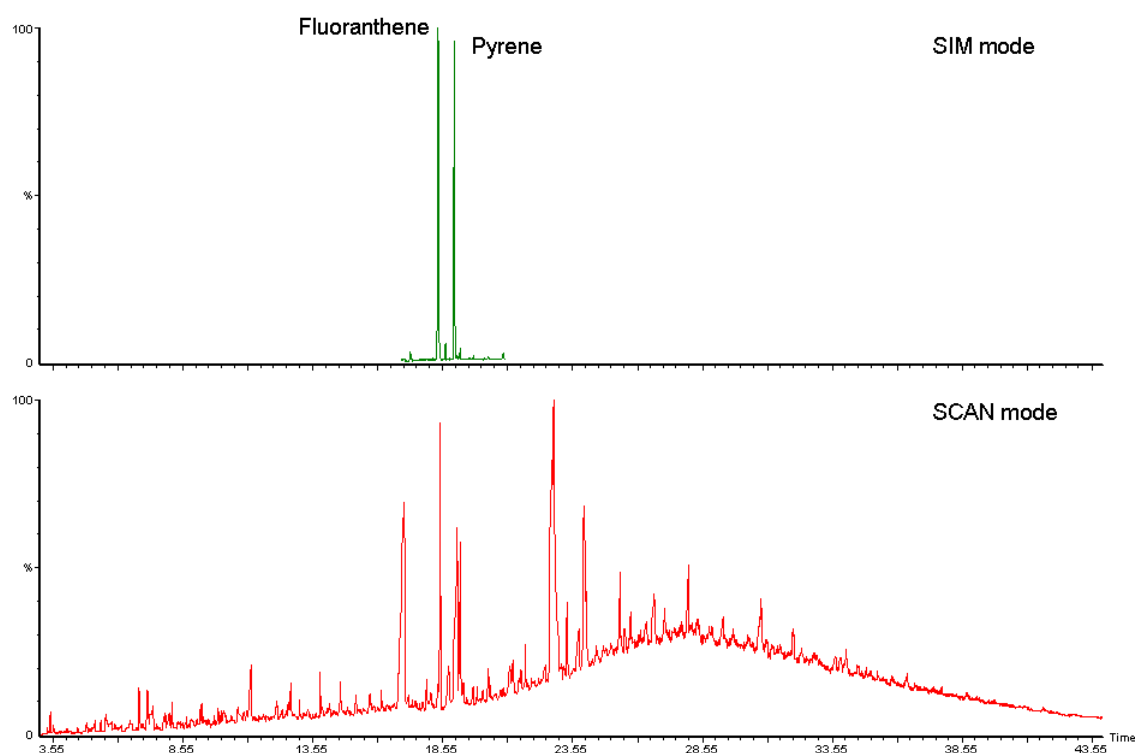


Figure 3.10. SCAN vs. SIM mode. Identification of fluoranthene and pyrene in reference material certificate (NIST 1649b urban dust).

The selected ions used in the identification of 16 EPA PAHs in this study for the SIM mode are listed in Table 3.1.

Table 3.1. Quantification ions of 16 EPA PAHs

PAH	Abbreviation	Ion (m/z)
Naphthalene	Naph	128
Acenaphthylene	Acy	152
Acenaphthene	Ace	154
Fluorene	FL	166
Phenanthrene	Phe	178
Anthracene	Ant	178
Fluoranthene	Ft	202
Pyrene	Pyr	202
Benzo[a]anthracene	BaA	228
Chrysene	Chry	228
Benzo[b]fluoranthene	BbFt	252
Benzo[k]fluoranthene	BkFt	252
Benzo[a]pyrene	BaP	252
Indeno[1,2,3-cd]pyrene	IP	276
Dibenzo[ah]anthracene	DBahA	278
Benzo[ghi]perylene	BghiP	278

Measuring peak areas or peak heights is the key to quantitative analysis. The use of peak heights provides acceptable accuracy in chromatograms that show sharp, narrow, defined and symmetric peaks. With this method it is possible to sacrifice the accuracy in favour of the simplicity and speed of the quantifications. However, the measuring of peak areas is the most used method of quantitative analysis when accuracy is required (Dyson, 1998).

After the quantification of the peak areas or peak heights, their mass or concentration in the sample can be measured with a calibration curve that relates the detector response to the injected sample amount. Due to the loss of analytes during the sample preparation, it is recommended to use the internal standard calibration. In this calibration method one or more substances are introduced as a fixed reference parameter, the concentration of which is kept constant in the standard solutions and is always added to the analysis sample at the same concentration. In the calibration curve, the area ratio between analyte and internal standard is plotted against the concentration ratio of both. From this curve it is possible to quantify an unknown sample by graphic or mathematic interpolation of the area ratio (analyte to internal

standard) in the calibration curve. The use of the internal standard in this method allows compensating the errors that affect the same proportion of the analyte and substance reference. This method achieves a higher precision in the quantitative determination than the external calibration. In the internal standard, the selected substance should display the following characteristics:

- The internal standard chosen must be stable to clean up and analyse and as inactive as possible.
- The properties of the standard should be comparable to those of the analyte concerning the sample preparation and analysis. For this reason the use of isotope labelled standards could be preferable.
- The internal standard must not be present in the original sample.
- In the chromatograms, the standard peak should be in the proximities of the peaks of interest.
- The use of several standards allows them to be used as retention time standards.
- The standard peak should avoid an overlap with matrix peaks or other components to achieve faultless integration.
- The quantifying mass of the internal standard should exclude interference by the matrix or other components.

In the study, deuterated PAHs have been used as internal standard. Table 3.2 shows the selected ions for deuterated PAHs in SIM mode.

Table 3.2. Quantification ions of deuterated PAHs

Deuterated PAH	Abbreviation	Ion (m/z)
Naphthalene-d ₈	Naph-d ₈	136
Biphenyl-d ₁₀	Bph-d ₁₀	164
Phenanthrene-d ₁₀	Phe-d ₁₀	188
Pyrene-d ₁₀	Pyr-d ₁₀	212
Benzo[a]anthracene-d ₁₂	BaA-d ₁₂	240
Benzo[a]pyrene-d ₁₀	BaP-d ₁₀	264
Benzo[ghi]perylene-d ₁₂	BghiP-d ₁₂	288

For the quantification, the 16 EPA PAHs were divided into groups according to their retention time (Table 3.3), so that each group was quantified by the most appropriate

internal standard (deuterated PAH with the most similar retention time to the group). A liquid certificated mixture of 16 EPA PAHs (SV Calibration Mix 5, Restek, 2000 $\mu\text{g mL}^{-1}$) and liquid deuterated mixture (Internal Standards MIX 37, Dr. Ehrenstorfer, 15 $\mu\text{g mL}^{-1}$ or Predeuterated internal standard PAH Mixture 6, Chiron, 200 $\mu\text{g mL}^{-1}$) were used during the study.

Table 3.3. Quantification groups of 16 EPA PAHs with their deuterated compound.

Group	PAH	Deuterated PAH
1	Naphthalene	Naphthalene-d ₈
2	Acenaphthylene	Biphenyl-d ₁₀
	Acenaphthene	
3	Fluorene	Phenanthrene-d ₁₀
	Phenanthrene	
4	Anthracene	Pyrene-d ₁₀
	Fluoranthene	
5	Pyrene	Benzo[a]anthracene-d ₁₂
	Benzo[a]anthracene	
6	Chrysene	Benzo[a]pyrene-d ₁₀
	Benzo[b]fluoranthene	
	Benzo[k]fluoranthene	
7	Benzo[a]pyrene	Benzo[ghi]perylene-d ₁₂
	Indeno[1,2,3-cd]pyrene	
	Dibenzo[ah]anthracene	
	Benzo[ghi]perylene	

The figures from 3.11 to 3.13 and from 3.14 to 3.20 show the identification of the 16 EPA and deuterated PAHs in SCAN and SIM mode, respectively. The results correspond to the analysis of a standard sample (filter injected with 50 ng of each EPA PAHs and 100 ng of each deuterated compound from liquid standard solutions).

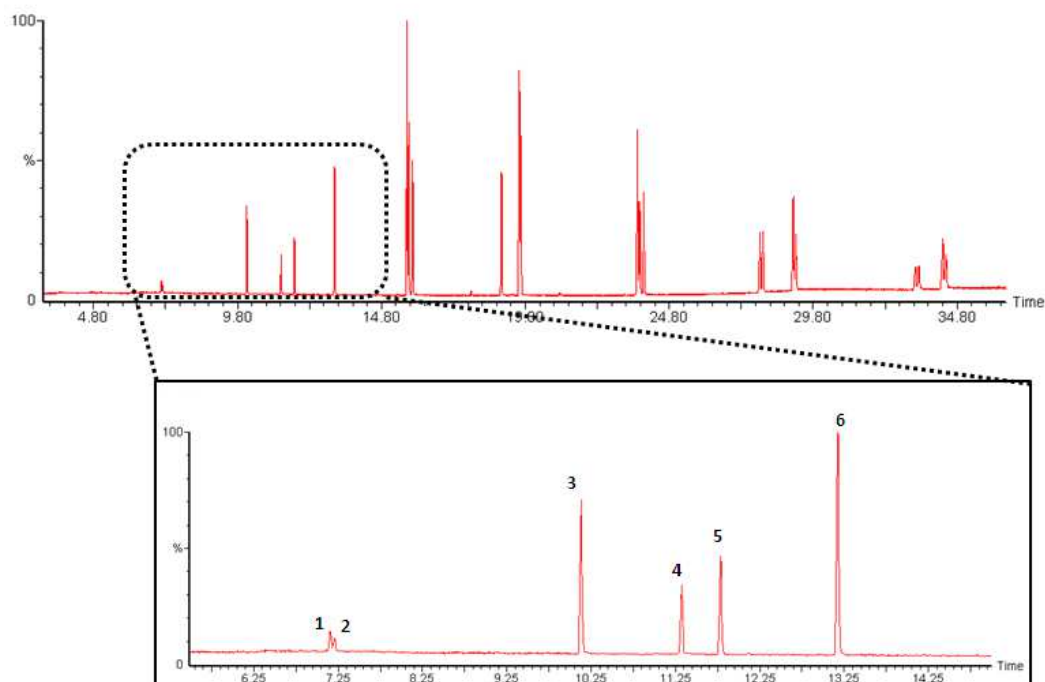


Figure 3.11. Identification of 16 EPA and deuterated PAHs in SCAN mode, from 0 to 15 min: 1) Naph-d₈, 2) Naph, 3) Bph-d₁₀, 4) Acy, 5) Ace, 6) FL.

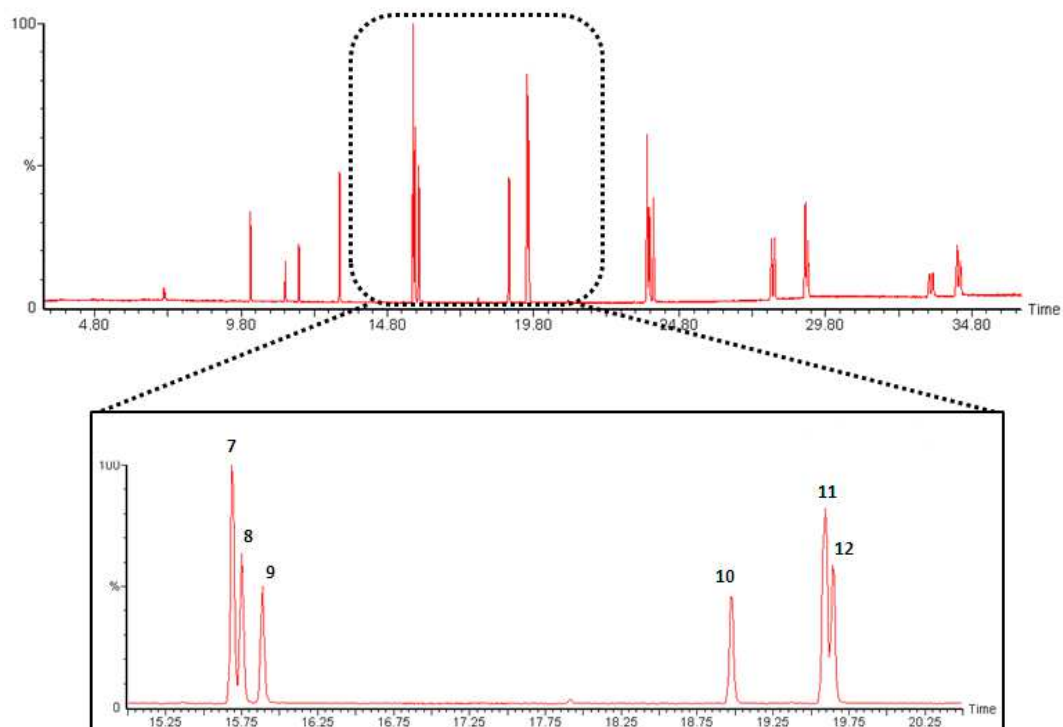


Figure 3.12. Identification of 16 EPA and deuterated PAHs in SCAN mode, from 15 to 20.5 min: 7) Phe-d₁₀, 8) Phe, 9) Ant, 10) Ft, 11) Pyr-d₁₀, 12) Pyr.

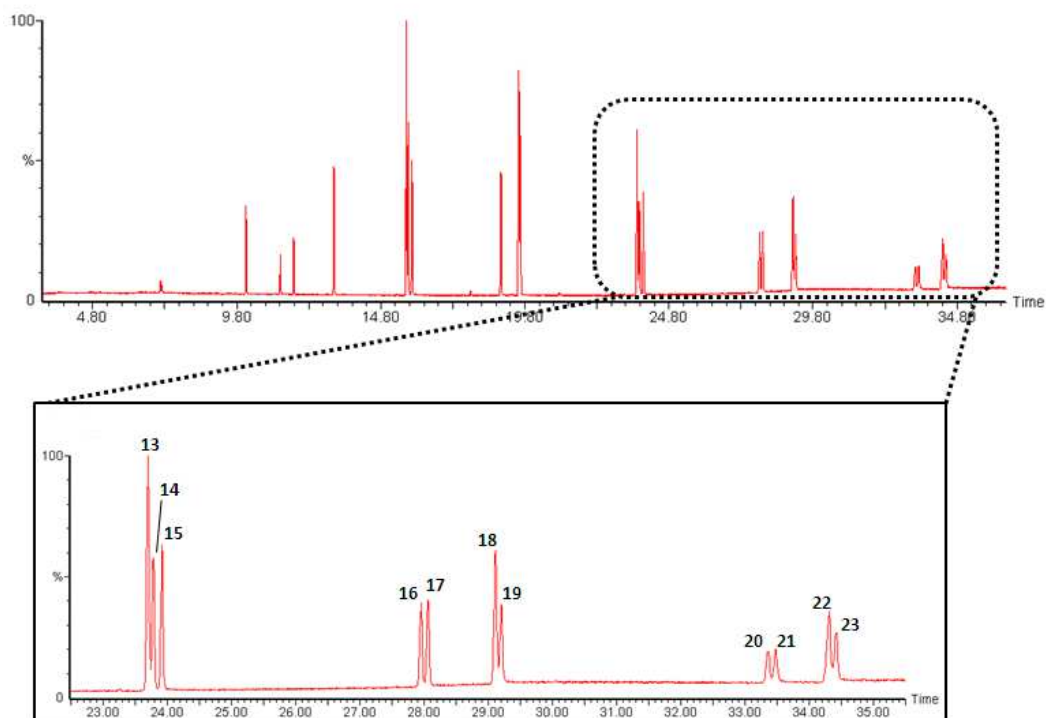


Figure 3.13. Identification of 16 EPA and deuterated PAHs in SCAN mode, from 22.5 to 35.5 min: 13) BaA-d₁₂, 14) BaA, 15) Chry, 16) BbFt, 17) BkFt, 18) BaP-d₁₀, 19) BaP, 20) IP, 21) DBahA, 22) BghiP-d₁₂, 23) BghiP.

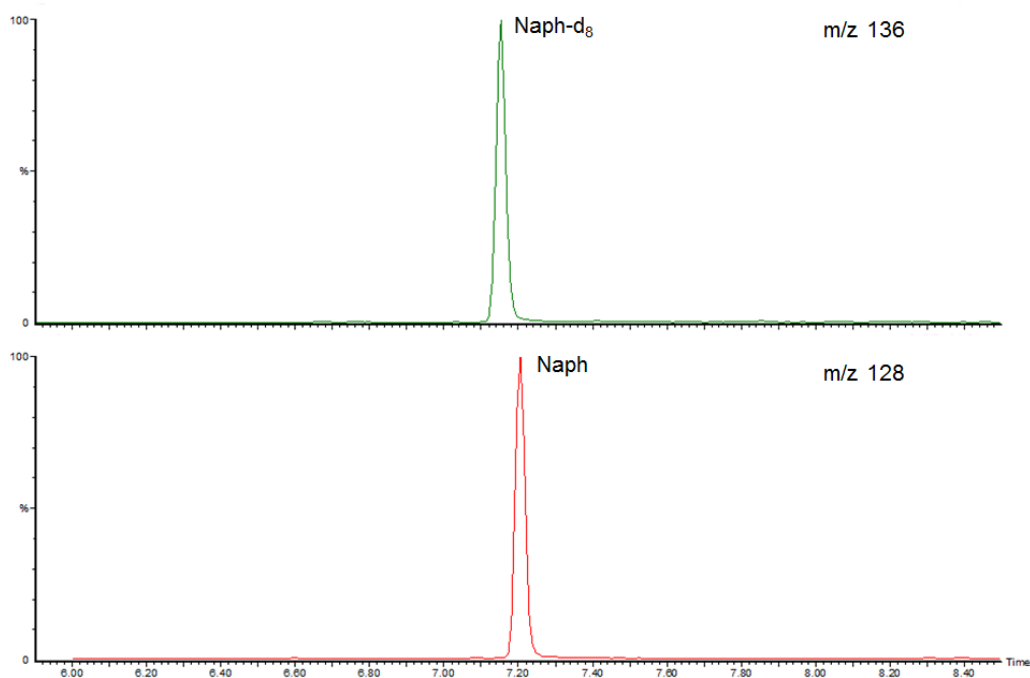


Figure 3.14. Identification of group 1 in SIM mode.

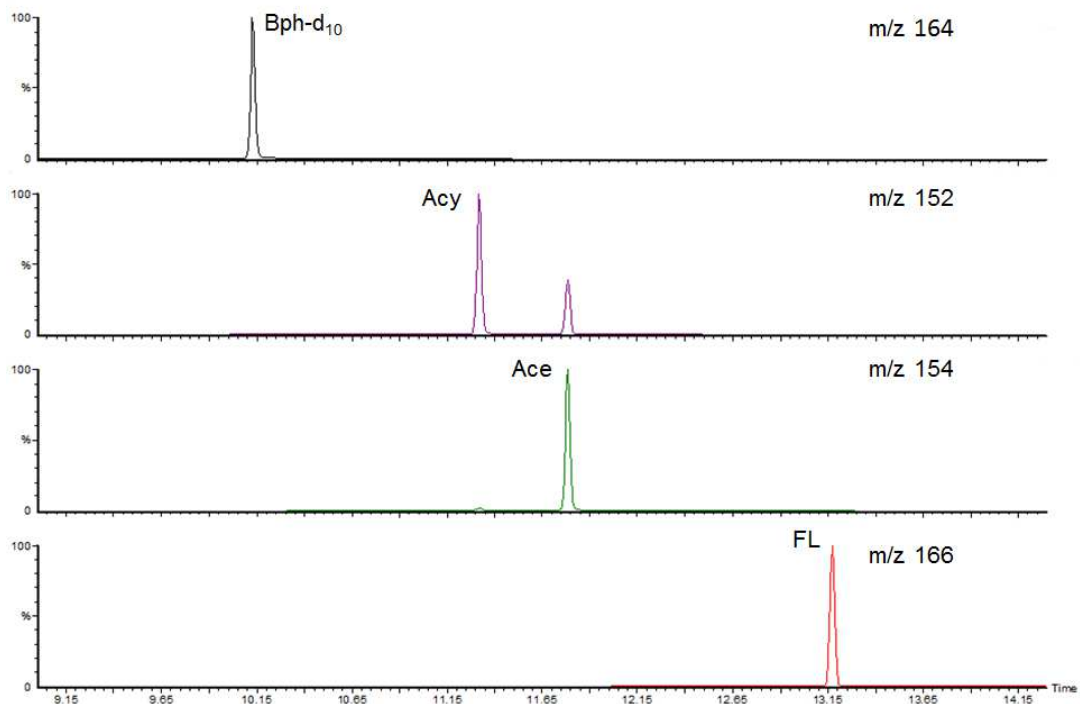


Figure 3.15. Identification of group 2 in SIM mode

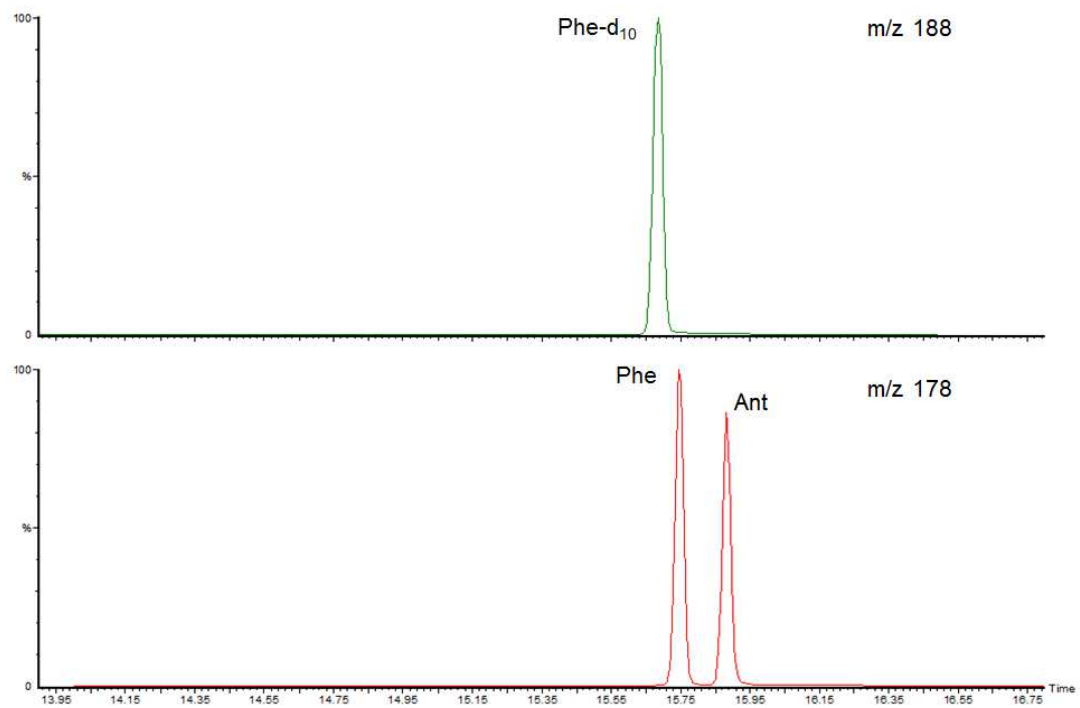


Figure 3.16. Identification of group 3 in SIM mode

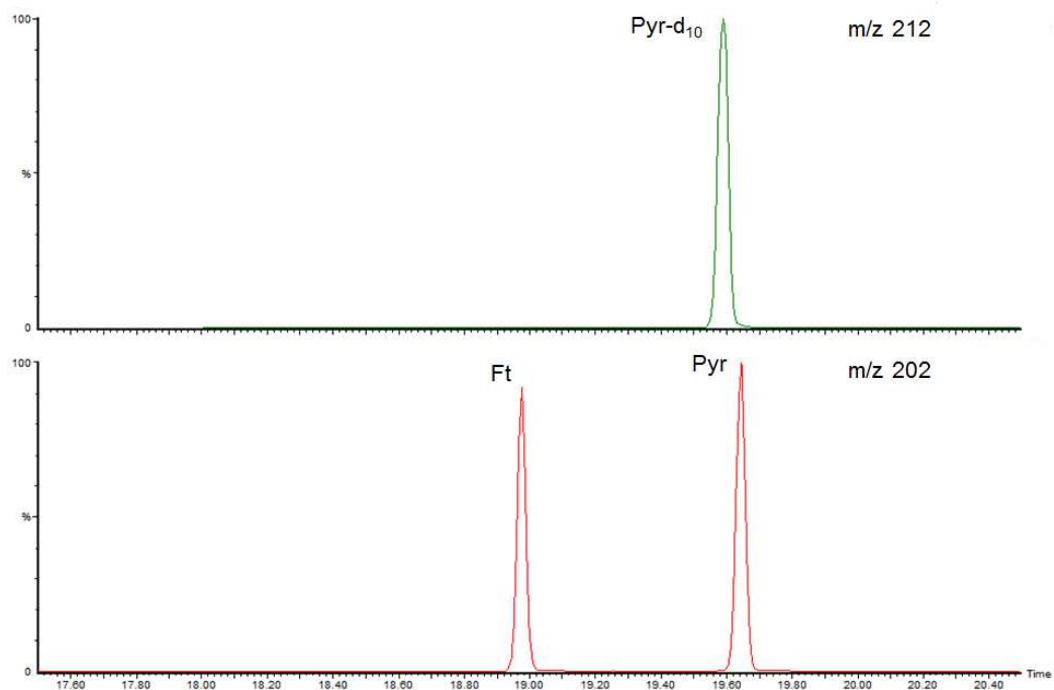


Figure 3.17. Identification of group 4 in SIM mode

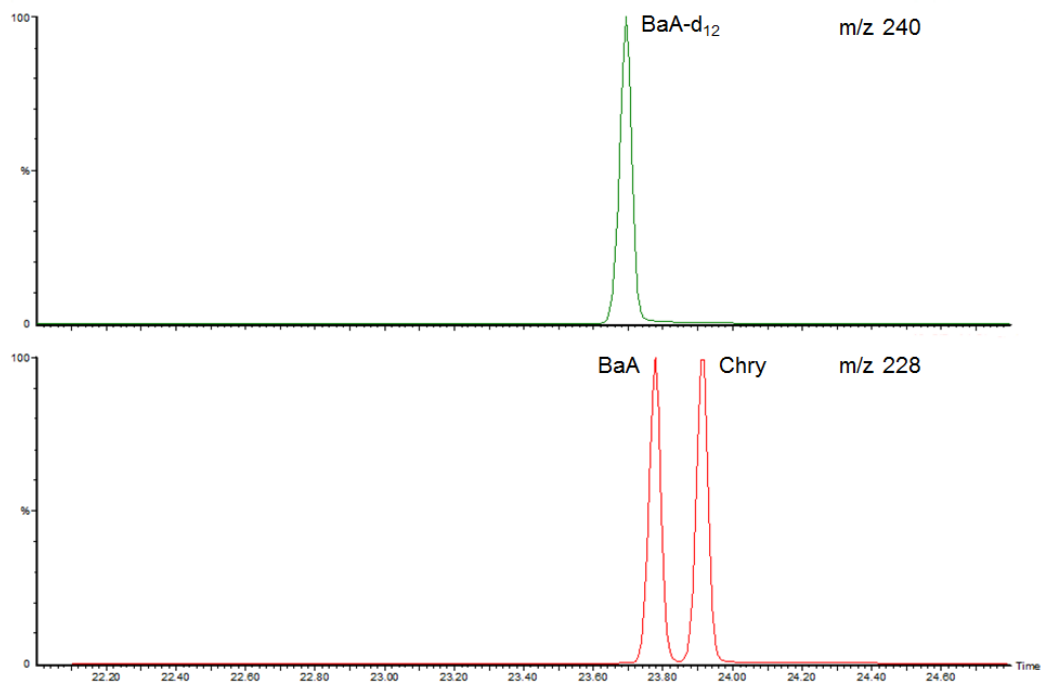


Figure 3.18. Identification of group 5 in SIM mode

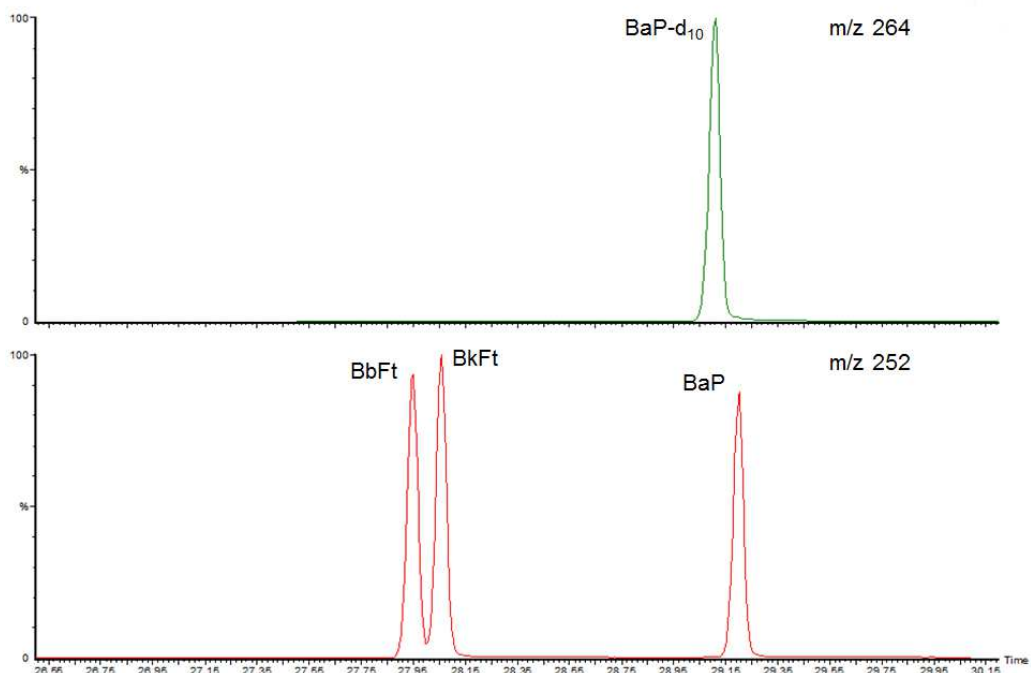


Figure 3.19. Identification of group 6 in SIM mode

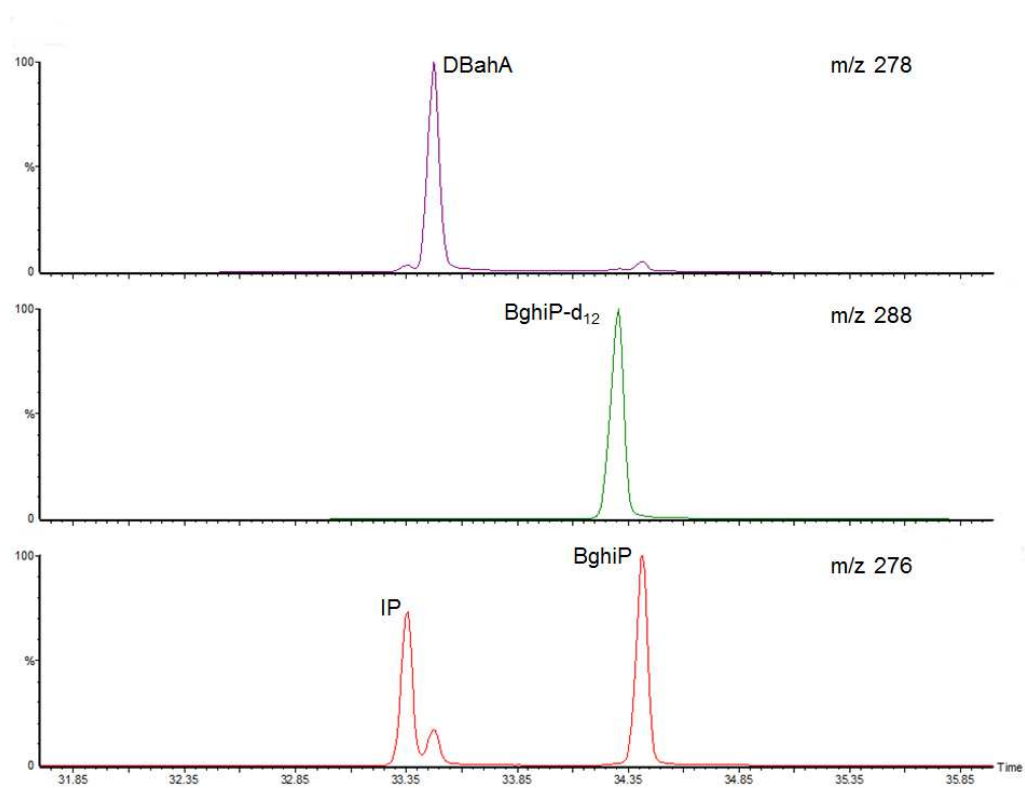


Figure 3.20. Identification of group 7 in SIM mode

3.1.4 Auxiliary equipment and gases.

Besides the sampling and analysis system, some auxiliary instruments and gases were necessary for the study.

The TD-GC/MS technique needed the following gases for correct operation:

- High Purity Helium ($\geq 99.999\%$). This was the carrier gas of the system. The gas was provided from 50 L gas bottle (Abelló Linde) at 200 bar. The working pressure of the bottle was approximately 4 bar.
- High Purity Nitrogen ($\geq 99.999\%$). This was used as “security gas” for the MS. When the carrier gas flow is shut off (by power cut or leak) automatically enter nitrogen gas to MS in order to prevent the entry of oxygen, which can damage the filament of the equipment. The gas was provided from 5 L gas bottle (Abelló Linde) at 200 bar. The working pressure of the bottle has been approximately 1 bar.
- Air. The air is used in the pneumatic system of the TD. This gas was provided by a zero air system designed by the Air Pollution research group at ETSI Bilbao (Figure 3.21):

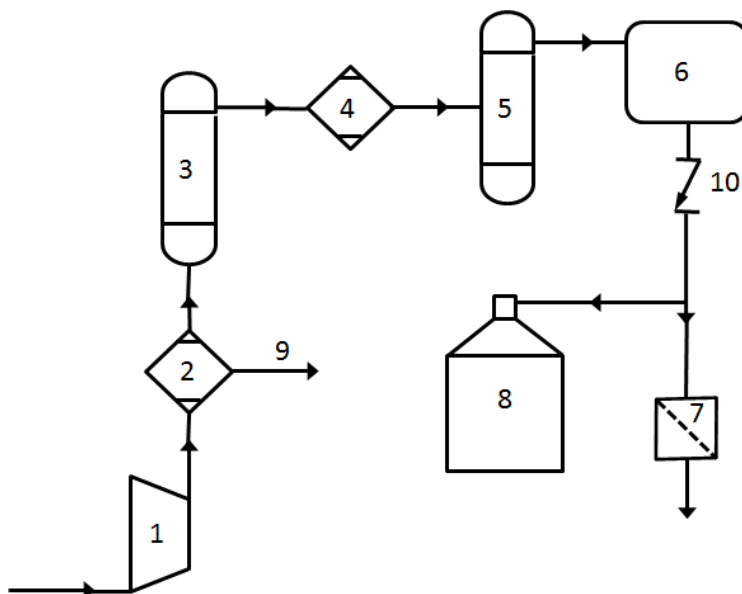


Figure 3.21. Flowchart of zero air system

Where:

1. Dry compressor “Jun-Air 1000”. 25 L min⁻¹ at 8 bar.

2. Compressed air refrigerated dryer.
 - Dew point = +2 °C at 8 bar.
 - Maximum flow = 360 L min⁻¹.
3. Buffer tank. 100 L at 6-8 bar.
4. Adsorption dryer “Ultrapac 2000 mini”.
 - Dew point = - 40 °C .
5. Dry air buffer tank. 100 L at 7.5-8 bar.
6. Zero air generator “Parker domnick hunter UHP-ZA ”
 - Flow = 3.5 L min⁻¹.
7. Filter.
8. Storage tank.
9. Purge.
10. Check valve.

Before entering the TD-GC/MS system, the helium and air lines passed through different filters to eliminate oxygen (oxygen trap, Perkin Elmer), hydrocarbons (hydrocarbon filter, Scientific Glass Technology) and moisture (safe glass moisture trap, Perkin Elmer), in order to guarantee the purity of the gases.

The turbomolecular pump of the mass spectrometer needs ambient temperatures below 30°C to work under air-cooling conditions (PerkinElmer, 2002). In order to achieve this requirement, the laboratory temperature was kept around 24°C by an air conditioning system.

3.2 Setting and use of TD-GC/MS software

The Clarus GC/MS is controlled by a personal computer based data system using the Microsoft Windows operating environment. The TurboMass software (Perkin Elmer) user interface allows a complete control of the GC/MS system from tuning and data acquisition (scanning or selected ion recording mode) through quantifying the results.

3.2.1 MS Tuning

Before acquiring data, it may be necessary to check the tuning conditions of the MS, and to modify one or more of the instrument tuning parameters in order to improve the

sensitivity of the SIM mode. The instrument can be tuned either manually or automatically from the instrument Tune page, which presents the next adjustable parameters (Figure 3.22):

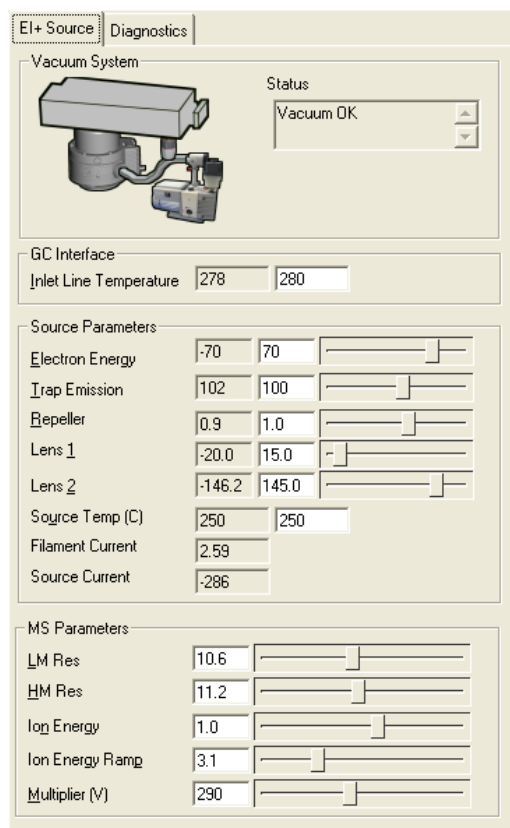


Figure 3.22. Instrument tune parameters in TurboMass software.

- Inlet line temperature. It controls the MS transfer line temperature, it was set at 280°C in this study.
- Electron energy. This is the potential energy of the electrons striking the analytes. 70 eV is the standard value to generate molecular ionization by electron impact. Furthermore, this is the set value to obtain the mass spectra of the TurboMass library. For this reason, electron energy of 70eV was selected in this study.
- Trap emission. This trap (charged with positive relative potential) attracts the electrons that did not strike the analytes.
- Repeller. This electrode “pushes” the ions out of the EI source. Increasing its voltage can improve sensitivity, but it may also distort peak shape. Its value

usually ranges between 0.1 and 1 V. Values higher than 3 indicates the necessity of cleaning the repeller.

- Lens 1 and 2. These lenses filter the ions before the detector.
- Source temperature. According to the manufacturer, the source temperature can be between 120 and 350°C. Low temperatures prevent molecular fragmentation, while high temperatures minimize the lifetime of the source. In this study the temperature was set at 250°C.
- Filament and source current. These parameters control the amount of electrical current flowing through the filament. Adjusting this can significantly change your signal intensity. The trade-off is filament lifetime. Generally, the filament current should be adjusted between 2.5 and 4.0 A. and the source current to at least twice the emission current.
- Low Mass Resolution (LM Res) and High Mass Resolution (HM Res). These parameters control the width (resolution) of the ion peaks.
- Ion energy and ion energy ramp. Both parameters control the acceleration of the ions out of the ion source. In graphical terms, the Ion Energy is the y-axis intercept and the Ion Energy Ramp is the slope of the line that defines this accelerating voltage. The effect of both parameters is interrelated.
- Multiplier. Its voltage is a key factor in sensitivity and dynamic range. Too low, and sensitivity can be severely reduced. Too high and the baseline is raised, lowering the dynamic range. Typical values are 400 to 600 V.

Periodically automatic adjustments of these parameters were made by the AutoTune option of the TurboMass software. This option automatically adjusts the parameters (except the inlet line and source temperature) in order to find the configuration that provides the best sensitivity. Nevertheless, these parameters can also be changed manually.

3.2.2 Data acquisition

TurboMass software allows setting up the SCAN and SIM functions that the MS will use to scan the instrument during an acquisition. The software facilitates the set-up of different retention windows for the acquisition of SIM groups, and the scan mass range that uses the MS during the acquisition. These scanning functions can be arranged to run either sequentially or concurrently during the acquisition (Figure 3.23).

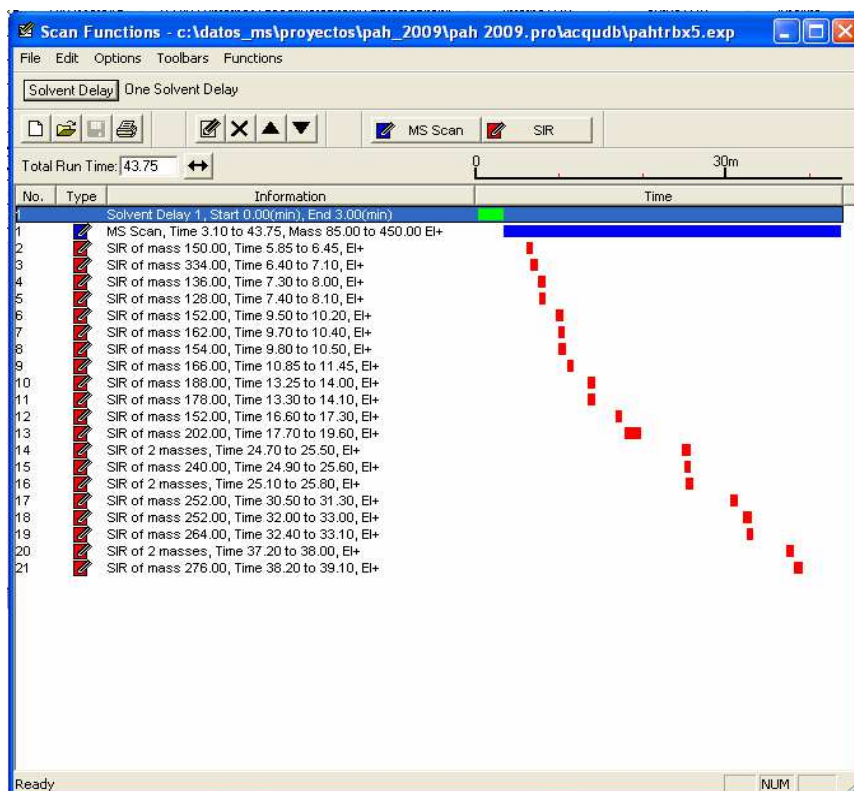


Figure 3.23. Example of SCAN and SIM windows configuration for 21 functions (function 1: SCAN; functions 2 – 21: SIM) by TurboMass software.

The SCAN parameters are set up by the MS scan function editor (Figure 3.24).

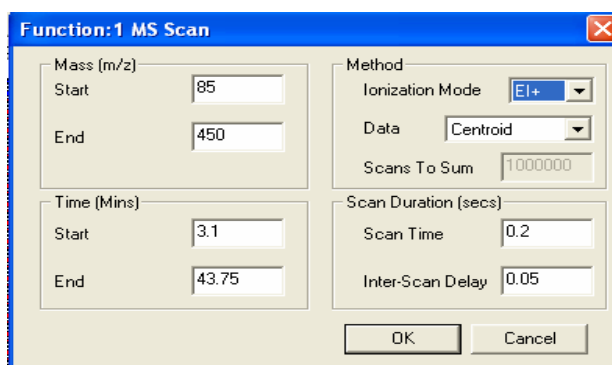


Figure 3.24. SCAN mode parameters for MS in TurboMass software

Where:

- Start and End Mass. Specifies the mass at which the scan will start and end. In this study the range of scanned mass was from 85 to 450 m/z.

- Start and End Time. Specifies the time at which the scan will start and end respectively. In this study the SCAN function started at 3.1 min and finished at 36.5 min.
- Ionization Mode. Specifies the ionization mode and polarity that will be used during the acquisition. The EI+ ionization was selected for this study.
- Data. Specifies the type of data to be collected and stored on disk. The available types are:
 - o Centroid. The data are stored as centroided, intensity, and mass assigned peaks.
 - o Continuum. Data are not centroided into peaks. Instead the signal received by the interface electronics is stored regularly to give an analogue intensity picture of the data being acquired.
 - o Multi-Channel Analysis (MCA). MCA data only show one intensity accumulated scan. As each scan is acquired, its intensity data are added to the accumulated summed data of previous scans.

During the study, centroid option was selected as type of data.

- Scans to Sum. For the MCA option, defines the number of scans to sum to create a spectrum.
- Scan times. Specifies the duration of each scan in seconds. In the study scans of 0.2 s were used.
- Inter-Scan Delay. Time in seconds between a scan finishing and the next one starting. During this period data are stored, but not acquired. Inter-Scan of 0.05 s was used in this study.

Similar to the SCAN function, the SIM mode has its own editor in the software (Figure 3.25).

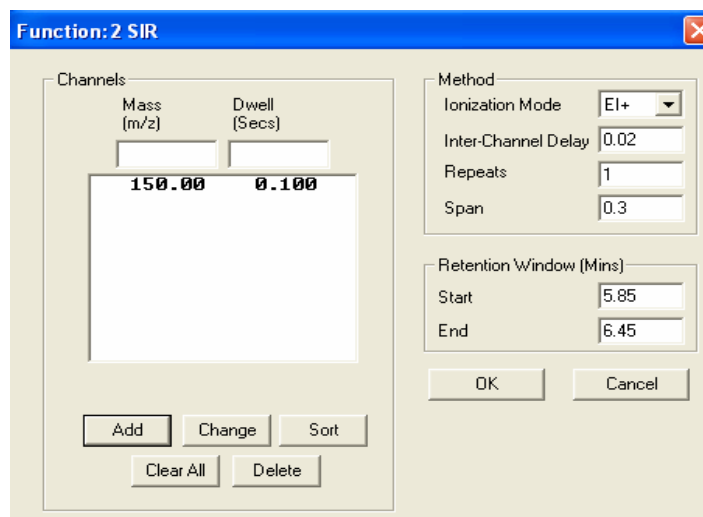


Figure 3.25. SIM mode parameters for MS in TurboMass software

Where:

- Mass. Specifies the mass to be monitored up to a maximum of 32.
- Dwell. Specifies the length of time in seconds for which the highlighted mass will be monitored.
- Ionization Mode. Specifies the ionization mode and polarity that will be used during the acquisition. For this study, EI+ ionization was selected.
- Inter-Channel Delay. Specifies the length of time in seconds between finishing monitoring the highlighted mass and starting monitoring the next mass in the function. During the study an inter-channel delay of 0.02 s was used.
- Repeats. In experiments with more than one function, this specifies the number of times we wish to execute this function per pass. A value of 1 was set to the study.
- Span. Specifies a small mass window applied centrally about the highlighted mass. During the acquisition this range will be scanned over the specified dwell time. This minimizes the chance of missing the top of the mass peak. SIM windows with spans of 0.3 were used during the study.
- Start and End Time. Specifies the time at which the scan will start and end.

TurboMass software allows using a mix of SCAN and SIM functions for the acquisition, this mode is known as Selected Ion and Full Ion Scanning (SIFI). This mode shows the universality of a full SCAN analysis, with the ability to library search, and the higher sensitivity of SIM. In the study the SIFI mode was applied in the MS method, the data acquisition was realized by a single full MS scan method that ran for the entire

chromatogram, and multiple SIM functions timed for the elution of specific compounds (Figure 3.23). Moreover, a solvent delay in the initial 3 minutes of the MS method was set to protect and thus extend the lifetime of the MS filament. The times of the different SIM windows were varied over the study in order to guarantee the acquisition of the target compounds.

3.2.3 Qualitative and quantitative analysis

TurboMass software enables the automated quantification of large numbers of samples within an analysis. Data can be acquired, processed, and reports printed without user intervention.

Initially, for quantification it is necessary to create a list of the target samples in the analytic study (Figure 3.26). These samples can be acquired manually, but more often they will be acquired automatically using an autosampler. This list of samples provides the information (for example sample type or standard concentrations) that TurboMass software requires to perform a complete analysis.

File Name	MS Method	GC Method	Sample ID	Conditions	Sample Type	MS Tune File	Conc. A	Conc. B	Calibration Curve	Quantity Method
020712b1	Traptest	Traptest		multiplier 400	Analyte	2012junio20				
020712b2	TGnew	TGr			Analyte	2012junio20				
020712b3	TGnew	TGr		multiplier 400	Analyte	2012junio20	25	25		
020712b4	TGnew	TGr			Analyte	2012junio20				
020712b5	TGnew	TGr		multiplier 400	Analyte	2012junio20	25	25	280612 int	020712 int
020712b6	TGnew	TGr		multiplier 400	Analyte	2012junio20	25	25	280612 int	020712 int
020712b7	TGnew	TGr		multiplier 400	Analyte	2012junio20	25	25	280612 int	020712 int
020712b8	TGnew	TGr		multiplier 400	Analyte	2012junio20	25	25	280612 int	020712 int
020712b9	TGnew	TGr		multiplier 400	Analyte	2012junio20	25	25	280612 int	020712 int
020712b10	TGnew	TGr		multiplier 400	Analyte	2012junio20	25	25	280612 int	020712 int
020712b11	TGnew	TGr		multiplier 400	Analyte	2012junio20	25	25	280612 int	020712 int
020712b12	TGnew	TGr		multiplier 400	Analyte	2012junio20	25	25	280612 int	020712 int
020712b13	TGnew	TGr		multiplier 400	Analyte	2012junio20	25	25	280612 int	020712 int
020712b14	TGnew	TGr		multiplier 400	Analyte	2012junio20	25	25	280612 int	020712 int

Figure 3.26. Sample list screen in TurboMass software

After the creation of the list of samples and the analyses, and before the integration or quantification can be performed, the quantitative method has to be created. TurboMass has an editor that allows for creating this method (Figure 3.27).

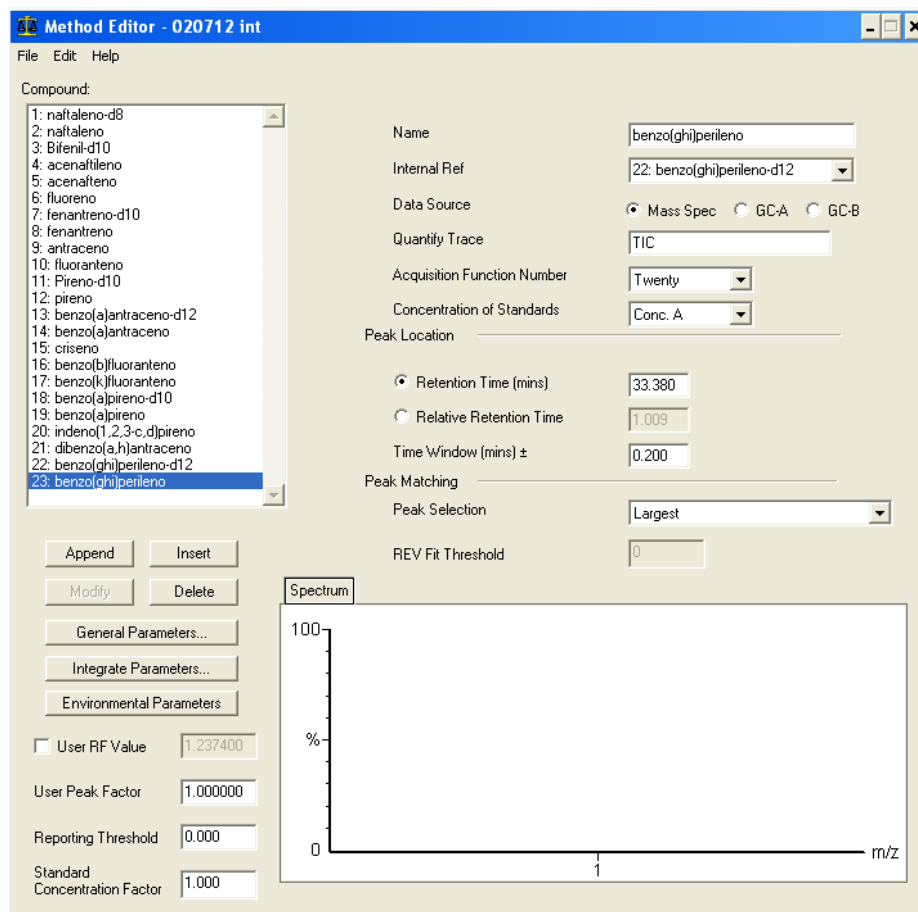


Figure 3.27. Quantitative method editor in TurboMass software

In this editor it is possible to fulfil the next tasks:

- Integration of a chromatogram trace to obtain peak information. The editor has diverse options that can improve the integration (Figure 3.28). These options are focused on the modification of the baseline position and the separation of partially resolved peaks by vertical drop lines.

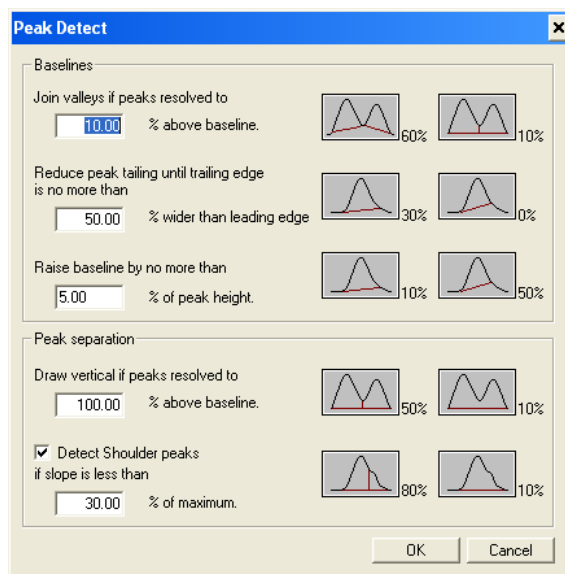


Figure 3.28. Peak detect options in quantitative method editor in TurboMass software.

- Location of the chromatogram peak relating to a specific compound from the list of detected peaks.
- Calculation of a response factor for the located peak.
- Formation of calibration curve. The editor options allow selecting the response type (external or internal) and curving type (average response factor, linear, quadratic, cubic or quartic) (Figure 3.29).

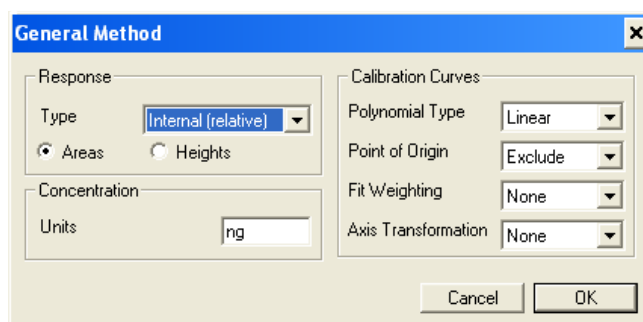


Figure 3.29. Calibration curve settings in quantitative method editor in TurboMass software.

3.2.4 Data quality control

Data quality control is essential to ensure the quality and reliability of the analytical data obtained. For this reason, retention times, peak areas and/or concentrations obtained for each PAH by TurboMass software were checked in order to detect errors. After error checking and correction, an Excel macro, designed by the Air Pollution research group at ETSI Bilbao, was applied to export the obtained results (from QSS to Excel) and to create the database in Excel.

3.3 Soxhlet extraction

During the study, the TD-GC/MS method was compared with the conventional technique (Soxhlet extraction-GC/MS). The Soxhlet extraction was performed by Büchi extraction system B-811 (Figure 3.30), an automated system that can be used to perform an extraction according to the original Soxhlet principle.



Figure 3.30. Büchi extraction system B-811(source: Büchi, 2016a).

The system mainly carries out three functions: extraction, rising and drying (Figure 3.31).

- Extraction. The sample is placed in the sampling tube of the B-811. There is a choice of four different procedures for the extraction.

- Rising. The valve is opened. The sampling tube is lifted up automatically. The rinsing ensures the removal of all sample residues from the outer side of the sampling tube and the inner side of the extraction chamber.
- Drying. The valve is closed while the low-level heating remains on. The solvent evaporates, is condensed in the condenser, and collected in the empty extraction chamber. This allows the solvent to be removed almost completely in the shortest possible time. The now highly-concentrated extract is available for further analysis.

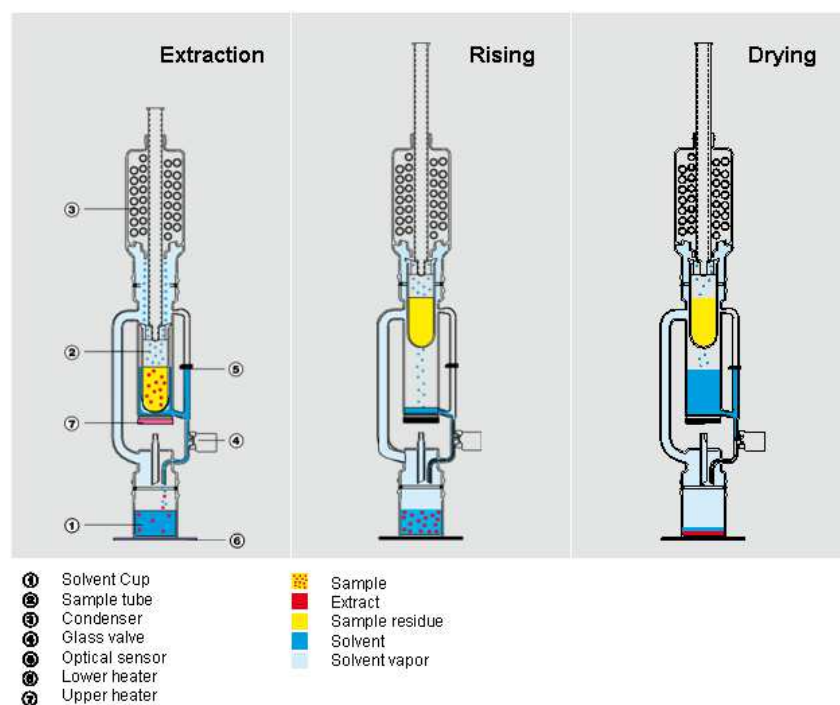


Figure 3.31. Operation of Büchi extraction system B-811 (source: Büchi, 2016b).

The B-811 has four different extraction procedures: Hot Extraction, Soxhlet Standard, Soxhlet Warm and Continuous Flow. This study used the Soxhlet Warm mode. The principle of this procedure is the same as that of the Soxhlet standard method, except that the upper-level heating is activated. First the solvent is evaporated, and condensed in the condenser where it flows into the sampling tube. As soon as the solvent level reaches the optical sensor, the glass valve opens and the solvent containing the dissolved analyte flows back into the solvent cup. As the sample is continually being extracted with fresh solvent, the analyte-solvent exchange is optimal. The increment of the temperature in the upper level improves the solubility of the analytes in the extraction chamber and thus reduces the duration of the complete extraction process.

In this study, decafluorobiphenyl, 4,4'-dibromooctafluorobiphenyl, 4,4'-dibromobiphenyl (Restek, 2000 $\mu\text{g mL}^{-1}$) and indeno[1,2,3-cd]pyrene-d12 (Chiron, 100 $\mu\text{g mL}^{-1}$) were used as recovery standard for the assessment of extraction efficiency.

Table 3.4 summarizes the extractor program used with the configuration of the lower and upper heater, and the duration for each stage.

Table 3.4. Configuration of the extraction system B-811 used in the study.

Method : Soxhlet Warm				
Stage	Process	Upper heater	Low heater	Duration (HH:MM)
1	Extraction	4	10	03:00
2	Washing	0	10	00:10
3	Drying	0	8	00:05
4	Drying	0	7	00:05
5	Drying	0	5	00:15

Chapter 4:

Development of TD-GC/MS method

4.1 Conditioning

Filters and solid adsorbent conditioning are essential stages to guarantee a good determination of the PAHs, reducing the interferences in the analysis.

4.1.1 Particulate phase

Initially, unconditioned filters were analysed (n=5) in order to confirm or refute the necessity of the conditioning stage. The results from different conditioning methods are presented in Figure 4.1, where logarithmic scales have been chosen in order to ease the comparison. These methods were:

- Packed sample tubes conditioning by muffle furnace. The sampling tubes loaded with filter punches were heated in a muffle furnace at 350°C for 14 h.
- Filter conditioning by muffle furnace. The filters were heated in a muffle furnace at 500°C for 24 h and introduced into the sampling tubes. This method has been used by several authors (Falkovich and Rudich, 2001; Gil-Moltó et al., 2009; Menezes and Cardeal, 2011).
- Packed sample tubes conditioning by thermal desorption unit. PerkinElmer Turbomatrix 150 ATD has a tube conditioning mode that enables packed sample tubes to be heated under controlled conditions for automated conditioning. In this study, the sampling tubes loaded with filter punches were heated in the ATD at 350°C (recommended maximum temperature in the tube oven by the manufacturer) with a desorb flow of 100 ml min⁻¹, minimum flow to speed up the removal of volatile contaminants (PerkinElmer, 2006), and for periods of either 30 min or 1 hour.

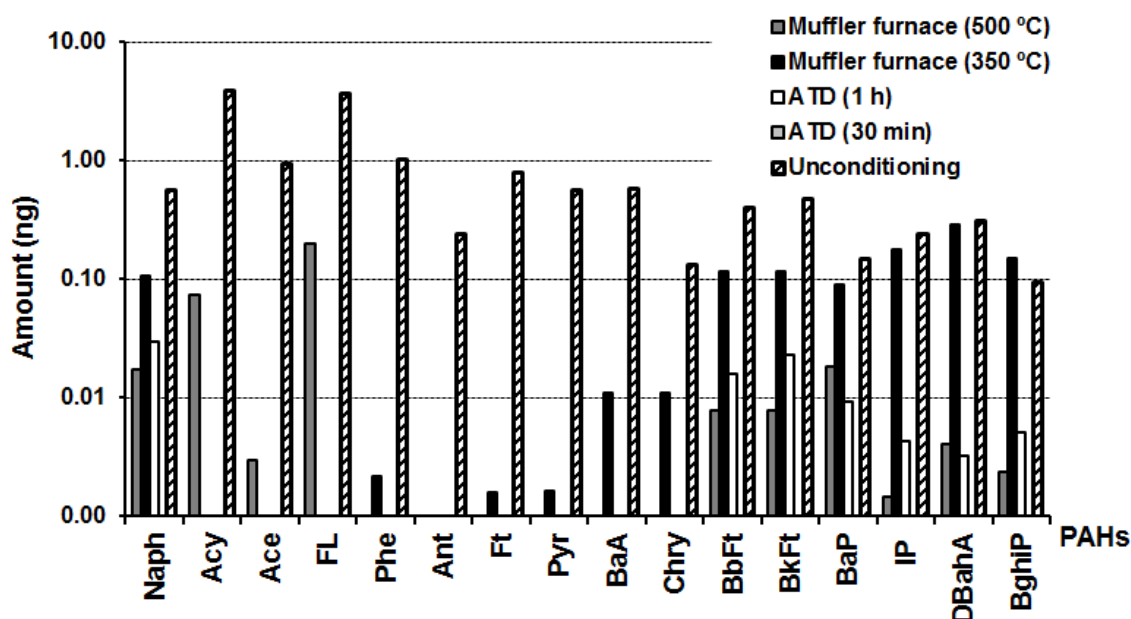


Figure 4.1. 16 EPA PAHs amount in the filter (ng) obtained from different conditioning methods, including the unconditioned samples.

In the comparison between the different conditioning methods (Figure 4.1), the PAH concentrations from unconditioned samples showed significantly higher values than the rest, especially in the 3 and 4-ring PAHs. This confirms the necessity of a previous conditioning process for the filters.

Among the conditioning methods, the conditioning by the automated thermal desorption unit presented significantly lower PAH concentrations (Figure 4.1). The conditioning time was not a critical parameter in these methods. In the case of conditioning by a muffle furnace, the filter conditioning out of the sample tube was more efficient than into it, with lower concentrations in most PAHs. The absence of flow through the sample tubes during the conditioning in this method, complicating the elimination of PAHs, could explain the concentration difference between both methods, especially in the heaviest compounds.

On the basis of the results, the filter conditioning by muffle furnace at 500°C during 24h and packed sample tube conditioning by ATD (during 30 min) were chosen as conditioning methods for this study.

4.1.2 Gas phase

The sample tubes with solid adsorbent were conditioned by ATD. The conditioning time was studied in order to optimize the process for samples with new and used solid adsorbents (Tenax GR or Tenax TA). The conditioning temperature was limited by the adsorbents, thus, a value of 350°C was used (the limit temperature, according to the manufacturer, for the studied adsorbents). Finally, a desorption flow of 100 ml min⁻¹ was used during the conditioning, i.e. the minimal flow recommended by the manufacturer to remove the compounds (PerkinElmer, 2006).

The conditioning times of 60 and 90 min were studied by samples packed with new Tenax GR adsorbent (n=5) and compared with unconditioned samples (n=3) (Table 4.1).

Table 4.1. Mean amount of 16 EPA PAHs (in ng) in new Tenax GR samples (n=5) after conditioning at 350°C for 60 and 90 min. Comparison with unconditioned Tenax GR samples (n=3). Standard deviation in brackets.

PAHs	Tenax GR (ng)		
	Unconditioned	60 min	90 min
Naph	1142.78 (242.77)	0.40 (0.11)	0.45 (0.19)
Acy	97.85 (14.07)	0 (0.01)	0 (0)
Ace	589.75 (22.15)	0 (0)	0 (0)
FL	315.29 (8.38)	0.06 (0.04)	0.03 (0.02)
Phe	301.60 (4.34)	0.50 (0.07)	0.35 (0.11)
Ant	4.23 (0.21)	0.24 (0.14)	0.24 (0.16)
Ft	35.59 (1.53)	0.17 (0.14)	0.15 (0.17)
Pyr	16.09 (1.17)	0.30 (0.18)	0.21 (0.26)
BaA	21.77 (7.16)	0.61 (0.12)	0.82 (0.16)
Chry	28.85 (3.97)	1.27 (0.15)	1.05 (0.22)
BbFt	5.03 (0.70)	0.39 (0.20)	0.14 (0.21)
BkFt	11.53 (1.15)	0.26 (0.13)	0.35 (0.50)
BaP	1.81 (1.62)	0.21 (0.23)	0.23 (0.53)
IP	4.81 (2.86)	0.78 (0.50)	0.60 (0.56)
DBahA	3.98 (1.20)	0.99 (1.30)	0.87 (0.85)
BghiP	2.66 (0.89)	0.79 (0.61)	0.68 (0.68)

The samples with unconditioned adsorbent showed the highest amount of PAHs, especially for the lightest PAHs with values higher than 300 ng (Table 4.1). Thus, the conditioning is a necessary stage to significantly reduce the interferences in the subsequent determination of PAHs.

In studying the conditioning time for the samples with Tenax GR, a significant reduction in the amount was observed from 60 min, mainly in the heavier PAHs, whereas any additional time beyond this did not significantly improve the removal of the compounds. For this reason, 60 min was considered the optimal time for conditioning samples with new Tenax GR.

The same test was carried out with new Tenax TA adsorbent. The results (Table 4.2) showed a similar pattern: the conditioning of adsorbent is again necessary, and 60 min were enough to guarantee a good clean-up of Tenax TA.

Table 4.2. Mean amount of 16 EPA PAHs (in ng) in new Tenax TA samples (n=3) after conditioning at 350°C for 60 and 90 min. Comparison with unconditioned Tenax TA samples (n=4). Standard deviation in brackets.

PAHs	Tenax TA (ng)		
	Unconditioned	60 min	90 min
Naph	42.01 (7.65)	3.05 (0.83)	2.98 (0.70)
Acy	3.03 (0.22)	0 (0.01)	0 (0)
Ace	8.85 (1.25)	0 (0)	0 (0)
FL	9.79 (0.88)	0 (0)	0 (0)
Phe	19.15 (1.30)	0 (0.01)	0 (0)
Ant	0.56 (0.85)	0 (0)	0 (0)
Ft	4.91 (0.35)	0 (0)	0 (0)
Pyr	1.62 (0.11)	0 (0)	0 (0)
BaA	5.35 (1.78)	0.44 (0.06)	0.23 (0.12)
Chry	63.67 (15.36)	0.16 (1.67)	0.30 (0.43)
BbFt	31.13 (6.02)	0.01 (0.67)*	0.04 (0.05)*
BkFt	74.70 (4.45)	0.01 (0.67)*	0.04 (0.05)*
BaP	26.11 (3.91)	0.06 (2.44)	0.07 (0.11)
IP	14.10 (9.48)	0.39 (0.34)	0.17 (0.16)
DBahA	1.94 (0.81)	0.31 (0.23)	0.12 (0.12)
BghiP	0.54 (0.09)	0.07 (0.07)	0.04 (0.04)

*Considering sum of BbFt + BkFt

After the analysis, the sampling tubes packed with solid adsorbent can be re-conditioned for future use. The re-conditioning time was tested for samples with previously used Tenax GR (n=4) and TA (n=4). As used samples do not require as long as samples with new adsorbent to remove interferences, (these are, in general, in lower quantities), re-conditioning times lower than 60 min (30 and 15 min) were tested in this study (Table 4.3). All samples in the test were reconditioned at 350°C.

Table 4.3. Mean amount of 16 EPA PAHs (in ng) in tubes packed with used Tenax Gr (n=4) and TA (n=4) after re-conditioning at 350°C for 15 and 30 min. Standard deviation in brackets.

PAHs	Tenax GR (ng)		Tenax TA (ng)	
	15 min	30 min	15 min	30 min
Naph	0 (0)	0 (0)	0.03 (0.02)	0.05 (0.01)
Acy	0 (0)	0 (0)	0.00 (0)	0.00 (0)
Ace	0 (0)	0 (0)	0.00 (0)	0.00 (0)
FL	0 (0)	0 (0)	0.00 (0)	0.00 (0)
Phe	0 (0)	0 (0)	0.04 (0.01)	0.04 (0)
Ant	0 (0)	0 (0)	0.01 (0)	0.01 (0)
Ft	0 (0)	0 (0)	0.02 (0.01)	0.02 (0)
Pyr	0 (0)	0 (0)	0.03 (0.01)	0.03 (0)
BaA	0.01 (0)	0 (0)	0.04 (0.01)	0.03 (0.01)
Chry	0 (0.01)	0 (0.01)	0.06 (0.02)	0.04 (0.01)
BbFt	0 (0)	0 (0)	0.08 (0.01)	0.10 (0)
BkFt	0 (0)	0 (0)	0.11 (0.03)	0.11 (0.01)
BaP	0.04 (0)	0.04 (0)	0.12 (0.04)	0.10 (0.02)
IP	0.06 (0.05)	0.01 (0.04)	0.02 (0.01)	0.02 (0.01)
DBahA	0.08 (0.01)	0.11 (0.01)	0.27 (0.09)	0.24 (0.10)
BghiP	0.59 (0.02)	0.36 (0.08)	0.15 (0.03)	0.16 (0.01)

After re-conditioning, both adsorbents showed similar amounts of PAHs, slightly higher for samples with used Tenax TA, especially in the heaviest PAHs. Regarding time, 15 and 30 min did not show significant differences in the amount of PAHs analysed, and both times provided a good clean-up of the samples (quantities for most of PAHs < 0.1 ng). The shorter time (15 min) was selected for the re-conditioning of both adsorbents.

4.2 Desorption stage

As explained in section 3.1.3, the thermal desorption in the ATD is performed in two stages: desorption in the sample tube and desorption in the trap.

4.2.1 Primary desorption (tube desorption)

In the primary desorption, the PAHs are desorbed from the filter or adsorbent by the tube oven, and they are carried, through helium flow, from sample tube to cold trap (where the analytes concentrate).

The conditions in the tube oven during this stage are key to guarantee an efficient desorption, thus, parameters such as the temperature and the time in the tube oven and the desorption flow were studied to optimize this process.

For particulate phase tests, each portion of pre-conditioned quartz fibre filter was spiked with 20 ng of PAHs solution ($20 \text{ ng } \mu\text{L}^{-1}$) prepared in methanol from a certified mixture of 16 EPA PAHs ($2000 \mu\text{g mL}^{-1}$, SV Calibration MIX 5, Restek Corporation, USA) solution. In contrast, for gas phase tests, each Tenax GR and Tenax TA sample was spiked with 50 ng and 25 ng of PAHs solution, respectively.

Temperature

Temperature for tube desorption is selected as high as possible. However, the range of possible temperatures is restricted by the packing/sample matrix stability, the lability of the components of interest and the temperature limitations of the system. In this study, the use of adsorbents such as Tenax TA and GR and the recommendations of the ATD manufacturer allow a maximum temperature of 350°C in the tube desorption stage. This value was used as conditioning and re-conditioning temperature (see section 4.1) and this has to be at least 25°C higher than that required for the analysis (PerkinElmer, 2007). Due to this fact, the maximum value of the temperature considered for the tube desorption stage was 320°C .

Particulate phase

Desorption temperatures of 280, 300 and 320°C in the tube were tested for the particulate phase. For each temperature, sample tubes (n=5) loaded with a 1/8 portion of pre-conditioned quartz fibre filter were used.

The areas (in %) obtained for each of the 16 EPA PAHs at the three temperatures were studied (Figure 4.2). The results demonstrated that an increase in the temperature of the oven tube enhances the desorption of PAHs. This improvement was remarkable in high molecular weight PAHs (IP, DBahA and BghiP). Finally, a value of 320°C was selected as temperature in the first desorption stage for the particulate phase.

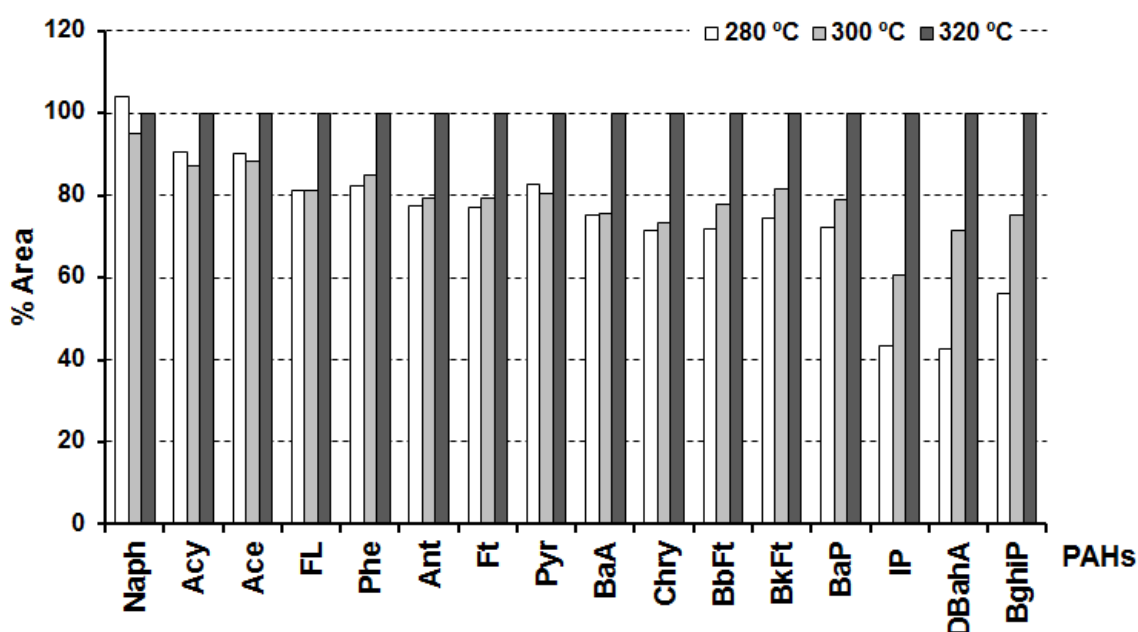


Figure 4.2. Area (in %) for each of the 16 EPA PAHs obtained in the study of the desorption temperature with tubes (n=5) loaded with filter.

Gas phase

The same values of desorption temperature (280, 300 and 320°C) were studied for tubes packed with Tenax GR and TA. In the test, for each temperature, tubes (n=5) packed with solid adsorbent (400 mg for Tenax GR and 250 mg for TA) were used.

The areas (in %) obtained for each of the 16 EPA PAHs at the three temperatures for Tenax GR (Figure 4.3) and TA (Figure 4.4) were studied.

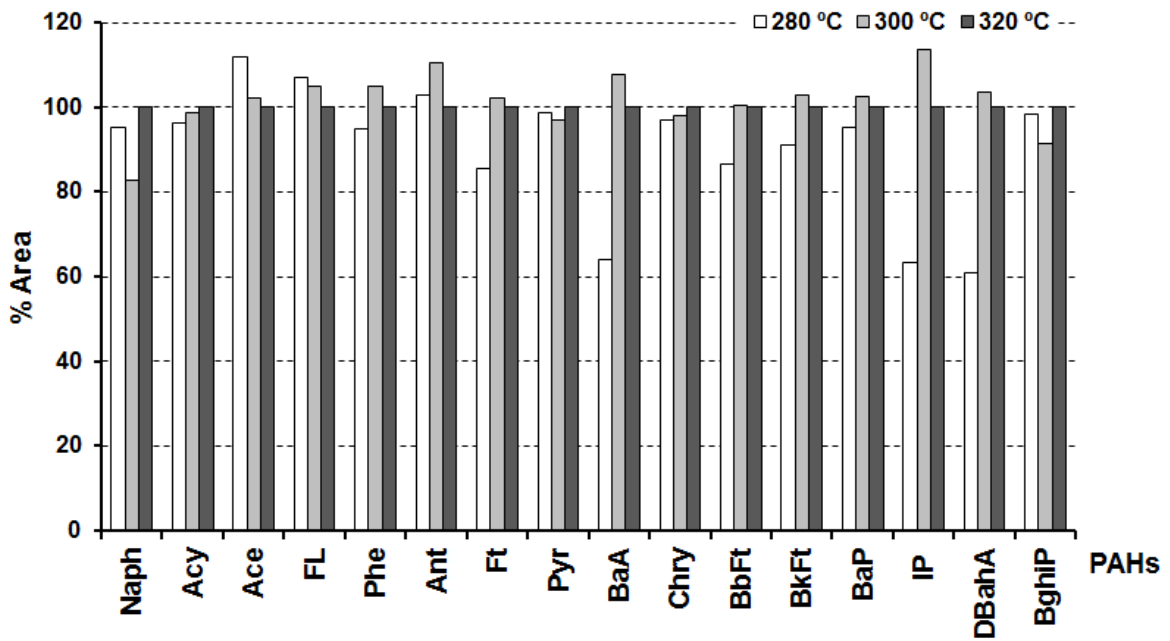


Figure 4.3. Area (in %) for each of the 16 EPA PAHs obtained in the study of the desorption temperature with tubes (n=5) packed with Tenax GR.

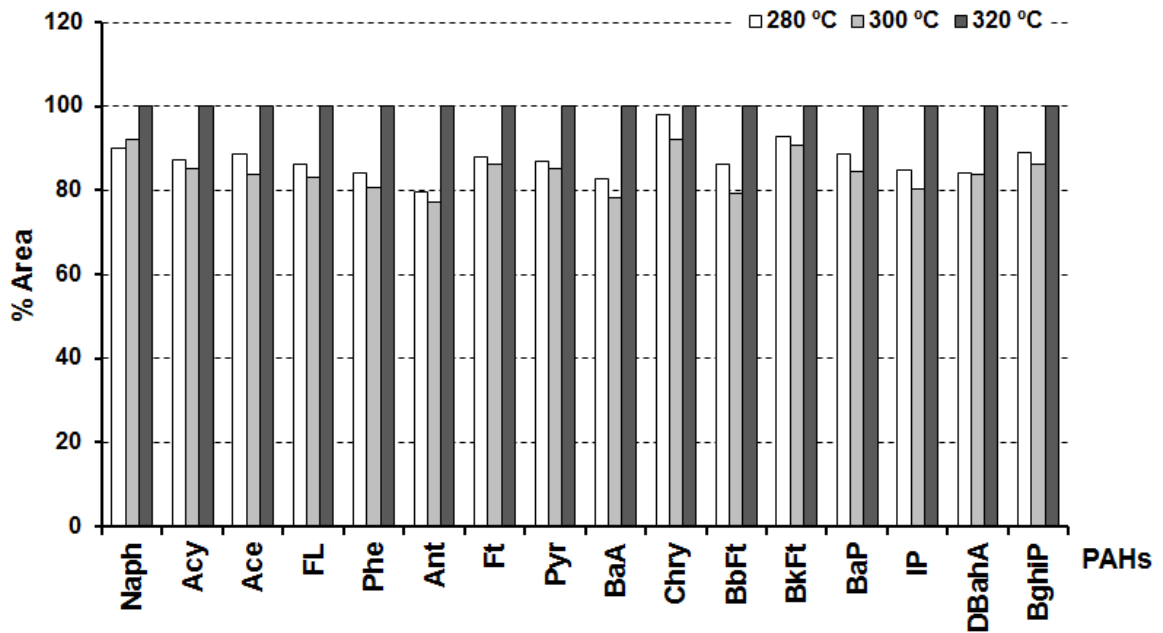


Figure 4.4. Area (in %) for each of the 16 EPA PAHs obtained in the study of the desorption temperature with tubes (n=5) packed with Tenax TA.

Observing the results, the samples with Tenax GR (Figure 4.3) showed high areas for the lightest PAHs at the three temperatures, especially at 300°C, whereas with the heavier PAHs, the highest temperatures (300 and 320°C) obtained better results. Finally, 300°C was selected as desorption temperature in the tube as it generally showed the highest areas in most PAHs. In the case of Tenax TA (Figure 4.4), the results clearly demonstrated that 320°C is the required temperature to obtain the highest efficiency in the tube desorption stage.

Time

Longer desorption times enable more efficient desorption, however, this could cause higher dispersion in the system and thus worsen compound detection. In order to find the best agreement between these two aspects, different desorption times were studied in both phases (particulate and gas).

Particulate phase

Three different desorption times were tested: 10, 15 and 20 min. Tubes (n=5) loaded with a 1/8 portion of a quartz fibre filter were studied for each. Figure 4.5 shows the area of chromatographic peak for each 16 of the EPA PAHs (in %) obtained for each desorption time.

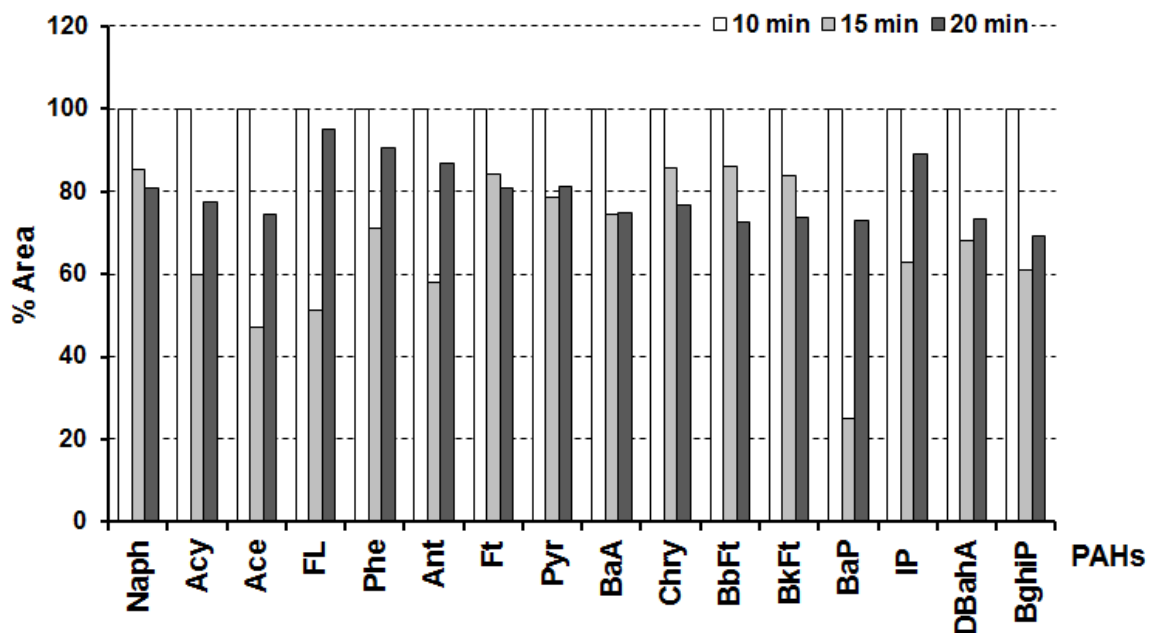


Figure 4.5. Area (in %) for each of the 16 EPA PAHs obtained in the study of desorption time with tubes (n=5) loaded with filter.

The lowest desorption time in the test (10 min) clearly showed significantly higher areas for most PAHs, indicating a more efficient desorption. This time was selected as desorption time in the tube.

Gas phase

Desorption times of 10, 20 and 30 min were studied with tubes packed with solid adsorbent (Tenax GR or Tenax TA). Figure 4.6 and 4.7 show the results of this test for Tenax GR and TA respectively.

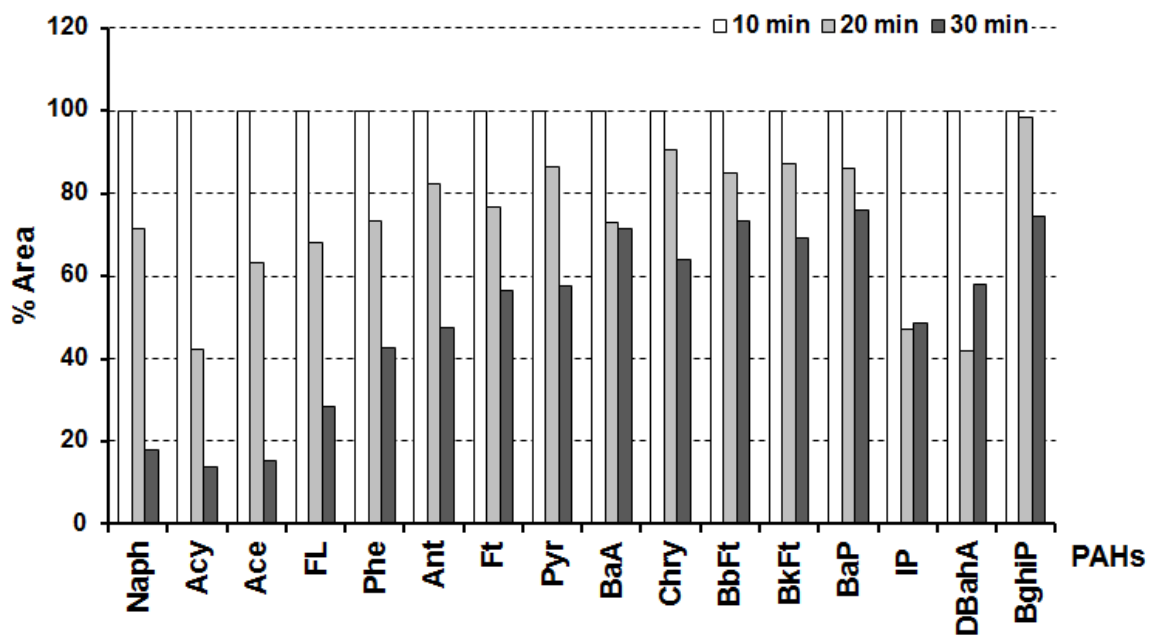


Figure 4.6. Area (in %) for each of the 16 EPA PAHs obtained in the study of desorption time with tubes (n=5) packed with Tenax GR.

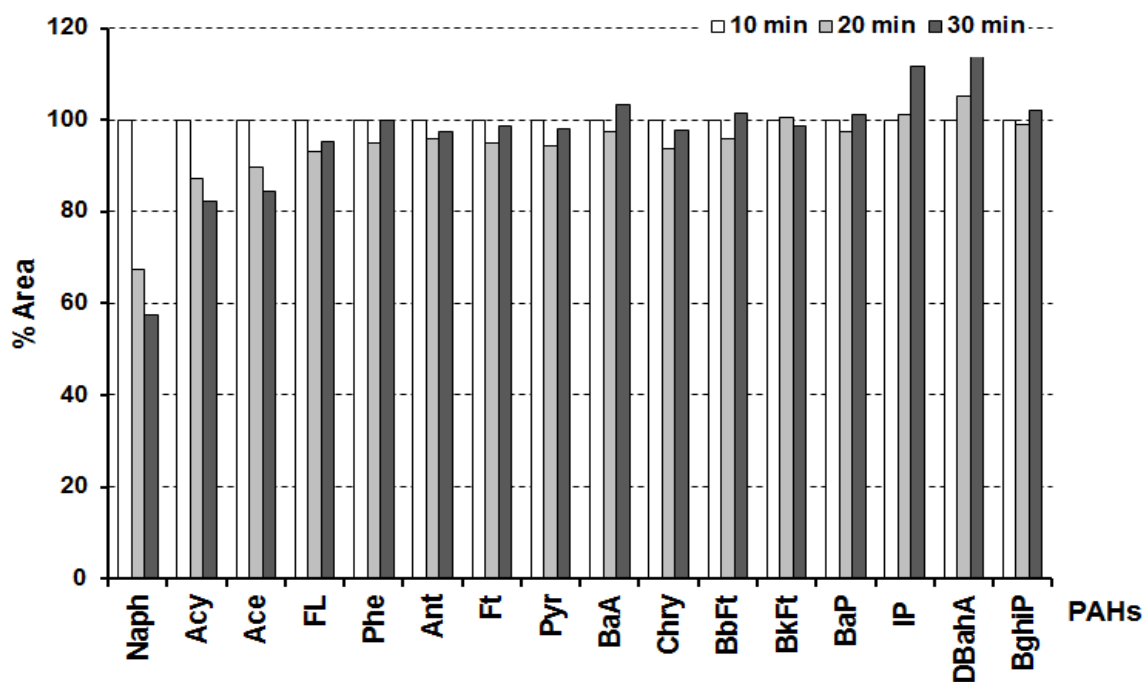


Figure 4.7. Area (in %) for each of the 16 EPA PAHs obtained in the study of desorption time with tubes (n=5) packed with Tenax TA.

In general, the desorption time tests with Tenax GR as packing matrix demonstrated that this parameter is more critical to the first desorption than the temperature (the differences in the area of chromatographic peak between the tested values were more significant). In contrast, the results for Tenax TA did not vary significantly with desorption time, except for the lightest PAHs where times longer than 10 min caused a distinct drop in the area of chromatographic peak. For both adsorbents (Tenax GR and TA) 10 min was the time with a more efficient desorption in the sample tube for most PAHs; thus this time was selected.

Desorption flow

The carrier gas flow that passes through sample tube guarantees the complete recovery of compounds from it and their transport until the trap (see section 3.1.4). Flows higher than 150 ml/min are not recommended, as they can generate problems in maintaining low temperatures in the trap zone during the first desorption stage (PerkinElmer, 2007). Different values of desorption flow were tested for the particulate and the gas phase.

Particulate phase

Desorption flows of 120 and 150 mL min⁻¹ were tested with a sampling tube loaded with filter (n=5 for each value). The area of chromatographic peak (in %) for low (2-3 rings: Naph, Ace, Acy, FL, Phe and Ant), middle (4 rings: Ft, Pyr, BaA and Chry) and high (5-6 rings: BbFt, BkFt, BaP, IP, DBahA and BghiP) molecular weight PAHs obtained by different desorption flows are shown in Figure 4.8.

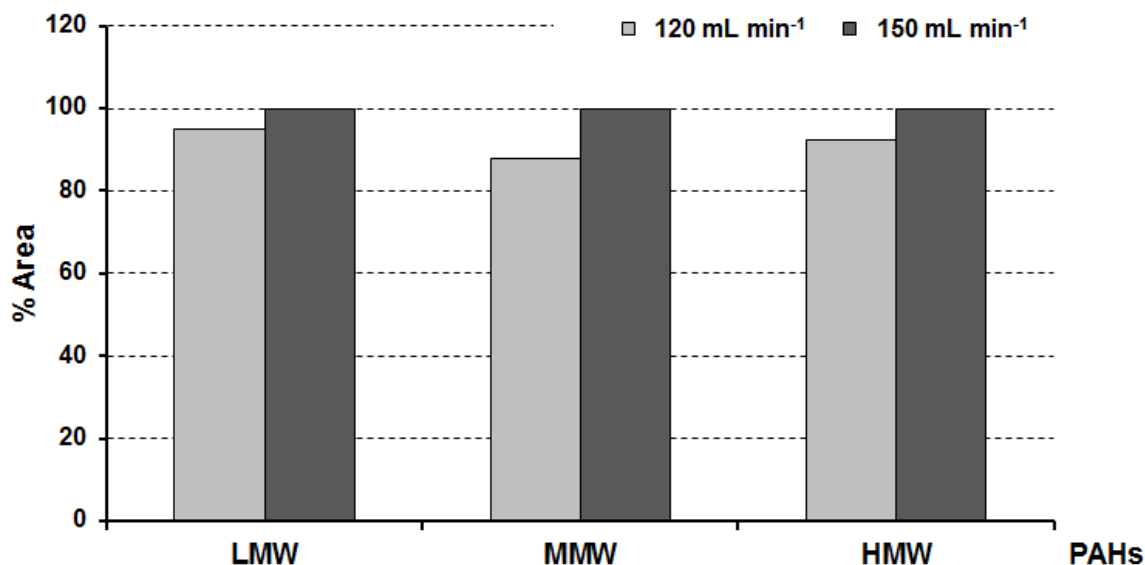


Figure 4.8. Area (in %) for LMW (low molecular weight), MMW (middle molecular weight) and HMW (high molecular weight) PAHs obtained with desorption flow of 120 and 150 mL min⁻¹.

Figure 4.8 shows that a flow of 150 mL min⁻¹ (the highest value allowed by the equipment) enables even more PAH desorption; therefore this flow was selected.

Gas phase

In this study, a group of 5 tubes packed with solid adsorbent were desorbed at different flows (80, 100 and 150 mL min⁻¹). The results with Tenax GR as adsorbent are presented in Figure 4.9, while those belonging to Tenax TA are shown in Figure 4.10.

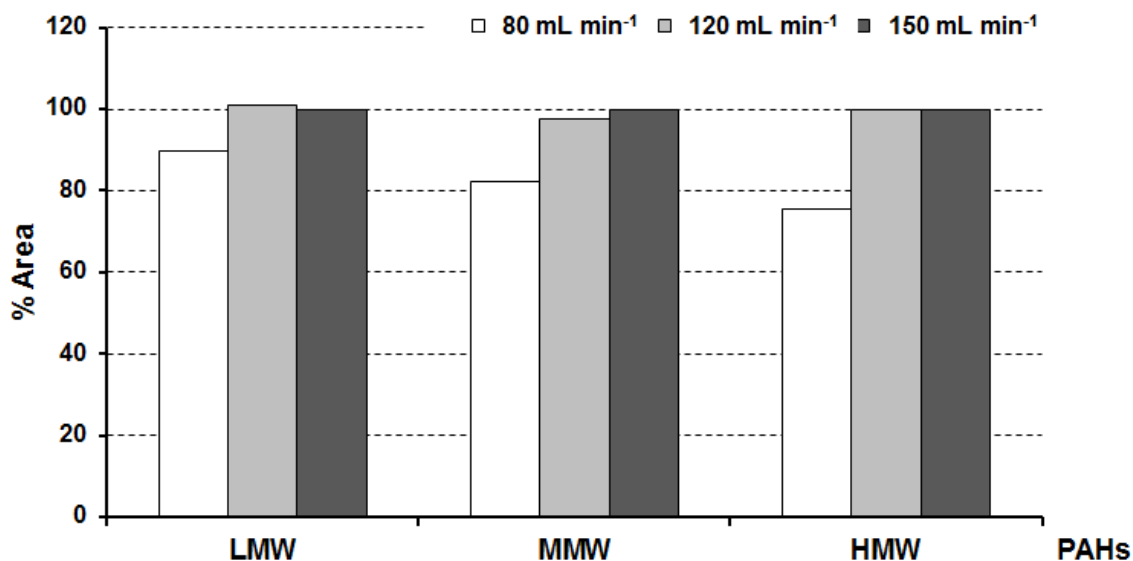


Figure 4.9. Area (in %) for LMW (low molecular weight), MMW (middle molecular weight) and HMW (high molecular weight) PAHs obtained in the study of desorption flow with tubes (n=5) packed with Tenax GR.

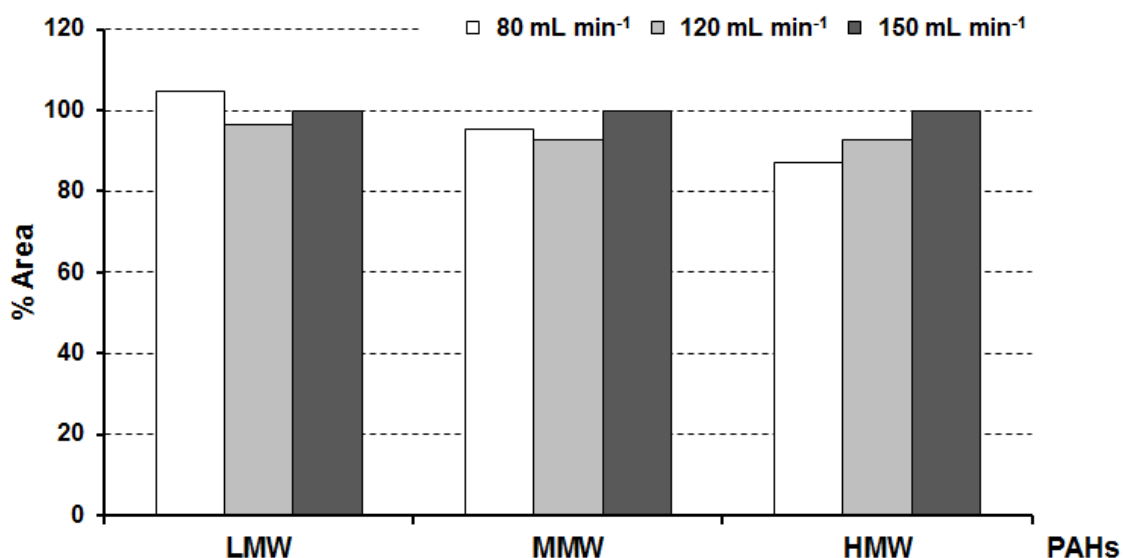


Figure 4.10. Area (in %) for LMW (low molecular weight), MMW (middle molecular weight) and HMW (high molecular weight) PAHs obtained in the study of desorption flow with tubes (n=5) packed with Tenax TA.

The first desorption stage with Tenax GR as packing matrix showed a significant improvement for desorption flows higher than 80 mL min⁻¹. Nevertheless, with higher

values, the areas of PAHs obtained by thermal desorption did not increase significantly, and were very similar to the results with 120 and 150 mL min⁻¹. Finally, the highest flow was selected as optimized value.

For Tenax TA, the results for MMW and HMW PAHs showed a similar pattern, but in this case the difference to the lowest flow was not as relevant. Again, the desorption flow of 150 mL min⁻¹ was chosen because it showed the highest areas for most PAHs.

Inlet split flow

As mentioned in the previous chapter, inlet split flow plays an important role during the primary desorption. This maintains a relatively high carrier gas flow through the sample tube, while at same time establishes a reasonably low flow through the cold trap, aiding the complete removal from the sample tube and analyte retention. After desorption, this flow also is used in the depressurization of samples tubes (PerkinElmer, 2007). Inlet splits of 0, 23 and 35 mL min⁻¹ were studied for tubes loaded with filter (n=5 for each flow) (Table 4.4).

Table 4.4. Area of chromatographic peak (in %) for each 16 EPA PAHs obtained in the study of the inlet split flow with tubes (n=5) loaded with filter.

PAHs	Inlet split flow		
	0 mL min ⁻¹	23 mL min ⁻¹	35 mL min ⁻¹
Naph	100	83	65
Acy	100	76	59
Ace	100	75	57
FL	100	73	54
Phe	100	73	56
Ant	100	72	56
Ft	100	72	63
Pyr	100	78	61
BaA	100	74	60
Chry	100	76	57
BbFt	100	79	63
BkFt	100	78	63
BaP	100	78	61
IP	100	77	56
DBahA	100	87	68
BghiP	100	91	78

Undoubtedly, the deactivation of the inlet split (0 mL min⁻¹) generated a significant improvement in PAH desorption (higher peak areas), because the complete sample, without purge, arrived in the cold trap. With the increase of inlet split to 23 and 35 mL min⁻¹, the sensitivity decreased (lower peak areas). Although an inlet split flow of 0 mL min⁻¹ showed the best results, it is recommended to activate this split in order to avoid the presence of unwanted compounds (permanent gases and water) in the trap. These could reduce the trap lifetime and interfere in the analysis. In order to find a compromise between these rules, intermediate flow (23 mL min⁻¹) was considered as the optimal value.

As the effect of the inlet split flow in the first desorption is independent of the used packing/sample matrix, the optimized value obtained by this test can be applied to both phases of PAHs.

4.2.2 Secondary desorption (trap desorption)

At the end of primary desorption in the tube, the second desorption in the Peltier trap starts automatically. This is quickly heated up to the maximum temperature, releasing the retained PAHs. A carrier gas flow, which passes through the trap during desorption, sweeps the compounds toward the chromatographic column.

In this section the trap temperature, the time, the desorption flow, and the outlet split flow were tested in order to optimize the secondary desorption. As the trap packing was the same for both PAH phases, the optimized values obtained by the tests of the tubes loaded with filter could be applied to the samples packed with adsorbent.

The tests were performed with the same tube conditions and amount of compounds as in the primary desorption for the particulate phase (n=5 spiked with 20 ng of each 16 EPA PAHs).

Temperature

The Peltier trap is a quartz tube packed with glass wool. The trap can be cooled electrically until -30°C and heated until 325°C. Its packing should be sufficiently weak to allow the complete desorption of the target analytes, and at the same time sufficiently strong to retain these when they are released in the primary desorption.

To enhance PAH desorption from the trap, its high temperature has to be as high as possible. This temperature depends on the trap packing and equipment stability as well as on the target compounds. In this study a value of 320°C (the value recommended by the manufacturer) was set, while its low temperature was tested for the next values: -15, -10 and -5 °C (Figure 4.11).

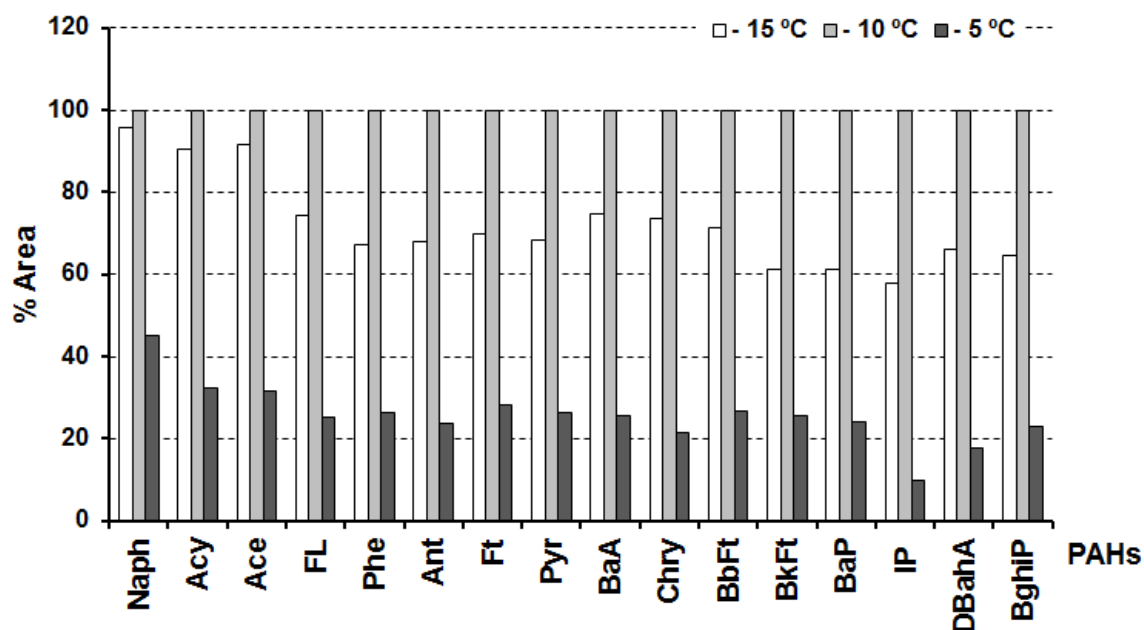


Figure 4.11. Area (in %) for each of the 16 EPA PAHs obtained in the study of the low trap temperature with tubes (n=5) loaded with filter.

The temperature in the Peltier trap is a critical parameter in secondary desorption, showing significantly changes in the sensitivity for different values. The temperature of -10 °C revealed the best results.

Time

Experiments with different trap heating durations (4, 6 and 12 min) were performed in order to evaluate the influence of this parameter on the analysis of the target compounds (Figure 4.12).

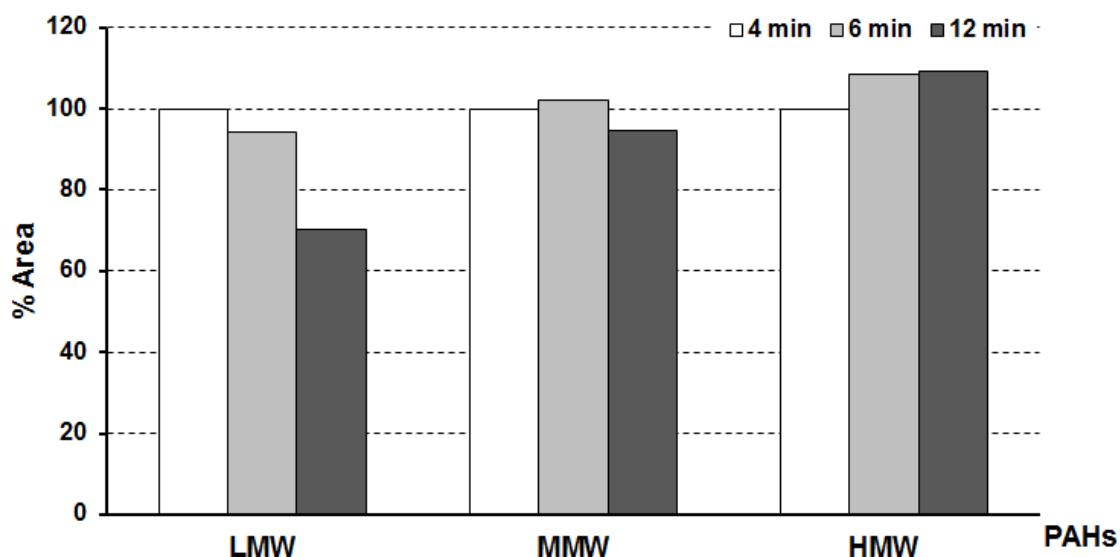


Figure 4.12. Area (in %) for LMW (low molecular weight), MMW (middle molecular weight) and HMW (high molecular weight) PAHs obtained in the study of the trap time with tubes (n=5) loaded with filter.

The results demonstrated that longer trap desorption times do not implicate a higher efficiency and consequently a better detection, 6 min showed a better response than 12. This is especially significant with the lightest PAHs (LMW) which could be affected by the exposure to high temperatures, generating losses. By contrast, the heavier PAHs (MMW and HMW) showed higher concentrations after longer trap desorption times, because they could need more time to be completely desorbed. Due to this, a trap duration of 6 min was selected as this value presented a good desorption for 16 target PAHs.

Outlet split flow

The outlet split flow plays a double function in the secondary desorption:

- It avoids system saturation and adapts the effluent flow to a capillary column flow, venting part of its effluent.
- It guarantees a high enough flow through the trap during desorption, facilitating the release of the analytes.

At least 10 mL min^{-1} of outlet split is necessary to minimize the air/water background on a mass spectrometer when atmospheric samples are analysed (PerkinElmer, 2007). Values of 10, 20 and 30 mL min^{-1} were tested (Figure 4.13)

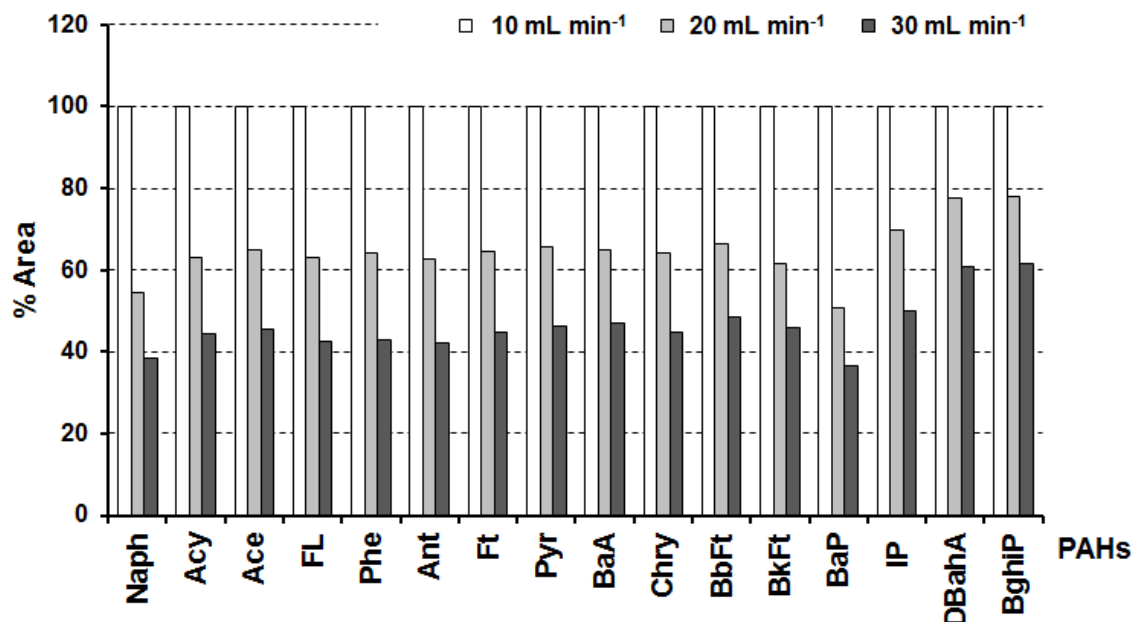


Figure 4.13. Area (in %) for each of the 16 EPA PAHs obtained in the study of the outlet split flow with tubes ($n=5$) loaded with filter.

The outlet split was a critical parameter in the trap desorption. The technique lost sensitivity with the increase of outlet split flow, which became significant between 10 and 20 mL min^{-1} . An outlet split flow of 10 mL min^{-1} was selected as optimal value for this parameter.

4.2.3 Desorption efficiency

The efficiency of the thermal desorption system for the determination of PAHs was studied for both phases (particulate and gas) with the optimized conditions selected in sections 4.2.1 and 4.2.2 (Table 4.5). To determine the efficiency in the tube (primary desorption), the sampling tubes (loaded and spiked with PAHs) were desorbed a second time. To test the efficiency in the trap (secondary desorption), an empty sampling tube was desorbed after each analysis.

Table 4.5. Optimized conditions for thermal desorption system

Primary desorption			Secondary desorption	
Parameter	Particulate	Gas	Parameter	
Tube temperature	320 °C	300 °C (Tenax GR) 320 °C (Tenax TA)	High trap temperature	320 °C
Time	10 min	10 min	Low trap temperature	-10 °C
Desorption flow	150 mL min ⁻¹	150 mL min ⁻¹	Time	6 min
Inlet split flow	23 mL min ⁻¹	23 mL min ⁻¹	Outlet split flow	10 mL min ⁻¹

The efficiency was calculated by the next expression

$$E(\%) = \left(\frac{A}{A+A^*} \right) \cdot 100 \quad (4.1)$$

where:

E is the efficiency in %.

A is the peak area of the analyte for the sampling tube analysis.

A* is the peak area of the analyte for second desorption of the sampling tube or for the empty tube.

Figure 4.14 shows the tube efficiencies obtained for each PAH in the particulate and gas (using Tenax TA as adsorbent) phases and the trap efficiency.

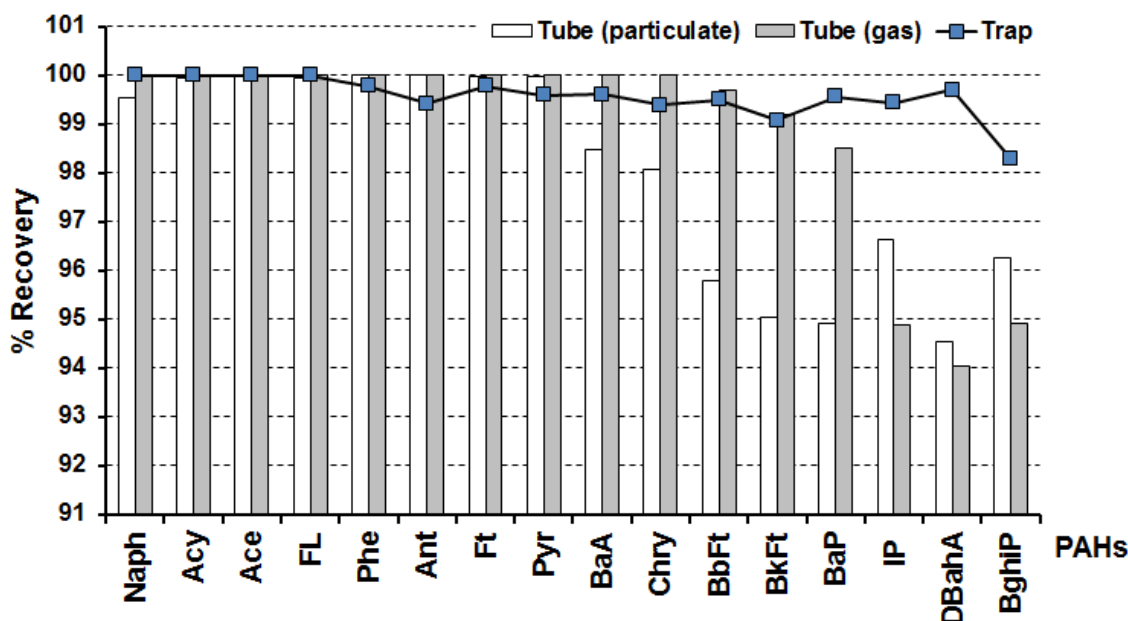


Figure 4.14. Recovery (in %) of the 16 EPA PAHs in the tube (particulate and gas phase) and in the trap.

The technique demonstrated a good efficiency with recoveries of the PAHs in the tube and trap higher than 94%.

4.3 Evaluation of analytical method

In this section analytical parameters such as linearity, precision, limit of detection and limit of quantification are calculated in order to evaluate the analytical method.

4.3.1 Linearity

The linearity of the ATD-GC/MS system was evaluated by calibration curve.

Particulate phase

During the calibration, 5 sampling tubes loaded with portions of quartz fibre filters were spiked with different amounts of PAHs (from 2.5 ng to 50 ng) and the same amount of deuterated compounds (50 ng). These samples were analysed to determine the linearity. Six-point calibration curves were plotted as the ratio of peak area

(analyte/deuterated) versus the ratio of amount in ng (analyte/deuterated). The determination coefficients were higher than 0.99 for most PAHs (Table 4.6), demonstrating that the technique has a good linearity in the determination of the particulate phase.

Gas phase

The calibration experiments were similar to the particulate phase. 10 sampling tubes packed with solid adsorbent (5 with Tenax GR and 5 with TA) were spiked with different amounts of PAHs (from 2.5 ng to 45 ng) and the same amount of deuterated compounds (25 ng). The ATIS system was used to introduce the compounds into the adsorbent in the gas phase. The technique, again, shows a good linearity with values of determination coefficients higher than 0.99 for most PAHs and for both adsorbents (Table 4.6).

Table 4.6. Coefficients of determination (R^2) of 16 EPA PAHs obtained in the linearity study for PAH particulate (filter) and gas phase (Tenax GR and TA).

PAHs	R^2		
	Filter	Tenax GR	Tenax TA
Naph	0.995	0.992	0.999
Acy	0.982	0.996	0.999
Ace	0.994	0.998	0.999
FL	0.988	0.989	0.999
Phe	0.981	0.997	0.996
Ant	0.998	0.991	0.996
Ft	0.996	0.999	0.999
Pyr	0.996	0.998	0.999
BaA	0.999	0.988	0.998
Chry	0.999	0.999	0.999
BbFt	0.999	0.997	0.996
BkFt	0.999	0.998	0.998
BaP	0.998	0.999	0.999
IP	0.991	0.963	0.993
DBahA	0.984	0.991	0.999
BghiP	0.993	0.999	0.996

Examples of calibration curves for BaP for each sampling media are shown in Figures 4.15, 4.16 and 4.17.

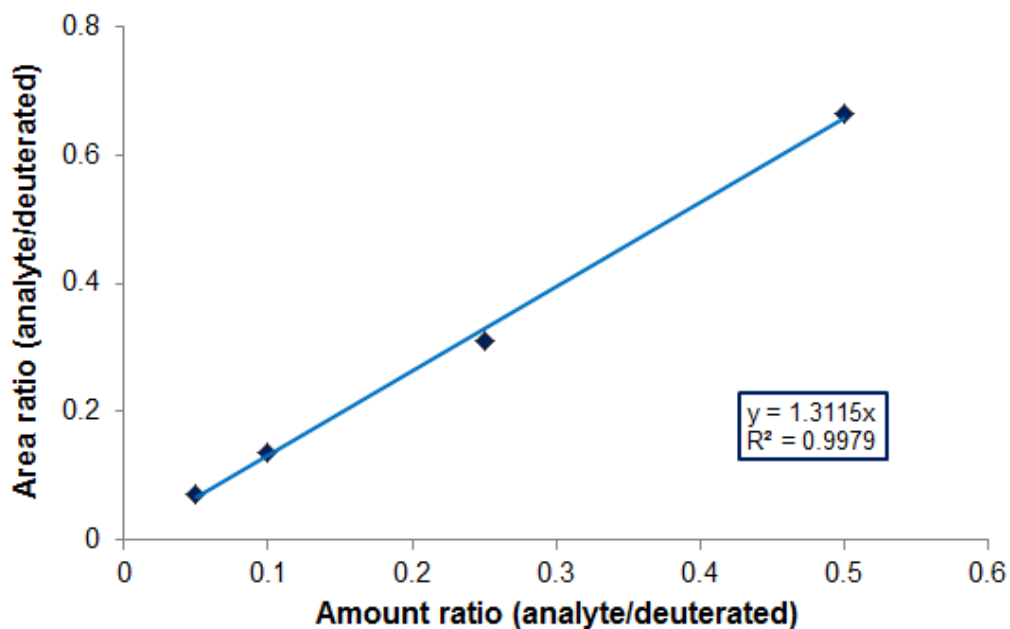


Figure 4.15. Calibration curve of BaP for particulate phase (filter).

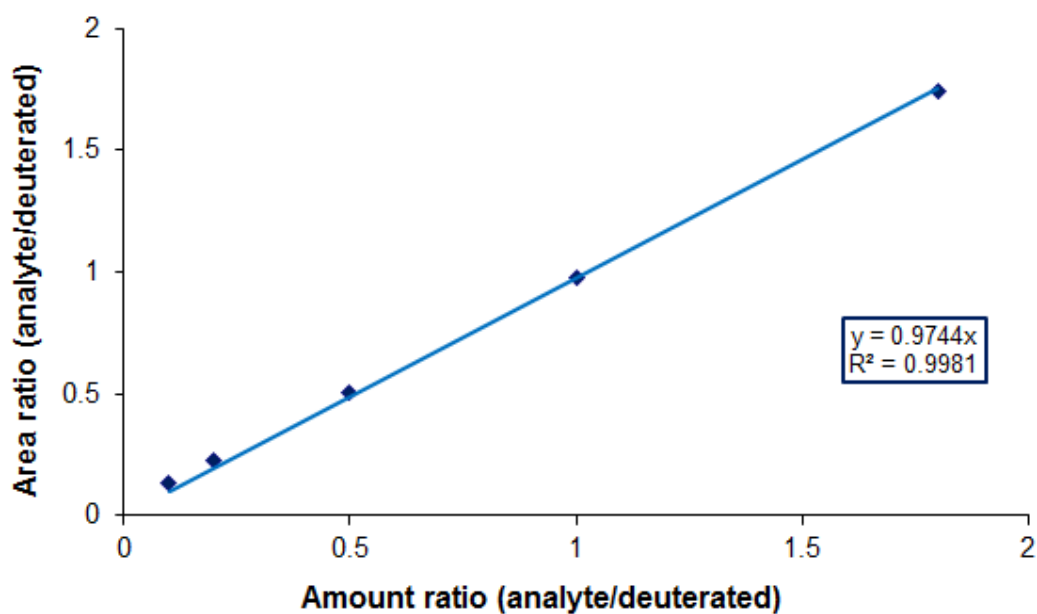


Figure 4.16. Calibration curve of BaP for gas phase (Tenax GR).

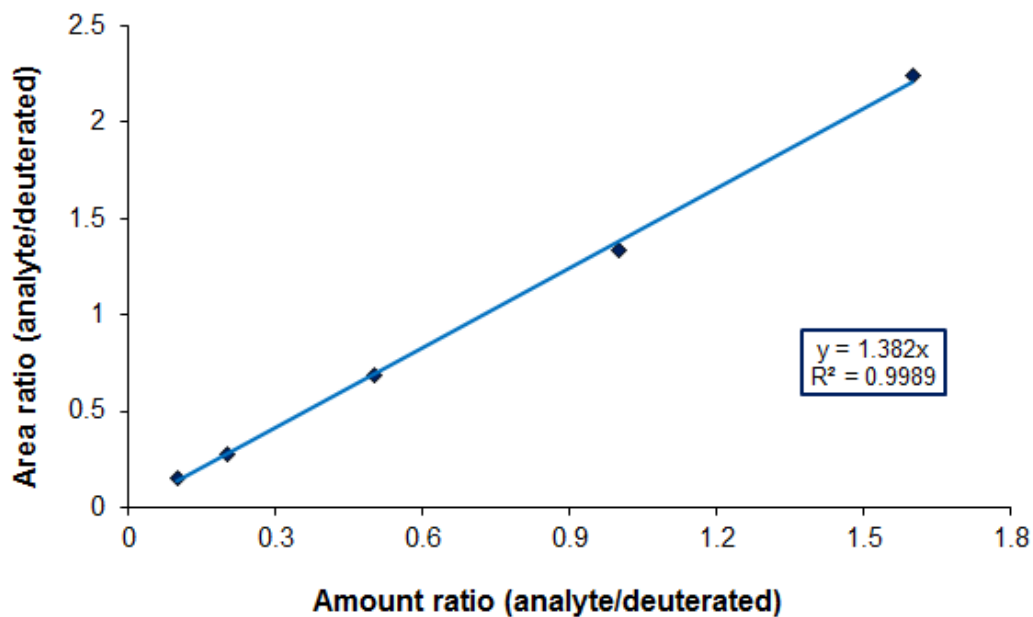


Figure 4.17. Calibration curve of BaP for gas phase (Tenax TA).

4.3.2 Precision

The precision of the analytical method was determined by the relative standard deviation (RSD).

Particulate phase

Replicate measurements of blank filters (n=10) spiked with the liquid standards for the fourth calibration point (25 ng for each PAH and 50 ng for each deuterated compound) were tested in order to determine the analytical precision of the technique (Table 4.7).

Gas phase

The test was performed by replicate measurements (n=10) for each studied adsorbent (Tenax GR and TA) spiked with the liquid standards for the fourth calibration point (25 ng for each PAH and deuterated compound).

Table 4.7. Relative standard deviation (RSD) in % of 16 EPA PAHs obtained in the precision study for the particulate (filter) and gas phase (Tenax GR and TA).

PAHs	RSD (%)		
	Filter	Tenax GR	Tenax TA
Naph	15.7	12.5	5.2
Acy	9.4	6.9	3.4
Ace	9.5	8.3	4.2
FL	11.1	5.8	7.8
Phe	8.9	13.6	3.4
Ant	9.1	9.7	3.7
Ft	11.1	7.9	3.7
Pyr	9.9	7.6	3.7
BaA	5.9	12.8	4.8
Chry	6.2	9.2	3.7
BbFt	5.8	8.8	4.4
BkFt	6.9	5.7	4.2
BaP	6.3	7.7	5.4
IP	10.8	11.2	5.5
DBahA	9.2	11.4	5.1
BghiP	4.9	4.2	4.3

The technique demonstrated good accuracy, with RSD < 10% for both phase. These results accomplish the quality objectives for ambient air PAHs stated by the ISO 12884:2000 (ISO, 2000), which establishes a precision of $\pm 25\%$. Between the two adsorbents, Tenax TA showed better precision with values of RSD < 6%.

4.3.3 Limit of detection, limit of quantification and method detection limit

The International Union of Pure and Applied Chemistry defined the limit of detection (LOD) as “the smallest amount of concentration of analyte in the sample that can be reliably distinguished from zero” (Thompson et al., 2002). The same federation described the limit of quantification (LQD) as “the concentration or amount below which the analytical method cannot operate with an acceptable precision”. Both limits are based on the signal-to-noise ratio; corresponding to a value of 3 and 10 times the noise level for LOD and LQD, respectively.

The method detection limit (MDL) is defined “as the minimum concentration of a substance that can be measured and reported with 99% confidence that the analyte concentration is greater than zero and is determined from analysis of a sample in a given matrix containing the analyte” (US-EPA, 2013). This method is based on standard deviation and is determined by the next expression:

$$\text{MDL} = t_{(n-1, 1-\alpha = 0.99)} \cdot \text{SD} \quad (4.2)$$

where:

- MDL is the method detection limit.
- $t_{(n-1, 1-\alpha = 0.99)}$ is the Student's t value appropriate for a 99% confidence level and a standard deviation estimate with n-1 degrees of freedom, n being the number of replicate samples.
- SD is the standard deviation of the replicate analyte.

In studies by other authors, the LOD values were commonly reported as the ultimate limit of detection although the MDL is more representative of actual or practical detection limits. The use of LOD values could be misleading in a practical sense, as they tend to be significantly lower than the MDL values (Foley and Dorsey, 1984; Kim and Kim, 2012).

In this study, the limits of target PAHs (MDLs, LODs and LQDs) for each phase (particulate and gas) were determined using liquid standards.

Particulate phase

MDLs, LODs and LQDs were calculated for each PAH in the lowest calibration standard (10 replicate sample tubes loaded with quartz filters and spiked with 2.5ng). The results obtained (Table 4.8) showed ranges of MDL from 0.19 ng to 1.67 ng (mean 0.75 ± 0.38 ng), of LOD from 0.01ng to 0.14 ng (mean 0.05 ± 0.04 ng) and of LQD from 0.02 ng to 0.47 ng (mean 0.16 ± 0.13 ng). The concentrations were calculated assuming the same sampling volume as in the application of the method (section 5), 240 m^3 (sampling flow of $30 \text{ m}^3 \text{ h}^{-1}$ during 8 h).

Table 4.8. Results of detection limit analysis of 16 EPA PAHs obtained by TD-GC/MS with sample tubes loaded with quartz filters.

PAHs	MDL		LOD		LQD	
	(ng)	(ng m ⁻³) ^a	(ng)	(ng m ⁻³) ^a	(ng)	(ng m ⁻³) ^a
Naph	1.32	5.51 · 10 ⁻³	0.14	5.84 · 10 ⁻⁴	0.47	1.95 · 10 ⁻³
Acy	0.81	3.39 · 10 ⁻³	0.04	1.60 · 10 ⁻⁴	0.13	5.32 · 10 ⁻⁴
Ace	0.86	3.57 · 10 ⁻³	0.03	1.37 · 10 ⁻⁴	0.11	4.56 · 10 ⁻⁴
FL	1.67	6.97 · 10 ⁻³	0.04	1.64 · 10 ⁻⁴	0.13	5.46 · 10 ⁻⁴
Phe	0.50	2.07 · 10 ⁻³	0.02	8.95 · 10 ⁻⁵	0.07	2.98 · 10 ⁻⁴
Ant	0.86	3.58 · 10 ⁻³	0.07	2.90 · 10 ⁻⁴	0.23	9.65 · 10 ⁻⁴
Ft	0.19	8.04 · 10 ⁻⁴	0.01	2.26 · 10 ⁻⁵	0.02	7.52 · 10 ⁻⁵
Pyr	0.33	1.37 · 10 ⁻³	0.01	4.30 · 10 ⁻⁵	0.03	1.43 · 10 ⁻⁴
BaA	0.27	1.13 · 10 ⁻³	0.01	2.71 · 10 ⁻⁵	0.02	9.04 · 10 ⁻⁵
Chry	0.98	4.09 · 10 ⁻³	0.03	1.39 · 10 ⁻⁴	0.11	4.63 · 10 ⁻⁴
BbFt	0.51	2.12 · 10 ⁻³	0.01	4.12 · 10 ⁻⁵	0.03	1.37 · 10 ⁻⁴
BkFt	0.67	2.79 · 10 ⁻³	0.10	4.17 · 10 ⁻⁴	0.33	1.39 · 10 ⁻³
BaP	0.69	2.87 · 10 ⁻³	0.06	2.46 · 10 ⁻⁴	0.20	8.20 · 10 ⁻⁴
IP	0.78	3.25 · 10 ⁻³	0.04	1.64 · 10 ⁻⁴	0.13	5.46 · 10 ⁻⁴
DBahA	0.81	3.39 · 10 ⁻³	0.11	4.74 · 10 ⁻⁴	0.38	1.58 · 10 ⁻³
BghiP	0.74	3.16 · 10 ⁻³	0.06	2.35 · 10 ⁻⁴	0.19	7.83 · 10 ⁻⁴
Mean	0.75	3.13 · 10 ⁻³	0.05	2.02 · 10 ⁻⁴	0.16	6.73 · 10 ⁻⁴
SD	0.38	1.56 · 10 ⁻³	0.04	1.67 · 10 ⁻⁴	0.13	5.55 · 10 ⁻⁴

^a Assuming a total sample volume of 240 m³ (30 m³ h⁻¹ during 8 h)

One aspect to consider is that the thermal desorption unit (PerkinElmer Turbomatrix 150 ATD) demanded continuous maintenance, especially the Peltier trap. A significant drop of the detection limits for the highest molecular weight PAHs (IP, DBahA and BghiP) is a sign that indicates that the Peltier trap needs maintenance.

Gas phase

In the determination of MDL, LOD and LOQ, 10 (packed with Tenax GR) and 9 (packed with Tenax TA) replicate sample tubes, spiked with the lowest calibration standard (2.5 ng) were used. The results obtained for Tenax GR and TA are shown in Table 4.9 and 4.10 respectively.

The samples with Tenax GR showed slightly higher limits than for TA and the particulate phase, with ranges of MDL from 0.29 ng to 1.65 ng (mean 0.70 ± 0.36 ng), of LOD from 0.02 ng to 0.92 ng (mean 0.15 ± 0.23 ng) and of LQD from 0.05 ng to 3.05 ng (mean 0.50 ± 0.81 ng).

For Tenax TA, MDL ranged from 0.24 ng to 0.48 ng (mean 0.34 ± 0.07 ng), while LOD and LOQ ranged from 0.01 ng to 0.25 ng (mean 0.06 ± 0.07 ng), and from 0.03 ng to 0.82 ng (mean 0.20 ± 0.25 ng), respectively.

Table 4.9. Results of detection limit analysis of 16 EPA PAHs obtained by TD-GC/MS with sample tubes packed with Tenax GR and Tenax TA.

PAHs	MDL (ng)		LOD (ng)		LQD (ng)	
	Tenax GR	Tenax TA	Tenax GR	Tenax TA	Tenax GR	Tenax TA
Naph	1.65	0.30	0.92	0.25	3.05	0.82
Acy	0.97	0.33	0.07	0.12	0.24	0.40
Ace	0.49	0.26	0.12	0.22	0.38	0.75
FL	0.71	0.24	0.04	0.06	0.15	0.20
Phe	0.68	0.32	0.15	0.04	0.51	0.14
Ant	0.63	0.37	0.41	0.05	1.36	0.17
Ft	0.54	0.32	0.02	0.02	0.05	0.06
Pyr	0.39	0.30	0.03	0.01	0.09	0.04
BaA	1.19	0.23	0.05	0.01	0.17	0.03
Chry	0.29	0.33	0.03	0.02	0.09	0.08
BbFt	0.57	0.31	0.02	0.01	0.06	0.03
BkFt	0.65	0.48	0.03	0.03	0.11	0.11
BaP	0.42	0.36	0.16	0.04	0.52	0.13
IP	1.14	0.45	0.06	0.01	0.20	0.04
DBahA	1.12	0.41	0.17	0.03	0.57	0.10
BghiP	0.58	0.44	0.08	0.03	0.25	0.09
Mean	0.70	0.34	0.15	0.06	0.50	0.20
SD	0.36	0.07	0.23	0.07	0.81	0.25

^a Assuming a total sample volume of 240 m³ (30 m³ h⁻¹ during 8 h)

The LODs for PAHs in the particulate phase obtained in this study showed similar values to those reported by other authors using the TD-GC/MS method (Table 4.10)

Table 4.10. LODs (in ng) obtained in this and other studies by the TD-GC/MS method (only for PAHs in the particulate phase).

PAHs	This study (filter)	(Gil-Moltó et al.; 2009)	(Cao et al.; 2013)
Naph	0.14	0.01	-
Acy	0.04	0.03	-
Ace	0.03	0.01	-
FL	0.04	0.01	-
Phe	0.02	0.01	0.16
Ant	0.07	0.03	0.12
Ft	0.01	0.01	0.06
Pyr	0.01	0.01	0.07
BaA	0.01	0.05	0.03
Chry	0.03	0.05	0.04
BbFt	0.01	0.05	0.06
BkFt	0.10	0.05	0.05
BaP	0.06	0.03	0.03
IP	0.04	0.03	0.04
DBahA	0.11	0.03	0.03
BghiP	0.06	0.03	0.07
Mean	0.05	0.03	0.06
SD	0.04	0.02	0.04

Also, the MDLs for PAHs in the particulate phase were compared to those obtained by solvent-based extraction. The TD-GC/MS method presented slightly lower limits (Table 4.11).

Table 4.11. Comparison of MDLs (in ng m⁻³) obtained in this study by TD-GC/MS to those obtained in other studies by the solvent-based extraction-GC/MS method (only for PAHs in the particulate phase). A sampling volume of 240 m³ was assumed in all studies.

PAHs	This study (filter)	(Adapted from Li et al., 2011)	(Adapted from Xu et al., 2012)	(Adapted from Delgado-Saborit et al., 2013)
Naph	5.51·10 ⁻³	0.06	-	5.42·10 ⁻⁴
Acy	3.39·10 ⁻³	0.06	6.05·10 ⁻³	1.08·10 ⁻³
Ace	3.57·10 ⁻³	0.05	6.23·10 ⁻³	1.62·10 ⁻³
FL	6.97·10 ⁻³	0.07	0.01	4.33·10 ⁻³
Phe	2.07·10 ⁻³	0.05	0.04	3.79·10 ⁻³
Ant	3.58·10 ⁻³	0.05	3.30·10 ⁻³	4.33·10 ⁻³
Ft	8.04·10 ⁻⁴	0.03	9.17·10 ⁻³	4.33·10 ⁻³
Pyr	1.37·10 ⁻³	0.03	0.01	4.87·10 ⁻³
BaA	1.13·10 ⁻³	0.03	0.01	5.42·10 ⁻³
Chry	4.09·10 ⁻³	0.03	3.12·10 ⁻³	4.87·10 ⁻³
BbFt	2.12·10 ⁻³	0.03	9.17·10 ⁻⁴	3.79·10 ⁻³
BkFt	2.79·10 ⁻³	0.02	8.25·10 ⁻⁴	4.33·10 ⁻³
BaP	2.87·10 ⁻³	0.03	8.98·10 ⁻⁴	0.01
IP	3.25·10 ⁻³	0.02	1.10·10 ⁻³	5.42·10 ⁻³
DBahA	3.39·10 ⁻³	0.03	3.21·10 ⁻⁴	4.87·10 ⁻³
BghiP	3.16·10 ⁻³	0.03	1.01·10 ⁻³	3.79·10 ⁻³
Mean	3.13·10 ⁻³	0.04	6.96·10 ⁻³	4.21·10 ⁻³
SD	1.56·10 ⁻³	0.01	9.29·10 ⁻³	2.13·10 ⁻³

4.4 Method Validation

NIST SRM 1649b urban dust was used to monitor the accuracy of the method when applied to atmospheric particulate samples.

To determine the accuracy and repeatability of the technique, approximately 10 mg of urban dust was weighted and placed on one-eighth of a 47 mm diameter quartz fibre filter which was rolled and put into a sampling tube. Silanized glass wool (Supelco Inc., Bellefonte, USA) was introduced at the end and the head of the sampling tubes in order to prevent system contamination. Prior to use, glass wool plugs and filters were heated at 350°C for 24 h to remove trace organic compounds. Before the analysis, filters were spiked with 1 µL of the deuterated PAH solution (25 ng µL⁻¹). Through this

process, 10 samples were prepared for validation. Table 4.12 shows the results obtained for each PAH, comparing the calculated concentration with the certified values.

Although the column used in this study demonstrated a good resolution for the 16 EPA PAHs, in the determination of real samples the presence of other PAHs can generate co-elution problems with the target compounds. The study carried out by R. Bordajandi et al. (2008) with the same type of column (with a non-polar stationary phase) demonstrated that some PAH pairs such as benzo[b]fluoranthene (BbFt)/benzo[j]fluoranthene (BjFt) and dibenzo[a,h]anthracene (DBahA)/dibenzo[a,c]anthracene (DBacA) co-elute in the same peak. The last certificate revision of SRM 1649b in December 2015 confirmed this fact, showing certificate values for the DBahA/DBacA pair (Table 4.12).

Table 4.12. TD-GC/MS method validation parameters for the 16 EPA PAHs in NIST SRM 1649b urban dust (n=10).

PAH	Experimental mean (ng) ^a	NIST certified value (ng) ^a	RSD (%)	Recovery (%)	Accuracy (%)
Naph	3694.41 ± 1082.45	26.75 ^b ± 2.98 ^b	46.33	13808.82	13708.82
Acy	6.97 ± 0.61	1.99 ^b ± 0.24 ^b	13.86	351.11	251.11
Ace	1.57 ± 0.19	2.03 ^b ± 0.41 ^b	19.53	77.25	-22.75
FL	2.06 ± 0.21	2.29 ^b ± 0.67 ^b	16.40	89.88	-10.12
Phe	42.70 ± 3.25	45.28 ^b ± 0.21 ^b	12.02	94.30	-5.70
Ant	12.59 ± 0.78	10.06 ^b ± 0.22 ^b	9.82	125.12	25.12
Ft	59.57 ± 3.22	67.91 ^b ± 0.41 ^b	8.56	87.71	-12.29
Pyr	51.76 ± 2.80	51.24 ± 1.44	8.56	101.01	1.01
BaA	19.26 ± 1.06	21.71 ^b ± 0.51 ^b	8.70	88.70	-11.30
Chry	26.17 ± 1.32	31.33 ± 0.29	7.95	83.52	-16.48
BbFt + BjFt	75.00 ± 6.17	81.34 ± 2.29	13.01	92.21	-7.79
BkFt	16.09 ± 1.37	17.51 ± 0.50	13.43	91.85	-8.15
BaP	20.38 ± 1.48	25.42 ^b ± 1.23 ^b	11.52	80.18	-19.82
IP	35.49 ± 1.94	29.74 ± 1.65	8.63	119.34	19.34
DBahA+DBacA	6.35 ± 0.93	6.02 ± 0.11	23.11	105.42	5.42
BghiP	37.21 ± 2.19	40.85 ^b ± 0.41 ^b	9.31	91.10	-8.90
Average^d	-	-	12.18	96.67	12.44

^a expanded uncertainty about the mean, with coverage factor, k = 2.

^b method dependent.

^c accuracy = (experimental value – certified value) × 100 / certified value.

^d except Naph and Acy.

The TD-GC/MS method showed good precision with mean RSD values of 12.18. The accuracy of the TD-GC/MS method ranged from -22.75% to 25.12%, while the average recovery efficiency was 96.67. These performance parameters of the TD-GC/MS method accomplish the quality objectives for ambient air PAHs stated by ISO 12884:2000 (ISO 2000), which establishes a precision of $\pm 25\%$, an accuracy of $\pm 20\%$, and a recovery efficiency between 75 and 125%. These requirements are accomplished for most PAHs; however there are some exceptions. The lowest molecular weight PAHs (Naph and Acy), with excessively high recoveries confirmed the overestimation of these compounds when analysed by the TD-GC/MS method. These compounds could suffer losses during the sample preparation due their high volatility. Besides, the presence of interfering compounds in the SRM and the low concentration of Acy could explain these overestimations. In consequence, both PAHs were excluded from the study.

In order to demonstrate the efficiency of the TD method as compared to other analytical methods, the conventional method (Soxhlet extraction) was also tested. In this study, between 300-500 mg of the NIST SRM 1694b urban dust were weighted and placed on one-eighth of a prebaked quartz fibre filter (a filter of 150 mm diameter heated in a muffle furnace at 350°C for 24h). Before folding the filter, it was spiked with 1 μL of a solution ($0.5 \text{ ng } \mu\text{L}^{-1}$) prepared in methanol from the recovery standards (decafluorobiphenyl, 4,4'-dibromooctafluorobiphenyl, 4,4'-dibromobiphenyl, Restek, $2000 \mu\text{g mL}^{-1}$ and indeno[1,2,3-cd]pyrene- d_{12} , Chiron, $100 \mu\text{g mL}^{-1}$). Through this process 7 samples were prepared for validation.

The samples were extracted with hexane in the Büchi Extraction System B-811 using Soxhlet Warm mode. This mode increases the solubility of the analytes, allowing an optimal extraction in 3 hours. The conditions of the extractor system in this study were summarized in section 3.

After the extraction process, the extracts of 5 mL were concentrated by a stream of dry nitrogen to a volume less than 0.5 mL. Finally, these extracts were diluted to 1.5 mL with methanol and 25 μL of a deuterated PAHs solution ($20 \text{ ng } \mu\text{L}^{-1}$) were spiked.

2 μL aliquots from each extract were injected into the GC/MS with split mode. Table 4.13 collects the timed events and the oven program used in the GC/MS during the validation of the Soxhlet method.

Table 4.13. Timed events and oven program used in direct injector mode.

Timed event			Oven program			
Event	Flow (mL min ⁻¹)	Time (min)	Ramp	Rate (°C min ⁻¹)	Temperature (°C)	Hold (min)
Split	0	-0.51	Initial	0	45	1
Split	50	1	1	20	200	0
Split	20	5	2	4	320	5

The average concentration (ng) obtained for each PAH and their values of precision and recovery are collected in Table 4.14. As in the validation of the TD method, the concentrations of BbFt and DBahA were considered as BbFt/BjFt and DBahA/DBacA, respectively, because these pairs co-elute in the same peak. The results showed a good recovery for 4, 5 and 6-ring PAHs with values between 72.84 and 131.25%; whereas the lightest PAHs (2 and 3-ring PAHs), except Phe, showed low recovery (< 70%). The loss of these analytes during the extraction process in the Soxhlet Warm mode (section 3.3) could be the main reason for these low recoveries. In the case of DBahA, although its co-elution with DBacA was considered, its recovery continued to be high (>200%). This indicates an overestimation in the determination of this compound by the Soxhlet process. Regarding precision and accuracy, the Soxhlet extraction-GC/MS showed worse results, with an average precision of 34.85 and values of accuracy $\geq \pm 20\%$ for some PAHs.

Table 4.14. Soxhlet extraction-GC/MS method validation parameters for the 16 EPA PAHs in SRM 1649b (n=7).

PAH	Experimental mean (ng) ^a	NIST certified value (ng) ^a	RSD (%)	Recovery (%)	Accuracy (%)
Naph	67.32 ± 18.60	391.64 ^b ± 35.43 ^b	33.84	17.19	-82.81
Acy	20.17 ± 5.91	79.90 ^b ± 9.48 ^b	35.86	25.24	-74.76
Ace	24.99 ± 5.41	81.56 ^b ± 16.48 ^b	26.53	30.65	-69.35
FL	32.60 ± 9.18	92.32 ^b ± 14.42 ^b	34.49	35.31	-64.69
Phe	1215.35 ± 331.78	1668.42 ^b ± 24.72 ^b	33.43	72.84	-27.16
Ant	104.55 ± 25.71	169.12 ^b ± 1.65 ^b	32.53	61.82	-38.18
Ft	2392.52 ± 559.83	2573.91 ^b ± 32.96 ^b	30.95	92.95	-7.05
Pyr	1914.67 ± 398.71	2054.18 ± 57.68	27.55	93.21	-6.79
BaA	808.28 ± 148.46	870.34 ^b ± 20.60 ^b	24.30	92.87	-7.13
Chry	1632.01 ± 464.16	1256.02 ± 11.54	37.62	129.94	29.94
BbFt+BjFt	3144.07 ± 800.72	3260.70 ± 91.88	33.69	96.42	-3.58
BkFt	921.46 ± 319.73	702.05 ± 20.19	45.90	131.25	31.25
BaP	1019.58 ± 271.00	1018.84 ^b ± 98.88 ^b	35.16	100.07	0.07
IP	1109.96 ± 296.97	1192.08 ± 65.92	35.39	93.11	-6.89
DBahA+DBacA	507.81 ± 176.18	241.30 ± 4.53	45.90	363.16	263.16
BghiP	2143.65 ± 580.24	1777.81 ^b ± 32.96 ^b	35.81	120.58	20.58
Average^d	-	-	34.85	120.69	36.82

^a expanded uncertainty about the mean, with coverage factor, k = 2.

^b method dependent.

^c accuracy = (experimental value – certified value) × 100 / certified value.

^d except Naph, Acy, Ace and FL.

Comparing both methods, the TD-CG/MS method demonstrated a better performance (good recovery, precision and accuracy) for the determination of PAHs. By contrast, the manipulation of the samples in the Soxhlet process meant losses of the light PAHs (2 and 3-ring) and an overestimation of some PAHs, especially of the DBahA.

4.5 Uncertainty of the method

According to the international standard (ISO 20988:2007) the uncertainty of a measurement is defined as “a parameter associated with the result of a measurement that characterizes the dispersion of the values that could reasonably be attributed to the measurand”. Estimation of uncertainty leads to better measurement reliability, renders data from inter-laboratory studies comparable, and helps to assess the

statistical significance of the difference between the measurement and a relevant reference value.

In this study the PAH concentrations in the air samples, expressed in ng m^{-3} , are obtained from the following equation:

$$\text{Concentration} (\text{ng} \cdot \text{m}^{-3}) = \frac{C (\text{ng} \cdot \text{m}^{-2}) \cdot A_{\text{sample}} (\text{m}^2)}{V_{\text{air}} (\text{m}^3)} \quad (4.3)$$

where:

- C is the concentration of the target compound obtained from the calibration, in ng m^{-2} .
- A_{sample} is the final area of the analysed filter, in m^2 .
- V_{air} is the volume of the air sampled, in m^3 .

According to Eq. 4.3, the uncertainty sources that contributed to the determination of particle PAHs in air by TD-GC/MS are:

- Calibration curves (Cal).
- Volume of sample (V_s).
- Volume of air (V_{air}).
- Recovery (R).

The uncertainty associated with the method (u_{comb}) was calculated by combining the uncertainty derived from each source (Eq. 4.4).

$$\left(\frac{u_{\text{comb}}}{C} \right)^2 = \left(\frac{u(\text{Cal})}{C} \right)^2 + \left(\frac{u(V_s)}{V_s} \right)^2 + \left(\frac{u(V_{\text{air}})}{V_{\text{air}}} \right)^2 + \left(\frac{u(R)}{R} \right)^2 \quad (4.4)$$

where:

- $u(\text{Cal})$ is the calibration uncertainty.
- $u(V_s)$ is the uncertainty derived from sample volume.
- $u(V_{\text{air}})$ is the uncertainty derived from air volume.
- $u(R)$ is the uncertainty derived from recovery.
- C is the amount of analyte, in ng.
- V_s is the volume of sample injected, in μL .
- V_{air} is the volume of air sampled, in m^3 .
- R is the recovery, dimensionless.

In order to compare TD-GC/MS to the conventional method, the uncertainty derived from the Soxhlet extraction-GC/MS was also calculated.

4.5.1 Uncertainty derived calibration curves $(u(\text{Cal})/C)^2$.

The uncertainty associated with calibration, $u(\text{Cal})$, was determined by taking the square root of the sum of the squares of the uncertainty derived from adjustment and preparation (standard and internal standard solutions) (Eq. 4.5).

$$\left(\frac{u(\text{Cal})}{C}\right)^2 = \left(\frac{u(C_x)}{C_x}\right)^2 + \sum_{i=1}^n \left(\frac{u(\text{std})}{C_{\text{std}}}\right)^2 + \sum_{j=1}^m \left(\frac{u(\text{is})}{C_{\text{is}}}\right)^2 \quad (4.5)$$

where:

- $(u(C_x)/C_x)^2$ is the uncertainty derived from linear least squares adjustment.
- $(u(\text{std})/C_{\text{std}})^2$ is the uncertainty derived from standard solution preparation.
- $(u(\text{is})/C_{\text{is}})^2$ is the uncertainty derived from internal standard solution preparation.
- n is the level of target compounds in the calibration curve.

m is the level of deuterated compounds in the calibration curve.

Uncertainty derived from linear least squares adjustment $(u(C_x)/C_x)^2$.

The uncertainty derived from the linear least squares adjustment is mainly due to the variability in the responses shown by the instrument, and it is evaluated from standard deviations of slope and intercept in calibration line. The relative uncertainty of the predicted analyte concentration $(u(C_x)/C_x)$ from linear least squares adjustment was calculated applying the following equation:

$$\left(\frac{u(C_x)}{C_x}\right)^2 = \frac{u_y}{(y-b)^2} + \frac{u_b}{(y-b)^2} + \frac{u_m}{(m)^2} \quad (4.6)$$

where:

- y is the mean value of the analytical response of the calibration curve.
- u_y is the uncertainty of the response deduced from its standard deviation (s_y/\sqrt{n}) , where n is the number of calibration points.

- b is the y-intercept of the calibration curve.
- u_b is the uncertainty of y-intercept deduced from its standard deviation (s_b/\sqrt{n}) , where n is the number of calibration points.
- m is the slope.
- u_m is the uncertainty of slope deduced from its standard deviation (s_m/\sqrt{n}) , where n is the number of calibration points.

In both methods (TD-GC/MS and Soxhlet extraction-GC/MS), calibration curves of five concentration levels were used to calculate this uncertainty. For example, $(u(C_x)/C_x)^2$ for BaP in TD-GC/MS was calculated in the following way:

- A calibration curve of BaP was performed (Figure 4.18), showing a slope value of 1.152 and a correlation coefficient of 0.998. The mean value of the area ratio (the analytical response of curve) was 0.831.

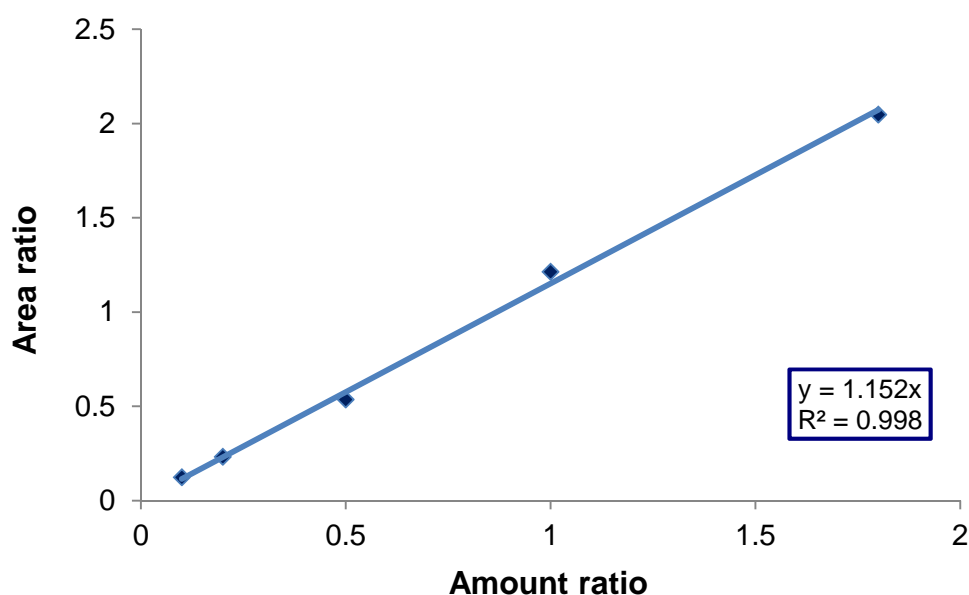


Figure 4.18. Calibration curve of BaP in TD-GC/MS used in the determination of $(u(C_x)/C_x)^2$.

- The uncertainties of area ratio (analytical response) and of slope for BaP in this curve were determined.

$$u_y = \frac{0.039}{\sqrt{5}} = 0.017 \quad (4.7)$$

$$u_m = \frac{0.018}{\sqrt{5}} = 8.05 \cdot 10^{-3} \quad (4.8)$$

- Finally, the relative ($u(C_x)/C_x$) for BaP was determined by Eq. 4.6.

$$\left(\frac{u(C_x)}{C} \right)^2 = \frac{(0.017)^2}{(0.831)^2} + \frac{(8.05 \cdot 10^{-3})^2}{(1.152)^2} = 4.91 \cdot 10^{-4} \quad (4.9)$$

$$\left(\frac{u(C_x)}{C} \right) = \left(\sqrt{4.91 \cdot 10^{-4}} \right) = 0.02 \quad (4.10)$$

Table 4.15 shows the relative uncertainty associated with the calibration curve for each PAH in both methods (TD-GC/MS and Soxhlet extraction-GC/MS). The results ranged between 0.02 and 0.06 for TD-GC/MS, and between 0.01 and 0.04 for Soxhlet extraction-GC/MS. This method showed lower uncertainty for the heaviest PAHs.

Table 4.15. Relative ($u(C_x)/C_x$) for each PAH in TD-GC/MS and Soxhlet extraction-GC/MS method.

PAH	$(u(C_x)/C_x)$	
	TD-GC/MS	Soxhlet extraction-GC/MS
Ace	0.04	-
FL	0.06	-
Phe	0.02	0.03
Ant	0.03	0.01
Ft	0.03	0.01
Pyr	0.03	0.03
BaA	0.02	0.03
Chry	0.04	0.02
BbFt	0.03	0.01
BkFt	0.04	0.02
BaP	0.02	0.04
IP	0.05	0.02
DBahA	0.05	0.03
BghiP	0.03	0.02

Uncertainty derived from standard solution preparation $(u(\text{std})/C_{\text{std}})^2$.

This uncertainty is a combination of the uncertainty of the glassware used and stock solutions. In this study, the standards were prepared using syringes (syr) and volumetric flask (flask). Eq. 4.11 and 4.12 were used to determine $(u(\text{std})/C_{\text{std}})^2$.

$$\left(\frac{u(\text{std})}{C_{\text{std}}}\right)^2 = \left(\frac{u(\text{stock})}{C_{\text{stock}}}\right)^2 + \left(\frac{u(f)}{f}\right)^2 \quad (4.11)$$

$$u(f) = \sqrt{\left(\frac{u(\text{syr})}{V_{\text{syr}}}\right)^2 + \left(\frac{u(\text{flask})}{V_{\text{flask}}}\right)^2} \quad (4.12)$$

where

- $u(f)$ is the uncertainty of the dilution factor, dimensionless.
- $u(\text{syr})$ is the uncertainty of the syringe.
- $u(\text{stock})$ is the uncertainty of the stock solution.
- $u(\text{flask})$ is the uncertainty of the volumetric flask.

- f is the dilution factor, dimensionless.
- C_{stock} is the amount of analyte in the stock solution, in ng.
- V_{syr} is the volume of the syringe, in μL .
- V_{flask} is the volume of the flask, in μL .

The $u(\text{syr})$ and $u(\text{flask})$ were calculated as the combination of the uncertainty coming from the calibration of the tool ($u(\text{syr}_{\text{cal}})$ or $u(\text{flask}_{\text{cal}})$), and the uncertainty source from the temperature ($u(T)$) (Eq. 4.13 and 4.14).

$$u(\text{syr}) = \sqrt{(u(\text{syr}_{\text{cal}}))^2 + (u(T))^2} \quad (4.13)$$

$$u(\text{flask}) = \sqrt{(u(\text{flask}_{\text{cal}}))^2 + (u(T))^2} \quad (4.14)$$

The uncertainties from the calibration of the item ($u(\text{syr}_{\text{cal}})$ and $u(\text{flask}_{\text{cal}})$) were calculated by using manufacturer's data (Table 4.16), assuming a rectangular distribution.

According to the Eurachem/Citac guide (2012), the temperature effect is the result of the variation in temperature in the laboratory which is generally accepted as $\pm 3^\circ\text{C}$ and can be calculated by the next equation:

$$u(T) = \frac{3 \cdot V \cdot Q}{1.73} \quad (4.15)$$

where

- $u(T)$ is the standard uncertainty of the temperature.
- V measured volume, in μL .
- Q is the coefficient of volume expansion of the solvent used in the preparation, in $^\circ\text{C}^{-1}$.

Table 4.16 introduces the manufacturer's specification data of items used to prepare the standard solution.

Table 4.16. The manufacturer's specification data of lab tools, PAH standard and solvents

Item	Amount	Manufacturer's specification
Volumetric flask	1mL	$\pm 2.50 \times 10^{-2} \text{ mL}^a$
Syringe	2; 25; 50; 125; 250; 500 μL	$\pm 1 \%$ nominal volume ^a
Internal Standard 16 EPA-PAHs	2000 $\mu\text{g mL}^{-1}$	$\pm 11.74 \text{ ng } \mu\text{L}^{-1}^b$
Internal deuterated PAHs	200 $\mu\text{g mL}^{-1}$	$\pm 4 \text{ ng } \mu\text{L}^{-1}^a$
Methanol thermal expansion (at 25°C)	-	$1.15 \times 10^{-3} \text{ }^\circ\text{C}^{-1}$
Methylene thermal expansion (at 25°C)	-	$1.44 \times 10^{-3} \text{ }^\circ\text{C}^{-1}$
Toluene thermal expansion (at 25°C)	-	$1.11 \times 10^{-3} \text{ }^\circ\text{C}^{-1}$
n-Hexane thermal expansion (at 25°C)	-	$1.14 \times 10^{-3} \text{ }^\circ\text{C}^{-1}$

^a accuracy.^b expanded uncertainty (95%).

In this study, the stock solution for the TD-GC/MS method was the standard certificated mixture of 16 EPA PAHs (SV Calibration Mix 5, Restek, 2000 $\mu\text{g mL}^{-1}$). To prepare the calibration standards (solutions of 2.5, 5, 12.5, 25, and 45 $\text{ng } \mu\text{L}^{-1}$), two dilution stages were necessary. In the first, 50 μL were removed from the stock solution and diluted in 1mL of methanol, obtaining a 100 $\text{ng } \mu\text{L}^{-1}$ solution. Subsequently, and depending on the target concentration of calibration solution, different volumes were removed from it and diluted with 1 mL of methanol (e.g. to obtain a concentration of 2.5 $\text{ng } \mu\text{L}^{-1}$; 25 mL of a 100 $\text{ng } \mu\text{L}^{-1}$ solution were necessary). These two dilution stages should be considered in the expression of uncertainty in the dilution, where the suffixes 1 and 2 mark the dilution stage (Eq.4.16).

$$u(f) = \sqrt{\left(\frac{u(\text{syr})_1}{V_{\text{syr}_1}}\right)^2 + \left(\frac{u(\text{flask})_1}{V_{\text{flask}_1}}\right)^2 + \left(\frac{u(\text{syr})_2}{V_{\text{syr}_2}}\right)^2 + \left(\frac{u(\text{flask})_2}{V_{\text{flask}_2}}\right)^2} \quad (4.16)$$

The uncertainty associated with the standard solution preparation was determined for each calibration level.

Tables 4.17 and 4.18 summarize the uncertainties obtained for each dilution stage and the calibration solution in the preparation of standard solutions.

Table 4.17. Uncertainty associated with syringe and volumetric flask during the standard solution preparation for each dilution stage (TD-GC/MS method).

Dilution stage	Solution concentration (ng μL^{-1})	V_{syr} (μL)	$u(\text{syr}_{\text{cal}})$ (μL)	$u(T)$ (μL)	$u(\text{syr})$ (μL)
1 st	100	50	0.289	0.125	0.315
2 nd	2.5	25	0.144	0.050	0.153
2 nd	5	50	0.289	0.100	0.306
2 nd	12.5	125	0.772	0.250	0.764
2 nd	25	250	1.443	0.501	1.528
2 nd	45	450	2.598	0.901	2.750

Dilution stage	Solution concentration (ng μL^{-1})	V_{flask} (μL)	$u(\text{flask}_{\text{cal}})$ (μL)	$u(T)$ (μL)	$u(\text{flask})$ (μL)
1 st ; 2 nd	100; 2.5; 5; 12.5; 25; 45	1000	14.434	2	14.572

Table 4.18. Uncertainties associated with dilution and standard solution preparation for each calibration solution (TD-GC/MS method).

Solution concentration (ng μL^{-1})	f	$u(f)$	C stock (ng μL^{-1})	$u(\text{stock})$ (ng μL^{-1})	$(u(\text{std})/C_{\text{std}})^2$
2.5	800	0.022	2000	5.814	$8.45 \cdot 10^{-6}$
5	400	0.022	2000	5.814	$8.45 \cdot 10^{-6}$
12.5	160	0.022	2000	5.814	$8.47 \cdot 10^{-6}$
25	80	0.022	2000	5.814	$8.53 \cdot 10^{-6}$
45	44	0.022	2000	5.814	$8.70 \cdot 10^{-6}$

The uncertainty associated with standard solution preparation presented similar values for the different calibration solutions (ranging between $8.45 \cdot 10^{-6}$ and $8.70 \cdot 10^{-6}$). The contribution of temperature in the uncertainty of syringe and volumetric flask was negligible.

The same calculations were performed for the Soxhlet extraction-GC/MS. In this method, the calibration standards (solutions of 0.1, 0.25, 0.5, 1 and 2.5 ng μL^{-1}) were prepared in three dilution stages:

- 50 μL were removed from the stock solution (SV Calibration Mix 5, Restek, 2000 $\mu\text{g mL}^{-1}$) and diluted in 1 mL of methanol, obtaining a 100 ng μL^{-1} solution.
- 100 μL of 100 ng μL^{-1} solution were diluted in 1 mL of methanol (10 ng μL^{-1} solution).

- Finally, from $10 \text{ ng } \mu\text{L}^{-1}$ solution, different volumes were removed and diluted to obtain the calibration solutions.

Table 4.19 shows the results obtained in the determination of the uncertainties associated with lab tools for the Soxhlet extraction-GC/MS method.

Table 4.19. Uncertainties associated with syringe and volumetric flask during the standard solution preparation for each dilution stage (Soxhlet extraction-GC/MS method).

Dilution stage	Solution concentration ($\text{ng } \mu\text{L}^{-1}$)	V_{syr} (μL)	$u(\text{syr}_{\text{cal}})$ (μL)	$u(\text{T})$ (μL)	$u(\text{syr})$ (μL)
1 st	100	50	0.289	0.125	0.315
2 nd	10	100	0.577	0.200	0.611
3 rd	0.1	10	0.058	0.020	0.061
3 rd	0.25	25	0.144	0.050	0.153
3 rd	0.5	50	0.289	0.100	0.306
3 rd	1	100	0.577	0.200	0.611
3 rd	2.5	250	1.443	0.501	1.528

Dilution stage	Solution concentration ($\text{ng } \mu\text{L}^{-1}$)	V_{flask} (μL)	$u(\text{flask}_{\text{cal}})$ (μL)	$u(\text{T})$ (μL)	$u(\text{flask})$ (μL)
1 st , 2 nd , 3 rd	100; 10; 2.5; 5; 12.5; 25; 45	1000	14.434	2	14.572

The results of Table 4.19 were used in the expressions 4.16 and 4.11, obtaining the same uncertainty in the preparation of the different calibration solutions, $8.45 \cdot 10^{-6}$. This value was the same as that obtained for the preparation of solutions of 2.5 and 5 $\text{ng } \mu\text{L}^{-1}$ in the TD-GC/MS method. Again, the effect of the temperature was negligible in the uncertainty associated with lab tools.

Uncertainty derived from internal standard solution preparation $(u(\text{is})/C_{\text{is}})^2$.

To determine the uncertainty associated with internal standard solution preparation the same methodology was used as in the assessment of $(u(\text{std})/C_{\text{std}})^2$.

In the TD-GC/MS, a solution of $25 \text{ ng } \mu\text{L}^{-1}$ was prepared from stock solution (Predeuterated internal standard PAH Mixture 6 Chiron, $200 \mu\text{g mL}^{-1}$), removing 125 μL and diluting them in 1 mL of methanol. For the Soxhlet extraction-GC/MS, the internal solution added to samples was the result of two dilution stages: 100 μL of stock

solution (the same as in the TD-GC/MS method) was removed and diluted in 1 mL of methanol, obtaining a $20 \text{ ng } \mu\text{L}^{-1}$; subsequently, $25 \text{ } \mu\text{L}$ from this solution were diluted in 1 mL of methanol to get a final concentration of $0.5 \text{ ng } \mu\text{L}^{-1}$.

The values of $(u(is)/C_{is})^2$ obtained for the TD-GC/MS and Soxhlet extraction-GC/MS methods were $3.62 \cdot 10^{-4}$ and $1.33 \cdot 10^{-4}$ respectively.

Once $(u(C_x)/C_x)^2$, $(u(std)/C_{std})^2$ and $(u(is)/C_{is})^2$ had been calculated, the uncertainty derived from the calibration curve was estimated according to Eq. 4.5. For BaP (determined by the TD-GC/MS method) the calculation was as follows:

$$\left(\frac{u(\text{Cal})}{C}\right)^2 = 4.91 \cdot 10^{-4} + 8.45 \cdot 10^{-6} + 8.45 \cdot 10^{-6} + 8.47 \cdot 10^{-6} + 8.53 \cdot 10^{-6} + 8.70 \cdot 10^{-6} + 3.62 \cdot 10^{-4} = 8.95 \cdot 10^{-4} \quad (4.17)$$

$$\frac{u(\text{Cal})}{C} = \left(\sqrt{8.95 \cdot 10^{-4}}\right) = 0.03 \quad (4.18)$$

The values of calibration uncertainty for both methods (TD-GC/MS and Soxhlet extraction-GC/MS) are summarized in Table 4.20.

Table 4.20. Relative ($u(\text{Cal})/C$) for each PAH in the TD-GC/MS and Soxhlet extraction-GC/MS methods.

PAH	$u(\text{Cal})/C$	
	TD-GC/MS	Soxhlet extraction-GC/MS
Ace	0.04	-
FL	0.06	-
Phe	0.03	0.03
Ant	0.04	0.02
Ft	0.04	0.02
Pyr	0.04	0.03
BaA	0.03	0.03
Chry	0.05	0.02
BbFt	0.04	0.01
BkFt	0.05	0.02
BaP	0.03	0.04
IP	0.05	0.02
DBahA	0.06	0.04
BghiP	0.03	0.02

The relative uncertainty associated with calibration in both methods showed similar values, between 0.02 and 0.04, for most PAHs. In both methods, the uncertainty derived from solution preparation (standard and internal standard) were negligible, being the linear least squares adjustment the main contributor to the calibration uncertainty.

4.5.2 Uncertainty derived from sample volume and from air flow $(u(V_s)/V_s)^2$ and $(u(V_{\text{air}})/V_{\text{air}})^2$.

In the TD-GC/MS the possible size variations in the cutting of the filter could be a source of uncertainty. Grandesso et al. (2013), analysing particle PAHs by TD-GC/MS method, estimated an uncertainty derived from cutting (u_{cut}/C_r) of $7.60 \cdot 10^{-3}$. Thus, this value was considered in this study for the TD-GC/MS method.

The term of $u(V_s)/V_s$ in the combined uncertainty expression (Eq. 4.4) was replaced by u_{cut}/C_r for the TD- GC/MS method.

In the Soxhlet extraction-GC/MS method the sample is injected directly into the CG/MS system, thus, the uncertainty associated with the sample in this case was the uncertainty of the syringe. The injected volume was 2 μL and relative $(u(V_s)/V_s)$ was calculated by the Eq. 4.13, obtaining a value of 0.01 for each PAH.

$(u(V_{\text{air}})/V_{\text{air}})^2$ is related to the uncertainty of the air sampler. In both methods (TD-GC/MS and Soxhlet extraction-GC/MS), the air sampler (Digitel DHA-80) worked at $30 \text{ m}^3 \text{ h}^{-1}$ during 8h (total volume of air collected per sample of 240 m^3). The relative uncertainty of this sampler in the flow (u_{sampler}) was estimated by the manufacturer in $\pm 1.03 \%$. This value was considered the relative $(u(V_{\text{air}})/V_{\text{air}})$ for both methods.

4.5.3 Uncertainty derived from recovery $(u(R)/R)^2$.

The data and results of the validation tests for both methods (section 4.6) were used for the estimation of recovery uncertainty, $(u(R)/R)^2$. This uncertainty can be calculated by using the following equations:

$$\left(\frac{u(R)}{R}\right)^2 = \left(\frac{u(C_{\text{obs}})}{C_{\text{obs}}}\right)^2 + \left(\frac{u(C_{\text{crm}})}{C_{\text{crm}}}\right)^2 \quad (4.19)$$

$$\left(\frac{u(C_{\text{obs}})}{C_{\text{obs}}}\right)^2 = \left(\frac{SD}{C_{\text{obs}} \cdot \sqrt{n}}\right)^2 \quad (4.20)$$

where:

- C_{obs} is the observed amount of analyte after extraction, in ng.
- C_{crm} is the amount of analyte in the certified reference material before extraction, in ng.
- R is the recovery of the compound, obtained from $C_{\text{obs}}/C_{\text{crm}}$.
- $(u(C_{\text{obs}})/C_{\text{obs}})^2$ is the uncertainty derived from the observed amount of analyte after the extraction.

- $(u(C_{\text{crm}})/C_{\text{crm}})^2$ is the uncertainty derived from the amount of analyte in the certified reference material before extraction.
- SD is the standard deviation of observed amount of analyte after extraction, ng.
- n the number of samples.

For BaP (determined by the TD-GC/MS method):

$$\left(\frac{u(C_{\text{obs}})}{C_{\text{obs}}}\right)^2 = \left(\frac{\text{SD}}{C_{\text{obs}} \cdot \sqrt{n}}\right)^2 = \left(\frac{2.35 \text{ ng}}{20.38 \text{ ng} \cdot \sqrt{10}}\right)^2 = 1.33 \cdot 10^{-3} \quad (4.21)$$

$$\left(\frac{u(C_{\text{crm}})}{C_{\text{crm}}}\right)^2 = \left(\frac{1.23 \text{ ng}}{25.42 \text{ ng}}\right)^2 = 2.36 \cdot 10^{-3} \quad (4.22)$$

$$\left(\frac{u(R)}{R}\right) = \left(\sqrt{1.33 \cdot 10^{-3} + 2.36 \cdot 10^{-3}}\right) = 0.06 \quad (4.23)$$

The R and relative $(u(R)/R)$ values for each PAH were determined for both methods (Table 4.21).

Table 4.21. Value of R and relative uncertainty associated with recovery obtained in TD-GC/MS and Soxhlet extraction-GC/MS for each PAH.

PAH	R		(u(R)/R)	
	TD-GC/MS	Soxhlet extraction-GC/MS	TD-GC/MS	Soxhlet extraction-GC/MS
Ace	0.77	-	0.12	-
FL	0.90	-	0.15	-
Phe	0.94	0.73	0.03	0.14
Ant	1.25	0.62	0.03	0.14
Ft	0.88	0.93	0.03	0.12
Pyr	1.01	0.93	0.03	0.11
BaA	0.89	0.93	0.03	0.09
Chry	0.84	1.30	0.03	0.14
BbFt ^a	0.92	0.96	0.04	0.13
BkFt	0.92	1.31	0.04	0.17
BaP	0.80	1.00	0.06	0.14
IP	1.20	0.93	0.04	0.14
DBahA ^b	1.05	2.10	0.07	0.17
BghiP	0.91	1.21	0.03	0.14

^a Results from BbFT + BjFT.^b Results from DBahA + DBacA.

The recovery of PAHs by TD-GC/MS showed lower uncertainty than the solvent-based method. The poor recovery of the PAHs in the Soxhlet process (section 4.6) could explain these results.

4.5.4 Combined uncertainty (u_{comb}/C)².

Finally, the combined uncertainty for 16 EPA PAHs in each method was calculated by Eq. 4.4.

Table 4.22 shows the relative combined uncertainty in % for each PAH in both methods. BaP (determined by the TD-GC/MS method) is given as an example calculation in Eq 4.24 and 4.25.

$$\left(\frac{u_{\text{comb}}}{C}\right)^2 = (0.03)^2 + (0.02)^2 + (7.60 \cdot 10^{-3})^2 + (0.06)^2 = 5 \cdot 10^{-3} \quad (4.24)$$

$$\left(\frac{u_{\text{comb}}}{C}\right) = \left(\sqrt{5 \cdot 10^{-3}}\right) \cdot 100 = 7\% \quad (4.25)$$

Table 4.22. u_{comb}/C and u_{expan}/C for 16 EPA PAHs in both methods.

PAH	u_{comb}/C (%)	
	TD-GC/MS	Soxhlet extraction-GC/MS
Ace	13	-
Fl	19	-
Phe	5	14
Ant	5	13
Ft	5	12
Pyr	5	11
BaA	4	10
Chry	6	15
BbFt ^a	6	13
BkFt	7	18
BaP	7	15
IP	7	14
DBahA ^b	9	18
BghiP	5	14

^a Results from BbFT + BjFt.

^b Results from DBahA + DBacA.

According to the results, the TD-GC/MS method was more reliable than Soxhlet extraction-GC/MS for the determination of particulate PAHs, with lower combined uncertainties (< 8% for most PAHs). The uncertainty associated with recovery was the main uncertainty source for both methods.

4.6 Determination of other PAHs in the particulate phase

The urban dust used to validate the method (section 4.6) contained other PAHs besides the 16 EPA PAHs. For this reason, it was considered to increase the number of PAHs determined by the technique. Table 4.23 shows, according to their elution order, the 16 EPA PAHs, the deuterated PAHs and the extra PAHs with their quantification ions.

Table 4.23. Quantification ions of 16 EPA PAHs and deuterated PAHs determined by the TD-GC/MS method (extra PAHs included).

PAH	Abbreviation	Ion (m/z)
Acenaphthene	Ace	154
Fluorene	FL	166
Phenanthrene-d ₁₀	Phe-d ₁₀	188
Phenanthrene	Phe	178
Anthracene	Ant	178
Fluoranthene	Ft	202
Pyrene-d ₁₀	Pyr-d ₁₀	212
Pyrene	Pyr	202
Benzo[ghi]fluoranthene	BghiFt	226
Benzo[c]phenanthrene	BcP	228
Cyclopenta[cd]pyrene	CPP	226
Benzo[a]anthracene-d ₁₂	BaA-d ₁₂	240
Benzo[a]anthracene	BaA	228
Triphenylene	Triph	228
Chrysene	Chry	228
Retene	Ret	234
Benzo[b]fluoranthene	BbFt	252
Benzo[jj]fluoranthene	BjFt	252
Benzo[k]fluoranthene	BkFt	252
Benzo[a]fluoranthene	BaFt	252
Benzo[e]pyrene	BePr	252
Benzo[a]pyrene-d ₁₀	BaP-d ₁₀	264
Benzo[a]pyrene	BaP	252
Perylene	Per	252
Dibenzo[a,j]anthracene	DBajA	278
Indeno[1,2,3-cd]pyrene	IP	276
Dibenzo[ac]anthracene	DBacA	278
Dibenzo[ah]anthracene	DBahA	278
Benzo[b]chrysene	BbC	278
Picene	Pic	278
Benzo[ghi]perylene-d ₁₂	BghiP-d ₁₂	288
Benzo[ghi]perylene	BghiP	278
Anthanthrene	Anthan	276
Coronene	Cor	300

To acquire the extra PAHs, their SIM windows were included in the MS configuration before validating the TD method. Hence, to determine these compounds, the same study was used (10 samples loaded with a 1/8 portion of a quartz fibre with approx. 10 mg of NIST SRM 1694b and 25 ng μL^{-1} of deuterated compounds).

The NIST mass spectral library, the retention times between analyte and internal standard, and a previous study performed by R. Bordajandi et al. (2008) with the same type of chromatographic column were used to identify the extra PAHs. Figures 4.19 to 4.22 show the identification of the target PAHs in the different SIM windows obtained in the analysis.

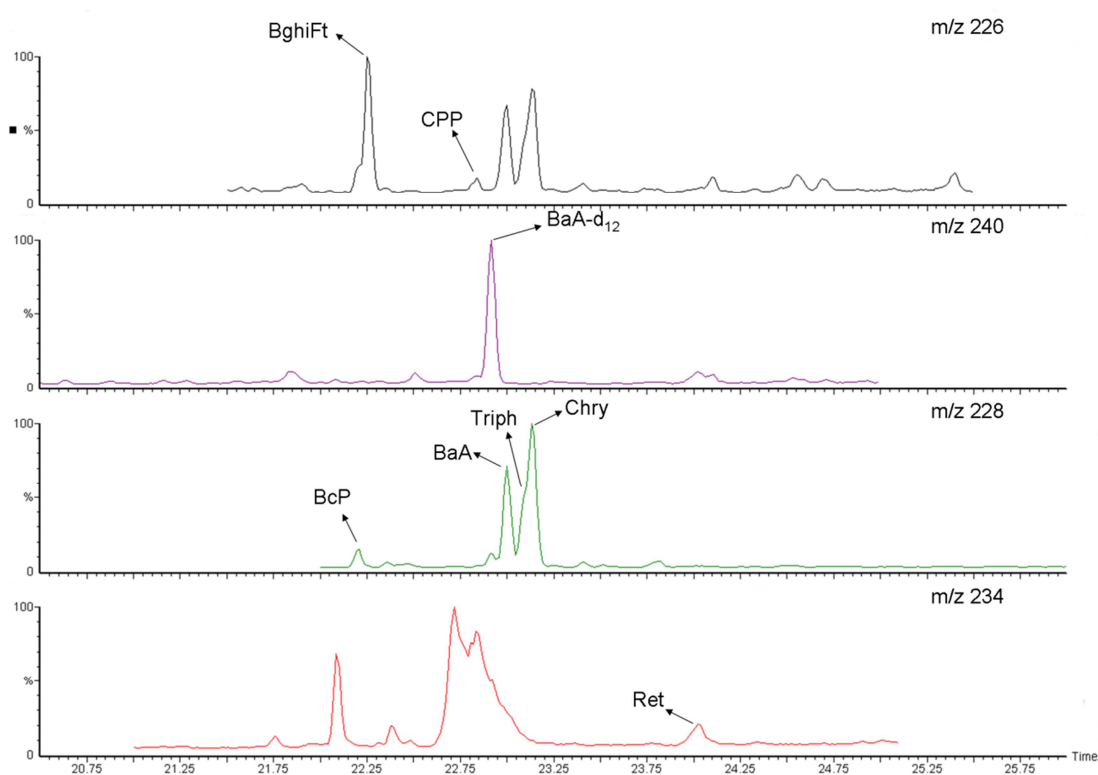


Figure 4.19. PAHs and deuterated PAHs in SIM windows (m/z 226,240,228 and 234) in the analysis of NIST SRM 1694b dust.

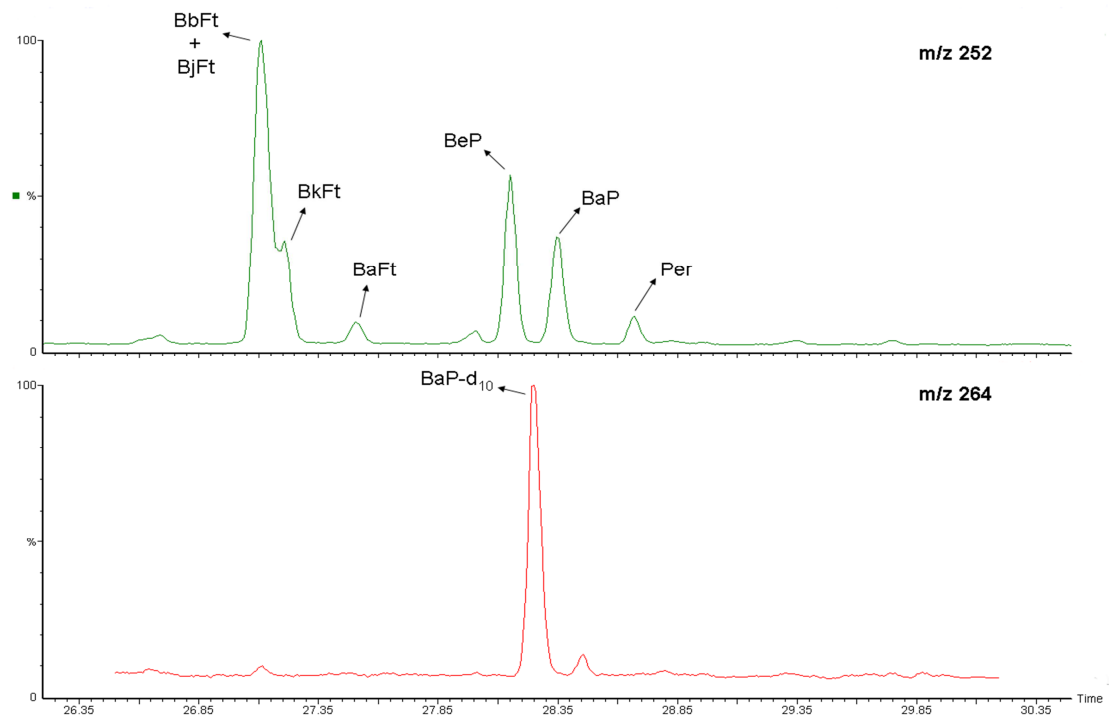


Figure 4.20. PAHs and deuterated PAHs in SIM windows (m/z 252 and 264) in the analysis of NIST SRM 1694b dust.

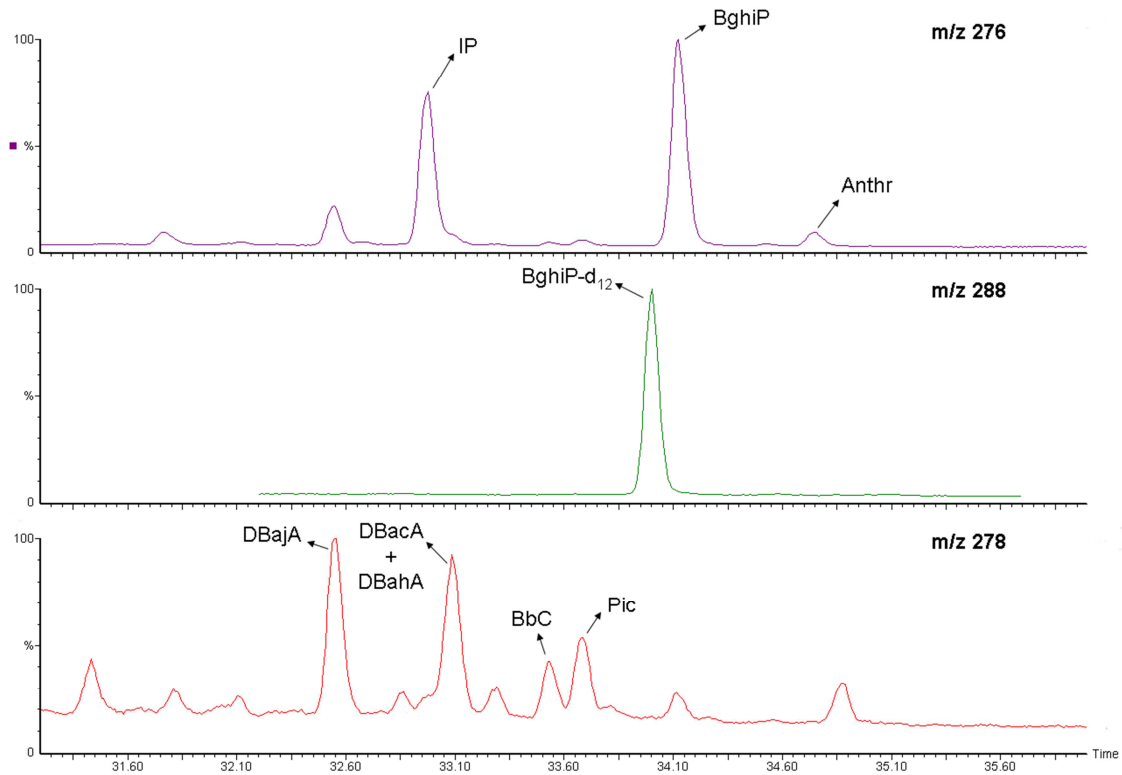


Figure 4.21. PAHs and deuterated PAHs in SIM windows (m/z 276, 288 and 278) in the analysis of NIST SRM 1694b dust.

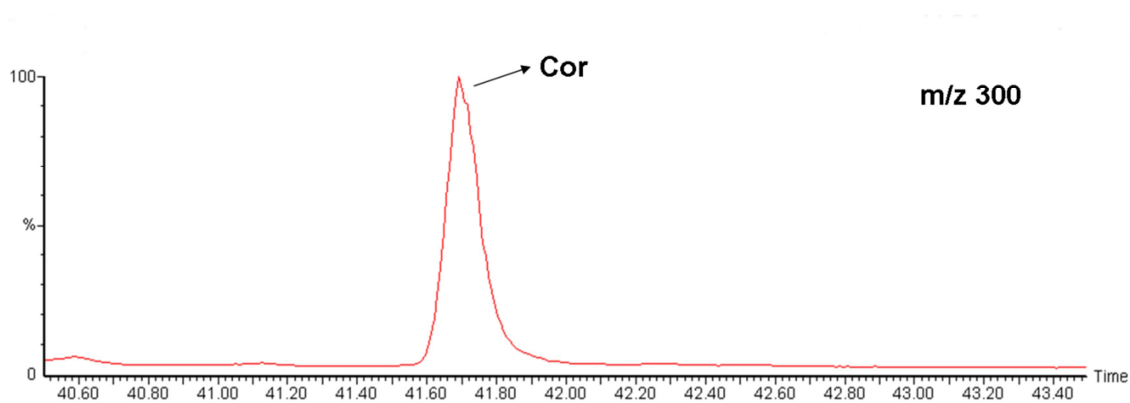


Figure 4.22. PAHs and deuterated PAHs in m/z 300 SIM window in the analysis of NIST SRM 1694b dust.

For the quantification, the relative response factors (RRFs) for each extra PAH were calculated by the next equation:

$$\text{RRF}_{\text{extra PAH}} = \frac{A_{\text{extra PAH}} \cdot C_{\text{ref PAH}}}{A_{\text{ref PAH}} \cdot C_{\text{extra PAH}}} \quad (4.26)$$

where:

$A_{\text{new PAH}}$ peak area of extra PAH.

$A_{\text{ref PAH}}$ peak area of reference PAH compound.

$C_{\text{new PAH}}$ extra PAH concentration in the NIST dust.

$C_{\text{ref PAH}}$ reference PAH concentration in the NIST dust.

Reference PAHs were selected according the following criteria: the nearest of the 16 EPA PAHs to each new one, which provides the least variation in the RRF. Table 4.24 collects the reference PAHs, RRFs and the coefficients of variation for each extra PAH.

Table 4.24. Reference PAH, RRFs and the coefficients of variation for each extra PAH.

New PAH	Reference PAH	RRF	CV (%)
BghiFt	BaA	1.29	6.68
BcP	BaA	0.76	13.17
CPP	BaA	0.31	15.14
Triph	BaA	0.69	16.10
Ret	BaA	1.13	25.62
BaFt	BkFt	0.99	11.34
BePr	BaP	1.31	4.10
Per	BaP	0.94	4.05
DBajA	IP	4.74	4.49
BbC	IP	1.08	6.16
Pic	IP	0.64	10.16
Anthran	BghiP	0.40	8.54
Cor	BghiP	0.54	15.76

The extra PAHs showed a range of RRFs between 0.03 and 3.27, with coefficients of variation of less than 15% for most compounds.

To conclude, the determination of the RRFs for these PAHs is a useful tool to have an initial estimation of their environmental concentration when the TD-CG/MS is applied to real samples.

Chapter 5:

**Determination of particle-bound
PAHs in urban area by
TD-GC/MS method**

5.1 Sampling site

The sampling site was the School of Engineering (longitude 2°56'56.24"W, latitude 3°15'44.86"N) of Bilbao city, northern Spain. The School of Engineering is located in the city centre of Bilbao, along the Nervión estuary that runs nearly 16 km from the centre of the city to the sea in a SE–NW direction. Bilbao has an oceanic climate with moderate temperatures, relative humidity is quite constant throughout the year, and rainfall is significant and frequent especially in spring and autumn. Moreover, this city is strongly influenced by land-sea breeze cycles during the day, channelized along the Nervión valley.

Bilbao city is the most populated area in the Basque Country and the tenth largest in Spain (approximately 350,000 in the city and 1 million inhabitants in the metropolitan area). In this urban area, local traffic and stationary emissions from the surrounding industries are considered as the major sources of atmospheric pollutants. Furthermore, the sampling site is highly affected by vehicle traffic due to the proximity of the A-8 highway (average daily volume of approximately 100,000 vehicles in 2013) and the city's main bus station (Figure 5.1).

In order to have a better characterization of the PAH emissions in the metropolitan area of Bilbao, the regional industrial sources were identified and located (Figure 5.2).

The information was obtained from PAH emission data recorded in the Basque E-PRTR (European Pollutant Release and Transfer Register) in 2013 and 2014. The steel and waste treatment industries were the industrial activities that emitted PAHs in the region during the sampling period.

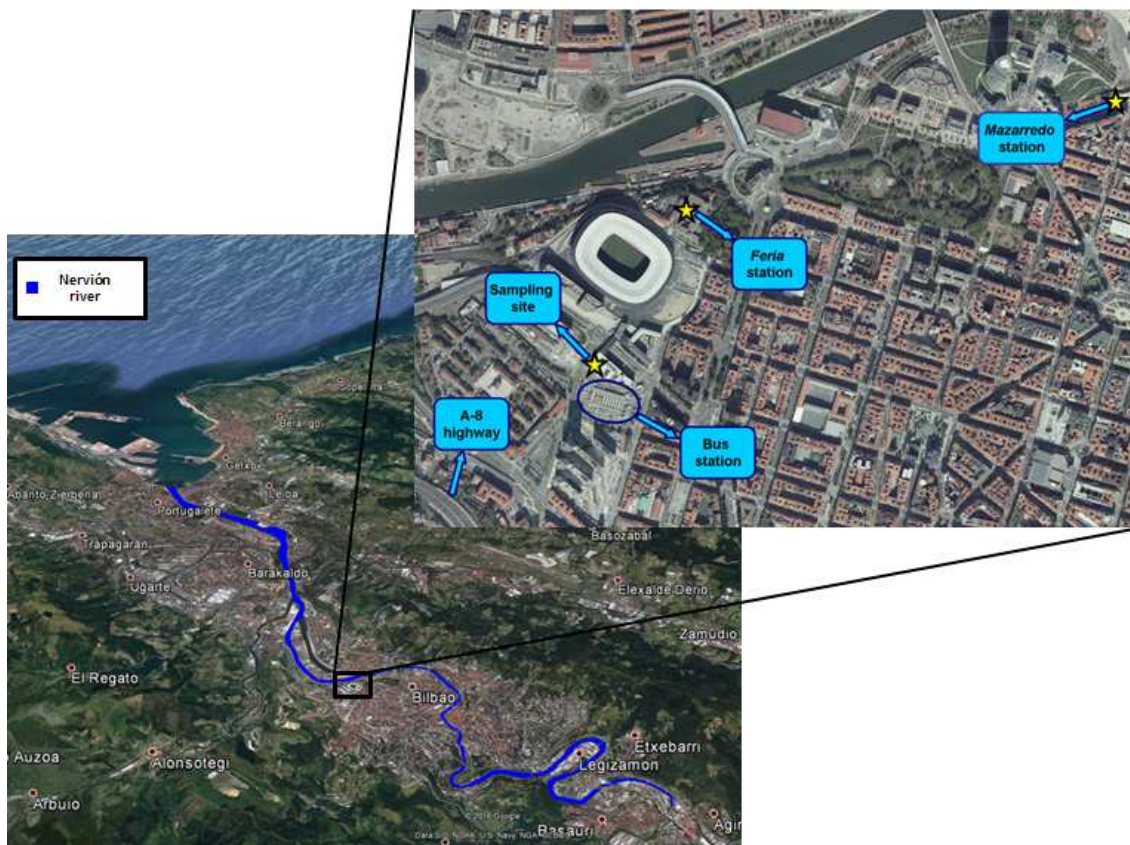


Figure 5.1. Geographical location of the sampling site in Bilbao city (Spain), and meteorological (*Feria*) and air pollution (*Mazarredo*) sampling stations (sources: Google Earth and GeoEuskadi).

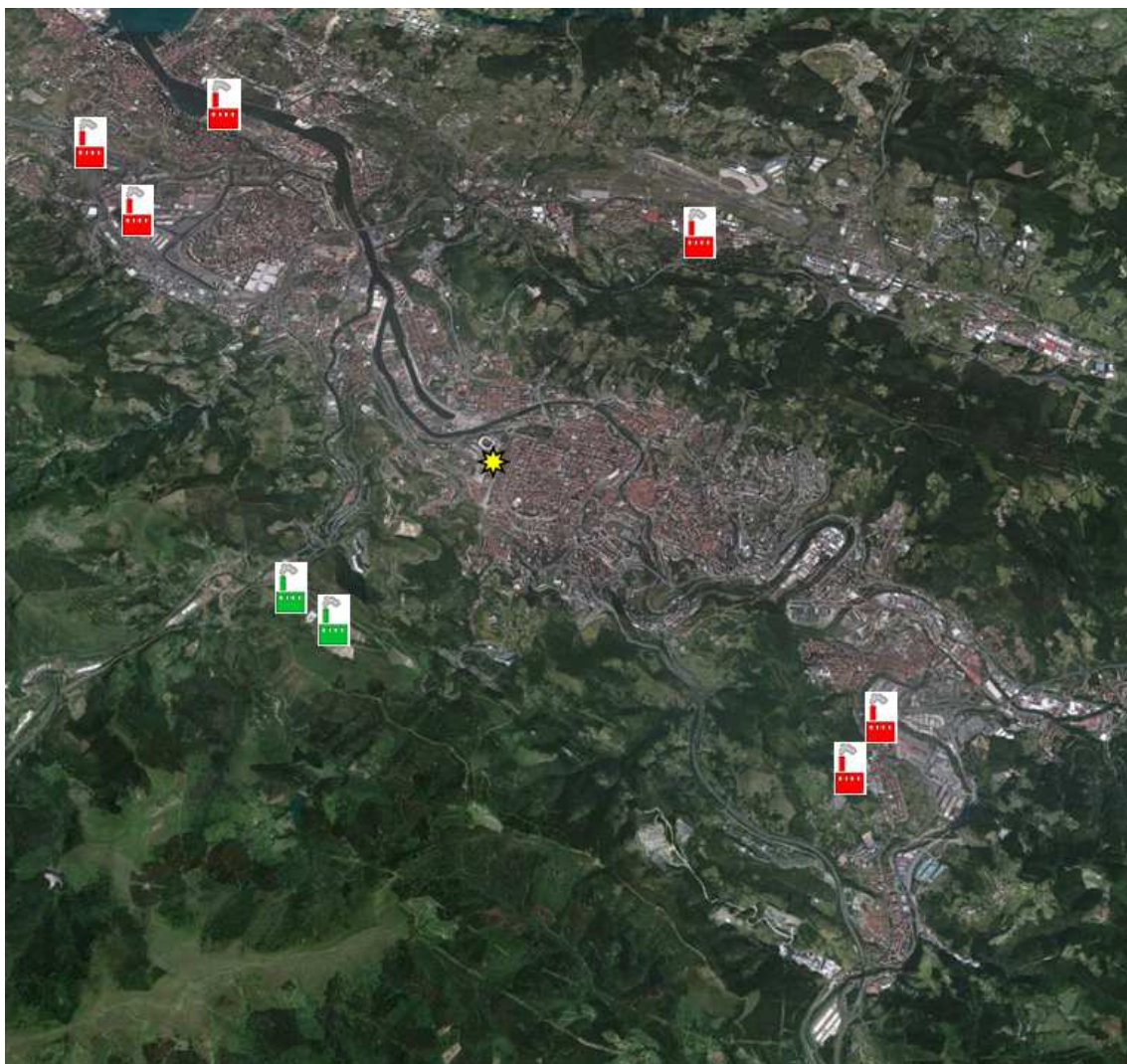


Figure 5.2. Industrial emissions of PAHs in the metropolitan area of Bilbao (years 2013 and 2014). Sampling site (yellow star), steel industry (red factory), and waste treatment industry (green factory) (sources: Google Earth and Basque E-PRTR).

The sampling campaign was conducted over 9 months: in July 2013, from September 2013 to March 2014, and in June 2014. PM_{10} samples were collected every 8 hours for seven consecutive days each month as follows: 04:00–12:00 h; 12:00–20:00 h, and 20:00–04:00h UTC (21 contiguous samples). These time intervals were chosen to study the influence of emission sources such as rush traffic hours on temporal variations of particle-bound PAH concentrations. Moreover, the sampling campaign was carried out in summer (01–08 July, 07–14 September), autumn (07–14 October, 11–18 November, 03–10 December,) winter (24–31 January, 21–28 February) and

spring (21–28 March and 7–14 June) , aiming at investigating their diurnal variation patterns under different meteorological conditions.

A total of 182 PM₁₀ samples were collected during the campaign, by using a high-volume sampler (Digitel DHA-80, Digitel Elektronik AG, Switzerland) operating at a flow rate of 30m³ h⁻¹. Previous to sampling, quartz fibre filters (150 mm diameter, Whatman International Ltd., United Kingdom) used as collection substrates were heated at 500°C for 24 h. After sampling, the filters were put into individual Petri dishes, wrapped in aluminium foil (pre-cleaned with n-hexane) to avoid photodegradation, and kept in a 4°C freezer until analysis (< 15 days) according to ISO 12884:2000 (ISO 2000).

5.2 Meteorological conditions and conventional pollutants concentrations

Meteorological and air regulated pollutant data used in this work were obtained from the weather network (*Feria* station, Basque Weather Service) and the Bilbao air pollution network (*Mazarredo* station, Basque Country Environment and Planning Department), respectively. These stations are located less than 500 meters (*Feria*) and approximately 1.5 km (*Mazarredo*) from the sampling point (Figure 5.1).

Table 5.1 and 5.2 summarize the meteorological conditions and air regulated pollutant concentrations that prevailed during the sampling campaign. In brief, the average temperature was between 7 and 22°C, June was the month with highest temperature and solar irradiation, and the relative humidity ranged from 56% to 85%. The atmospheric pressure was between 1011 and 1029 mbar, while rainfall was significant in November, January and March (values between 2.9–4 L m⁻², 2.2–4.8 L m⁻², and 0.9–3.2 L m⁻², respectively).

Wind varied significantly along the year, influenced by sea/land interaction (Figure 5.3). The predominant wind directions were west-northwest (WNW), north-west (NW), east-southeast (ESE) and east-south (SE) for the whole sampling period, during which the wind speed varied from 0.69 to 4.72 m s⁻¹.

Atmospheric dynamics are heavily influenced by complex topography and sea/land interactions. Sea/land and mountain/valley breezes occur with relatively high frequency, especially in stable atmospheric situations. Thus, local phenomena interact with the prevailing synoptic meteorology, producing a specific atmospheric dynamic that affects Bilbao's urban climate. In the daytime, WNW-NW wind directions are

common during spring and summer in relation with higher influence of the sea breeze. In contrast, night-time winds in SE-ESE directions are more frequent in autumn and winter, being related to cold air drainage flows (i.e. mountain breeze) (Millán et al., 1987; Acero et al., 2013).

Regarding air pollutant data, the highest concentration levels generally coincided with the morning or afternoon periods, except in February where they coincided with the night period (Table 5.2). December was the month with the highest pollutant concentrations, except for O₃, for which the lowest concentrations were registered. Among these pollutants, NO₂ is well-known to be a traffic-related air pollutant, thus its diurnal pattern shows peaks during morning and afternoon rush hour traffic (Figure 5.4).

Table 5.1. Meteorological conditions during the sampling campaign. Standard deviations in brackets.

Parameter	Period*	July-13	September-13	October-13	November-13	December-13	January-14	February-14	March-14	June-14
Wind speed (m s ⁻¹)	M	0.82 (0.67)	0.75 (0.34)	1.40 (0.66)	3.03 (2.05)	1.13 (0.89)	3.46 (2.09)	3.43 (1.24)	2.91 (2.04)	0.82 (0.63)
	A	4.11 (1.27)	1.20 (0.72)	1.31 (0.43)	2.77 (1.72)	0.69 (0.39)	4.35 (2.29)	3.09 (1.50)	4.72 (1.38)	4.27 (1.33)
	N	1.03 (0.59)	2.31 (0.66)	1.34 (0.73)	2.66 (2.23)	1.30 (0.66)	3.94 (2.23)	2.45 (1.47)	3.12 (2.79)	1.14 (0.60)
Prevailing wind direction	M	NW	E and SE	ESE	NW and WNW	ESE	SSW	SE and SSW	SE	NE and WNW
	A	NW and WNW	WNW	NW and WNW	WNW	WNW	WSW	NW	NW	NW
	N	WNW and SE	ESE	ESE	NW and WNW	ESE	WNW	SE	WNW	WNW
Temperature (°C)	M	19 (2)	17 (1)	14 (2)	11 (3)	8 (2)	9 (3)	11 (2)	10 (2)	21 (2)
	A	21 (3)	19 (2)	17 (2)	12 (3)	12 (1)	11 (3)	13 (3)	11 (2)	22 (2)
	N	18 (1)	16 (2)	13 (2)	12 (3)	7 (2)	10 (3)	10 (3)	9 (2)	19 (1)
Atmospheric Pressure (mbar)	M	1022 (3)	1023 (2)	1020 (3)	1024 (7)	1029 (2)	1011 (10)	1018 (5)	1016 (2)	1018 (4)
	A	1021 (3)	1022 (3)	1020 (3)	1026 (5)	1028 (3)	1011 (11)	1019 (6)	1015 (4)	1018 (4)
	N	1022 (3)	1023 (2)	1021 (3)	1025 (6)	1029 (3)	1012 (12)	1018 (6)	1015 (5)	1020 (3)
Solar irradiation (W m ⁻²)	M	327 (160)	214 (89)	138 (72)	39 (20)	90 (44)	55 (19)	130 (64)	134 (102)	374 (156)
	A	389 (200)	207 (98)	162 (80)	43 (26)	103 (54)	68 (24)	196 (78)	176 (108)	443 (162)
	N	0 (0)	0 (0)	0 (0)	0 (0)	0 (0)	0 (0)	0 (0)	0 (0)	0 (0)

Note: diurnal periods correspond to morning (M): 04:00–12:00 h, afternoon (A): 12:00–20:00 h and night (N): 20:00–04:00 h UTC.

Table 5.1. (continued) Meteorological conditions during the sampling campaign. Standard deviations in brackets.

Parameter	Period*	July-13	September-13	October-13	November-13	December-13	January-14	February-14	March-14	June-14
Rainfall (L m ⁻²)	M	0.01 (0.01)	0.11 (0.26)	0.01 (0.01)	4.01 (5.62)	0 (0)	2.23 (2.89)	0.94 (1.80)	0.94 (1.76)	0 (0)
	A	0.01 (0.02)	0.12 (0.28)	0.16 (0.28)	3.10 (4.45)	0 (0)	4.79 (2.77)	0.93 (2.37)	1.24 (1.55)	0 (0)
	N	0.04 (0.09)	0.10 (0.24)	0.01 (0.01)	2.94 (4.43)	0.07 (0.19)	3.80 (2.50)	0 (0)	3.21 (5.24)	0.06 (0.15)
Relative Humidity (%)	M	79 (8)	81 (5)	77 (4)	82 (11)	78 (8)	75 (11)	56 (12)	72 (5)	67 (11)
	A	75 (9)	72 (11)	65 (14)	81 (11)	65 (9)	74 (10)	57 (13)	68 (4)	64 (12)
	N	85 (6)	83 (5)	81 (4)	83 (10)	82 (7)	80 (8)	66 (15)	77 (8)	78 (10)

Note: diurnal periods correspond to morning (M): 04:00–12:00 h, afternoon (A): 12:00–20:00 h and night (N): 20:00–04:00 h UTC.

Table 5.2. Air regulated pollutant concentrations during the sampling campaign. Standard deviations in brackets.

Parameter	Period*	July-13	September-13	October-13	November-13	December-13	January-14	February-14	March-14	June-14
NO ($\mu\text{g m}^{-3}$)	M	19.93 (8.27)	34.11 (13.21)	58.05 (23.61)	11.45 (5.30)	72.38 (35.19)	21.54 (18.51)	14.04 (8.58)	15.53 (11.74)	17.25 (8.39)
	A	6.51 (1.61)	6.86 (1.62)	10.32 (2.71)	13.13 (4.19)	65.52 (52.60)	8.93 (3.25)	11.66 (2.35)	6.39 (1.06)	5.59 (1.17)
	N	5.45 (1.78)	9.79 (5.32)	19.20 (7.28)	5.32 (0.96)	45.30 (31.03)	5.34 (1.68)	15.05 (9.27)	5.55 (3.68)	3.21 (1.39)
NO ₂ ($\mu\text{g m}^{-3}$)	M	33.54 (10.36)	35.36 (9.87)	53.86 (10.11)	37.58 (12.16)	55.66 (9.66)	47.95 (17.51)	43.63 (17.62)	39.04 (17.50)	41.93 (7.77)
	A	18.32 (4.60)	22.96 (5.56)	37.38 (8.96)	47.38 (13.97)	67.73 (17.17)	38.41 (9.36)	44.82 (6.75)	30.14 (6.51)	20.77 (4.88)
	N	29.59 (15.15)	32.45 (11.45)	49.02 (11.02)	25.07 (11.94)	53.27 (7.98)	25.27 (9.81)	54.57 (15.43)	27.46 (19.66)	25.09 (13.62)
NO _x ($\mu\text{g m}^{-3}$)	M	64.05 (19.99)	88.07 (27.80)	143.32 (45.70)	55.19 (19.10)	167.16 (59.47)	81.18 (44.04)	65.11 (30.63)	64.17 (34.60)	68.54 (19.97)
	A	28.39 (5.46)	33.55 (7.51)	53.14 (12.26)	67.54 (19.97)	168.46 (96.09)	52.25 (13.67)	62.86 (9.13)	39.98 (8.12)	29.42 (6.31)
	N	38.04 (17.52)	47.32 (17.11)	78.50 (21.51)	33.16 (13.44)	123.04 (48.23)	33.70 (11.93)	77.73 (27.58)	36.18 (25.25)	30.16 (15.49)
SO ₂ ($\mu\text{g m}^{-3}$)	M	2.39 (1.59)	7.78 (2.30)	11.91 (3.86)	5.55 (3.01)	9.94 (3.85)	7.43 (1.15)	7.93 (1.74)	0.43 (0.23)	11.41 (4.85)
	A	1.26 (0.39)	3.77 (1.96)	5.79 (2.12)	5.41 (2.52)	7.53 (4.48)	6.71 (1.09)	7.80 (1.47)	0.30 (0.06)	6.46 (1.03)
	N	1.24 (0.34)	5.43 (2.64)	9.41 (3.52)	4.96 (2.12)	9.67 (4.73)	6.63 (1.12)	9.67 (3.26)	0.32 (0.13)	8.04 (3.28)
O ₃ ($\mu\text{g m}^{-3}$)	M	21.66 (6.88)	26.13 (9.01)	12.34 (3.26)	37.39 (13.97)	9.14 (2.70)	31.29 (12.73)	34.96 (12.00)	42.72 (19.01)	34.16 (6.08)
	A	35.84 (11.73)	57.11 (10.78)	46.41 (10.10)	32.25 (13.85)	19.55 (12.35)	39.34 (8.16)	41.11 (4.48)	58.46 (7.42)	66.96 (11.09)
	N	18.80 (5.24)	20.13 (13.31)	11.54 (14.04)	46.86 (21.20)	8.54 (4.80)	45.71 (10.04)	18.49 (14.94)	50.61 (28.31)	42.59 (13.30)

Note: diurnal periods correspond to morning (M): 04:00–12:00 h, afternoon (A): 12:00–20:00 h and night (N): 20:00–04:00 h UTC.

Table 5.2. (continued) Air regulated pollutant concentrations during the sampling campaign. Standard deviations in brackets.

Parameter	Period*	July-13	September-13	October-13	November-13	December-13	January-14	February-14	March-14	June-14
Benzene ($\mu\text{g m}^{-3}$)	M	0.25 (0.14)	0.09 (0.04)	0.65 (0.28)	0.45 (0.13)	0.80 (0.23)	0.36 (0.08)	0.33 (0.07)	0.43 (0.23)	0.32 (0.15)
	A	0.11 (0.12)	0.06 (0.04)	0.29 (0.11)	0.47 (0.25)	0.93 (0.50)	0.29 (0.06)	0.42 (0.14)	0.30 (0.06)	0.09 (0.04)
	N	0.12 (0.05)	0.12 (0.06)	0.46 (0.24)	0.42 (0.27)	0.93 (0.34)	0.31 (0.09)	0.54 (0.13)	0.32 (0.13)	0.26 (0.09)
Toluene ($\mu\text{g m}^{-3}$)	M	2.29 (1.51)	2.38 (0.85)	6.37 (2.84)	2.09 (0.78)	5.09 (2.51)	1.80 (0.98)	1.77 (0.78)	2.49 (2.04)	4.10 (1.81)
	A	0.90 (0.62)	0.88 (0.27)	2.69 (1.34)	2.63 (0.94)	7.05 (5.57)	1.85 (0.66)	1.93 (0.38)	1.36 (0.61)	1.39 (0.63)
	N	1.91 (1.11)	1.83 (0.73)	4.79 (2.49)	1.42 (0.74)	6.02 (4.86)	1.04 (0.32)	3.15 (1.09)	1.42 (1.29)	2.94 (1.94)
O-xylene ($\mu\text{g m}^{-3}$)	M	1.94 (1.27)	2.12 (0.76)	5.14 (2.17)	1.50 (0.60)	4.70 (2.66)	1.39 (0.81)	1.36 (0.65)	1.64 (1.30)	3.07 (1.23)
	A	0.61 (0.42)	0.78 (0.48)	1.82 (0.80)	2.16 (0.68)	5.47 (4.50)	1.62 (0.72)	1.49 (0.35)	0.90 (0.42)	0.96 (0.51)
	N	1.34 (0.68)	1.57 (0.79)	3.74 (1.59)	1.10 (0.61)	4.61 (2.95)	0.84 (0.43)	2.67 (1.12)	1.16 (1.26)	1.49 (1.04)

Note: diurnal periods correspond to morning (M): 04:00–12:00 h, afternoon (A): 12:00–20:00 h and night (N): 20:00–04:00 h UTC.

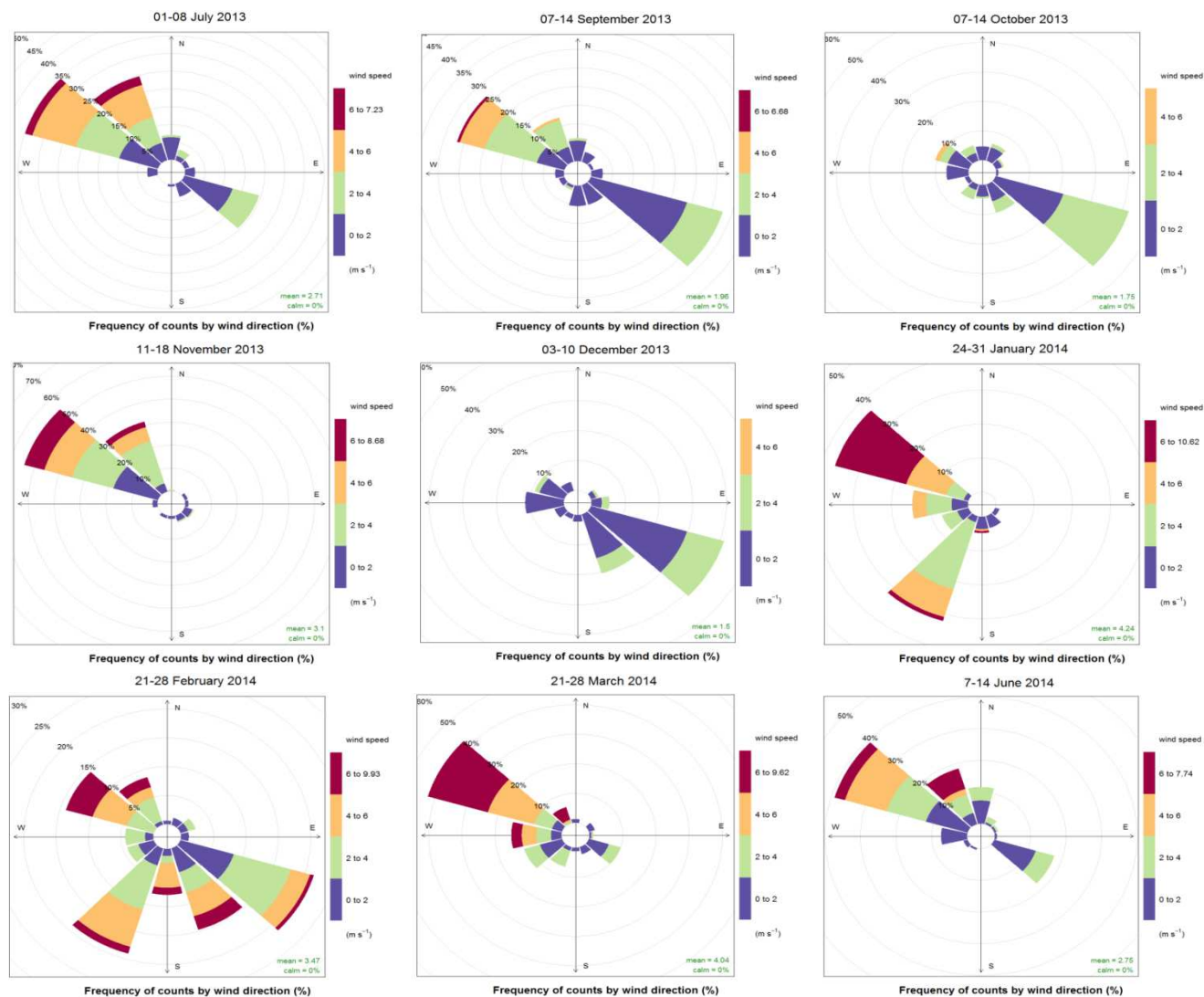


Figure 5.3. Wind rose showing the wind speed and direction frequencies at Bilbao city for the sampling periods of the campaign (based on hourly data).

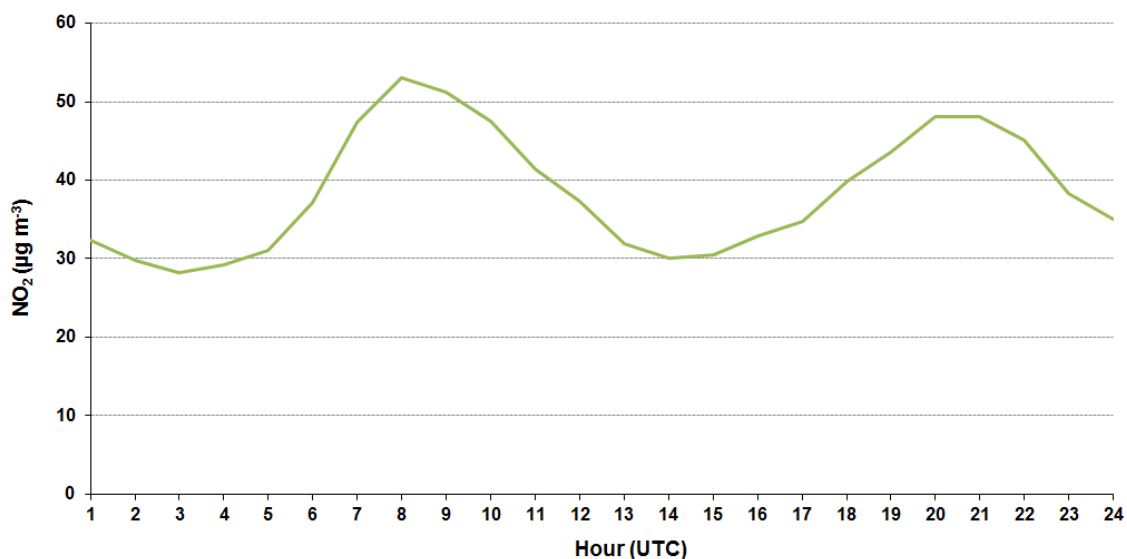


Figure 5.4. Average diurnal NO₂ concentration (µg m⁻³) in Bilbao city during sampling campaign.

5.3 Results of the sampling campaign

Table 5.3 presents the descriptive statistics (number of valid data, mean, standard deviation, median, minimum and maximum) for individual and total PAH concentrations measured over the whole sampling period. The Ace concentrations were not measured because of their low concentrations (small chromatographic peak) together with the presence of numerous interferences (with the same quantification ion and a similar retention time), which significantly complicated the identification and quantification of this compound in Bilbao's ambient air.

Table 5.3. Descriptive statistics of the individual and total particle-bound PAH concentrations (diurnal and sampling period-averaged data).

PAH	Period	N	Mean (ng m ⁻³)	SD (ng m ⁻³)	Median (ng m ⁻³)	Min. (ng m ⁻³)	Max. (ng m ⁻³)
FL	M	62	0.09	0.09	0.06	0.01	0.61
	A	60	0.08	0.06	0.06	0.02	0.28
	N	60	0.08	0.07	0.06	0.01	0.35
	Total	182	0.08	0.07	0.06	0.01	0.61
Phe	M	62	0.20	0.13	0.16	0.04	0.73
	A	60	0.18	0.14	0.14	0.06	0.80
	N	60	0.15	0.09	0.13	0.03	0.42
	Total	182	0.17	0.12	0.15	0.03	0.80
Ant	M	62	0.05	0.06	0.04	0.01	0.48
	A	60	0.05	0.05	0.03	0.01	0.32
	N	60	0.04	0.04	0.03	4.00·10 ⁻³	0.27
	Total	182	0.04	0.05	0.03	4.00·10 ⁻³	0.48
Ft	M	62	0.28	0.21	0.22	0.06	1.20
	A	60	0.31	0.27	0.24	0.04	1.38
	N	60	0.19	0.16	0.13	0.03	0.77
	Total	182	0.26	0.22	0.19	0.03	1.38
Pyr	M	62	0.29	0.22	0.23	0.05	1.04
	A	60	0.32	0.28	0.25	0.04	1.48
	N	60	0.19	0.16	0.14	0.02	0.73
	Total	182	0.27	0.23	0.20	0.02	1.48
BaA	M	62	0.16	0.18	0.08	0.02	0.78
	A	60	0.16	0.26	0.08	0.02	1.45
	N	60	0.15	0.21	0.05	0.01	1.00
	Total	182	0.16	0.22	0.07	0.01	1.45
Chry	M	62	0.24	0.21	0.18	0.04	0.91
	A	60	0.22	0.26	0.12	0.04	1.35
	N	60	0.22	0.24	0.13	0.03	1.08
	Total	182	0.22	0.24	0.13	0.03	1.35
BbFt	M	60	0.47	0.57	0.26	0.04	2.41
	A	57	0.53	1.01	0.17	0.06	5.98
	N	58	0.50	0.66	0.22	0.03	3.54
	Total	175	0.50	0.76	0.21	0.03	5.98

Table 5.3. (continued) Descriptive statistics of the individual and total particle-bound PAH concentrations (diurnal and sampling period-averaged data).

PAH	Period	N	Mean (ng m ⁻³)	SD (ng m ⁻³)	Median (ng m ⁻³)	Min. (ng m ⁻³)	Max. (ng m ⁻³)
BkFt	M	59	0.17	0.16	0.10	0.02	0.67
	A	57	0.20	0.30	0.08	0.03	1.41
	N	58	0.18	0.19	0.11	0.01	0.83
	Total	174	0.18	0.23	0.10	0.01	1.41
BaP	M	58	0.15	0.18	0.09	0.02	0.73
	A	57	0.14	0.20	0.08	0.01	1.16
	N	55	0.17	0.22	0.09	0.01	1.04
	Total	170	0.16	0.20	0.09	0.01	1.16
IP	M	55	0.16	0.19	0.10	0.01	0.92
	A	52	0.16	0.26	0.08	0.01	1.52
	N	54	0.18	0.26	0.09	1.00·10 ⁻³	1.32
	Total	161	0.17	0.24	0.09	1.00·10 ⁻³	1.52
DBahA	M	51	0.05	0.06	0.03	4.00·10 ⁻⁴	0.38
	A	47	0.05	0.06	0.03	3.00·10 ⁻³	0.35
	N	45	0.05	0.05	0.04	3.00·10 ⁻⁴	0.27
	Total	143	0.05	0.06	0.03	3.00·10 ⁻⁴	0.38
BghiP	M	60	0.21	0.17	0.16	0.02	0.92
	A	57	0.21	0.22	0.13	0.04	1.03
	N	57	0.20	0.19	0.15	0.01	0.95
	Total	174	0.20	0.19	0.15	0.01	1.03
BghiFt	M	40	0.19	0.17	0.13	0.03	0.74
	A	40	0.20	0.20	0.14	0.01	0.87
	N	38	0.18	0.19	0.09	0.02	0.64
	Total	118	0.20	0.19	0.13	0.01	0.87
BcP	M	61	0.05	0.05	0.04	0.01	0.23
	A	60	0.06	0.08	0.04	4.00·10 ⁻³	0.40
	N	60	0.05	0.06	0.02	0.01	0.25
	Total	181	0.06	0.06	0.03	4.00·10 ⁻³	0.40
CPP	M	25	0.05	0.10	0.01	4.00·10 ⁻³	0.45
	A	27	0.06	0.14	0.02	0.01	0.75
	N	21	0.11	0.23	0.01	3.00·10 ⁻³	0.95
	Total	73	0.07	0.16	0.01	3.00·10 ⁻³	0.95

Table 5.3. (continued) Descriptive statistics of the individual and total particle-bound PAH concentrations (diurnal and sampling period-averaged data).

PAH	Period	N	Mean (ng m ⁻³)	SD (ng m ⁻³)	Median (ng m ⁻³)	Min. (ng m ⁻³)	Max. (ng m ⁻³)
Triph	M	59	0.14	0.10	0.12	0.02	0.51
	A	54	0.13	0.12	0.09	0.03	0.62
	N	51	0.15	0.16	0.08	0.02	0.74
	Total	164	0.14	0.13	0.10	0.02	0.74
BaFt	M	49	0.04	0.05	0.03	4.00·10 ⁻³	0.21
	A	48	0.05	0.08	0.02	3.00·10 ⁻³	0.39
	N	44	0.05	0.07	0.02	3.00·10 ⁻³	0.32
	Total	141	0.05	0.07	0.02	3.00·10 ⁻³	0.39
BeP	M	58	0.26	0.28	0.16	0.01	1.08
	A	56	0.24	0.37	0.09	0.02	1.83
	N	55	0.27	0.31	0.14	0.01	1.50
	Total	169	0.26	0.32	0.13	0.01	1.83
Per	M	55	0.03	0.04	0.02	3.00·10 ⁻³	0.15
	A	54	0.03	0.03	0.02	2.00·10 ⁻³	0.14
	N	50	0.04	0.04	0.02	2.00·10 ⁻³	0.19
	Total	159	0.03	0.04	0.02	2.00·10 ⁻³	0.19
DBaja	M	37	0.01	0.01	3.00·10 ⁻³	4.00·10 ⁻⁴	0.03
	A	38	0.01	0.01	2.00·10 ⁻³	2.00·10 ⁻⁴	0.06
	N	36	0.01	0.01	3.00·10 ⁻³	2.00·10 ⁻⁴	0.04
	Total	111	0.01	0.01	2.00·10 ⁻³	2.00·10 ⁻⁴	0.06
BbC	M	20	0.01	5.00·10 ⁻³	0.01	3.00·10 ⁻³	0.02
	A	19	0.01	0.01	0.01	4.00·10 ⁻³	0.05
	N	23	0.01	0.01	0.01	2.00·10 ⁻³	0.05
	Total	62	0.01	0.01	0.01	2.00·10 ⁻³	0.05
Pic	M	21	0.02	0.03	0.01	4.00·10 ⁻³	0.13
	A	19	0.03	0.06	0.01	4.00·10 ⁻³	0.24
	N	23	0.03	0.04	0.01	3.00·10 ⁻³	0.14
	Total	63	0.03	0.04	0.01	3.00·10 ⁻³	0.24
Anthran	M	18	0.03	0.03	0.02	3.00·10 ⁻³	0.10
	A	12	0.02	0.04	0.01	3.00·10 ⁻³	0.13
	N	18	0.05	0.07	0.02	0.01	0.26
	Total	48	0.03	0.05	0.02	3.00·10 ⁻³	0.26

Table 5.3. (continued) Descriptive statistics of the individual and total particle-bound PAH concentrations (diurnal and sampling period-averaged data).

PAH	Period	N	Mean (ng m ⁻³)	SD (ng m ⁻³)	Median (ng m ⁻³)	Min. (ng m ⁻³)	Max. (ng m ⁻³)
Cor	M	18	0.09	0.09	0.04	0.01	0.26
	A	17	0.10	0.13	0.04	0.01	0.44
	N	18	0.11	0.13	0.06	0.01	0.40
	Total	53	0.10	0.12	0.04	0.01	0.44
Σ 25PAHs	M	62	3.12	2.71	2.14	0.59	12.55
	A	60	3.21	3.98	1.91	0.42	21.68
	N	60	2.94	3.06	1.80	0.41	14.65
	Total	182	3.09	3.27	2.06	0.41	21.68

Over the sampling campaign, the average concentration of individual PAHs ranged from 0.01 ± 0.01 to 0.50 ± 0.76 ng m⁻³, while the mean for total PAHs (Σ 25PAHs) was of 3.09 ± 3.27 ng m⁻³. The BaP showed a mean concentration of 0.16 ± 0.22 ng m⁻³, below the target value established by European legislation (1 ng m⁻³, annual mean) (EUD, 2008), and a maximum concentration of 1.16 ng m⁻³.

The mean diurnal period concentration of individual PAHs showed values between 0.01 ± 0.01 and 0.47 ± 0.57 ng m⁻³ for the morning period, between 0.01 ± 0.01 and 0.53 ± 1.01 ng m⁻³ for the afternoon period, and between 0.01 ± 0.01 and 0.50 ± 0.66 ng m⁻³ for the night period. The mean total PAH concentration (Σ 25PAHs) was 3.12 ± 2.71 , 3.21 ± 3.98 , and 2.94 ± 3.06 ng m⁻³ for morning, afternoon and night periods, respectively.

Total PAHs showed slightly higher concentrations in the afternoon period, whereas in terms of individual PAHs, the results did not indicate a predominant period because the levels for each PAH were equally distributed among diurnal periods.

Among the PAHs, BbFt was the major contributor to total PAHs. The mean concentration of this compound was 0.5 ± 0.76 ng m⁻³. Additionally, the most abundant PAHs found were, in order of importance, Pyr > Ft > BeP > Chry. Urban areas with a strong traffic impact are characterized by the high presence of these compounds in PM₁₀ fraction (Aldabe et al., 2012; Callén et al., 2013a).

Besides BeP, among the extra PAHs (not included in the EPA list), compounds such as BghiFt and Triph also showed a high mean concentration ($> 0.10 \text{ ng m}^{-3}$).

The results showed mean values of PAHs higher than the median values, indicating a positively skewed distribution. This behaviour also produces large data dispersion, which can be observed in a standard deviation higher than the mean for most of PAHs.

5.3.1 Temporal evolution: diurnal variability

The average diurnal period and weekly concentration of individual and total PAHs ($\Sigma 25$ PAHs), as well as the contribution of PAH-ring groups to the PM_{10} fraction for each month ($n=9$) of the sampling campaign, are shown in Table A.1 (in Appendix A) and 5.4., respectively.

Table 5.4. Diurnal period (n=7) and weekly (n=21) mean concentrations (ng m^{-3}) of total PAHs ($\Sigma 25\text{PAHs}$) and contribution (in %) of PAH-ring groups to the PM_{10} fraction during the sampling period. Standard deviation in brackets.

PAH	Period	July-13	September-13	October-13	November-13	December-13
$\Sigma 25 \text{ PAHs}$	M	2.09(0.82)	2.34(0.81)	4.73(2.94)	2.14(0.99)	8.79(2.76)
	A	1.35(0.29)	1.54(0.34)	2.72(0.64)	4.51(3.15)	12.67(6.70)
	N	1.71(0.63)	2.11(1.61)	2.44(0.93)	1.78(1.24)	10.74(3.01)
	Mean	1.73(0.67)	2.00(1.06)	3.30(2.02)	2.85(2.33)	10.63(4.50)
2-3 rings %	M	16(5)	17(4)	10(4)	14(5)	7(2)
	A	17(2)	16(4)	11(1)	13(4)	5(1)
	N	18(7)	15(6)	10(1)	17(8)	5(1)
	Mean	17(5)	16(5)	10(2)	15(6)	6(1)
4 rings %	M	42(7)	37(6)	38(7)	47(7)	31(3)
	A	39(9)	42(6)	43(6)	39(10)	33(4)
	N	33(5)	39(9)	37(4)	34(6)	28(3)
	Mean	38(8)	39(7)	39(6)	40(9)	31(4)
≥ 5 rings %	M	41(7)	46(7)	53(10)	39(9)	62(5)
	A	42(10)	42(7)	46(6)	48(13)	62(4)
	N	48(11)	46(9)	53(4)	49(11)	66(3)
	Mean	44(9)	45(7)	50(8)	46(12)	63(5)

Table 5.4. (continued) Average diurnal period (n=7) and weekly (n=21) concentrations (ng m⁻³) of total PAHs (Σ 25PAHs) and contribution (in %) of PAH-ring groups to the PM₁₀ fraction during the sampling period. Standard deviation in brackets.

PAH	Period	January-14	February-14	March-14	June-14	Jul. - Jun.
Σ 25 PAHs	M	1.99(1.52)	1.67(0.50)	1.68(1.16)	2.66(1.40)	3.12(2.71)
	A	1.85(0.28)	2.15(0.65)	1.57(0.69)	1.80(1.16)	3.21(3.98)
	N	0.96(0.38)	3.36(1.66)	1.55(1.59)	2.73(1.55)	2.94(3.06)
	Mean	1.60(0.99)	2.40(1.24)	1.60(1.15)	2.38(1.37)	3.09(3.27)
2-3 rings %	M	13(8)	14(1)	10(3)	11(4)	13(5)
	A	12(3)	12(3)	11(4)	13(7)	12(5)
	N	12(4)	14(7)	12(7)	7(4)	12(7)
	Mean	13(6)	13(4)	11(5)	11(6)	12(6)
4 rings %	M	45(8)	39(7)	43(6)	33(5)	39(9)
	A	47(7)	43(5)	45(7)	33(19)	41(9)
	N	38(6)	34(7)	37(9)	25(11)	34(7)
	Mean	43(8)	39(8)	42(8)	31(12)	38(9)
\geq 5rings %	M	42(9)	47(2)	46(9)	56(7)	48(11)
	A	41(7)	45(6)	44(6)	54(17)	47(11)
	N	50(5)	52(10)	52(11)	68(13)	53(11)
	Mean	44(8)	48(9)	47(9)	59(13)	49(11)

Over the sampling campaign, the mean diurnal period concentration of individual PAHs ranged from $5 \cdot 10^{-4} \pm 5 \cdot 10^{-4}$ to $2.75 \pm 1.89 \text{ ng m}^{-3}$, whereas for total PAHs ($\Sigma 25\text{PAHs}$) was between 0.96 ± 0.38 and $12.67 \pm 6.70 \text{ ng m}^{-3}$. A different pattern was observed during the sampling campaign according to the diurnal sampling periods. Thus, in July, September, October and January most of the PAHs displayed the highest individual concentrations during the morning periods, ranging from $1 \cdot 10^{-3} \pm 3 \cdot 10^{-4}$ to $0.77 \pm 0.74 \text{ ng m}^{-3}$. In contrast, in November and December the afternoon was the period with highest individual PAH concentrations (from $3 \cdot 10^{-3} \pm 2 \cdot 10^{-3}$ to $2.75 \pm 1.89 \text{ ng m}^{-3}$). Finally, in February and June, the individual PAHs reached the highest concentrations during the night periods, ranging from $3 \cdot 10^{-3} \pm 1 \cdot 10^{-3}$ to $0.42 \pm 0.25 \text{ ng m}^{-3}$. March did not show a predominant diurnal period.

The diurnal average BaP concentration ranged from $0.04 \pm 0.01 \text{ ng m}^{-3}$ to $0.70 \pm 0.28 \text{ ng m}^{-3}$; $0.21 \pm 0.24 \text{ ng m}^{-3}$ on average. This PAH presented higher concentration levels in the morning or at night (except in November). The observed results were also comparable to those reported previously in similar urban environments in Spain: Zaragoza: $0.089 \pm 0.34 \text{ ng m}^{-3}$ (warm period) and $0.48 \pm 0.48 \text{ ng m}^{-3}$ (cold period) (Callén et al., 2011), and Barcelona: $0.29 \pm 0.34 \text{ ng m}^{-3}$ (annual average) (Reche et al., 2012); and higher than the values measured in less populated and traffic affected cities: Ciudad Real: $0.014 \pm 0.007 \text{ ng m}^{-3}$ (autumn) and $0.035 \pm 0.050 \text{ ng m}^{-3}$ (winter) (Villanueva et al., 2015).

These results also clearly showed that the contribution of the more volatile compounds to the total PAHs measured in this study (i.e. 3-ring PAHs: FL, Phe and Ant) was low ($5 \pm 1\% - 18 \pm 7\%$), but quite constant during the diurnal sampling periods (12% on average). This is likely due to their predominant presence in the gaseous phase (Kameda et al., 2011), according to which their concentration in the particulate phase was lower in July and September, when higher temperatures (9°C higher than the average temperature in December) promote their volatilisation.

In contrast, the high molecular weight (HMW) PAHs (≥ 5 -ring) and middle molecular weight (MWM) PAHs (4-ring) accounted for $25 \pm 11\% - 47 \pm 7\%$ and $39 \pm 9\% - 68 \pm 13\%$ of the total PAH content respectively, showing a significant diurnal variation (ANOVA, $p < 0.05$). In this sense, high molecular and middle molecular weight PAHs followed a different diurnal pattern, in which high molecular weight PAHs presented their maximum contribution levels at night, when the contribution of the middle

molecular weight PAHs was minimal. The photodegradation of HMW light-sensitive compounds (5 and 6-ring PAHs are more readily destroyed by photochemical degradation than the 3 and 4-ring compounds) combined with the temperature inversions and the changes in the sources (Xu et al., 2013) could explain this pattern.

Finally, the seasonal variations of PAHs were significant (ANOVA, $p < 0.05$), showing higher values in the sampling week of October, November and December (autumn) than those obtained in July and September (summer) (Tables 5.4 and A1). Furthermore, some of the PAHs reached their maximum concentration levels during the night period. The changes over the course of the day in source strengths, the dispersion of material due to diurnal changes in meteorological factors (particularly atmospheric stability), the atmospheric reactivity, and the changes in temperature of the atmosphere could explain these variations in the PAH concentrations.

5.4 PAH source assessment

5.4.1 Diagnostic ratios analysis

The diagnostic ratios reported in the literature have been extensively used to identify the main emission sources of PAHs in urban environments (section 1.8.1).

In this regard, source identification can be improved by using various ratios and performing a relative comparison between them (Ravindra et al., 2008). Thus, cross plots of several ratios and their cut-off values for various sources are illustrated according to the months (Figure 5.5.A and B) and diurnal periods (Figure 5.5.C and D). The PAH diagnostic ratios calculated include Ant/Ant+Phe; Ft/Ft+Pyr; BaA/BaA+Chry and IP/IP+BghiP, whose values are detailed in Table 5.5.

Table 5.5. Diurnal period (n=7) and weekly (n=21) mean diagnostic ratios of PAHs over the sampling period (n=182). Standard deviation in brackets.

Ratios	Period	July	September	October	November	December
Ant/(Ant+Phe)	M	0.14 (0.03)	0.15 (0.03)	0.19 (0.03)	0.24 (0.11)	0.16 (0.02)
	A	0.15 (0.04)	0.16 (0.03)	0.19 (0.04)	0.30 (0.08)	0.18 (0.02)
	N	0.13 (0.03)	0.15 (0.04)	0.19 (0.03)	0.27 (0.10)	0.23 (0.06)
	Mean	0.14 (0.03)	0.15 (0.03)	0.19 (0.03)	0.27 (0.10)	0.19 (0.04)
Ft/(Ft+Pyr)	M	0.49 (0.03)	0.47 (0.02)	0.47 (0.02)	0.50 (0.04)	0.49 (0.03)
	A	0.52 (0.02)	0.47 (0.04)	0.47 (0.03)	0.49 (0.03)	0.49 (0.01)
	N	0.50 (0.03)	0.49 (0.03)	0.49 (0.03)	0.53 (0.02)	0.50 (0.01)
	Mean	0.50 (0.03)	0.48 (0.03)	0.48 (0.03)	0.51 (0.03)	0.50 (0.02)
BaA/(BaA+Chry)	M	0.32 (0.06)	0.42 (0.14)	0.42 (0.01)	0.30 (0.10)	0.46 (0.04)
	A	0.30 (0.05)	0.37 (0.14)	0.50 (0.16)	0.38 (0.03)	0.47 (0.04)
	N	0.30 (0.07)	0.34 (0.05)	0.39 (0.05)	0.30 (0.09)	0.48 (0.03)
	Mean	0.31 (0.06)	0.38 (0.12)	0.43 (0.10)	0.32 (0.08)	0.47 (0.04)
IP/(IP+BghiP)	M	0.40 (0.03)	0.39 (0.04)	0.46 (0.06)	0.24 (0.09)	0.49 (0.06)
	A	0.38 (0.02)	0.40 (0.02)	0.42 (0.02)	0.27 (0.12)	0.48 (0.10)
	N	0.44 (0.08)	0.41 (0.04)	0.45 (0.03)	0.29 (0.15)	0.54 (0.06)
	Mean	0.41 (0.06)	0.40 (0.03)	0.45 (0.04)	0.27 (0.12)	0.50 (0.07)
BaA/BaP	M	1.07 (0.84)	1.00 (0.20)	0.99 (0.16)	1.08 (0.07)	1.12 (0.23)
	A	1.24 (1.60)	0.86 (0.21)	1.02 (0.08)	1.26 (0.28)	1.29 (0.13)
	N	0.63 (0.13)	1.02 (0.68)	0.87 (0.14)	0.87 (0.39)	1.03 (0.21)
	Mean	0.97 (0.99)	0.96 (0.41)	0.96 (0.14)	1.07 (0.32)	1.15 (0.22)
BbFt/BkFt	M	2.10 (0.59)	2.64 (0.75)	3.06 (0.38)	2.29 (0.28)	3.66 (1.11)
	A	1.74 (0.73)	1.92 (0.72)	2.48 (0.59)	1.99 (0.53)	3.89 (1.06)
	N	1.87 (0.64)	2.54 (0.81)	2.79 (0.51)	1.80 (0.22)	3.73 (0.74)
	Mean	1.91 (0.64)	2.37 (0.79)	2.77 (0.53)	2.01 (0.40)	3.75 (0.94)
BaP/BghiP	M	0.55 (0.17)	0.65 (0.15)	0.95 (0.31)	0.77 (0.11)	0.77 (0.18)
	A	0.53 (0.22)	0.55 (0.12)	0.67 (0.13)	0.67 (0.20)	0.90 (0.20)
	N	0.57 (0.17)	0.61 (0.12)	0.75 (0.15)	0.84 (0.48)	1.05 (0.12)
	Mean	0.55 (0.18)	0.60 (0.13)	0.79 (0.24)	0.76 (0.31)	0.90 (0.20)
BghiP/IP	M	1.54 (0.20)	1.57 (0.26)	1.20 (0.31)	3.68 (1.69)	1.08 (0.26)
	A	1.61 (0.16)	1.52 (0.15)	1.38 (0.11)	3.79 (2.92)	1.17 (0.44)
	N	1.34 (0.40)	1.44 (0.20)	1.21 (0.13)	4.02 (4.24)	0.89 (0.22)
	Mean	1.49 (0.29)	1.51 (0.21)	1.26 (0.21)	3.84 (3.00)	1.05 (0.32)

Table 5.5. (continued) Diurnal period (n=7) and weekly (n=21) mean diagnostic ratios of PAHs over the sampling period (n=182). Standard deviation in brackets.

Ratios	Period	January	February	March	June	Jul. – Jun.
Ant/(Ant+Phe)	M	0.23 (0.11)	0.17 (0.05)	0.13 (0.02)	0.20 (0.03)	0.18 (0.07)
	A	0.26 (0.14)	0.16 (0.04)	0.16 (0.03)	0.24 (0.04)	0.20 (0.08)
	N	0.25 (0.09)	0.20 (0.05)	0.17 (0.04)	0.25 (0.06)	0.20 (0.07)
	Mean	0.25 (0.11)	0.18 (0.05)	0.15 (0.04)	0.23 (0.05)	0.19 (0.07)
Ft/(Ft+Pyr)	M	0.49 (0.04)	0.50 (0.02)	0.53 (0.05)	0.50 (0.02)	0.49 (0.03)
	A	0.49 (0.03)	0.48 (0.03)	0.54 (0.04)	0.51 (0.02)	0.49 (0.03)
	N	0.52 (0.02)	0.50 (0.02)	0.57 (0.07)	0.55 (0.05)	0.52 (0.04)
	Mean	0.50 (0.03)	0.49 (0.03)	0.55 (0.05)	0.52 (0.04)	0.50 (0.04)
BaA/(BaA+Chry)	M	0.40 (0.11)	0.51 (0.12)	0.33 (0.18)	0.25 (0.11)	0.42 (0.16)
	A	0.42 (0.07)	0.61 (0.18)	0.34 (0.11)	0.23 (0.08)	0.44 (0.18)
	N	0.27 (0.06)	0.67 (0.17)	0.25 (0.14)	0.15 (0.09)	0.37 (0.18)
	Mean	0.37 (0.10)	0.60 (0.17)	0.31 (0.14)	0.21 (0.10)	0.38 (0.15)
IP/(IP+BghiP)	M	0.27 (0.12)	0.40 (0.11)	-	0.29 (0.16)	0.37 (0.12)
	A	0.32 (0.07)	0.32 (0.08)	0.22 (0.02)	0.33 (0.06)	0.36 (0.09)
	N	0.20 (0.13)	0.40 (0.08)	0.41 (5.00·10 ⁻³)	0.26 (0.12)	0.38 (0.13)
	Mean	0.27 (0.12)	0.38 (0.09)	0.29 (0.11)	0.29 (0.12)	0.37 (0.12)
BaA/BaP	M	1.54 (0.54)	0.97 (0.28)	1.70 (0.70)	1.13 (0.19)	1.16 (0.47)
	A	1.65 (0.30)	1.07 (0.15)	1.88 (0.52)	1.06 (0.98)	1.24 (0.67)
	N	0.98 (0.13)	1.12 (0.37)	1.46 (0.91)	0.89 (0.44)	0.97 (0.43)
	Mean	1.39 (0.45)	1.06 (0.27)	1.69 (0.67)	1.04 (0.64)	1.13 (0.54)
BbFt/BkFt	M	2.63 (0.59)	2.45 (0.85)	2.17 (0.71)	2.77 (1.15)	2.64 (0.93)
	A	2.56 (0.43)	2.85 (0.60)	2.57 (0.76)	2.34 (0.34)	2.48 (0.86)
	N	2.17 (0.17)	3.16 (0.85)	2.71 (0.79)	2.02 (0.50)	2.53 (0.84)
	Mean	2.45 (0.46)	2.82 (0.79)	2.49 (0.74)	2.38 (0.96)	2.55 (0.87)
BaP/BghiP	M	0.50 (0.13)	0.63 (0.11)	0.76 (0.32)	0.48 (0.17)	0.68 (0.23)
	A	0.44 (0.14)	0.78 (0.20)	0.83 (0.35)	0.46 (0.15)	0.64 (0.24)
	N	0.39 (0.09)	0.90 (0.25)	0.70 (0.39)	0.29 (0.08)	0.70 (0.30)
	Mean	0.44 (0.13)	0.77 (0.22)	0.77 (0.33)	0.44 (0.16)	0.67 (0.26)
BghiP/IP	M	3.53 (2.68)	1.67 (0.78)	-	4.36 (4.94)	2.28 (2.23)
	A	2.22 (0.72)	2.24 (0.66)	3.50 (0.38)	2.11 (0.52)	2.04 (1.30)
	N	5.94 (6.40)	1.56 (0.52)	1.44 (0.03)	4.21 (3.92)	2.38 (3.11)
	Mean	3.02 (1.95)	1.82 (0.70)	2.91 (1.45)	3.79 (3.87)	2.24 (2.32)

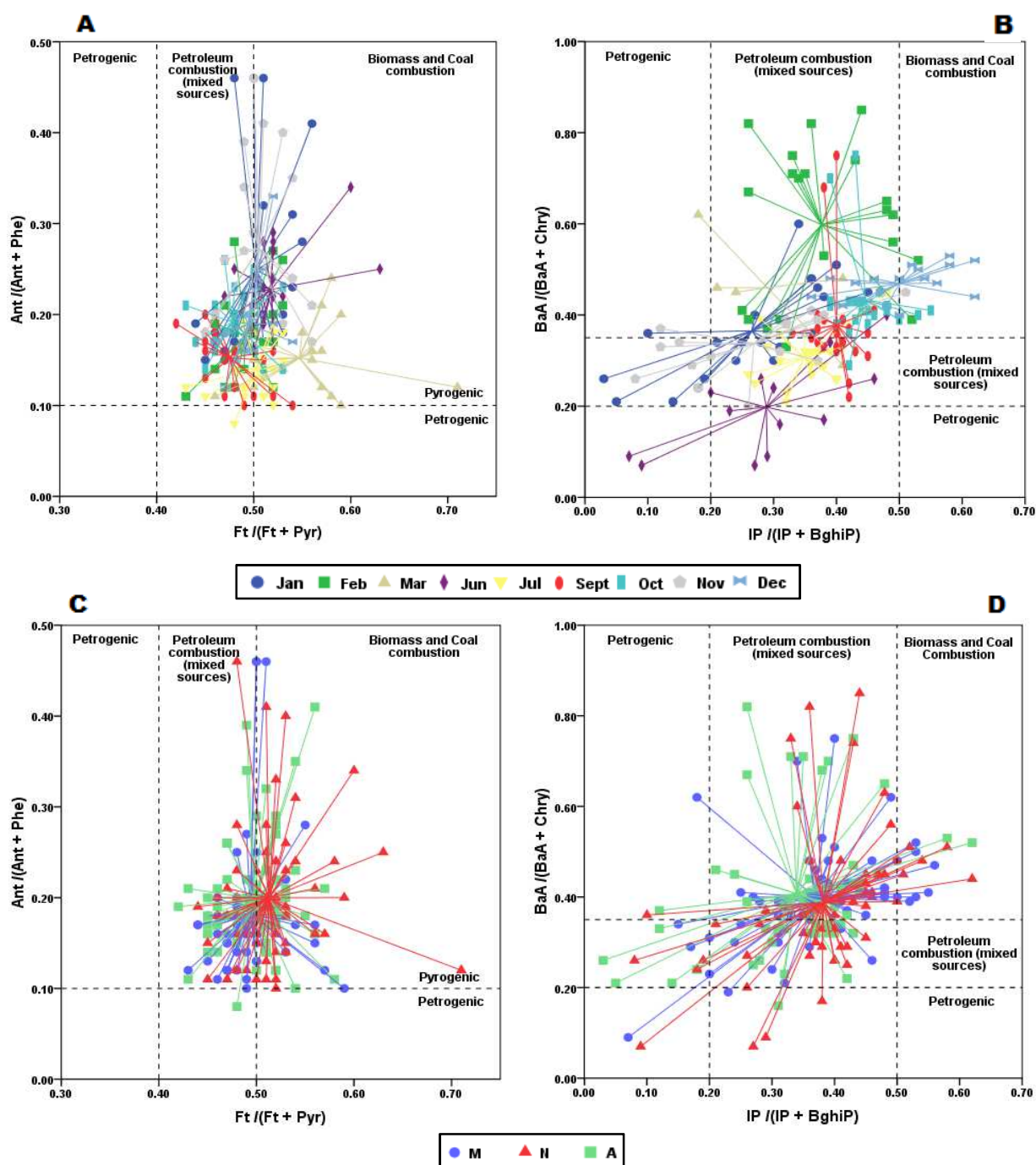


Figure 5.5. Cross plots for the ratios Ft/(Ft+Pyr) vs Ant/(Ant+Phe) according to the (A) month and (C) diurnal period, and IP/(IP+BghiP) vs BaA/(BaA+Chry) according to the (B) month and (D) diurnal period.

As illustrated in Figure 5.5, the binary ratios calculated enabled us to discriminate between pyrogenic and petrogenic sources in the urban area. These results ($\text{Ant}/(\text{Ant}+\text{Phe}) > 0.1$, $\text{Ft}/(\text{Ft}+\text{Pyr}) > 0.4$, $\text{IP}/(\text{IP}+\text{BghiP})$ and $\text{BaA}/(\text{BaA}+\text{Chry}) > 0.2$) clearly indicated the predominance of pyrogenic sources (Yunker et al., 2002). Moreover,

these cross plots also allowed us to distinguish between different pyrogenic forms that pointed out a mixed contribution from petroleum combustion as well as coal/biomass burning. In particular, the average value of the Ft/(Ft+Pyr) ratio obtained in this study was 0.50 ± 0.04 , which indicated the predominance of vehicular emissions (Varea et al., 2011) over other pyrogenic PAH sources (average Ant/(Ant+Phe) value = 0.19 ± 0.07) (Table 5.5). Interestingly, Ft/(Ft+Pyr) values tended to be higher than 0.5 during the afternoon and night periods, which suggests a coal/biomass combustion source (Figure 5.5.C). In contrast, most of the morning periods were located in the petroleum combustion area, pointing out the prevalence of vehicle exhaust emissions during that period. This mixed contribution was especially evident in November and January, which showed a different pattern highlighted by higher values of the Ant/(Ant+Phe) and Ft/(Ft+Pyr) ratios (Figure 5.5.A). In contrast, March, with the highest values of Ft/(Ft+Pyr) ratio, suggested the predominance of coal/biomass combustion sources. A different trend was also confirmed by the results obtained for the BaA/(BaA+Chry) (average = 0.38 ± 0.15) and IP/(IP+BghiP) ratios (average = 0.37 ± 0.12), whose values differentiated in a similar way November, January, February and June from the other months (Figure 5.5.B). Even more, these values also suggested that December was more influenced by coal/biomass combustion sources, not showing a clear differentiation between the different diurnal periods.

In addition, BaA/BaP, BbFt/BkFt, BaP/BghiP and BghiP/IP ratios were calculated (Table 5.5) in order to distinguish between gasoline and diesel exhausts in vehicular emissions. The average values obtained: 1.13 ± 0.54 (BaA/BaP); 2.55 ± 0.87 (BbFt/BkFt); 0.67 ± 0.26 (BaP/BghiP); 2.24 ± 2.32 (BghiP/IP), suggested that the main contribution of traffic emissions could be due to diesel vehicles (Slezakova et al., 2010; Callén et al., 2011; Oliveira et al., 2011; Sisovic et al., 2012). Nevertheless, these diagnostic ratios only indicate potential sources without providing the distribution of PAHs for each source. Thus, receptor models were also applied in an attempt to identify PAH profiles.

5.4.2 UNMIX

The last version of the UNMIX model, UNMIX 6.0 (US-EPA, 2007) was used to apportion the potential sources of PAHs and their contributions. Before starting the modelling, the database was checked to find data below the method detection limit (MDL), missing data and outliers. The missing data were replaced by the geometric

mean and the outliers (6 samples) were left out. Only IP and DBahA showed data below MDL and also the higher number of missing data (Table 5.6).

Table 5.6. Number of acceptable data, data below the MDL, and missing data for each PAH in the database.

PAH	Acceptable	< MDL	Missing
FL	182	0	6
Phe	182	0	6
Ant	182	0	6
Ft	182	0	6
Pyr	182	0	6
BaA	182	0	6
Chry	182	0	6
BbFt	175	0	13
BkFt	174	0	14
BeP	170	0	18
BaP	170	0	18
IP	160	1	27
DBahA	135	8	45
BghiP	173	0	15

In order to provide source composition as mass fraction (US-EPA, 2007), a variable that accounts for the total PAH concentration was set as Total Variable and added to the input species.

Initially, no feasible solution was found that included all species. Different combinations and the “suggest exclusion” function were used until finding a feasible solution with a clear interpretability of the factors. Finally, UNMIX identified 3 sources for PAH species (excluding FL, Ant, BeP and DBahA) with min. R^2 value of 0.92 and min. S/N value of 4.18. These results achieves the recommend values (min. $R^2 > 0.8$ and min. S/N > 2) set by US EPA to ensure that the solution is feasible (US-EPA, 2007). The concentrations of PAHs predicted by the UNMIX model were well correlated with the experimentally measured concentrations ($R^2 = 1$) (Figure 5.6). The source profiles resolved by the UNMIX model are presented in Table 5.7.

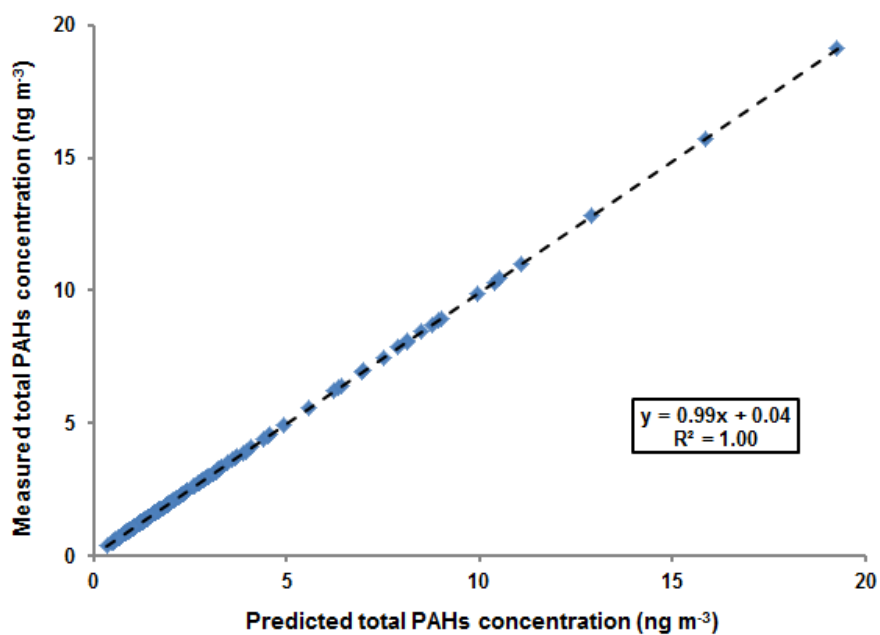


Figure 5.6. Measured vs. predicted total PAH concentrations (ng m⁻³) in UNMIX model

Table 5.7. Source profiles (in ng m⁻³) obtained from UNMIX.

PAH	Factor		
	1	2	3
Phe	0.02	0.11	0.04
Ft	0.03	0.15	0.08
Pyr	0.03	0.16	0.08
BaA	0.01	0.04	0.11
Chry	0.06	0.08	0.08
BbFt	0.26	0.00	0.23
BkFt	0.12	0.03	0.03
BaP	0.00	0.03	0.11
IP	0.00	0.02	0.13
BghiP	0.02	0.07	0.09
PAHs (%)	27	31	42

Factor 1 was characterized by high loadings on BbFt and BkFt and moderate on Chry. As some of these compounds were suggested as markers from natural gas home appliances (Rogge et al., 1993; Bourotte et al., 2005; Lee and Kim, 2007), coal

combustion processes (Wan et al. 2006; Ravindra et al. 2008), and combustions of oil (Mantis et al., 2005). Thus; this factor may be associated with a mix of stationary sources (Masiol et al., 2012).

In contrast, Factor 2 was strongly related to 3 to 4-ring PAHs (Phe, Ft and Pyr), which are usually emitted by electric arc furnaces in the steel/iron industry (Baraniecka et al., 2010; Gomes, 2016). This technology is used in the local industry for the production of steel (see Figure 5.2). Thus; this factor could be associated with the steel industry.

Finally, Factor 3 was characterized by the highest molecular weight PAHs, i.e. BaA, BbFt, BaP, IP and BghiP, all of which are characteristic of vehicle emissions (He et al., 2014; Lv et al., 2016).

5.4.3 Positive matrix factorization (PMF)

PMF 5.0 (US-EPA, 2014) was used to apportion the contribution from emission sources. The model requires two input matrices: one for measured concentration of the species (C) and one for the estimated uncertainty of the concentration. The uncertainty for each variable was calculated using the concentration and the MDL. If C was above the MDL, the uncertainty was the value obtained by the methodology explained in Chapter 4. In contrast, if C was below the MDL, C and the uncertainty were replaced by MDL/2 and $0.2C + MDL/3$, respectively (Tauler et al., 2009). For missing values, geometric mean concentration and four times this mean were used for the C and uncertainty, respectively (Kim and Hopke, 2007).

The methodology reported in the EPA PMF 5.0 user guide (US-EPA, 2014) was used to optimize the model solution. This is summarized in the next processes:

Categorization of variables. In the PMF model the user can specify whether a species is “Strong”, “Weak” or “Bad”. As a first approach, Paatero and Hopke (2003) suggested use of the signal-to-noise (S/N) ratio for each species as classification rule. Consequently, a species is classified as “Strong” if its S/N ratio is greater than 2, “Weak” if it is between 0.2 and 2, and “Bad” if it is less than 0.2. “Bad” variables are excluded from the dataset; the uncertainties for “Weak” variables are tripled, and uncertainties of “Strong” variables remain unchanged. In this study, all species showed a S/N ratio greater than 3, except for DBahA that had a ratio of 1.7 due to the 24% missing values (Table 5.6). Hence, DBahA was defined as “Weak” variable. The

variable for the total PAH concentration was specified as Total Variable and automatically categorized as weak to lower its influence in the final PMF results.

Extra model uncertainty. This uncertainty encompasses various errors that are not considered measurement or analytical errors, such as the variation of source profiles and the chemical reactivity of species in the atmosphere (US-EPA, 2014). This study explored an extra uncertainty range between 0 and 15%. Finally, a value of 10% was found appropriate.

Outliers. Before running the PMF, it is recommended to check the temporal pattern of the samples in order to detect unusual data. In this study, 6 samples (the same as in the application of UNMIX) were excluded from the model.

Fitting parameters. In order to guarantee a good match between observed (input data) and predicted (modelled) values the correlation coefficient (R^2) and slopes of individual PAHs should be larger than 0.6 and near 1, respectively. If a species showed $R^2 < 0.6$ the user should evaluate whether this has to be down-weighted or excluded from the model. In the initial PMF run, FL and Ant showed a poor correlation ($R^2 < 0.6$), thus, these species were down-weighted, defining them as “Weak” variables for final analysis.

The value of the Q function (Eq. 1.4) is the other parameter that determines the goodness of fit of the input data. The Q (robust) is calculated excluding outliers, while the Q (true) is calculated including all points. In this study, the stability of PMF was analysed by checking both Q and by comparing the Q (robust) with the Q (theoretical). This Q represents the perfect fit of the model and is determined by the next expression (Callén et al., 2014):

$$Q(\text{theoretical}) = (n \cdot s) + [(n \cdot w) / 3] - (n \cdot f) \quad (5.1)$$

where n is the number of samples, s is the number of strong samples, w is the number of weak species, and f is the number of expected factors. The model will show a reasonable fit if the value of Q (robust) is within $\pm 50\%$ of the Q (theoretical).

In order to ensure that the solution is the global minimum, the model was run from 20 random starting points and the lowest Q (robust) for the 20 runs was used as the final solution.

Factor rotations. The non-negativity constraint of PMF is not enough to ensure that there is a unique solution (rotational ambiguity). The Fpeak is a built-in function in PMF that is used to assess and reduce the rotational ambiguity. The basic role of Fpeak is to create new matrices by forcing rows and columns of F and G matrices to be added or subtracted to or from each other (depending on the positive or negative Fpeak value) (Reff et al., 2007). Fpeak values from -1.4 to 0.8 were used to test the rotational ambiguity of the solution in this study. Values beyond this range were not tested because they generate changes of the Q value higher than 5% (US EPA, 2014).

Model errors. The PMF model software allows evaluating the variability in the solution by two error estimation methods: displacement (DISP) and Bootstrap (BS) analysis. The DISP explores the rotational ambiguity in a PMF solution by assessing the largest range of source profile values without an appreciable increase in the Q value. In contrast, BS is used to detect and estimate disproportionate effects of a small set of observations on the solution and also, partially, effects of rotational ambiguity (US EPA, 2014). To ensure the robustness of the statistics, 100 bootstrap runs were performed in this study, using a minimum correlation value (R value) of 0.60.

The UNMIX results (3 sources) were used as guide to the initial selection of the number of factors in PMF. From three-factor to five-factor solutions were explored in PMF. Finally, a three-factor model provided the best fit, having a theoretical Q value of 1698.7 and a robust Q value of 2672.9.

The total variable (total PAH concentration) showed very good fit between observed and predicted data, with a correlation coefficient (R^2) of 0.99 and a slope of 1 (Figure 5.7). Besides, the individual species were well adjusted, with R^2 higher than 0.78 for the most of them.

Altering the Fpeak value was not found to result in substantially better source profiles. Therefore, base run result (Fpeak = 0) was selected.

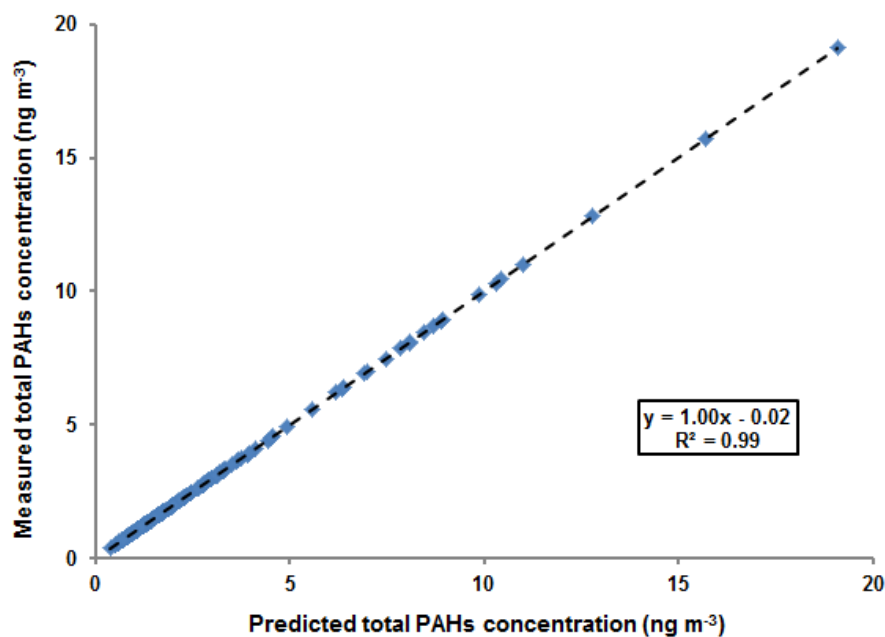


Figure 5.7. Measured vs. predicted total PAH concentration (ng m⁻³) in PMF model

Finally, DISP and BS methods did not show factor swaps (factors change so much that they exchange identities, indicating a “not-well-defined solution”), and at least 93 bootstrap factors are mapped to each base factor, meaning a relatively stable result.

The three-factor model showed a similar profile to the UNMIX factors (Figure 5.8.). Factor 1 showed a significant contribution of Chry, BbFt, BkFt and BeP. Natural gas, coal and oil combustion could be the main sources of these compounds; consequently, the factor was associated with a mix of stationary sources.

Factor 2 had a similar source profile to factor 2 from UNMIX. This factor was more influenced by lower molecular weight PAHs, with contributions higher than 60% of FL, Phe, Ant, Ft and Pyr. These compounds, as mentioned in the factor 2 from the UNMIX analysis, may be attributed to the production of steel by electric arc furnaces. Therefore, this factor was associated with steel industry emissions.

Factor 3 showed high proportions of BaA (62%), BaP (74%), IP (100%), DBaH (99%) and BghiP (68%), a similar profile to the vehicular emission factor (factor 3) from the UNMIX analysis. Thus, this factor could be representative of vehicle emissions.

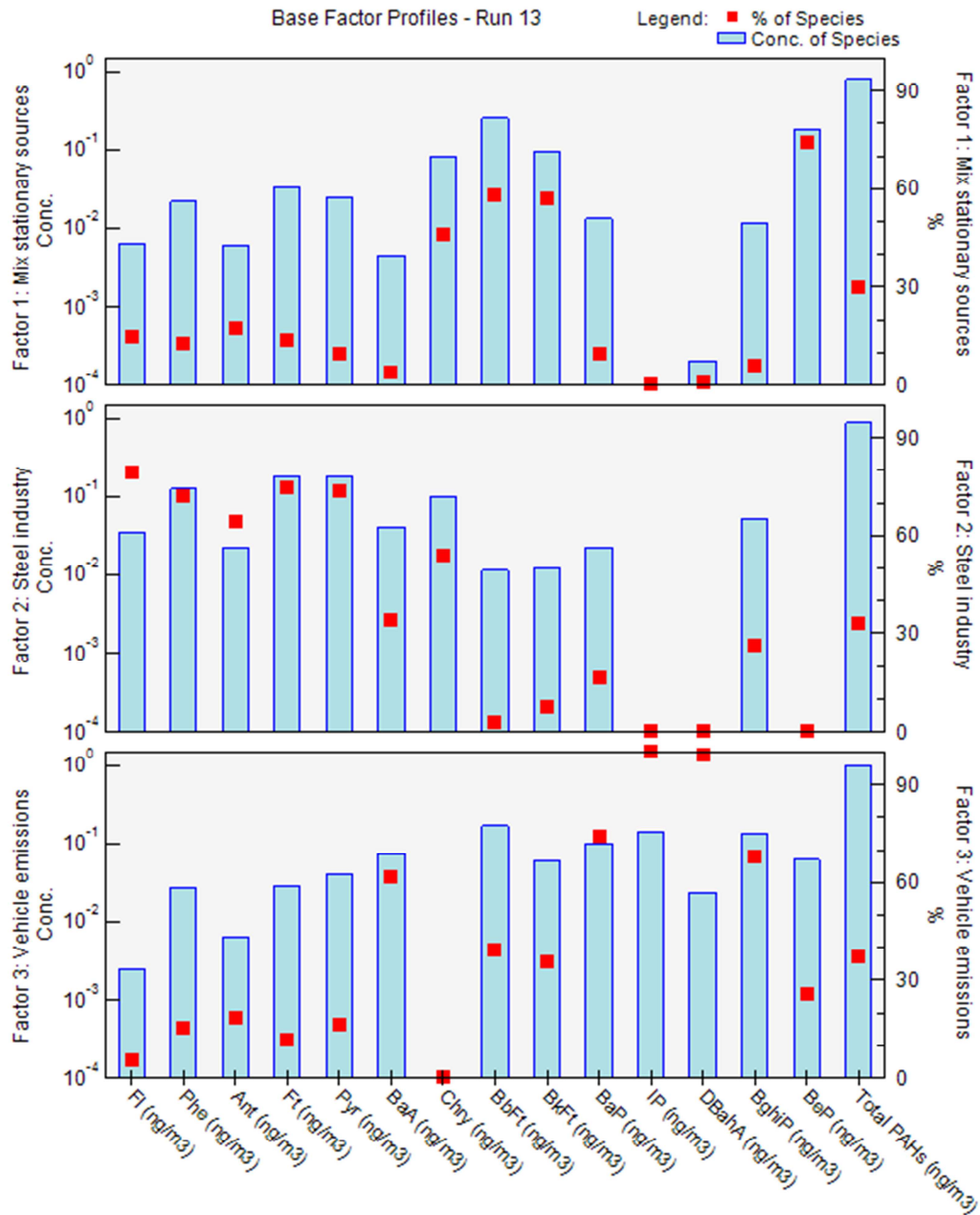


Figure 5.8. PMF factor profiles.

Total PAH contributions of the three sources showed a similar percentage, being slightly higher for vehicle emissions (Figure 5.9).

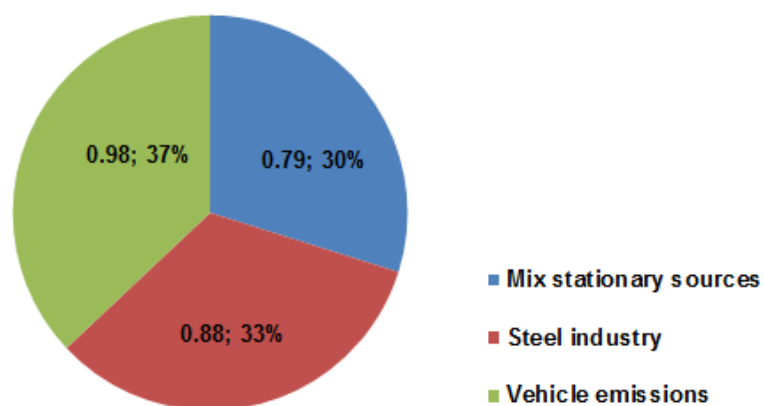


Figure 5.9. Total PAH source contribution (ng m⁻³; %) by PMF model in Bilbao city

In order to better characterize the sources, the BaP/(BaP+BeP) ratio was studied in the samples with the highest contribution of PAHs (> 60%) in one of three sources. This ratio is usually used as atmospheric particle ageing marker and also as a marker of photodegradation of gaseous and particle PAHs (Oliveira et al., 2011). The results showed that samples with the vehicular exhausts as the main contributor of PAHs had ratio values around 0.5, indicating freshly emitted particles. In contrast, when the main contributor of PAHs was a mix of stationary sources or the steel industry, the samples showed mainly BaP/(BaP+BeP) ratio values less than 0.5, meaning photolysis and therefore ageing particles.

Also, to help in the identification and characterization of the sources, a bivariate polar plot derived from the openair software (Carslaw and Ropkins, 2012) was used with the PMF factor and NO₂ concentrations (Figure 5.10).

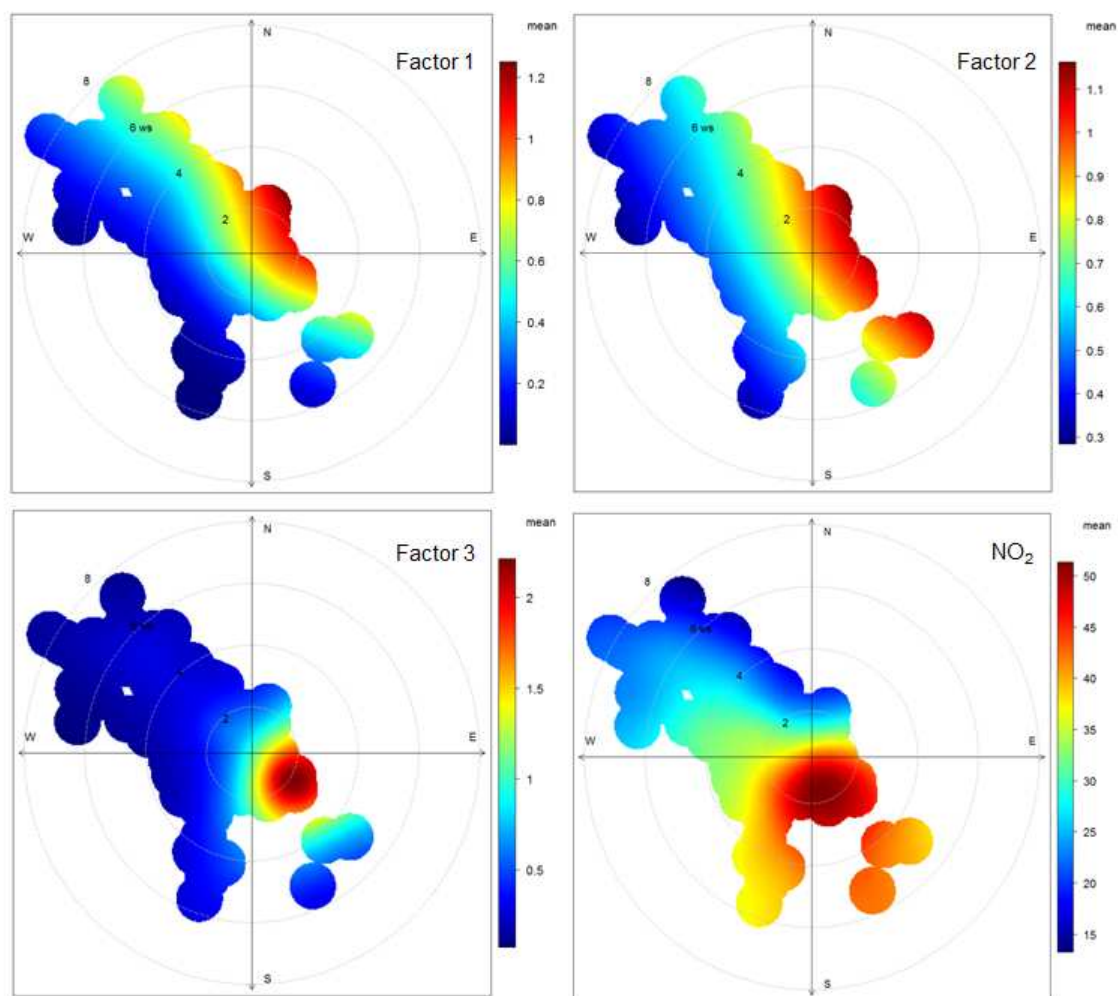


Figure 5.10. Bivariate polar plot of PMF factor concentrations (ng m^{-3}) and of NO_2 concentrations ($\mu\text{g m}^{-3}$) at Bilbao city (8-hour mean concentrations).

Bivariate polar plots show how the concentration of a species varies jointly with wind speed and wind direction in polar coordinates. Wind direction together with wind speed can be highly effective at discriminating different emission sources (Uria-Tellaetxe and Carslaw, 2014). For this reason, the use of 8-hour means in the bivariate polar plot could complicate the identification of emission sources, as wind direction and speed vary significantly in shorter time periods, losing information in the final plot. As a consequence, the plots obtained for factor 1 and 2 showed a similar pattern (the highest PAH concentrations in the NW-SE direction); complicating the discrimination between the sources of both factors (Figure 5.10).

In contrast, the bivariate polar plot for factor 3 showed a different pattern (the impact of this was more localized in the SE direction), matching the NO_2 (traffic-related air

pollutant) (figure 5.10). This could confirm that both pollutants (factor 3 and NO₂) were emitted from the same source, urban traffic.

5.5. Effect of meteorology

The ambient meteorological factors could greatly affect the PAH concentrations. In order to elucidate the most influenced meteorological factors depending on the diurnal period, Pearson correlation coefficients between PAH concentrations and the meteorological variables were calculated in Table 5.8.

Table 5.8. Pearson correlation coefficients of PAHs with meteorological parameters depending on the diurnal period (n=61 per diurnal period).

PAH	Period	Wind speed	Temperature	Pressure	Rain	Humidity	Irradiation
FL	M	-0.21	-0.01	0.03	-0.21	0.04	-0.01
	A	-0.19	0.00	0.31*	-0.07	0.10	-0.05
	N	-0.14	-0.01	0.21	-0.21	-0.11	
Phe	M	-0.44**	-0.04	0.33**	-0.29*	0.24	-0.05
	A	-0.51**	-0.21	0.38**	-0.05	0.18	-0.32*
	N	-0.40**	-0.19	0.44**	-0.36**	0.14	
Ant	M	-0.16	-0.10	0.02	-0.09	0.15	-0.13
	A	-0.24	-0.18	0.32*	0.15	0.32*	-0.36**
	N	-0.20	-0.17	0.40**	-0.19	0.10	
Ft	M	-0.28*	-0.30*	0.39**	-0.14	0.26*	-0.25*
	A	-0.53**	-0.35**	0.36**	-0.04	0.12	-0.41**
	N	-0.30*	-0.36**	0.44**	-0.30*	0.11	
Pyr	M	-0.30*	-0.31*	0.39**	-0.13	0.27*	-0.27*
	A	-0.57**	-0.36**	0.37**	-0.04	0.11	-0.43**
	N	-0.32*	-0.36**	0.45**	-0.31*	0.12	
BaA	M	-0.27*	-0.32*	0.32*	-0.23	0.19	-0.22
	A	-0.47**	-0.31*	0.34**	-0.06	0.03	-0.27*
	N	-0.19	-0.47**	0.39**	-0.24	0.08	
Chry	M	-0.32*	-0.08	0.35**	-0.26*	0.29*	-0.17
	A	-0.42**	-0.25	0.34**	-0.04	0.14	-0.28*
	N	-0.22	-0.20	0.38**	-0.23	0.16	
BbFt	M	-0.27*	-0.22	0.40**	-0.25	0.17	-0.14
	A	-0.40**	-0.23	0.34**	-0.08	0.07	-0.20
	N	-0.21	-0.34**	0.35**	-0.25	0.08	
BkFt	M	-0.29*	-0.11	0.37**	-0.27*	0.24	-0.08
	A	-0.37**	-0.22	0.28*	0.12	0.24	-0.25
	N	-0.27*	-0.13	0.33**	-0.28*	0.14	
BeP	M	-0.33**	-0.06	0.38**	-0.26*	0.21	-0.06
	A	-0.39**	-0.16	0.38**	-0.16	0.07	-0.17
	N	-0.17	-0.13	0.24	-0.19	0.05	
BaP	M	-0.25	-0.25*	0.34**	-0.22	0.18	-0.18
	A	-0.47**	-0.25	0.36**	-0.08	0.01	-0.22
	N	-0.17	-0.47**	0.38**	-0.23	0.13	

** Significant correlation significant at the 0.01 level (2 tailed).

* Significant correlation significant at the 0.05 level (2 tailed).

Diurnal periods correspond to morning (M): 04:00–12:00 h, afternoon (A): 12:00–20:00 h and night (N): 20:00–04:00 h UTC.

Table 5.8. (continued) Pearson correlation coefficients of PAHs with meteorological parameters depending on the diurnal period (n=61 per diurnal period).

PAH	Period	Wind speed	Temperature	Pressure	Rain	Humidity	Irradiation
IP	M	-0.19	-0.33**	0.34**	-0.24	0.16	-0.16
	A	-0.45**	-0.21	0.27*	-0.01	0.03	-0.20
	N	-0.14	-0.43**	0.35**	-0.19	0.15	
DBahA	M	-0.03	-0.23	0.28*	-0.20	0.02	-0.11
	A	-0.44**	-0.14	0.26*	0.04	0.05	-0.16
	N	-0.12	-0.47**	0.23	-0.16	0.08	
BghiP	M	-0.28*	-0.28*	0.37**	-0.28*	0.21	-0.17
	A	-0.44**	-0.23	0.28*	0.14	0.18	-0.27*
	N	-0.21	-0.39**	0.41**	-0.26*	0.19	
Σ14PAHs	M	-0.32*	-0.23	0.40**	-0.26*	0.23	-0.18
	A	-0.47**	-0.26*	0.36**	-0.04	0.11	-0.27*
	N	-0.25	-0.35**	0.41**	-0.28*	0.12	

** Significant correlation significant at the 0.01 level (2 tailed).

* Significant correlation significant at the 0.05 level (2 tailed).

Diurnal periods correspond to morning (M): 04:00–12:00 h, afternoon (A): 12:00–20:00 h and night (N): 20:00–04:00 h UTC.

The significant meteorological parameters ($p < 0.05 - 0.01$, Table 5.8) for most of the PAHs were wind speed, temperature, and atmospheric pressure, whereas solar irradiation and rainfall did not have a significant influence on most of them. Humidity had no clear influence on the PAHs variation, probably due to the narrow humidity range during the sampling period (see Table A.1). Significant negative correlations of PAHs related to wind speed and temperature, and positive correlations of PAHs with ambient pressure, have been also observed in other studies (Barrado et al., 2012; Augusto et al., 2013; Callén et al., 2014).

During the nights and the mornings, the atmospheric temperature showed significant negative correlations ($p < 0.05-0.01$, Table 5.8). At night, lower temperatures generally result in temperature inversion under lower solar irradiation (Wu et al., 2014). In the morning, higher temperatures increase the atmospheric degradation pathways of PAHs through chemical or photochemical reactions, as well as their participation in the gas phase (He et al., 2014).

The wind had an important role in the atmospheric dispersion and dilution of PAHs, especially during the morning and afternoon period. In the spring and summer, the breeze cycles generate strong NW and WNW winds (from sea to land) which enhance the dispersion of pollutants, reaching their maximum value in the afternoon and disappearing during the night. This local dispersion mechanism changes in autumn when the sea breeze effect disappears and the wind is more persistent (Millán et al., 1987; Acero et al., 2013). At this time of year (autumn and winter) the prevailing winds are from SE and ESE, which are frequently associated with cold air drainage flows (i.e. mountain/valley breeze). This breeze starts after sunset and persists until the first hours after sunrise, enhancing the PAH concentration. If synoptic situations are adequate the effect of these winds can extend until midday (Acero et al., 2013).

During the sampling campaign, the effect of breeze cycles was clearly observed in Bilbao city, generating stronger afternoon winds in spring and summer (Figure 5.11) that matched the significant drops in pollutant concentration (for example for NO₂ levels in Figure 5.12, and for Σ 25PAH concentrations in Table 5.4). In contrast, the absence of these winds during autumn and winter (Figure 5.11) increased the concentration of pollutants during the afternoon (as can be observed in Table 5.4 for Σ 25PAHs). In the case of NO₂, the peak concentration appeared to be related to afternoon rush hour traffic (Figure 5.12).

Finally, significant positive correlations ($p < 0.05-0.01$, Table 5.8) were found between the atmospheric pressure and ambient particle-bound PAH concentrations during the nights and afternoons. A higher ambient pressure leads to reduced volatilisation (from particle surfaces) together with enhanced condensation of semi-volatile organic compounds on particles (Bandowe et al., 2014). In particular, it is interesting to note that the highest particle concentrations of PAHs found in December were measured under a “blocking anticyclonic episode”, when higher atmospheric pressures resulted in a lower dispersion of these pollutants due to lower temperatures and inversion phenomena.

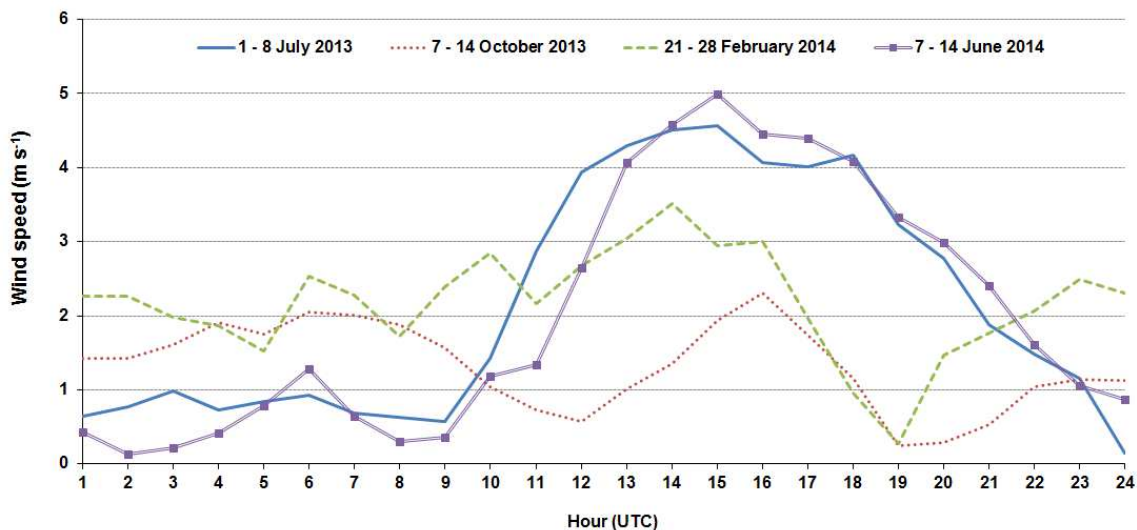


Figure 5.11. Average diurnal wind speed (m s^{-1}) in Bilbao city. Seasonal comparison.

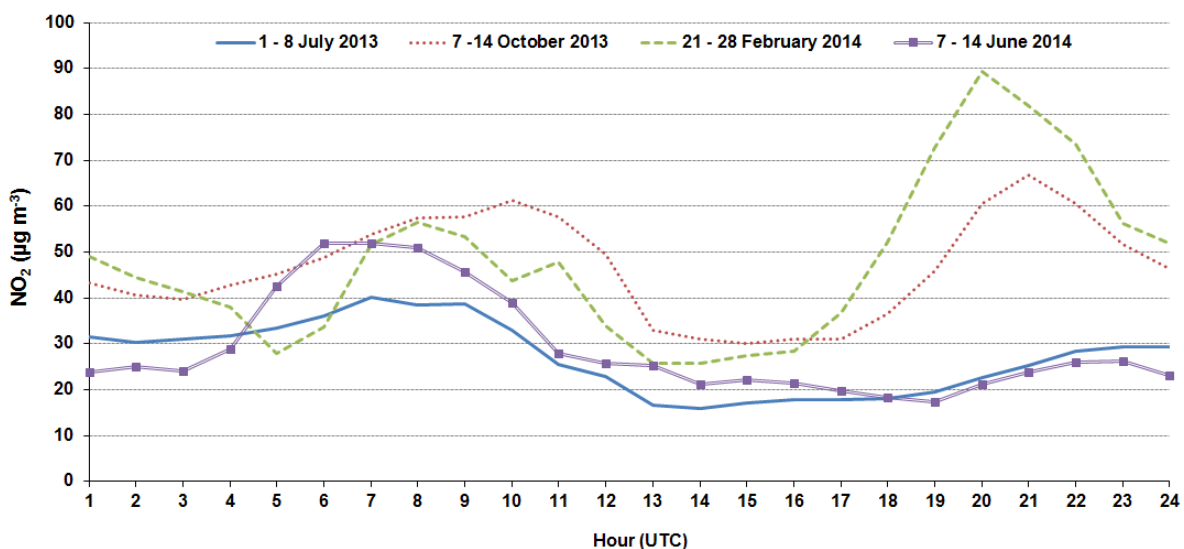


Figure 5.12. Average diurnal NO_2 concentration ($\mu\text{g m}^{-3}$) in Bilbao city. Seasonal comparison.

5.6 Carcinogenic potential assessment

The carcinogenic potency associated with the measured PAHs in Bilbao city during the sampling campaign was calculated by Eq. 1.1, using the values of TEFs reported by Malcolm and Dobson (1994). The carcinogenic potential for each time bin is shown in Table 5.9.

Table 5.9. Diurnal period (n=7) and weekly (n=21) mean BaP_{eq} concentrations (ng m⁻³) over the sampling period. Standard deviation in brackets.

Period	M	A	N	Mean
Jul-13	0.18(0.09)	0.13(0.05)	0.19(0.09)	0.17(0.08)
Sept-13	0.22(0.07)	0.16(0.06)	0.21(0.14)	0.20(0.10)
Oct-13	0.57(0.43)	0.26(0.06)	0.28(0.11)	0.37(0.29)
Nov-13	0.13(0.11)	0.38(0.30)	0.16(0.12)	0.22(0.22)
Dec-13	0.90(0.35)	1.27(0.77)	1.29(0.46)	1.14(0.55)
Jan-14	0.11(0.08)	0.10(0.02)	0.06(0.02)	0.09(0.05)
Feb-14	0.17(0.09)	0.21(0.10)	0.37(0.21)	0.25(0.16)
Mar-14	0.08(0.09)	0.06(0.05)	0.10(0.16)	0.08(0.10)
Jun-14	0.17(0.07)	0.13(0.08)	0.16(0.05)	0.15(0.07)
Jul. - Jun.	0.28(0.32)	0.28(0.42)	0.30(0.39)	0.29(0.38)

Note: 8 h periods corresponding to morning (M): 04:00–12:00 h UTC, afternoon (A): 12:00–20:00 h UTC and night (N): 20:00–04:00 h UTC

Over the sampling campaign, the diurnal period mean BaP_{eq} concentration ranged from 0.06 ± 0.02 to 1.29 ± 0.46 ng m⁻³. The carcinogenic potency showed great variability, (RSD: 23-151%; median: 51%), reaching its highest level in December. Morning and night were the diurnal periods that showed the highest BeP_{eq} values (from 0.10 ± 0.16 to 0.57 ± 0.43 ng m⁻³), except in November where the afternoon was the period with the highest carcinogenic potency (0.38 ± 0.30 m⁻³).

Among PAHs, BaP was the most important BaP_{eq} contributor, with percentages of 31-56%. The following compounds (mean value) were BbFt (16%), DBahA (16%), BkFt (6%), IP (5%), and BaA (5%), respectively (Table 5.10). These six PAHs accounted for > 94% of the total BaP_{eq}.

Table 5.10. Mean contribution of individual PAHs to BaP_{eq} (in %,) during the sampling campaign.

PAHs	Jul-13 (n=21)	Sep-13 (n=21)	Oct-13 (n=21)	Nov-13 (n=21)	Dec-13 (n=21)	Jan-14 (n=21)	Feb-14 (n=21)	March-14 (n=21)	Jun-14 (n=21)	Jul-Jun (n=189)
Ant	0	0	0	0	0	1	0	0	0	0
Ft	1	1	1	1	1	2	1	1	1	1
BaA	4	5	5	5	6	8	5	7	3	5
Chry	1	1	1	1	1	1	0	1	1	1
BbFt	11	10	13	19	19	13	10	19	29	16
BkFt	7	4	4	11	5	5	4	7	14	6
BeP	1	1	1	2	1	1	0	1	3	1
BaP	52	51	56	47	50	53	51	44	31	49
IP	7	5	5	4	6	5	4	5	3	5
DBahA	16	20	13	8	12	10	24	13	14	16
BghiP	1	1	1	1	1	1	1	1	1	1

Finally, during the sampling campaign the inhalation cancer risk (ICR) due to particle PAH exposure was calculated by Eq. 1.2. The World Health Organization (WHO) suggested the IUR_{BaP} of $8.7 \cdot 10^{-5} \text{ m}^3/\text{ng}$ for the lifetime 70-year PAH exposure, assuming one is exposed to the average level of one unit BaP concentration ($1 \text{ ng}/\text{m}^3$). This value was based on an epidemiology study on coke-oven workers in Pennsylvania. (WHO, 2000). Table 5.11 shows the PAH-induced inhalation lifetime cancer risks obtained during the sampling campaign.

Table 5.11. Diurnal period (n=7) and weekly (n=21) mean ICR during the sampling campaign (based on the IUR_{BaP} of the WHO).

Period	ICR			
	M	A	N	Mean
Jul-13	$1.60 \cdot 10^{-5}$	$1.11 \cdot 10^{-5}$	$1.61 \cdot 10^{-5}$	$1.46 \cdot 10^{-5}$
Sept-13	$1.94 \cdot 10^{-5}$	$1.35 \cdot 10^{-5}$	$1.82 \cdot 10^{-5}$	$1.70 \cdot 10^{-5}$
Oct-13	$4.96 \cdot 10^{-5}$	$2.29 \cdot 10^{-5}$	$2.43 \cdot 10^{-5}$	$3.23 \cdot 10^{-5}$
Nov-13	$1.13 \cdot 10^{-5}$	$3.29 \cdot 10^{-5}$	$1.35 \cdot 10^{-5}$	$1.92 \cdot 10^{-5}$
Dec-13	$7.84 \cdot 10^{-5}$	$1.11 \cdot 10^{-4}$	$1.12 \cdot 10^{-4}$	$9.94 \cdot 10^{-5}$
Jan-14	$9.93 \cdot 10^{-6}$	$8.60 \cdot 10^{-6}$	$5.53 \cdot 10^{-6}$	$8.02 \cdot 10^{-6}$
Feb-14	$1.48 \cdot 10^{-5}$	$1.81 \cdot 10^{-5}$	$3.20 \cdot 10^{-5}$	$2.17 \cdot 10^{-5}$
Mar-14	$6.54 \cdot 10^{-6}$	$5.43 \cdot 10^{-6}$	$8.99 \cdot 10^{-6}$	$6.99 \cdot 10^{-6}$
Jun-14	$1.47 \cdot 10^{-5}$	$1.12 \cdot 10^{-5}$	$1.40 \cdot 10^{-5}$	$1.33 \cdot 10^{-5}$
Jul. - Jun.	$2.47 \cdot 10^{-5}$	$2.48 \cdot 10^{-5}$	$2.63 \cdot 10^{-5}$	$2.53 \cdot 10^{-5}$

Note: 8 h periods corresponding to morning (M): 04:00–12:00 h UTC, afternoon (A): 12:00–20:00 h UTC and night (N): 20:00–04:00 h UTC

The inhalation cancer risks calculated based on the WHO guideline ranged from $5.43 \cdot 10^{-6}$ to $1.12 \cdot 10^{-4}$ over the sampling campaign, December being the month with the highest risk levels. Morning and night were the diurnal periods that showed the highest ICR values (from $5.53 \cdot 10^{-6}$ to $1.12 \cdot 10^{-4}$), except in November where it was the afternoon ($3.29 \cdot 10^{-5}$).

Regarding the acceptable cancer risk level, the US-EPA (2001) advises that one in a million (10^6) over an average lifetime of 70 years is the acceptable or inconsequential risk level, and a one in ten thousand level (10^4) is considered serious. During the sampling campaign there were no episodes that exceed the WHO unit risk ($8.7 \cdot 10^{-5} \text{ m}^3/\text{ng}$ per $1 \text{ ng}/\text{m}^3$ of BaP) except in December where the ICR exceeded this value, especially in the afternoon and at night. As previously mentioned in section 5.5, the

sampling week of this month was characterized by a “blocking anticyclonic episode” that eased the accumulation of particulate PAHs. This episode meant a considerable risk for human health.

Chapter 6:

Conclusions

This Ph.D. thesis has developed and validated an analytical method based on thermal desorption extraction for determining PAHs in gas and particulate phase. The use of this solvent-free extraction technique has showed numerous advantages (less sample manipulation and analysis time, reduced exposure risk, and higher sensitivity and reliability) that make the TD-GC/MS method a better alternative than the conventional method (liquid extraction-GC/MS) for the analysis of these pollutants.

The following conclusions can be drawn from the present study:

Development of TD-GC/MS method

- The conditioning of the sampling media is an essential stage to remove the interferences in the analysis of PAHs. Among the different conditioning protocols, conditioning with the thermal desorption unit (PerkinElmer Turbomatrix 150 TD) enabled a good conditioning of the samples at a relative high temperature (350°C) and within a short time (≤ 30 min).
- Tube and trap temperature, time, desorption and split flows (inlet and outlet) were critical parameters in the thermal desorption of PAHs. The optimized TD method showed an efficient desorption of PAHs (gas and particulate phase) with recoveries of PAHs higher than 94%. The two versions of Tenax (GR and TA) used in this study did not present significant differences in the thermal desorption of gas PAHs.
- The TD-GC-MS method showed limits of detection (LODs) < 0.1 ng, while method detection limits (MDL) were < 1 ng, slightly lower values compared with solvent-based extraction-GC/MS methods.
During the study, the method demanded continuous Peltier trap maintenance because the contamination in it affected the highest molecular weight PAHs (IP, DBahA and BghiP), significantly increasing their detection limits.
- The results obtained in the validation of TD-GC/MS by standard reference material (urban dust) demonstrated that this is a reliable method to determine particulate PAHs in aerosol samples (good linearity, precision and accuracy). Nevertheless, the application of the method to quantify the lowest molecular weight PAHs (Naph and Ace) can generate overestimation of these compounds in the aerosol samples.

- The uncertainty associated with recovery was the main source of uncertainty in the TD-GC/MS method. Furthermore, this method showed a lower uncertainty (< 8% for most PAHs) than the conventional method (solvent-based extraction and GC/MS analysis).
- Besides 16 EPA PAHs, the TD-GC/MS method enabled the determination of other PAHs in aerosol samples (e.g. benzo[e]pyrene).

Application of TD-GC/MS method

- The application of the TD-GC/MS method to characterize the particle-bound PAHs (in PM₁₀) obtained by high temporal resolution samples in an urban area (Bilbao city) enabled observing the diurnal and seasonal variation of these compounds. Over the sampling campaign, the average concentration of individual PAHs ranged from 0.01 ± 0.01 to 0.50 ± 0.76 ng m⁻³, while mean diurnal period concentration of $\Sigma 25$ PAHs (16 EPA PAHs + extra PAHs) ranged from 0.96 ± 0.38 and 12.67 ± 6.70 ng m⁻³. Factors such as the changes in the contributions of PAH sources and the meteorological conditions could be the main reasons of these variations.
The most abundant PAHs found were, in order of importance, BbFt > Pyr > Ft > BeP > Chry.
- The potential PAH sources identified by the receptor models (UNMIX and PMF) in Bilbao city were the local steel industry, a mix of stationary sources and the traffic. Their contributions were similar (between 30% and 37%) without a predominant PAH source in the region.
- Meteorological parameters such as wind speed, temperature, and atmospheric pressure significantly influenced the PAH concentrations determined in the urban area of Bilbao. The local sea breeze cycles (predominant during spring and summer) played an important role in the atmospheric dispersion and dilution of PAHs (especially during the afternoon period).
- The PAHs measured in Bilbao city during the sampling campaign showed the highest carcinogenic potential during the morning and at night. BaP, BbFt, DBahA, BkFt, IP and BaA were the main contributors to carcinogenic potential,

accounting for > 94%. The sampling week of December (characterized by a “blocking anticyclonic episode”) was the only episode where the inhalation of particulate PAHs implied a considerable risk for human health (inhalation cancer risk > $8.7 \cdot 10^{-5}$).

Chapter 7:

Bibliography

1. Acero JA, Arrizabalaga J, Kupski S, Katschner L. Deriving an Urban Climate Map in coastal areas with complex terrain in the Basque Country (Spain). *Urban Clim.* 2013; 4: 35-60.
2. Agilent Technologies. Focusing on Volatiles. Thermal desorption: Introduction and Principles. Available: <http://www.chem.agilent.com/cag/country/principles.pdf> [last accessed: September 2016].
3. Ahmad UK, Ujang Z, Woon CH, Indran S, Mian MN. Development of extraction procedures for the analysis of polycyclic aromatic hydrocarbons and organochlorine pesticides in municipal sewage sludge. *Water Sci. Technol.* 2004; 50(9):137-144.
4. Alam MS, Delgado-Saborit JM, Stark CP, Harrison RM. Investigating PAH relative reactivity using congener profiles, quinone measurements and back trajectories. *Atmos. Chem. Phys.* 2014; 14: 2467-2477.
5. Albinet A, Leoz-Garziandia E, Budzinski H, Villenave E. Polycyclic aromatic hydrocarbons (PAHs), nitrated PAHs and oxygenated PAHs in ambient air of the Marseilles area (South of France): concentrations and sources. *Sci. Total Environ.* 2007; 384: 280-292.
6. Aldabe J, Santamaría C, Elustondo D, Parra A, Foan L, Simon V, Santamaría JM. Polycyclic aromatic hydrocarbons (PAHs) sampled in aerosol at different sites of the western Pyrenees in Navarra (Spain). *Environ. Eng. Manag. J.* 2012; 11: 1049-1058.
7. Amador-Muñoz O, Bazán-Torija S, Villa-Ferreira SA, Villalobos-Pietrini R, Bravo-Cabrera JL, Munive-Colín Z, Hernández-Mena L, Saldarriaga-Noreña H, Murillo-Tovar MA. Opposing seasonal trends for polycyclic aromatic hydrocarbons and PM10: Health risk and sources in southwest Mexico City. *Atmos. Res.* 2013; 122: 199-212.
8. American Society for Testing and Materials (ASTM). Standard test method for determination of gaseous and particulate PAHs in ambient air (collection on sorbent-backed filters with GC/MS analysis). Designation: D6209-98; 2004.
9. Armstrong B, Hutchinson E, Unwin J, Fletcher T. Lung cancer risk after exposure to polycyclic aromatic hydrocarbons: a review and meta-analysis. *Environ. Health Persp.* 2004; 112: 970-978.
10. Atkinson RW, Fuller GW, Anderson HR, Harrison RM, Armstrong B. Urban ambient particle metrics and health: a time-series analysis. *Epidemiology.* 2010; 21:501-11.
11. Augusto S, Pereira MJ, Máguas C, Branquinho C. A step towards the use of biomonitors as estimators of atmospheric PAHs for regulatory purposes. *Chemosphere.* 2013; 92(5): 626-632.

12. Aydin YM, Kara M, Dumanoglu Y, Odabasi M, Elbir T. Source apportionment of polycyclic aromatic hydrocarbons (PAHs) and polychlorinated biphenyls (PCBs) in ambient air of an industrial region in Turkey. *Atmos. Environ.* 2014; 97: 271–285.
13. Bach PB, Kelley MJ, Tate RC, McCrory DC. Screening for lung cancer: a review of the current literature. *Chest.* 2003; 123(1):72-82.
14. Balasubramanian R, He J. Trace analysis of persistent organic pollutants in the air using accelerated solvent extraction. In: Zereini F, Wiseman C (eds.), *Urban Airborne Particulate Matter: Origins, Chemistry, Fate and Health Impacts*. Springer, Heidelberg, 2010; 127-144.
15. Bandowe BA, Meusel H, Huang RJ, Ho K, Cao J, Hoffmann T, Wilcke W. PM_{2.5}-bound oxygenated PAHs, nitro-PAHs and parent-PAHs from the atmosphere of a Chinese megacity: seasonal variation, sources and cancer risk assessment. *Sci. Total Environ.* 2014; 473-474: 77-87.
16. Baraniecka J, Pyrzyńska K, Szewczyńska M, Pośniak M, Dobrzyńska E. Emission of polycyclic aromatic hydrocarbons from selected processes in steelworks. *J. Hazard. Mater.* 2010; 183(1-3):111-115.
17. Barrado AI, García S, Barrado E, Pérez RM. PM_{2.5}-bound PAHs and hydroxy-PAHs in atmospheric aerosol samples: Correlations with season and with physical and chemical factors. *Atmos. Environ.* 2012; 49: 224-232.
18. Baumard P, Budzinski H, Garrigues P, Dizer H, Hansen PD. (1999): Polycyclic aromatic hydrocarbons in recent sediments and mussels (*Mytilus edulis*) from the Western Baltic: occurrence, bioavailability and seasonal variations. *Mar. Environ. Res.* 1999; 47: 17-47.
19. Björklund E, Nilsson T, Bøwadt S. 2000. Pressurised liquid extraction of persistent organic pollutants in environmental analysis. *Trends Anal. Chem.* 2000; 19(7): 434-45.
20. Blachnik C. Comparison of Buchi extraction system B-811 with classic Soxhlet extraction. Buchi information bulletin, 2002.
21. Bordajandi LR, Dabrio M, Ulberth F, Emons H. Optimisation of the GC-MS conditions for the determination of the 15 EU foodstuff priority polycyclic aromatic hydrocarbons. *J. Sep. Sci.* 2008; 31(10): 1769-1778.
22. Boström CE, Gerde P, Hanberg A, Jernstrom B, Johansson C, Kyrklund T, Rannug A, Törnqvist M, Victorin K, Westerholm R. Cancer risk assessment, indicators, and guidelines for polycyclic aromatic hydrocarbons in the ambient air. *Environ. Health Persp.* 2002; 110 (3): 451-88.

23. Bourotte C, Forti MC, Taniguchi S, Bicego MC, Lotufo PA. A wintertime study of PAHs in fine and coarse aerosols in Sao Paulo city, Brazil. *Atmos. Environ.* 2005; 39: 3799–3811.
24. Büchi. Extraction System B-811 / B-811 LSV Available: <http://www.buchi.com/en/products/extraction/extraction-system-b-811-b-811-lsv> [last accessed: September 2016a].
25. Büchi. Extraction System B-811 brochure. Available: <http://www.masontechnology.ie/files/documents/Buchi15.pdf> [last accessed: September 2016b].
26. Callén MS, López JM, Mastral AM. Characterization of PM₁₀-bound polycyclic aromatic hydrocarbons in the ambient air of Spanish urban and rural areas. *J. Environ. Monitor.* 2011; 13(2):319-327.
27. Callén MS, López JM, Iturmendi A, Mastral AM. Nature and sources of particle associated polycyclic aromatic hydrocarbons (PAH) in the atmospheric environment of an urban area. *Environ. Pollut.* 2013a; 183: 166-174.
28. Callén MS, López JM, Mastral AM. Influence of organic and inorganic markers in the source apportionment of airborne PM₁₀ in Zaragoza (Spain) by two receptor models. *Environ Sci Polut R.* 2013b; 20(5): 3240-3251.
29. Callén MS, Iturmendi A, López JM. Source apportionment of atmospheric PM_{2.5}-bound polycyclic aromatic hydrocarbons by a PMF receptor model. Assessment of potential risk for human health. *Environ. Pollut.* 2014; 195:167-177.
30. Cao J-J, Zhu C-S, Tie X-X, Geng F-H, Xu H-M, Ho SSH, Wang G-H, Han Y-M, Ho K-F. Characteristics and sources of carbonaceous aerosols from Shanghai, China. *Atmos. Chem. Phys.* 2013; 13: 803-817.
31. Carslaw DC, Ropkins K. Openair — an R package for air quality data analysis. *Environ Model Softw.* 2012; 27-28: 52-61.
32. Chantara S, Sangchan W. Sensitive analytical method for particle-bound polycyclic aromatic hydrocarbons: A case study in Chiang Mai, Thailand. *Sci. Asia.* 2009; 35: 42-48.
33. Chaspoul F, Barban G, Gallice P. Simultaneous GC/MS analysis of polycyclic aromatic hydrocarbons and their nitrated derivatives in atmospheric particulate matter from workplaces. *Polycycl. Aromat. Comp.* 2005; 25(2): 157-167.
34. Cheng H, Deng Z, Chakraborty P, Liu D, Zhang R, Xu Y, Luo C, Zhang G, Li J. A comparison study of atmospheric polycyclic aromatic hydrocarbons in three Indian cities using PUF disk passive air samplers. *Atmos. Environ.* 2013; 73:16-21.

35. Cheruiyot NK, Lee WJ, Mwangi JK, Wang LC, Lin NH, Lin YC, Cao J, Zhang R, Chang-Chien GP. An overview: Polycyclic aromatic hydrocarbon emissions from the stationary and mobile sources and in the ambient air. *Aerosol Air Qual. Res.* 2015; 15: 2730–2762.
36. Coker D. Personal monitoring techniques for gases and vapours. *Int. Environ. Saf. J.* 1979; 43-44.
37. Coker DT, van den Hoed N, Saunders KJ, Tindle PE. A monitoring method for gasoline vapour giving detailed composition: *Ann. Occup. Hyg.* 1989; 33 (1): 15-26.
38. Connell DW. *Basic Concepts of Environmental Chemistry, second edition.* CRC Press, Florida, 2005; 36-43.
39. Council Decision 2004/259/EC of 19 February 2004 concerning the conclusion, on behalf of the European Community, of the 1988 Protocol to the 1979 Convention on Long Range Transboundary Air Pollution on Persistent Organic Pollutants [OJ L 81 of 19.03.2004]. Available: <http://eur-lex.europa.eu/legal-content/EN/TXT/?uri=CELEX:32004D0259> [last accessed: September 2016].
40. Delgado-Saborit JM, Alam MS, Godri Pollitt KJ, Stark C, Harrison RM. Analysis of atmospheric concentrations of quinones and polycyclic aromatic hydrocarbons in vapour and particulate phases. *Atmos. Environ.* 2013; 77: 974–982.
41. Delhomme O, Millet M. Characterisation of particulate polycyclic aromatic hydrocarbons in the east of France urban areas. *Environ. Sci. Pollut. Res.* 2012; 19: 1791-1799.
42. Di Filippo P, Riccardi C, Pomata D, Buiarelli F. Concentrations of PAHs, and nitro- and methyl-derivatives associated with a size-segregated urban aerosol. *Atmos. Environ.* 2010; 44: 2742-2749.
43. Digital Elektronik AG. Digital Aerosol Sampler DH-80 Manual. Hegnau, Switzerland, 2010.
44. Ding LC, Ke F, Wang DKW, Dann T, Austin CC. A new direct thermal desorption-GC/MS method: organic speciation of ambient particulate matter collected in Golden, BC. *Atmos. Environ.* 2009; 43 (32): 4894-4902.
45. Duan JC, Bi XH, Tan JH, Sheng GY, Fu JM. The differences of the size distribution of polycyclic aromatic hydrocarbons (PAHs) between urban and rural sites of Guangzhou, China. *Atmos. Res.* 2005; 78: 190-203.
46. Dyson N. *Chromatographic Integration Methods, second edition.* Royal Society of Chemistry, Cambridge, UK, 1998, pp. 83-85.

47. Eberly SI. EPA PMF 1.1 User's Guide, U.S. Environmental Protection Agency, Research Triangle Park, NC, 2005.
48. Esworthy R. Air quality: EPA's 2013 changes to the particulate matter (PM) standard. Congressional Research Service 7-5700, n. R42934; 2013. p. 6.
49. Eurachem/Citac guide. In: S.L.R. Ellison, A. Williams (eds.), *Quantifying Uncertainty in Analytical Measurement, third edition*, 2012.
50. European Commission (EC). The Working Group on polycyclic aromatic hydrocarbons, ambient air pollution by polycyclic aromatic hydrocarbons (PAH); Position Paper, July 27th 2001). Available: http://europa.eu.int/comm/environment/air/pdf/pp_pah.pdf [last accessed: September 2016].
51. European Committee for Standardization (CEN). Standard method for the measurement of the concentration of BaP in ambient air. UNE-EN 15549. Brussels, 2008.
52. European Environment Agency (EEA). European Union Emission Inventory Report 1990-2014 under the UNECE Convention on Long-range Transboundary Air Pollution (LRTAP). EEA Technical Report No 16/2016. Publications Office for Official Publications of the European Union, Luxembourg, 2016.
53. European Union Directive (EUD). Directive 2008/50/EC of the European Parliament and of the Council of 21 May 2008 on Ambient Air Quality and Cleaner Air for Europe. Off. J. Eur. Union L 2008; 152: 1-44.
54. Falkovich AH, Rudich Y. Analysis of semivolatile organic compounds in atmospheric aerosols by direct sample introduction thermal desorption GC/MS. *Environ. Sci. Technol.* 2001; 35(11): 2326-2333.
55. Foley JP, Dorsey JG. Clarification of the limit of detection in chromatography. *Chromatographia.* 1984; 18: 503-511.
56. Galarneau E. Source specificity and atmospheric processing of airborne PAHs: implications for source apportionment. *Atmos. Environ.* 2008; 42(35):8139–8149.
57. García I, Ignacio M, Mouteira A, Cobas J, Carro M. Assisted solvent extraction and ion-trap tandem mass spectrometry for the determination of polychlorinated biphenyls in mussels. Comparison with other extraction techniques. *Anal. Bioanal. Chem.* 2008; 390: 729-737.
58. Gil-Moltó J, Varea M, Galindo N, Crespo J. Application of an automatic thermal desorption-gas chromatography-mass spectrometry system for the analysis of

- polycyclic aromatic hydrocarbons in airborne particulate matter. *J. Chromatogr. A*. 2009; 1216(9): 1285-1289.
59. Golomb D, Ryan D, Underhill J, Wade T, Zemba S. Atmospheric deposition of toxics onto Massachusetts bay-II. Polycyclic aromatic hydrocarbons. *Atmos. Environ.* 1997; 31: 1361-1368.
60. Golomb D, Barry G, Fisher G, Varanusupakul P, Koleda M, Rooney T. Atmospheric deposition of polycyclic aromatic hydrocarbons near New England coastal waters. *Atmos. Environ.* 2001; 35: 6245-6258.
61. Gomes JFP. Emission of high toxicity airborne pollutants from electric arc furnaces during steel production. In: Cavaliere P (ed.), *Ironmaking and Steelmaking Processes*. Springer International Publishing Switzerland. 2016, 223-235.
62. Grandesso E, Pérez Ballesta P, Kowalewski K. Thermal desorption GC-MS as a tool to provide PAH certified standard reference material on particulate matter quartz filters. *Talanta*. 2013; 105: 101-108.
63. Grandesso E, Pérez Ballesta P. Derivatization and analysis of levoglucosan and PAHs in ambient air particulate matter by moderate temperature thermal desorption coupled with GC/MS. *Anal. Methods*. 2014; 6(17): 6900-6908.
64. Guerin TF. The extraction of aged polycyclic aromatic hydrocarbon (PAH) residues from a clay soil using sonication and a Soxhlet procedure: a comparative study. *J. Environ. Monit.* 1999;1(1):63-67.
65. Gupta S, Kumar K, Srivastava A, Srivastava A, Jain VK. Size distribution and source apportionment of polycyclic aromatic hydrocarbons (PAHs) in aerosol particle samples from the atmospheric environment of Delhi, India. *Sci. Total Environ.* 2011; 409(22):4674-4680.
66. Gustafsson O, Nilsson N, Bucheli TD. Dynamic colloid-water partitioning of pyrene through a coastal Baltic spring bloom. *Sci. Total Environ.* 2001; 35(20): 4001-4006.
67. Guzmán-Torres D, Eiguren-Fernández A, Cicero-Fernández P, Maubert-Franco M, Retama-Hernández A, Ramos Villegas R, Miguel HA. Effects of meteorology on diurnal and nocturnal levels of priority polycyclic aromatic hydrocarbons and elemental and organic carbon in PM10 at a source and a receptor area in Mexico city. *Atmos. Environ.* 2009; 43: 2693-2699.
68. Haynes BS. Soot and hydrocarbons in combustion. In: Bartok W, Sarofim AF, (eds.), *Fossil Fuel Combustion: A Source Book*. Wiley, New York; 1991, 261-326.

69. Hawthorne SB, Grabanski CB, Martin E, Miller DJ. Comparisons of soxhlet extraction, pressurized liquid extraction, supercritical fluid extraction and subcritical water extraction for environmental solids: recovery, selectivity and effects on sample matrix. *J. Chromatogr. A.* 2000; 892(1-2):421-433.
70. He JB, Fan SX, Meng QZ, Sun Y, Zhang J, Zu F. Polycyclic aromatic hydrocarbons (PAHs) associated with fine particulate matters in Nanjing, China: distributions, sources and meteorological influences. *Atmos. Environ.* 2014; 89: 207–215.
71. Henry RC. Multivariate receptor modeling by N-dimensional edge detection. *Chemometr. Intell. Lab.* 2003; 65: 179–189.
72. Ho SS, Yu JZ. In-injection port thermal desorption and subsequent gas chromatography-mass spectrometric analysis of polycyclic aromatic hydrocarbons and n-alkanes in atmospheric aerosol samples. *J. Chromatogr. A.* 2004; 1059(1-2): 121-129.
73. Holdren MW, Smith DL. Performance of Automated Gas Chromatographs Used in the 1990 Atlanta Study. In Proceedings of the 1991 U.S. EPA/A&WMA International Symposium on Measurement of Toxic and Related Air Pollutants. Air and Waste Management Association. Pittsburgh, USA; 1991.
74. Hopke PK, Ito K, Mar T, Christensen WF, Eatough DJ, Henry RC, Kim E, Laden F, Lall R, Larson TV, Liu H, Neas L, Pinto J, Stölzel M, Suh H, Paatero P, Thurston GD. PM source apportionment and health effects: 1. Intercomparison of source apportionment results. *J. Expo. Sci. Environ. Epidemiol.* 2006; 16(3): 275-286.
75. Hu M, Jing-Hong Z, Chun-Feng D, Liang H, Ya-Feng G. Thermal desorption-gas chromatography or gas chromatograph-mass spectrometry for analysis of semi-volatile compounds on atmospheric particulate matters. *Chinese J. Anal. Chem.* 2014; 42(7): 931-936.
76. Huma B, Yadav S, Attri AK. Profile of particulate-bound organic compounds in ambient environment of Srinagar: a high-altitude urban location in the North-Western Himalayas. *Environ Sci. Pollut. Res Int.* 2016; 23(8): 7660-7675.
77. Inomata Y, Kajino M, Sato K, Ohara T, Kurokawa JI, Ueda H, Tang N, Hayakawa K, Ohizumi T, Akimoto H. Emission and Atmospheric Transport of Particulate PAHs in Northeast Asia. *Environ. Sci. Technol.* 2012; 46: 4941-4949.
78. International Agency for Research on Cancer (IARC). Agents Classified by the IARC Monographs. Available: http://monographs.iarc.fr/ENG/Classification/latest_classif.php [last accessed: September 2016].

79. International Organization for Standardization (ISO). Ambient air. Determination of total (gas and particle-phase) PAHs. Collection on sorbent-backed filters with GC/MS analyses. ISO 12884:2000.
80. International Organization for Standardization (ISO). Workplace air quality - Sampling and analysis of volatile organic compounds by solvent desorption/gas chromatography. Part 1: Pumped sampling method. ISO 16200-1:2001.
81. International Organization for Standardization (ISO). Stationary source emissions. Determination of gas and particle-phase PAHs. ISO 11338:2003.
82. International Organization for Standardization (ISO). Ambient air. Determination of particle-phase polycyclic aromatic hydrocarbons by high performance liquid chromatography. ISO 16362:2005.
83. International Organization for Standardization (ISO). Air quality - Guidelines for estimating measurement uncertainty. ISO 20988:2007.
84. Itoh N, Numata M, Aoyagi Y, Yarita T. Comparison of low-level polycyclic aromatic hydrocarbons in sediment revealed by Soxhlet extraction, microwave-assisted extraction, and pressurized liquid extraction. *Anal. Chim. Acta.* 2008; 612: 44-52.
85. Joa K, Panova E, Irha H, Teinemaa E, Lintelmann J, Kirso U. Determination of polycyclic aromatic hydrocarbons (PAHs) in oil shale processing wastes: current practice and new trends. *Oil Shale.* 2009; 26: 59-72.
86. Kadam SU, Tiwari BK, O'Donnell CP. Application of novel extraction technologies for bioactives from marine algae. *J. Agric. Food Chem.* 2013; 61(20):4667-4675.
87. Kalberlah F, Frijus-Plessen N, Hassauer M. Toxicological criteria for the risk assessment of polyaromatic hydrocarbons (PAHs) in existing chemicals. Part 1: the use of equivalent factors. *Altlasten-Spektrum.* 1995; 5:231-237.
88. Kameda T, Akiyama A, Toriba A, Tang N, Hayakawa K. Atmospheric formation of hydroxynitropyrenes from a photochemical reaction of particle-associated 1-nitropyrene. *Environ. Sci. Technol.* 2011; 45(8): 3325-3332.
89. Karaca G, Cindoruk SS, Tasdemir Y. Migration of polycyclic aromatic hydrocarbons (PAHs) in urban treatment sludge to the air during PAH removal applications. *J. Air Waste Manage.* 2014; 64(5):568-77.
90. Karthikeyan S, Balasubramanian R, See SW. Optimization and validation of a low temperature microwave-assisted extraction method for analysis of polycyclic aromatic hydrocarbons in airborne particulate matter. *Talanta.* 2006; 69:79-86.

91. Keyte IJ, Harrison RM, Lammel G. Chemical reactivity and long-range transport potential of polycyclic aromatic hydrocarbons--a review. *Chem. Soc. Rev.* 2013; 42(24):9333-9391.
92. Khairy MA, Lohmann R. Source apportionment and risk assessment of polycyclic aromatic hydrocarbons in the atmospheric environment of Alexandria, Egypt. *Chemosphere.* 2013; 91(7): 895-903.
93. Kim E, Hopke P. Comparison between sample-species specific uncertainties and estimated uncertainties for the source apportionment of the speciation trends network data. *Atmos. Environ.* 2007; 41: 567–575.
94. Kim Y-H, Kim K-H. Ultimate detectability of volatile organic compounds: how much further can we reduce their ambient air sample volumes for analysis? *Anal. Chem.* 2012; 84, 8284-8293.
95. Kim KH, Jahan SA, Kabir E, Brown RJC. A review of airborne polycyclic aromatic hydrocarbons (PAHs) and their human health effects. *Environ. Int.* 2013; 60: 71-80.
96. Kim Y-H, Kim K-H. A simple methodological validation of the gas/particle fractionation of polycyclic aromatic hydrocarbons in ambient air. *Sci. Rep.* 2015; 5: 11679.
97. Kolb B. Headspace sampling with capillary columns. *J. Chromatogr. A.* 1999; 842 (1-2): 163-205.
98. Kronholm J, Kettune J, Hartonen K, Riekkola ML, Pressurized hot water extraction of n-alkanes and polyaromatic hydrocarbons in soil and sediment from oil shale industry district in Estonia. *J. Soils Sediment.* 2004; 4(2): 107-114.
99. Larsen RK, Baker JE. Source apportionment of polycyclic aromatic hydrocarbons in the urban atmosphere: a comparison of three methods. *Environ Sci Technol.* 2003; 37(9): 1873-1881.
100. Lau EV, Gan S, Ng HK. Extraction techniques for polycyclic aromatic hydrocarbons in soils. *Inter. J. Anal. Chem.* 2010; 10:1 -9.
101. Lazarov B, Swinnen R, Spruyt M, Goelen E, Stranger M, Desmet G, Wauters E. Optimisation Steps of an Innovative Air Sampling Method for Semi Volatile Organic Compounds. *Atmos. Environ.* 2013; 79: 780-786.
102. Lee RGM, Jones KC. The influence of meteorology and air masses on daily atmospheric PCB and PAH concentrations at an UK site. *Environ. Sci. Technol.* 1999; 33: 705-712.

103. Lee RGM, Coleman P, Jones JL, Jones KC, Lohmann R. Emission factors and importance of PCDD/Fs, PCBs, PCNs, PAHs and PM10 from the domestic burning of coal and wood in the UK. *Environ. Sci. Technol.* 2005; 39: 1436-1447.
104. Lee JY, Kim YP. Source apportionment of the particulate PAHs at Seoul, Korea: impact of long range transport to a megacity. *Atmos. Chem. Phys.* 2007; 7: 3587–3596.
105. Lee BK. Sources, Distribution and Toxicity of Polyaromatic Hydrocarbons (PAHs) in Particulate Matter. In: Villanyi V (ed.), *Air Pollution*. Sciyo, India, 2010, pp. 99-101.
106. Leung PY, Wan HT, Billah MB, Cao JJ, Ho KF, Wong CK. Chemical and biological characterization of air particulate matter 2.5, collected from five cities in China. *Environ. Pollut.* 2014; 194:188-195.
107. Li W, Peng Y, Shi J, Qiu W, Wang J, Bai Z. Particulate polycyclic aromatic hydrocarbons in the urban Northeast Region of China: profiles, distributions and sources. *Atmos. Environ.* 2011; 45: 7664–7671.
108. Li X, Kong S, Yin Y, Li L, Yuan L, Li Q, Xiao H, Chen K. Polycyclic aromatic hydrocarbons (PAHs) in atmospheric PM2.5 around 2013 Asian Youth Games period in Nanjing. *Atmos. Res.* 2013; 174: 85-96.
109. Li W , Wang C , Wang H , Chen J , Shen H , Shen G , Huang Y , Wang R , Wang B , Zhang Y , Chen H , Chen Y , Su S , Lin N , Tang J , Li Q , Wang X , Liu J , Tao S. Atmospheric polycyclic aromatic hydrocarbons in rural and urban areas of northern China. *Environ. Pollut.* 2014; 192: 83-90.
110. Liao CM, Chiang KC (2006) Probabilistic assessment for personal exposure to carcinogenic polycyclic aromatic hydrocarbons in Taiwanese temples. *Chemosphere* 63:1610-1619.
111. Lima ALC, Farrington JW, Reddy CM. Combustion-derived polycyclic aromatic hydrocarbons in the environment—a review. *Environ. Forensics.* 2005; 6: 109-131.
112. Lin YC, Lee WJ, Hou HC. PAH emissions and energy efficiency of palm-biodiesel blends fueled on diesel generator. *Atmos. Environ.* 2006; 40: 3930-3940.
113. Liu LB, Liu Y, Lin JM, Tang N, Hayakawa K, Maeda T. Development of analytical methods for polycyclic aromatic hydrocarbons (PAHs) in airborne particulates: a review. *J. Environ. Sci. China.* 2007; 19(1):1-11.
114. Liu JW, Li J, Lin T, Liu D, Xu Y, Chaemfa C, Qi SH, Liu FB, Zhang G. Diurnal and nocturnal variations of PAHs in the Lhasa atmosphere, Tibetan Plateau:

- implication for local sources and the impact of atmospheric degradation processing. *Atmos. Res.* 2013; 124: 34-43.
115. Liu Y, Wang S, Lohmann R, Yu N, Zhang Ch, Gao Y, Zhao J, Ma L. Source apportionment of gaseous and particulate PAHs from traffic emission using tunnel measurements in Shanghai, China. *Atmos. Environ.* 2015; 107: 129-136.
116. Löndahl J, Massling A, Pagels J, Swietlicki E, Vaclavik E, Loft S. Size-Resolved Respiratory-Tract Deposition of Fine and Ultrafine Hydrophobic and Hygroscopic Aerosol Particles during Rest and Exercise. *Inhal. Toxicol.* 2007; 19: 109-116.
117. Lottmann A, Cadé E, Geagea ML, Delhomme O, Grand C, Veilleraud C, Rizet A-L, Mirabel P, Millet M. Separation of molecular tracers sorbed onto atmospheric particulate matter by flash chromatography. *Anal. Bioanal. Chem.* 2007; 387: 1855-1861.
118. Lundstedt S, Haglund P, Oberg L. Degradation and formation of polycyclic aromatic compounds during bioslurry treatment of an aged gasworks soil. *Environ. Toxicol. Chem.* 2003; 22 (7): 1413-1420.
119. Lung SC, Wu MJ, Lin CC. Customers exposure to PM_{2.5} and polycyclic aromatic hydrocarbons in smoking/nonsmoking sections of 24-h coffee shops in Taiwan. *J. Expo. Anal. Env. Epid.* 2004a; 14: 529-535.
120. Lung SC, Guo KJ, Chen PY, Tsai PF, Chen PC. Participants' exposure to PM_{2.5} and gaseous/particulate polycyclic aromatic hydrocarbons during the Ma-tsu Goddess parade. *J Expo. Anal. Env. Epid.* 2004b; 14: 536–543.
121. Luque de Castro MD, Priego-Capote F. Soxhlet extraction: Past and present panacea. *J. Chromatogr. A.* 2010;1217(16):2383-2389.
122. Lv Y, Li X, Xu TT, Cheng TT, Yang X, Chen JM, Linuma Y, Herrmann H. Size distributions of polycyclic aromatic hydrocarbons in urban atmosphere: sorption mechanism and source contributions to respiratory deposition. *Atmos. Chem. Phys.* 2016; 16: 2971–2983.
123. Ma WL, Li YF, Qi H, Sun DZ, Liu LY, Wang DG. Seasonal variations of sources of polycyclic aromatic hydrocarbons (PAHs) to a northeastern urban city, China. *Chemosphere.* 2010; 79(4): 441-447.
124. Ma WL, Sun DZ, Shen WG, Yang M, Qi H, Liu LY, Shen JM, Li YF. Atmospheric concentrations, sources and gas-particle partitioning of PAHs in Beijing after the 29th Olympic Games. *Environ. Pollut.* 2011; 159(7): 1794-1801.
125. Mackay D, Shiu WY, Ma KC. *Illustrated Handbook of Physical-Chemical Properties and Environmental Fate for Organic Chemicals, Vol. II, Polynuclear*

- Aromatic Hydrocarbons, Polychlorinated Dioxins, and Dibenzofurans*. Lewis Publishers, Michigan, USA, 1992.
126. Malcom HM, Dobson S. *The calculation of an environmental assessment level (EAL) for atmospheric PAHs using relative potencies*. Department of the Environment, London, UK, 1994; 34-46.
127. Malinowski ER. *Factor analysis in chemistry, third edition*. Wiley, New York, 2002.
128. Mandalakis M, Tsapakis M, Tsoga A, Stephanou EG. Gas-particle concentrations and distribution of aliphatic hydrocarbons, PAHs, PCBs and PCDD/Fs in the atmosphere of Athens (Greece). *Atmos. Environ.* 2002; 36: 4023-4035.
129. Manahan SE. *Environmental Chemistry, 6th edition*. Lewis Publishers, Florida, USA, 1994.
130. Mantis J, Chaloulakou A, Samara C. PM10-bound polycyclic aromatic hydrocarbons (PAHs) in the Greater Area of Athens, Greece. *Chemosphere*. 2005; 59: 593-604.
131. Manura J. Selection of GC guard columns for use with GC cryo-trap. Sci. Instrument Services Inc., 1999. Application Note 24a.
132. Marr LC, Dzepina K, Jimenez JL, Reisen F, Bethel HL, Arey J, Gaffney JS, Marley NA, Molina LT, Molina MJ. Sources and transformations of particle-bound polycyclic aromatic hydrocarbons in Mexico City. *Atmos. Chem. Phys.* 2006; 6: 1733-1745.
133. Martins GV, Martins S, Martins AO, Basto MC, Silva GV. Determination of gaseous polycyclic aromatic hydrocarbons by a simple direct method using thermal desorption-gas chromatography-mass spectrometry. *Environ. Monit. Assess.* 2013; 185(8): 6447-6457.
134. Masiol M, Centanni E, Squizzato S, Hofer A, Pecorari E, Rampazzo G, Pavoni B. GC-MS analyses and chemometric processing to discriminate the local and long-distance sources of PAHs associated to atmospheric PM2.5. *Environ. Sci. Pollut. R.* 2012; 19(8): 3142-3151.
135. Mastral AM, Callén MS. A review on polycyclic aromatic hydrocarbon (PAH) emissions from energy generation. *Environ. Sci. Technol.* 2000; 34 (15): 3051-3057.
136. Menezes HC, de Lourdes Cardeal Z. Determination of polycyclic aromatic hydrocarbons from ambient air particulate matter using a cold fiber solid phase microextraction gas chromatography-mass spectrometry method. *J. Chromatogr. A.* 2011; 1218(21): 3300-3305.

137. Mercier F, Glorennec P, Blanchard O, Le Bot B. Analysis of semi-volatile organic compounds in indoor suspended particulate matter by thermal desorption coupled with gas chromatography/mass spectrometry. *J. Chromatogr. A*. 2012; 1254: 107-114.
138. Millán MM, Otamendi JE, Alonso LA, Ureta L. 1987, Experimental Characterization of Atmospheric Diffusion in Complex Terrain with Land-Sea Interactions. *JAPCA*. 1987; 37(7): 807-811.
139. Mitchell K, Steere DE, Taylor JA, Manicom B, Fisher JE, Sienicki EJ, Chiu C, Williams P. Impact of diesel fuel aromatics on particulate, PAH and nitro-PAH emissions. SAE Emission Technology Collection, 1994. No. 942053.
140. MonAirNet project. Passive air sampling. Available: <http://www.monairnet.eu/index-en.php?pg=methods--passive-air-sampling> [last accessed: October 2015].
141. Morville S, Delhomme O, Millet M. Seasonal and diurnal variations of atmospheric PAH concentrations between rural, suburban and urban areas. *Atmos. Pollut. Res.* 2011; 2: 366-373.
142. Motelay-Massei A, Garban B, Tiphagne-larcher K, Chevreuil M, Ollivon D. Mass balance for polycyclic aromatic hydrocarbons in the urban watershed of Le Havre (France): Transport and fate of PAHs from the atmosphere to the outlet. *Water Res.* 2006; 40(10): 1995-2006.
143. Muller P, Leece B, Raha D, Li-Muller A. Scientific Criteria Document for Multimedia Standards Development, Polycyclic Aromatic Hydrocarbons (PAH). Part 1: Hazard Identification and Dose-Response Assessment; Standard Development Branch, Ontario Ministry of Environment and Energy: Toronto, Ontario, 1997.
144. National Institute for Occupational Safety and Health (NIOSH). Method: 5515, Issue 2. Polynuclear aromatic hydrocarbons by GC. 1994.
145. National Institute for Occupational Safety and Health (NIOSH). Method: 5506, Issue 3. Polynuclear aromatic hydrocarbons by HPLC. 1998.
146. Nisbet ICT, LaGoy PK. Toxic equivalency factors (TEFs) for polycyclic aromatic hydrocarbons (PAHs). *Regul. Toxicol. Pharm.* 1992; 16(3): 290-300.
147. Norris G, Duvall R, Brown S, and Bai S. EPA Positive Matrix Factorization (PMF) 5.0 fundamentals and user guide. Prepared for the U.S. Environmental Protection Agency Office of Research and Development, Washington, DC, 2014 (EPA/600/R-14/108; STI-910511-5594-UG).
148. Office of the Federal Registration (OFR). Appendix A: priority pollutants. Fed Reg. 1982; 47: 52309.

149. Oliveira C, Martins N, Tavares J, Pio C, Cerqueira M, Matos M, Silva H, Oliveira C, Camões F. Size distribution of polycyclic aromatic hydrocarbons in a roadway tunnel in Lisbon, Portugal. *Chemosphere*. 2011; 83(11):1588-1596.
150. Omar N, Radzi Bin Abas M, Ketuly K, Tahir N. Concentrations of PAHs in atmospheric particles (PM-10) and roadside soil particles collected in Kuala Lumpur, Malaysia. *Atmos. Environ*. 2002; 36: 247-54.
151. Ortiz R, Vega S, Gutierrez R, Gibson R, Schettino B, Ramirez MD. Presence of polycyclic aromatic hydrocarbons (PAHs) in top soils from rural terrains in Mexico City. *B. Environ. Contam. Tox*. 2012; 88:428-432.
152. Paatero P, Tapper U. Positive matrix factorization: a non-negative factor model with optimal utilization of error estimates of data values. *Environmetrics*. 1994; 5: 111-126.
153. Paatero P. Least-squares formulation of robust non-negative factor analysis. *Chemometr. Intell. Lab*. 1997; 37: 23-35.
154. Paatero P. The Multilinear Engine-A table-driven least squares program for solving multilinear problems, including the n-way parallel factor analysis model. *J. Comput. Graph. Stat*. 1999; 8: 854-888.
155. Paatero P, Hopke PK. Discarding or downweighting high-noise variables in factor analytic models. *Anal. Chim. Acta*. 2003; 490: 277-289.
156. Paatero P, Eberly S, Brown SG, Norris GA. Methods for estimating uncertainty in factor analytic solutions. *Atmos. Meas. Tech*. 2014; 7: 781-797.
157. Pandey SK, Kim KH, Brown RJC. A review of techniques for the determination of polycyclic aromatic hydrocarbons in air. *Trends Anal. Chem*. 2011; 30: 1716-1739.
158. Park SS, Kim YJ, Kang CH. Atmospheric polycyclic aromatic hydrocarbons in Seoul, Korea. *Atmos. Environ*. 2002; 36(17): 2917-2924.
159. Park SU, Kim JG, Jeong MJ, Song BJ. Source identification of atmospheric polycyclic aromatic hydrocarbons in industrial complex using diagnostic ratios and multivariate factor analysis. *Arch. Environ. Con. Tox*. 2011; 60(4):576-589.
160. PerkinElmer. Clarus 500 MS Hardware Guide. PerkinElmer, Inc., UK, 2002.
161. PerkinElmer. TurboMass Software. User's Guide. PerkinElmer, Inc. UK, 2006.
162. PerkinElmer. TurboMatrix Series Thermal Desorbers. User's Guide. PerkinElmer, Inc., UK, 2007.

163. Pietrogrande MC, Abbaszade G, Schnelle-Kreis J, Bacco D, Mercuriali M, Zimmermann R. Seasonal variation and source estimation of organic compounds in urban aerosol of Augsburg, Germany. *Environ. Pollut.* 2011; 159(7):1861-1868.
164. Piñeiro-Iglesias M, López-Mahía P, Vázquez-Blanco E, Muniategui-Lorenzo S, Prada-Rodríguez D, Fernández-Fernández E. Microwave assisted extraction of polycyclic aromatic hydrocarbons from atmospheric particulate samples. *Fresen. J. Anal. Chem.* 2000; 367(1): 29-34.
165. Pleil JD, Vette AF, Rappaport SM. Assaying particle-bound polycyclic aromatic hydrocarbons from archived PM_{2.5} filters. *J. Chromatogr. A.* 2004;1033 (1): 9-17.
166. Portet-Koltalo F, Oukebdane K, Dionnet F, Desbène PL. De l'intérêt de l'utilisation de la pyridine pour l'extraction par micro-ondes des hydrocarbures aromatiques polycycliques à partir des particules de suies émises à l'échappement d'un moteur Diesel. *Spectra Analyse.* 2007; 254: 28-36.
167. Poster DL, Schantz MM, Sander LC, Wise SA. Analysis of polycyclic aromatic hydrocarbons (PAHs) in environmental samples: a critical review of gas chromatographic (GC) methods. *Anal. Bioanal. Chem.* 2006; 386(4): 859-881.
168. Queensland Government. High and low volume air samplers. Available: <https://www.qld.gov.au/environment/pollution/monitoring/air-pollution/samplers/> [last accessed: October 2015].
169. Rajput N, Lakhani A. Polycyclic aromatic hydrocarbons: sources, distribution, and health implications. In: Gurjar BR, Molina LT, Ojha CSP (eds.), *Air Pollution Health and Environmental Impacts*. CRC Press, Florida, 2010; 229-248.
170. Ramos L, Kristenson EM, Brinkman UA. Current use of pressurised liquid extraction and subcritical water extraction in environmental analysis. *J. Chromatogr. A.* 2002; 975: 3-29.
171. Ravindra K, Mor S, Ameena, Kamyotra JS, Kaushik CP. Variation in spatial pattern of criteria air pollutants before and during initial rain of monsoon. *Environ. Monit. Assess.* 2003; 87: 145–153.
172. Ravindra K, Bencs L, Wauters E, Hoog J, Deutsch F, Roekens E, Bleux N., Berghmans P, Van Grieken R. Seasonal and site-specific variation in vapour and aerosol phase PAHs over Flanders (Belgium) and their relation with anthropogenic activities. *Atmos. Environ.* 2006; 40: 771–785.
173. Ravindra K, Sokhi R, Grieken RV. Atmospheric polycyclic aromatic hydrocarbons: source attribution, emission factors and regulation. *Atmos. Environ.* 2008; 42: 2895-2921.

174. Ré N, Kataoka VM, Cardoso CA, Alcantara GB, de Souza JB. Polycyclic aromatic hydrocarbon concentrations in gas and particle phases and source determination in atmospheric samples from a semiurban area of Dourados, Brazil. *Arch. Environ. Con. Tox.* 2015; 69(1): 69-80.
175. Reche C, Moreno T, Amato F, Viana M, van Drooge BL, Chuang HC, Bérubé K, Jones T, Alastuey A, Querol X. A multidisciplinary approach to characterise exposure risk and toxicological effects of PM₁₀ and PM_{2.5} samples in urban environments. *Ecotoxi. Environ. Safe.* 2012; 78: 327-335.
176. Reff A, Eberly SI, Bhave PV. Receptor modeling of ambient particulate matter data using positive matrix factorization: review of existing methods. *J. Air Waste Manag. Assoc.* 2007; 57(2):146–154.
177. Reisen F, Arey J. Atmospheric reactions influence seasonal PAH and nitro-PAH concentrations in the Los Angeles basin. *Environ. Sci. Technol.* 2005; 39:64–73.
178. Ré-Poppi N, Santiago-Silva M. Polycyclic aromatic hydrocarbons and other selected organic compounds in ambient air of Campo Grande City, Brazil. *Atmos. Environ.* 2005; 39 (16): 2839-2850.
179. Rice HR, Baker BA. Workplace hazards to women's reproductive health. *Minn. Med.* 2007; 90(9): 44-7.
180. Ringuet J, Albinet A, Leoz-Garziandia E, Budzinski H, Villenave E. Diurnal/nocturnal concentrations and sources of particulate-bound PAHs, OPAHs and NPAHs at traffic and suburban sites in the region of Paris (France). *Sci. Total Environ.* 2012; 437: 297-305.
181. Rivera-Figueroa AM, Ramazan KA, Finlayson-Pitts BJ. Fluorescence, absorption, and excitation spectra of polycyclic aromatic hydrocarbons as a tool for quantitative analysis. *J. Chem. Educ.* 2004, 81 (2): 242-245.
182. Rogge WF, Hildemann LM, Mazurek MA, Cass GR, Simoneit BRT. Sources of fine organic aerosol. 5. Natural gas home appliances. *Environ. Sci. Technol.* 1993; 27:2736–2744.
183. Rynö M, Rantanen L, Papaioannou E, Konstandopoulos AG, Koskentalo T, Savela K. Comparison of pressurized fluid extraction, Soxhlet extraction and sonication for the determination of polycyclic aromatic hydrocarbons in urban air and diesel exhaust particulate matter. *J. Environ. Monit.* 2006; 8(4):488-493.
184. Santana Rodríguez JJ, Padron Sanz C. Fluorescence techniques for the determination of polycyclic aromatic hydrocarbons in marine environment: An overview. *Analisis.* 2000; 28: 710-717.

185. Sasaki JC, Arey J, Eastmond DA, Parks KK, Grosovsky AJ. Genotoxicity induced in human lymphoblasts by atmospheric reaction products of naphthalene and phenanthrene. *Mutat. Res. Gen. Tox. En.* 1997; 393: 23-35.
186. Scientific Instrument Services Inc (SIS). Adsorbent resins guide. Available: <http://www.sisweb.com/index/referenc/resins.htm> [last accessed: October 2016].
187. Sharma H, Jain VK, Khan ZH. Characterization and source identification of polycyclic aromatic hydrocarbons (PAHs) in the urban environment of Delhi. *Chemosphere*. 2007; 66(2): 302-310.
188. Shen JC, Shao X G. A comparison of accelerated solvent extraction, Soxhlet extraction, and ultrasonicassisted extraction for analysis of terpenoids and sterols in tobacco. *Anal. Bioanal. Chem.* 2005; 383: 1003-1008.
189. Shen HZ, Huang Y, Wang R, Zhu D, Li W, Shen GF, Wang B, Zhang YY, Chen YC, Lu Y, Chen H, Li TC, Sun K, Li BG, Liu WX, Liu JF, Tao S. Global atmospheric emissions of polycyclic aromatic hydrocarbons from 1960 to 2008 and future predictions. *Environ. Sci. Technol.* 2013; 47:6415-6424.
190. Sigma-Aldrich. ATIS Adsorbent Tube Injector System. Available: <http://www.sigmaaldrich.com/catalog/product/supelco/28521u?lang=es®ion=ES> [last accessed: September 2016].
191. Sišović A, Pehnec G, Jakovljević I, Silović Hujčić M, Vađić V, Bešlić I. Polycyclic aromatic hydrocarbons at different crossroads in Zagreb, Croatia. *Bull. Environ. Contam. Toxicol.* 2012; 88(3):438-442.
192. Slezakova K, Castro D, Pereira MC, Moralis S, Delerue-Matos C, Alvim-Ferraz MC. Influence of traffic emissions on the carcinogenic polycyclic aromatic hydrocarbons in outdoor breathable particles. *J. Air Waste Manag. Assoc.* 2010; 60 (4): 393-401
193. Slezakova K, Castro D, Delerue-Matos C, Alvim-Ferraz MC, Morais S, Pereira, MC. Impact of vehicular traffic emissions on particulate-bound PAHs: Levels and associated health risks. *Atmos. Res.* 2013; 127: 141-147.
194. Smith KEC, Northcott GL, Jones KC. Influence of the extraction methodology on the analysis of polycyclic aromatic hydrocarbons in pasture vegetation. *J. Chromatogr. A.* 2006; 1116(1-2):20-30.
195. Spanish Ministry of Agriculture, Food and Environment. Spain Inventory Report 1990-2014. Available: http://www.ceip.at/ms/ceip_home1/ceip_home/status_reporting/2016_submission/ [last accessed: August 2016].

196. Sparring S, Bowadt S, Svensmark B, Bjorklund E. Comprehensive comparison of classic Soxhlet extraction with Soxtec extraction, ultrasonication extraction, supercritical fluid extraction, microwave assisted extraction and accelerated solvent extraction for the determination of polychlorinated biphenyls in soil. *J. Chromatogr. A*. 2005; 1090: 1-9.
197. Stephens DL Jr, McFadden T, Heath OD, Mauldin RF. The effect of sonication on the recovery of polycyclic aromatic hydrocarbons from coal stack ash surfaces. *Chemosphere*. 1994; 28(10):1741–1747.
198. Subramanyam V, Valsaraj KT, Thibodeaux LJ, Reible DD. Gas-to-particle partitioning of polycyclic aromatic hydrocarbons in an urban atmosphere. *Atmos. Environ*. 1994; 28: 3083-3091.
199. Sun F, Littlejohn D, Gibson MD. Ultrasonication extraction and solid phase extraction clean-up for determination of US EPA 16 priority pollutant polycyclic aromatic hydrocarbons in soils by reversed-phase liquid chromatography with ultraviolet absorption detection. *Anal. Chim. Acta*. 1998; 364(1-3): 1-11.
200. Tauler R. Viana M. Querol X. Alastuey A. Flight RM. Wentzell PD. Hopke PK. Comparison of the results obtained by four receptor modelling methods in aerosol source apportionment studies. *Atmos. Environ*. 2009; 43: 3989-3997.
201. Teixeira EC, Mattiuzi CD, Agudelo-Castañeda DM, Garcia Kde O, Wiegand F. Polycyclic aromatic hydrocarbons study in atmospheric fine and coarse particles using diagnostic ratios and receptor model in urban/industrial region. *Environ. Monit. Assess*. 2013; 185(11): 9587-9602.
202. Teknokroma. Meta X5 capillar columns Available: <http://www.teknokroma.es/UserFiles/GC/Columnas%20Capilares%20Teknokroma/Meta.X5/Meta.X5.pdf> [last accessed: September 2016].
203. Thompson M, Ellison SLR, Wood R. Harmonized guidelines for single-laboratory validation of methods of analysis (IUPAC technical report). *Pure Appl. Chem*. 2002; 74: 835-855.
204. Tobiszewski M, Namieśnik J. PAH diagnostic ratios for the identification of pollution emission sources. *Environ. Pollut*. 2012; 162: 110-119.
205. Tsapakis M, Stephanou E G. Occurrence of gaseous and particulate polycyclic aromatic hydrocarbons in the urban atmosphere: Study of sources and ambient temperature effect on the gas/particle concentration and distribution. *Environ Pollut*. 2005; 133: 147-156.
206. United Nations Economic Commission for Europe (UNECE). Convention on longrange trans-boundary air pollution. United Nations Economic Commission for Europe, Geneva, 1979.

207. U.S. Environmental Protection Agency (US-EPA). Compendium Method TO-17. Determination of Volatile Organic Compounds in Ambient Air Using Active Sampling Onto Sorbent Tubes. Cincinnati, Ohio, 1999a.
208. U.S. Environmental Protection Agency (US-EPA). Method TO-13A. Determination of polycyclic aromatic hydrocarbons (PAHs) in ambient air using gas chromatography/mass spectrometry (GC/MS). Cincinnati, Ohio, 1999b.
209. U.S. Environmental Protection Agency (US-EPA). Risk Assessment Guidance for Superfund. In: Human Health Evaluation Manual (Part E, Supplemental Guidance for Dermal Risk Assessment), vol. I. EPA/540/R/99/005, Washington DC, USA Office of Emergency and Remedial Response, 2001.
210. U.S. Environmental Protection Agency (US-EPA). EPA Unmix 6.0 Fundamentals and User Guide. USEPA Office of Research and Development, 2007.
211. U.S. Environmental Protection Agency (US-EPA). Guidelines establishing test procedures for the analysis of pollutants (Part 136, Appendix B. Definition and procedure for the determination of the method detection limit-Revision 1.11). U.S. Code of Federal Regulations, Title 40; Washington, USA, 2013; 344-347.
212. U.S. Environmental Protection Agency (US-EPA). EPA Positive Matrix Factorisation (PMF) 5.0 Fundamentals and User Guide. USEPA Office of Research and Development, 2014.
213. U.S. Environmental Protection Agency (US-EPA). Integrated Risk Information System (IRIS). Available: <http://cfpub.epa.gov/ncea/iris/index.cfm?fuseaction=iris.showSubstanceList> [last accessed: October 2016].
214. Uria-Tellaetxe I, Carslaw DC. Conditional bivariate probability function for source identification. *Environ. Modell. Softw.* 2014; 59: 1-9.
215. Valavanidis A, Fiotakis K, Vlachogianni T. Airborne particulate matter and human health: toxicological assessment and importance of size and composition of particles for oxidative damage and carcinogenic mechanisms. *J. Environ. Sci. Heal C.* 2008; 26: 339-362.
216. Van Drooge BL, Nikolova I, Ballesta PP. Thermal desorption gas chromatography-mass spectrometry as an enhanced method for the quantification of polycyclic aromatic hydrocarbons from ambient air particulate matter. *J. Chromatogr. A.* 2009; 1216(18): 4030-4039.
217. Van Drooge BL, Grimalti JO. Persistent Organic Pollutants in the European Atmosphere. In: Viana M (ed.), *The Handbook of Environmental Chemistry Vol.*

- 26: *Urban air quality in Europe*. Springer-Verlag Berlin Heidelberg. 2013; 75-100.
218. Van Jaarsveld JA, Van Pul WAJ, De Leeuw FAAM. (1997). Modelling transport and deposition of persistent organic pollutants in the European region. *Atmos. Environ.* 1997; 31: 1011-1024.
219. Varea M, Galindo N, Gil-Moltó J, Pastor C, Crespo J. Particle-bound polycyclic aromatic hydrocarbons in an urban, industrial and rural area in the western Mediterranean. *J. Environ. Monitor.* 2011; 13(9):2471-2476.
220. Vasilakos C, Levi N, Maggos T, Hatzianestis J, Michopoulos J, Helmis C. Gas-particle concentration and characterization of sources of PAHs in the atmosphere of a suburban area in Athens, Greece. *J. Hazard. Mater.* 2007; 140: 45-51.
221. Vestenius M, Leppanen S, Anttila P, Kyllonen K, Hatakka J, Hellen H, Hyvarinen AP, Hakola H. Background concentrations and source apportionment of polycyclic aromatic hydrocarbons in south-eastern Finland. *Atmos. Environ.* 2011; 45(20): 3391–3399.
222. Villanueva F, Tapia A, Cabañas B, Martínez E, Albaladejo J. Characterization of particulate polycyclic aromatic hydrocarbons in an urban atmosphere of central-southern Spain. *Environ. Sci. Pollut. Res. Int.* 2015; 22(23):18814-18823.
223. Walgraeve C, Chantara S, Sopajaree K, De Wispelaere P, Demeestere K, Van Langenhove H. Quantification of PAHs and oxy-PAHs on airborne particulate matter in Chiang Mai, Thailand, using gas chromatography high resolution mass spectrometry. *Atmos. Environ.* 2015; 107: 262-272.
224. Wan X, Chen J, Tian F, Sun W, Yang F, Saiki K. Source apportionment of PAHs in atmospheric particulates of Dalian: factor analysis with nonnegative constraints and emission inventory analysis. *Atmos. Environ.* 2006; 40:6666–6675.
225. Wang Y, Raj A, Chung SH. A PAH growth mechanism and synergistic effect on PAH formation in counterflow diffusion flames. *Combust. Flame.* 2013; 160 (9): 1667-1676.
226. Wania F, Mackay D. Tracking the distribution of persistent organic pollutants. *Environ. Sci. Technol.* 1996; 30: 390-396.
227. Wauters E, Van Caeter P, Desmet G, David F, Devos C, Sandra P. Improved accuracy in the determination of polycyclic aromatic hydrocarbons in air using 24 h sampling on a mixed bed followed by thermal desorption capillary gas chromatography-mass spectrometry. *J. Chromatogr. A.* 2008;1190 (1-2):286-293.

228. Wei C, Han Y, Bandowe BA, Cao J, Huang RJ, Ni H, Tian J, Wilcke W. Occurrence, gas/particle partitioning and carcinogenic risk of polycyclic aromatic hydrocarbons and their oxygen and nitrogen containing derivatives in Xi'an, central China. *Sci. Total Environ.* 2015; 505: 814-822.
229. Wells PG, McCallum GP, Lam KC, Henderson JT, Ondovcik SL. Oxidative DNA damage and repair in teratogenesis and neurodevelopmental deficits. *Birth Defects Res. C.* 2010; 90(2): 103-109.
230. Westerholm R, Lin H. A multivariate statistical analysis of fuel-related Polycyclic Aromatic Hydrocarbon emission from heavy-duty diesel vehicles. *Environ. Sci. Technol.* 1994; 28: 962-972
231. Wild SR, Jones KC. Polynuclear aromatic hydrocarbons in the United Kingdom environment: A preliminary source inventory and budget. *Environ. Pollut.* 1995; 88: 91-108.
232. Williams ML. Atmospheric dispersal of pollutants and the modelling of air pollution. In: Harrison RM (ed.), *Pollution: Causes, Effects and Control*, 5th edition. The Royal Society of Chemistry, Cambridge, 1996; 225-243.
233. Wiriya W, Prapamontol T, Chantara S. PM10-bound polycyclic aromatic hydrocarbons in Chiang Mai (Thailand): seasonal variations, source identification, health risk assessment and their relationship to air-mass movement. *Atmos. Res.* 2013; 124: 109-122.
234. Woolfenden E. Sorbent-based sampling methods for volatile and semi-volatile organic compounds in air Part 1: Sorbent-based air monitoring options. *J. Chromatogr. A.* 2010; 1217(16): 2674-2684.
235. Woolfenden E. Thermal desorption for gas chromatography. In: Poole CF (ed), *Gas Chromatography*. Elsevier, USA, 2012; 235-289.
236. World Health Organization (WHO). Air Quality Guideline for Europe, 2nd ed. WHO, Copenhagen, 2000. WHO Regional Publications: European Series, No.91.
237. Wu SP, Tao S, Liu WX. Particle size distributions of polycyclic aromatic hydrocarbons in rural and urban atmosphere of Tianjin, China. *Chemosphere.* 2006; 62(3): 357-367.
238. Wu Y, Yang L, Zheng X, Zhang SJ, Song SJ, Li JQ, Hao JM. Characterization and source apportionment of particulate PAHs in the roadside environment in Beijing. *Sci. Total Environ.* 2014; 470-471: 76-83.
239. Xu Y, Zhang Y-L, Li J, Gioia R, Zhang G, Li X-D, Spiro B, Bhatia RS, Jones KC. The spatial distribution and potential sources of polycyclic aromatic

- hydrocarbons (PAHs) over the Asian marginal seas and the Indian and Atlantic Oceans. *J. Geophys. Res.* 2012; 117 (D7) D07302.
240. Xu HM, Tao J, Ho SSH, Ho KF, Cao JJ, Li N, Chow J C, Wang GH, Han YM, Zhang RJ, Watson JG, Zhang JQ. Characteristics of fine particulate non-polar organic compounds in Guangzhou during the 16th Asian Games: Effectiveness of air pollution controls. *Atmos. Environ.* 2013; 76: 94-101.
241. Yadav S, Tandon A, Attri AK. Characterization of aerosol associated non-polar organic compounds using TD-GC-MS: a four year study from Delhi, India. *J. Hazard. Mater.* 2013; 252-253: 29-44.
242. Yagishita M, Kageyama S, Ohshima S, Matsumoto M, Aoki Y, Goto S, Nakajima D. Atmospheric concentration and carcinogenic risk of polycyclic aromatic hydrocarbons including benzo[c]fluorene, cyclopenta[c,d]pyrene, and benzo[j]fluoranthene in Japan. *Atmos. Environ.* 2015; 115: 263-268.
243. Yang F, Zhai Y, Chen L, Li C, Zeng G, He Y. The seasonal changes and spatial trends of particle associated polycyclic aromatic hydrocarbons in the summer and autumn in Changsha City. *Atmos. Res.* 2010; 96: 122-130.
244. Yu JZ, Huang XH, Ho SS, Bian Q. Nonpolar organic compounds in fine particles: quantification by thermal desorption-GC/MS and evidence for their significant oxidation in ambient aerosols in Hong Kong. *Anal. Bioanal. Chem.* 2011; 401(10): 3125-3139.
245. Yuan Y, Jin L, Wang L, Li Z, Zhang L, Zhu H, Finnell R H, Zhou G, Ren A. Levels of PAH-DNA adducts in placental tissue and the risk of fetal neural tube defects in a Chinese population. *Reprod. Toxicol.* 2013; 37: 70-5.
246. Yunker MB, Macdonald RW, Vingarzan R, Mitchell RH, Goyette D, Sylvestre S. PAHs in the Fraser River basin: a critical appraisal of PAH ratios as indicators of PAH source and composition. *Org. Geochem.* 2002; 33(4): 489–515.
247. Zhang L, Wang Y, Wu D, Xu M, Chen J. Microwave-assisted extraction of polyphenols from *Camellia oleifera* fruit hull. *Molecules.* 2011; 16(6): 4428-4437.
248. Zhu L, Lu H, Chen S, Amagai T. Pollution level, phase distribution and source analysis of polycyclic aromatic hydrocarbons in residential air in Hangzhou, China. *J. Hazard. Mater.* 2009; 162 (2-3):1165-1170.

Appendix A

Table A.1. Diurnal period (n=7) and weekly (n=21) mean concentrations (ng m⁻³) of individual PAHs during the sampling period. Standard deviation in brackets.

PAH	Period	July-13	September-13	October-13	November-13	December-13
FL	M	0.09(0.07)	0.14(0.07)	0.05(0.02)	0.05(0.02)	0.13(0.07)
	A	0.07(0.04)	0.08(0.04)	0.04(0.01)	0.11(0.08)	0.12(0.08)
	N	0.12(0.12)	0.09(0.02)	0.04(0.02)	0.09(0.08)	0.11(0.05)
	Mean	0.10(0.08)	0.10(0.05)	0.04(0.01)	0.08(0.07)	0.12(0.07)
Phe	M	0.21(0.07)	0.20(0.06)	0.27(0.11)	0.15(0.04)	0.39(0.17)
	A	0.14(0.04)	0.14(0.04)	0.21(0.04)	0.27(0.17)	0.44(0.24)
	N	0.16(0.05)	0.14(0.04)	0.17(0.07)	0.14(0.13)	0.33(0.06)
	Mean	0.17(0.06)	0.16(0.05)	0.22(0.09)	0.19(0.14)	0.39(0.17)
Ant	M	0.03(0.01)	0.04(0.01)	0.06(0.02)	0.06(0.04)	0.08(0.04)
	A	0.02(0.01)	0.03(0.01)	0.05(0.02)	0.13(0.10)	0.09(0.05)
	N	0.02(0.01)	0.03(0.01)	0.04(0.01)	0.07(0.10)	0.10(0.03)
	Mean	0.03(0.01)	0.03(0.01)	0.05(0.02)	0.09(0.09)	0.09(0.04)
Ft	M	0.22(0.09)	0.21(0.08)	0.33(0.14)	0.28(0.13)	0.70(0.30)
	A	0.15(0.07)	0.19(0.06)	0.34(0.10)	0.43(0.22)	0.94(0.39)
	N	0.13(0.04)	0.16(0.07)	0.20(0.07)	0.17(0.15)	0.61(0.13)
	Mean	0.17(0.08)	0.19(0.07)	0.29(0.12)	0.30(0.19)	0.74(0.31)
Pyr	M	0.23(0.09)	0.24(0.09)	0.38(0.16)	0.29(0.15)	0.72(0.27)
	A	0.14(0.06)	0.21(0.08)	0.39(0.10)	0.43(0.17)	0.97(0.40)
	N	0.13(0.04)	0.18(0.08)	0.20(0.07)	0.15(0.13)	0.59(0.12)
	Mean	0.17(0.08)	0.21(0.08)	0.32(0.14)	0.29(0.18)	0.76(0.31)

Note: diurnal periods correspond to morning (M): 04:00–12:00 h, afternoon (A): 12:00–20:00 h and night (N): 20:00–04:00 h UTC.

Table A.1. (continued) Diurnal period (n=7) and weekly (n=21) mean concentrations (ng m⁻³) of individual PAHs during the sampling period. Standard deviation in brackets.

PAH	Period	July-13	September-13	October-13	November-13	December-13
BaA	M	0.08(0.04)	0.13(0.06)	0.32(0.21)	0.08(0.06)	0.47(0.22)
	A	0.04(0.01)	0.06(0.02)	0.13(0.03)	0.21(0.15)	0.78(0.45)
	N	0.06(0.03)	0.12(0.15)	0.14(0.06)	0.07(0.08)	0.69(0.21)
	Mean	0.06(0.04)	0.10(0.10)	0.20(0.15)	0.12(0.12)	0.64(0.32)
Chry	M	0.18(0.10)	0.19(0.11)	0.45(0.32)	0.17(0.07)	0.53(0.19)
	A	0.11(0.30)	0.10(0.04)	0.15(0.08)	0.34(0.24)	0.82(0.40)
	N	0.12(0.04)	0.24(0.31)	0.21(0.08)	0.14(0.09)	0.75(0.22)
	Mean	0.14(0.07)	0.18(0.19)	0.27(0.23)	0.22(0.17)	0.69(0.29)
BbFt	M	0.23(0.14)	0.26(0.11)	0.77(0.74)	0.24(0.17)	1.60 (0.49)
	A	0.12(0.03)	0.13(0.05)	0.33(0.19)	0.78(0.80)	2.75(1.89)
	N	0.20(0.12)	0.22(0.21)	0.34(0.17)	0.29(0.27)	2.08(0.87)
	Mean	0.19(0.11)	0.20(0.15)	0.48(0.48)	0.45(0.54)	2.12(1.23)
BkFt	M	0.12(0.09)	0.10(0.03)	0.24(0.23)	0.10(0.07)	0.45(0.12)
	A	0.08(0.04)	0.07(0.02)	0.13(0.06)	0.49(0.59)	0.69(0.40)
	N	0.13(0.08)	0.08(0.05)	0.12(0.05)	0.16(0.15)	0.55(0.16)
	Mean	0.11(0.07)	0.08(0.04)	0.16(0.14)	0.26(0.39)	0.56(0.26)
BaP	M	0.10(0.06)	0.12(0.04)	0.34(0.26)	0.09(0.06)	0.44(0.20)
	A	0.06(0.03)	0.07(0.02)	0.13(0.03)	0.16(0.09)	0.60(0.35)
	N	0.09(0.06)	0.11(0.07)	0.16(0.07)	0.08(0.06)	0.70(0.28)
	Mean	0.09(0.05)	0.10(0.05)	0.21(0.17)	0.11(0.08)	0.57(0.29)

Note: diurnal periods correspond to morning (M): 04:00–12:00 h, afternoon (A): 12:00–20:00 h and night (N): 20:00–04:00 h UTC.

Table A.1. (continued) Diurnal period (n=7) and weekly (n=21) mean concentrations (ng m⁻³) of individual PAHs during the sampling period. Standard deviation in brackets.

PAH	Period	July-13	September-13	October-13	November-13	December-13
IP	M	0.09(0.03)	0.12(0.03)	0.30(0.20)	0.05(0.05)	0.54(0.23)
	A	0.06(0.02)	0.09(0.03)	0.14(0.02)	0.15(0.17)	0.69(0.52)
	N	0.10(0.06)	0.12(0.07)	0.17(0.06)	0.06(0.07)	0.81(0.39)
	Mean	0.08(0.05)	0.11(0.05)	0.20(0.14)	0.09(0.12)	0.67(0.38)
DBahA	M	0.02(0.01)	0.03(0.01)	0.05(0.03)	0.01(0.01)	0.13(0.12)
	A	0.03(0.02)	0.05(0.04)	0.05(0.03)	0.04(0.06)	0.15(0.12)
	N	0.03(0.03)	0.04(0.03)	0.04(0.02)	0.01(0.01)	0.15(0.07)
	Mean	0.03(0.02)	0.04(0.03)	0.05(0.03)	0.02(0.04)	0.14(0.10)
BghiP	M	0.17(0.06)	0.18(0.05)	0.32(0.15)	0.11(0.08)	0.55(0.19)
	A	0.12(0.03)	0.13(0.05)	0.20(0.03)	0.32(0.36)	0.63(0.28)
	N	0.16(0.07)	0.16(0.09)	0.20(0.06)	0.10(0.05)	0.66(0.21)
	Mean	0.15(0.06)	0.16(0.07)	0.24(0.11)	0.18(0.23)	0.61(0.22)
BghiFt	M	-	-	-	0.10(0.05)	0.38(0.15)
	A	-	-	-	0.15(0.06)	0.57(0.26)
	N	-	-	-	0.05(0.02)	0.34(0.10)
	Mean	-	-	-	0.10(0.06)	0.43(0.20)
BcP	M	0.02(0.01)	0.01(0.01)	0.03(0.02)	0.03(0.02)	0.15(0.06)
	A	0.01(3.00·10 ⁻³)	0.02(0.01)	0.04(0.01)	0.05(0.02)	0.24(0.12)
	N	0.01(0.01)	0.03(0.03)	0.03(0.01)	0.01(5.00·10 ⁻³)	0.14(0.04)
	Mean	0.01(0.01)	0.20(0.02)	0.04(0.02)	0.03(0.02)	0.17(0.09)

Note: diurnal periods correspond to morning (M): 04:00–12:00 h, afternoon (A): 12:00–20:00 h and night (N): 20:00–04:00 h UTC.

Table A.1. (continued) Diurnal period (n=7) and weekly (n=21) mean concentrations (ng m⁻³) of individual PAHs during the sampling period. Standard deviation in brackets.

PAH	Period	July-13	September-13	October-13	November-13	December-13
CPP	M	-	-	-	-	0.19(0.20)
	A	-	-	-	-	0.36(0.34)
	N	-	-	-	-	0.40(0.36)
	Mean	-	-	-	-	0.32(0.30)
Triph	M	0.14(0.10)	0.11(0.06)	0.18(0.10)	0.07(0.03)	0.22(0.04)
	A	0.07(0.04)	0.06(0.02)	0.10(0.03)	0.09(0.05)	0.31(0.21)
	N	0.07(0.04)	0.16(0.26)	0.11(0.05)	0.05(0.02)	0.26(0.07)
	Mean	0.10(0.07)	0.11(0.15)	0.13(0.08)	0.07(0.04)	0.26(0.12)
BaFt	M	-	0.02(0.01)	0.05(0.03)	0.03(0.01)	0.14(0.05)
	A	-	0.01(3.00·10 ⁻³)	0.03(0.01)	0.06(0.05)	0.23(0.12)
	N	-	0.02(0.01)	0.03(0.02)	0.02(0.01)	0.21(0.07)
	Mean	-	0.02(0.01)	0.04(0.02)	0.04(0.03)	0.19(0.09)
BeP	M	0.10(0.05)	0.17(0.08)	0.42(0.36)	0.15(0.09)	0.71(0.17)
	A	0.08(0.02)	0.08(0.04)	0.21(0.11)	0.26(0.21)	1.07(0.65)
	N	0.10(0.06)	0.17(0.21)	0.19(0.10)	0.13(0.12)	0.76(0.16)
	Mean	0.09(0.05)	0.14(0.13)	0.27(0.24)	0.38(0.15)	0.84(0.40)
Per	M	0.02(0.01)	0.03(0.01)	0.07(0.05)	0.02(0.01)	0.08(0.04)
	A	0.01(0.01)	0.01(0.01)	0.03(0.01)	0.03(0.02)	0.09(0.04)
	N	0.03(0.02)	0.02(0.02)	0.03(0.02)	0.01(4.00·10 ⁻³)	0.13(0.05)
	Mean	0.02(0.01)	0.02(0.01)	0.04(0.04)	0.02(0.02)	0.10(0.05)

Note: diurnal periods correspond to morning (M): 04:00–12:00 h, afternoon (A): 12:00–20:00 h and night (N): 20:00–04:00 h UTC.

Table A.1. (continued) Diurnal period (n=7) and weekly (n=21) mean concentrations (ng m⁻³) of individual PAHs during the sampling period. Standard deviation in brackets.

PAH	Period	July-13	September-13	October-13	November-13	December-13
DBaja	M	-	3.00·10 ⁻³ (1.00·10 ⁻³)	0.01(5.00·10 ⁻³)	1.00·10 ⁻³ (1.00·10 ⁻³)	0.02(0.01)
	A	-	1.00·10 ⁻³ (4.00·10 ⁻⁴)	3.00·10 ⁻³ (1.00·10 ⁻³)	3.00·10 ⁻³ (2.00·10 ⁻³)	0.02(0.02)
	N	-	2.00·10 ⁻³ (1.00·10 ⁻³)	4.00·10 ⁻³ (2.00·10 ⁻³)	1.00·10 ⁻³ (2.00·10 ⁻⁴)	0.03(0.01)
	Mean	-	2.00·10 ⁻³ (1.00·10 ⁻³)	5.00·10 ⁻³ (4.00·10 ⁻³)	1.00·10 ⁻³ (1.00·10 ⁻³)	0.02(0.01)
BbC	M	-	5.00·10 ⁻³ (5.00·10 ⁻⁴)	6.00·10 ⁻³ (2.00·10 ⁻³)	4.00·10 ⁻³ (-)	0.01 (7.00·10 ⁻³)
	A	-	5.00·10 ⁻³ (5.00·10 ⁻⁴)	5.00·10 ⁻³ (1.00·10 ⁻³)	5.00·10 ⁻³ (-)	0.02(0.02)
	N	0.01(0.01)	5.00·10 ⁻³ (1.00·10 ⁻³)	6.00·10 ⁻³ (1.00·10 ⁻³)	-	0.03(0.02)
	Mean	0.01(0.01)	5.00·10 ⁻³ (1.00·10 ⁻³)	6.00·10 ⁻³ (1.00·10 ⁻³)	5.00·10 ⁻³ (1.00·10 ⁻³)	0.02(0.02)
Pic	M	0.01(-)	0.01(2.00·10 ⁻³)	0.01(7.00·10 ⁻³)	0.01(-)	0.06(0.04)
	A	-	6.00·10 ⁻³ (2.00·10 ⁻³)	0.01(2.00·10 ⁻³)	7.00·10 ⁻³ (-)	0.10(0.10)
	N	0.01(2.00·10 ⁻⁴)	0.01(4.00·10 ⁻³)	8.00·10 ⁻³ (2.00·10 ⁻³)	-	0.09(0.05)
	Mean	0.01(3.00·10 ⁻⁴)	7.00·10 ⁻³ (3.00·10 ⁻³)	0.01(4.00·10 ⁻³)	0.01(1.00·10 ⁻³)	0.08(0.06)
Anthran	M	-	0.02(0.10)	0.03(0.20)	-	0.06(0.04)
	A	-	7.00·10 ⁻³ (6.00·10 ⁻³)	5.00·10 ⁻³ (4.00·10 ⁻³)	-	0.13(-)
	N	-	0.02(0.02)	0.03(0.01)	-	0.13(0.11)
	Mean	-	0.01(0.01)	0.02(0.02)	-	0.10(0.08)
Cor	M	-	-	-	-	0.19(0.07)
	A	-	-	-	-	0.23(0.15)
	N	-	-	-	-	0.26(0.12)
	Mean	-	-	-	-	0.23(0.11)

Note: diurnal periods correspond to morning (M): 04:00–12:00 h, afternoon (A): 12:00–20:00 h and night (N): 20:00–04:00 h UTC.

Table A.1. (continued) Diurnal period (n=7) and weekly (n=21) mean concentrations (ng m⁻³) of individual PAHs during the sampling period. Standard deviation in brackets.

PAH	Period	January-14	February-14	March-14	June-14	Jul. - Jun.
FL	M	0.11(0.22)	0.10(0.04)	0.05(0.03)	0.06(0.02)	0.09(0.09)
	A	0.07(0.08)	0.09(0.03)	0.06(0.05)	0.07(0.06)	0.08 (0.06)
	N	0.03(0.03)	0.17(0.08)	0.06(0.05)	0.04(0.02)	0.08(0.07)
	Mean	0.07(0.13)	0.12(0.07)	0.06(0.04)	0.06(0.04)	0.08(0.07)
Phe	M	0.16(0.19)	0.11(0.03)	0.12(0.08)	0.16(0.04)	0.20(0.13)
	A	0.12(0.03)	0.13(0.04)	0.10(0.04)	0.10(0.03)	0.18(0.14)
	N	0.06(0.02)	0.17(0.05)	0.08(0.06)	0.08(0.02)	0.15(0.09)
	Mean	0.11(0.11)	0.14(0.05)	0.10(0.06)	0.11(0.05)	0.17(0.12)
Ant	M	0.09(0.17)	0.02(0.01)	0.02(0.01)	0.04(0.01)	0.05(0.06)
	A	0.05(0.04)	0.02(0.01)	0.02(0.01)	0.03(0.01)	0.05(0.05)
	N	0.02(0.01)	0.04(0.02)	0.02(0.01)	0.03(0.01)	0.04(0.04)
	Mean	0.05(0.10)	0.03(0.02)	0.02(0.01)	0.03(0.01)	0.04(0.05)
Ft	M	0.25(0.18)	0.16(0.07)	0.20(0.12)	0.18(0.06)	0.28(0.21)
	A	0.26(0.04)	0.21(0.10)	0.21(0.09)	0.16(0.19)	0.31(0.27)
	N	0.09(0.04)	0.20(0.08)	0.11(0.08)	0.12(0.06)	0.19(0.16)
	Mean	0.20(0.13)	0.19(0.08)	0.17(0.10)	0.15(0.12)	0.26(0.22)
Pyr	M	0.27(0.21)	0.16(0.08)	0.18(0.11)	0.18(0.06)	0.29(0.22)
	A	0.27(0.07)	0.24(0.12)	0.19 (0.09)	0.15(0.18)	0.33(0.28)
	N	0.09(0.04)	0.20(0.09)	0.10(0.09)	0.09(0.03)	0.19(0.16)
	Mean	0.21(0.15)	0.20(0.10)	0.15(0.09)	0.14(0.11)	0.27(0.23)

Note: diurnal periods correspond to morning (M): 04:00–12:00 h, afternoon (A): 12:00–20:00 h and night (N): 20:00–04:00 h UTC.

Table A.1. (continued) Diurnal period (n=7) and weekly (n=21) mean concentrations (ng m⁻³) of individual PAHs during the sampling period. Standard deviation in brackets.

PAH	Period	January-14	February-14	March-14	June-14	Jul. - Jun.
BaA	M	0.12(0.13)	0.07(0.02)	0.08(0.11)	0.06(0.01)	0.16(0.18)
	A	0.09(0.02)	0.11(0.06)	0.09(0.06)	0.05(0.03)	0.17(0.25)
	N	0.04(0.01)	0.21(0.15)	0.06(0.09)	0.03(0.02)	0.15(0.21)
	Mean	0.08(0.08)	0.13(0.11)	0.07(0.08)	0.05(0.02)	0.16(0.22)
Chry	M	0.14(0.07)	0.07(0.02)	0.45(0.32)	0.26(0.24)	0.24(0.21)
	A	0.13(0.05)	0.06(0.02)	0.14(0.08)	0.19(0.17)	0.22(0.26)
	N	0.11(0.05)	0.08(0.03)	0.13(0.12)	0.27(0.25)	0.22(0.24)
	Mean	0.12(0.06)	0.07(0.02)	0.14(0.10)	0.24(0.21)	0.22(0.24)
BbFt	M	0.16(0.12)	0.16(0.07)	0.18(0.14)	0.53(0.48)	0.47(0.57)
	A	0.13(0.03)	0.21(0.08)	0.24(0.18)	0.33(0.26)	0.53(1.00)
	N	0.10(0.04)	0.42(0.25)	0.32(0.39)	0.69(0.45)	0.50(0.66)
	Mean	0.13(0.07)	0.26(0.19)	0.23(0.24)	0.52(0.42)	0.50(0.76)
BkFt	M	0.06(0.03)	0.06(0.03)	0.09(0.07)	0.21(0.16)	0.17(0.16)
	A	0.05(0.01)	0.08(0.04)	0.10(0.09)	0.15(0.14)	0.20(0.30)
	N	0.04(0.02)	0.15(0.11)	0.10(0.12)	0.38(0.27)	0.18(0.19)
	Mean	0.05(0.02)	0.10(0.07)	0.09(0.09)	0.25(0.21)	0.18(0.23)
BaP	M	0.06(0.04)	0.07(0.02)	0.05(0.05)	0.06(0.02)	0.15(0.18)
	A	0.05(0.01)	0.11(0.05)	0.07(0.06)	0.06(0.03)	0.14(0.20)
	N	0.04(0.01)	0.20(0.13)	0.09(0.09)	0.04(0.01)	0.17(0.22)
	Mean	0.05(0.03)	0.13(0.10)	0.06(0.06)	0.05(0.03)	0.16(0.20)

Note: diurnal periods correspond to morning (M): 04:00–12:00 h, afternoon (A): 12:00–20:00 h and night (N): 20:00–04:00 h UTC.

Table A.1. (continued) Diurnal period (n=7) and weekly (n=21) mean concentrations (ng m⁻³) of individual PAHs during the sampling period. Standard deviation in brackets.

PAH	Period	January-14	February-14	March-14	June-14	Jul. - Jun.
IP	M	0.05(0.04)	0.09(0.07)	0.09(-)	0.06(0.05)	0.16(0.19)
	A	0.07(0.03)	0.07(0.05)	0.02(0.01)	0.05(0.02)	0.16(0.26)
	N	0.03(0.02)	0.14(0.07)	0.11(0.01)	0.04(0.03)	0.18(0.26)
	Mean	0.05(0.03)	0.10(0.07)	0.07(0.05)	0.05(0.04)	0.17(0.24)
DBahA	M	0.01(0.01)	0.06(0.06)	0.01(-)	0.02(0.01)	0.05(0.06)
	A	0.01(0.01)	0.05(0.05)	0.01(0.01)	0.04(0.01)	0.05(0.06)
	N	- (-)	0.06(0.04)	0.03(0.02)	0.02(0.01)	0.05(0.05)
	Mean	0.01(0.01)	0.06(0.05)	0.02(0.02)	0.03(0.01)	0.05(0.06)
BghiP	M	0.13(0.07)	0.12(0.04)	0.11(0.18)	0.13(0.04)	0.21(0.17)
	A	0.14(0.07)	0.13(0.04)	0.08(0.08)	0.15(0.13)	0.21(0.22)
	N	0.11(0.05)	0.21(0.11)	0.08(0.08)	0.09(0.03)	0.20(0.19)
	Mean	0.12(0.06)	0.15(0.08)	0.08(0.11)	0.12(0.08)	0.20(0.19)
BghiFt	M	0.12(0.06)	0.14(0.09)	0.30(0.24)	0.07(0.03)	0.19(0.17)
	A	0.12(0.02)	0.20(0.12)	0.27(0.10)	0.04(0.03)	0.22(0.20)
	N	0.06(0.03)	0.34(0.25)	0.24(0.19)	0.04(0.01)	0.18(0.19)
	Mean	0.10(0.05)	0.23(0.18)	0.27(0.17)	0.05(0.03)	0.20(0.19)
BcP	M	0.04(0.02)	0.05(0.03)	0.08(0.06)	0.02(0.01)	0.05(0.05)
	A	0.04(7.00·10 ⁻³)	0.08(0.05)	0.10(0.04)	0.02(0.02)	0.06(0.08)
	N	0.02(7.00·10 ⁻³)	0.12(0.09)	0.07(0.05)	0.01(8.00·10 ⁻³)	0.05(0.06)
	Mean	0.03(0.01)	0.09(0.07)	0.08(0.05)	0.02(0.01)	0.06(0.06)

Note: diurnal periods correspond to morning (M): 04:00–12:00 h, afternoon (A): 12:00–20:00 h and night (N): 20:00–04:00 h UTC.

Table A.1. (continued) Diurnal period (n=7) and weekly (n=21) mean concentrations (ng m⁻³) of individual PAHs during the sampling period. Standard deviation in brackets.

PAH	Period	January-14	February-14	March-14	June-14	Jul. - Jun.
CPP	M	0.06(0.03)	0.01(2.00·10 ⁻³)	0.02(0.02)	0.01(3.00·10 ⁻³)	0.05(0.10)
	A	0.06(0.02)	0.01(5.00·10 ⁻³)	0.02(0.01)	0.01(3.00·10 ⁻³)	0.06(0.14)
	N	-	0.01(3.00·10 ⁻³)	0.02(0.01)	7.00·10 ⁻³ (3.00·10 ⁻³)	0.11(0.23)
	Mean	0.06(0.02)	0.01(3.00·10 ⁻³)	0.02(0.01)	0.01(3.00·10 ⁻³)	0.07(0.16)
Triph	M	0.07(0.02)	0.16(0.12)	0.11(0.10)	0.18(0.16)	0.14(0.10)
	A	0.08(0.02)	0.21(0.13)	0.09(0.06)	0.17(0.17)	0.13(0.12)
	N	0.06(0.01)	0.34(0.23)	0.08(0.07)	0.13(0.10)	0.15(0.16)
	Mean	0.07(0.02)	0.24(0.18)	0.09(0.07)	0.16(0.14)	0.14(0.13)
BaFt	M	0.02(0.01)	0.01(0.01)	0.01(0.01)	0.01(6.00·10 ⁻³)	0.04(0.05)
	A	0.02(4.00·10 ⁻³)	0.01(0.01)	0.02(0.01)	7.00·10 ⁻³ (3.00·10 ⁻³)	0.05(0.08)
	N	0.01(4.00·10 ⁻³)	0.03(0.02)	0.02(0.02)	6.00·10 ⁻³ (1.00·10 ⁻³)	0.05(0.07)
	Mean	0.02(0.01)	0.02(0.02)	0.02(0.01)	0.01(5.00·10 ⁻³)	0.05(0.07)
BeP	M	0.09(0.05)	0.05(0.04)	0.07(0.07)	0.43(0.36)	0.26(0.28)
	A	0.08(0.02)	0.08(0.04)	0.09(0.09)	0.26(0.20)	0.24(0.37)
	N	0.06(0.03)	0.19(0.12)	0.32(0.15)	0.67(0.53)	0.27(0.31)
	Mean	0.07(0.03)	0.11(0.10)	0.13(0.13)	0.45(0.40)	0.26(0.32)
Per	M	0.02(0.01)	0.01(4.00·10 ⁻³)	0.02(0.02)	0.01(0.01)	0.03(0.04)
	A	0.01(3.00·10 ⁻³)	0.02(0.01)	0.01(4.00·10 ⁻³)	7.00·10 ⁻³ (5.00·10 ⁻³)	0.03(0.03)
	N	0.01(4.00·10 ⁻³)	0.04(0.03)	0.03(7.00·10 ⁻³)	0.02(0.02)	0.04(0.04)
	Mean	0.01(0.01)	0.02(0.02)	0.02(0.01)	0.01(0.01)	0.03(0.04)

Note: diurnal periods correspond to morning (M): 04:00–12:00 h, afternoon (A): 12:00–20:00 h and night (N): 20:00–04:00 h UTC.

Table A.1. (continued) Diurnal period (n=7) and weekly (n=21) mean concentrations (ng m⁻³) of individual PAHs during the sampling period. Standard deviation in brackets.

PAH	Period	January-14	February-14	March-14	June-14	Jul. - Jun.
DBaja	M	1.00·10 ⁻³ (3.00·10 ⁻⁴)	2.00·10 ⁻³ (3.00·10 ⁻⁴)	7.00·10 ⁻³ (-)	1.00·10 ⁻³ (1.00·10 ⁻³)	6.00·10 ⁻³ (7.00·10 ⁻³)
	A	1.00·10 ⁻³ (1.00·10 ⁻³)	2.00·10 ⁻³ (3.00·10 ⁻⁴)	2.00·10 ⁻³ (-)	1.00·10 ⁻³ (1.00·10 ⁻³)	5.00·10 ⁻³ (0.01)
	N	5.00·10 ⁻⁴ (5.00·10 ⁻⁴)	4.00·10 ⁻³ (2.00·10 ⁻³)	7.00·10 ⁻³ (5.00·10 ⁻⁴)	2.00·10 ⁻³ (1.00·10 ⁻³)	7.00·10 ⁻³ (0.01)
	Mean	1.00·10 ⁻³ (1.00·10 ⁻³)	3.00·10 ⁻³ (2.00·10 ⁻³)	6.00·10 ⁻³ (3.00·10 ⁻³)	1.00·10 ⁻³ (1.00·10 ⁻³)	0.01(0.01)
BbC	M	-	-	-	-	7.00·10 ⁻³ (5.00·10 ⁻³)
	A	-	-	-	-	0.01(0.01)
	N	-	3.00·10 ⁻³ (1.00·10 ⁻³)	-	-	0.01(0.01)
	Mean	-	3.00·10 ⁻³ (1.00·10 ⁻³)	-	-	0.01(0.01)
Pic	M	-	-	-	-	0.02(0.03)
	A	-	-	-	-	0.03(0.06)
	N	-	0.01(2.00·10 ⁻³)	-	-	0.03(0.04)
	Mean	-	0.01(2.00·10 ⁻³)	-	-	0.03(0.04)
Anthran	M	-	4.00·10 ⁻³ (2.00·10 ⁻⁵)	-	-	0.03(0.03)
	A	0.01(6.00·10 ⁻³)	9.00·10 ⁻³ (-)	-	-	0.02(0.04)
	N	-	0.02(0.01)	-	-	0.05(0.07)
	Mean	0.01(6.00·10 ⁻³)	0.01(0.01)	-	-	0.03(0.05)
Cor	M	0.03(0.02)	0.02(0.01)	-	-	0.09(0.09)
	A	0.03(0.04)	0.02(0.01)	-	-	0.10(0.13)
	N	0.03(0.02)	0.05(0.04)	-	-	0.11(0.13)
	Mean	0.03(0.03)	0.03(0.03)	-	-	0.10(0.12)

Note: diurnal periods correspond to morning (M): 04:00–12:00 h, afternoon (A): 12:00–20:00 h and night (N): 20:00–04:00 h UTC.

Appendix B

List of Publications

- 1. Diurnal variation of particle-bound PAHs in an urban area of Spain using TD-GC/MS: influence of meteorological parameters and emission sources.**
I. Elorduy, S. Elcoroaristizabal, N. Durana, J.A. García, L. Alonso. *Atmospheric Environment* 2016; 138: 87-98.

List of Contributions to Conferences

- 1. Diurnal variability of particle-bound PAHs in an urban area of Spain using TD-GC/MS.**
S. Elcoroaristizabal, I. Elorduy, N. Durana, J.A. García, L. Alonso. 39th International Symposium on Environmental Analytical Chemistry. Hamburg, Germany. July 2016. Contribution: Poster.
- 2. Analysis of PAHs in airborne particles by thermal desorption-GC/MS in an urban area.**
I. Elorduy, N. Durana, S. Elcoroaristizabal, J.A. García, M. Navazo, M.C. Gómez, J. Iza, L. Alonso. 38th International Symposium on Environmental Analytical Chemistry. Lausanne, Switzerland. June 2014. Contribution: Poster.
- 3. Chemometric determination of PAHs in aerosol samples.**
S. Elcoroaristizabal, J.A. García, N. Durana, L. Alonso, J.L. Ilardia, I. Elorduy, J. Iza. Conferentia Chemometrica. Sopron, Hungary. September 2013. Contribution: Poster.
- 4. Development of thermal desorption and fluorescence techniques for measuring ambient air PAHs.**
I. Elorduy, S. Elcoroaristizabal, N. Durana, J.A. García, L. Alonso. GRACCIE Workshop. Santander, Spain. December 2012. Contribution: Oral presentation.
- 5. Development and application of two sensitive methods for determination of PAH in urban areas.**
S. Elcoroaristizabal, N. Durana, J.A. García, L. Alonso, J.L. Ilardia, I. Elorduy, J. Iza. Urban Environmental Pollution (UEP). Amsterdam, the Netherlands. June 2012. Contribution: Poster.

Paper:

**Diurnal variation of particle-bound PAHs in
an urban area of Spain using TD-GC/MS:
influence of meteorological parameters and
emission sources**

Iñaki Elorduy, Saioa Elcoroaristizabal, Nieves Durana
Jose Antonio García, Lucio Alonso

Atmospheric Environment 138 (2016) 87- 98



Contents lists available at ScienceDirect

Atmospheric Environment

journal homepage: www.elsevier.com/locate/atmosenv

Diurnal variation of particle-bound PAHs in an urban area of Spain using TD-GC/MS: Influence of meteorological parameters and emission sources



I. Elorduy*, S. Elcoroaristizabal, N. Durana, J.A. García, L. Alonso

Chemical and Environmental Engineering Department, School of Engineering, University of the Basque Country, Alameda de Urquijo s/n, E-48013, Bilbao, Spain

HIGHLIGHTS

- Short-term data analysis of 13 PM₁₀-bound PAHs pointed out different diurnal patterns.
- BbFt, Pyr, Ft and Chry were the major contributors to total PAHs in PM₁₀.
- Traffic and industrial sources influenced PAHs diurnal variability.
- The most influential meteorological factors were temperature, wind speed and pressure.
- Ozone was one of the main controlling factors except during the night time.

ARTICLE INFO

Article history:

Received 23 March 2016
 Received in revised form
 6 May 2016
 Accepted 8 May 2016
 Available online 10 May 2016

Keywords:

Diurnal PAHs
 TD-CG/MS
 Emission sources
 Meteorological parameters
 Binary diagnostic ratios
 Principal component analysis

ABSTRACT

Short-term particulate concentrations of 13 polycyclic aromatic hydrocarbons (PAHs) in PM₁₀ were determined in the urban area of Bilbao (Spain). The analysis was performed by thermal desorption coupled with gas chromatography-mass spectrometry (TD-GC/MS), which enabled to use three diurnal periods of 8 h sampling basis time resolution. A total of 105 PM₁₀ samples were collected during 5 months in 2013.

Diurnal average concentration of total PAHs (Σ 13 PAHs) ranged from 1.18 to 9.78 ng m⁻³; and from 0.06 to 0.70 ng m⁻³ for benzo[a]pyrene. The presence of high concentrations of benzo[b]fluoranthene, pyrene, fluoranthene and chrysene, and the significant PAHs diurnal variations due to the sampling period, pointed out the influence of mixing anthropogenic sources and meteorological conditions.

The diurnal pattern of source contributions was assessed by binary diagnostic ratios and principal component analysis (PCA). These results showed the prevalence of pyrogenic sources coming from traffic and coal/coke combustion sources. Moreover, the PCA differentiated a diurnal pattern of source contributions. The influence of meteorological factors was studied by Pearson correlation analysis and multiple linear regression. Three factors, temperature, wind speed and atmospheric pressure, were identified as the most significant ones affecting diurnal PAHs concentrations. Finally, PCA of the PAHs levels, regulated atmospheric pollutants and meteorological parameters showed that diurnal PAHs concentrations were mainly influenced by variations in the emission sources, atmospheric oxidants such as ozone, and temperature conditions. These results provide further insight into the PAHs diurnal patterns in urban areas by using higher temporal resolutions.

© 2016 Elsevier Ltd. All rights reserved.

1. Introduction

Polycyclic aromatic hydrocarbons (PAHs) are a group of

ubiquitous organic pollutants generated as by-products of incomplete combustion processes of organic matter (Finlayson-Pitts and Pitts, 2000), and primarily emitted from anthropogenic sources (Ravindra et al., 2008). In ambient air, PAHs have received increased attention in recent years because their widespread occurrence poses an environmental and health concern due to their persistence: 4 PAHs are included in the Convention on Long-Range

* Corresponding author.

E-mail address: inaki.elorduy@ehu.es (I. Elorduy).

Transboundary Air Pollution Protocol on Persistent Organic Pollutants (UNECE, 1979; Council of the European Union, 2004); and toxicity: some PAHs have been identified as human carcinogens with also well-known mutagenic properties (IARC, 1983). Due to these features, several international agencies have listed them as priority pollutants. The United States Environmental Protection Agency (US-EPA) includes 16 PAHs (16 EPA-PAHs) (OFR, 1982), whereas the European Union Directive 2004/107/EC11 (EUD, 2005) on ambient air quality sets a target value for benzo[a]pyrene of 1 ng m^{-3} in the PM_{10} fraction (annual average), taken as indicator for total particulate carcinogenic PAHs.

In urban areas, the assessment of ambient air polycyclic aromatic hydrocarbons is an important issue because the risk associated with human exposure is higher considering the population density (Sharma et al., 2007; Sogri, 2007). Specifically, in urban and suburban areas, the most toxic PAHs (5 and 6 rings) are linked to the respirable fraction of the particulate matter ($\text{PM}_{2.5}$ = aerodynamic diameter $\leq 2.5 \mu\text{m}$) (Sheu et al., 1997), which can contribute to, or even enhance, their adverse health effects. Accordingly, many urban air pollution studies have been focused on PAHs bound to particulate matter, particularly PM_{10} (aerodynamic diameter $\leq 10 \mu\text{m}$) and $\text{PM}_{2.5}$ (Villar-Vidal et al., 2014; Elcoroaristizabal et al., 2014; Jamhari et al., 2014), in order to assess their concentration, distribution and sources. However, most of the studies rarely achieved temporal resolution measurements higher than 24 h. This time resolution seems not sufficient to comprehend their variability, fate and behavior in the atmosphere (Ringuet et al., 2012a), since the PAH composition of aerosols can vary according to the diurnal changes in the sources, meteorological conditions and atmospheric reactivity (Alam et al., 2014). Hence, short time PAH monitoring studies are more conducive.

At present, some studies have investigated the diurnal variation of particle-bound PAHs, but most of them have been conducted at time resolutions of 12 h (Ringuet et al., 2012a; Liu et al., 2013; Wu et al., 2014), while there are still few studies performed at higher temporal sampling resolutions in urban areas (Guzmán-Torres et al., 2009; Morville et al., 2011; Delhomme and Millet, 2012). This is likely due to the limits of detection of the current analytical procedures used, which limits the temporal resolution of PAHs in ambient air.

The most frequently used approach in standard procedures relies on solvent extraction of the particles absorbed onto the filters and quantification by chromatographic methods, namely gas chromatography-mass spectroscopy (GC-MS) and high-performance liquid chromatography (HPLC-UV/Vis or HPLC-FLD) (Poster et al., 2006). These measurements tend to be laborious, relatively expensive, and time-consuming. As a consequence, a number of solvent-free sample preparation techniques have been developed, among which, thermal desorption-gas chromatography/mass spectrometry (TD-GC/MS) appears as a simple alternative that overcomes the main drawbacks of the solvent extraction approaches (Van Drooge et al., 2009). First, TD-GC/MS does not require sample pretreatment, avoiding matrix extraction, concentration and clean-up steps, which decreases the time, uncertainty and cost of the analysis, and reduces the likelihood of sample contamination and losses. Second, this sensitive technique offers method detection limits lower than those based on conventional extraction methods (Kim and Kim, 2015). Finally, only a small amount of the filter sample is required for detecting individual organic compounds. All of this potentially allows the use of shorter sampling times for monitoring PAH pollution in urban aerosols.

In spite of these facts, scarce TD-GC/MS applications have been published focused on the analysis of particle-bound PAHs. In 2008, Bates et al. (2008) evaluated the technique for measuring airborne

4–6 ring PAHs collected onto quartz filters for a period of 24 h, providing a more readily automated and sensitive alternative. Later, Gil-Moltó et al. (2009) demonstrated the capability of the TD-GC/MS technique to quantify 12 particle-bound PAHs in the PM_{10} and $\text{PM}_{2.5}$ fractions collected with low volume samplers. However, these and other studies do not offer any new advantage from the point of view of the sampling methodology, even though TD/GC-MS enables the analysis of high temporal resolution samples for source apportionment purposes. For instance, Jeon et al. (2001) used 2 h filter samples to study the main source patterns of organic PM components, and Van Drooge et al. (2009) applied this method in short-term monitoring (3 h) in order to identify PAH temporal variations in PM_{10} . Nevertheless, these campaigns were conducted over a relative low number of samples (45 and 56 in total, respectively).

In this work, TD-GC/MS technique has been employed to investigate the diurnal variability of 13 PM_{10} -bound EPA-PAHs in an urban area of Spain (Bilbao city). The TD-GC/MS method was validated by using a Standard Reference Material (SRM 1649b), which demonstrated a good performance (accuracy, precision and recovery efficiency) and sensitivity. This enabled to measure PAHs levels in urban aerosols over 8 h sampling periods. The sampling campaign was conducted during 5 months in 2013, collecting a total of 105 PM_{10} samples in order to assess their diurnal trends under different environmental conditions. Moreover, potential controlling factors (physicochemical and meteorological parameters) and emission sources were studied to provide a deeper insight on the diurnal variability of PAHs in this urban area.

2. Materials and methods

2.1. Sampling site and campaign

The sampling site was located at the School of Engineering (longitude $2^{\circ}56'56.24''\text{W}$, latitude $3^{\circ}15'44.86''\text{N}$) of Bilbao city, northern Spain. The School of Engineering is sited in the city center of Bilbao, which is located along an estuary that runs nearly 16 km from the center of the city to the sea in a SE–NW direction. Bilbao has an oceanic climate with moderate temperatures, relative humidity is quite constant throughout the year, and rainfall is significant and frequent especially in spring and autumn. Moreover, this city is strongly influenced by land-sea breeze cycles during the day, channelized along the *Nervión* and *Kadagua* valleys.

Bilbao city is the most populated area in the Basque Country and the tenth largest in Spain (approximately 350,000 in the city and 1 million inhabitants in the metropolitan area). In this urban area, local traffic and stationary emissions from the surrounding industries are considered as the major sources of atmospheric pollutants. Further, the sampling site is highly affected by vehicle traffic due to the proximity of the A-8 highway (average daily volume of approximately 100,000 vehicles in 2013) and the city's main bus station (Fig. 1).

The sampling campaign was conducted over 5 months: July 2013 and from September to December 2013. PM_{10} samples were collected every 8 h for seven consecutive days each month as follows: 04:00–12:00 h; 12:00–20:00 h, and 20:00–04:00 h UTC (21 contiguous samples from Monday to Sunday). These time intervals were chosen to study the influence of emission sources such as rush traffic hours on temporal variations of particle-bound PAHs concentrations. Moreover, the sampling campaign was carried out in summer (July), autumn (September, October, November) and winter (December), aiming at investigating their diurnal variation patterns under different meteorological conditions.

A total of 105 PM_{10} samples were collected during the campaign using a high volume sampler (Digitel DHA-80, Digitel Elektronik



Fig. 1. Geographical location of the sampling site in Bilbao city (Spain), and meteorological (*Feria*) and air pollution (*Mazarredo*) sampling stations (sources: Google Earth and GeoEuskadi).

AG, Switzerland) operating at a flow rate of $30 \text{ m}^3 \text{ h}^{-1}$. Previously to sampling, quartz fiber filters (150 mm diameter, Whatman International Ltd., United Kingdom) used as collection substrates, were heated at $500 \text{ }^\circ\text{C}$ for 24 h. After sampling, the filters were put into individual Petri dishes, wrapped in aluminum foil (pre-cleaned with *n*-hexane) to avoid photodegradation, and kept in a $4 \text{ }^\circ\text{C}$ freezer until analysis (<15 days) according to ISO 12884:2000 (ISO, 2000).

2.2. Meteorological conditions and air regulated pollutants concentrations

Meteorological and air regulated pollutants data used in this work were obtained from the weather network (*Feria* station, Basque Weather Service) and the Bilbao air pollution network (*Mazarredo* station, Basque Country Environment and Planning Department), respectively. These stations are located less than 500 m (*Feria*) and approximately 1.5 km (*Mazarredo*) from the sampling point (Fig. 1).

Table A.1 (appendix A: supplementary information) summarizes the meteorological conditions and air regulated pollutant concentrations prevailing during the sampling campaign.

2.3. PAHs analysis: thermal desorption-chromatographic conditions

Filter samples were randomly cut into 8 portions of 1 cm^2 and introduced into stainless-steel tubes (90 mm length \times 6 mm O.D. \times 5 mm I.D., Perkin Elmer S.L., Spain). This was performed in the same way as other studies (Ringuet et al., 2012b; Grandesso et al., 2013), which demonstrated good homogeneity results when using small sections of the filters. Then, PAHs analysis was

carried out using an automatic thermal desorber unit (Turbomatrix 150 ATD, Perkin Elmer S.L., Spain) coupled by a fused silica capillary transfer line (0.32 mm I.D.) to a GC/MS detector (Agilent 5973, Agilent Technologies S.L., Spain). The chromatographic separation of PAHs was conducted on a Meta.X5 (silphenylene phase) capillary column: 30 m length \times 0.25 mm I.D. \times 0.25 μm film thickness (Teknokroma, Spain).

Thermal desorption was performed under the following conditions: dry-purge for 1 min at room temperature, sampling tube desorption at $320 \text{ }^\circ\text{C}$ for 10 min using helium carrier gas at 150 mL min^{-1} , trapping at $-10 \text{ }^\circ\text{C}$, and finally trap desorption at $325 \text{ }^\circ\text{C}$ for 6 min. The helium gas carrier pressure employed in the GC/MS system was 21 psi and the column temperature was programmed as follows: initial temperature $100 \text{ }^\circ\text{C}$ for 3 min, ramp of $10 \text{ }^\circ\text{C min}^{-1}$ until $250 \text{ }^\circ\text{C}$, ramp of $5 \text{ }^\circ\text{C min}^{-1}$ until $320 \text{ }^\circ\text{C}$, and finally temperature held at $320 \text{ }^\circ\text{C}$ for 10 min. The total analysis time was 42 min per sample. The temperature of the both transfer lines (from TD to GC and from GC to MS) was held at $280 \text{ }^\circ\text{C}$, whereas the source temperature was $250 \text{ }^\circ\text{C}$. Simultaneous full scan (SCAN) and selective ion monitoring (SIM) modes were used for the identification and quantification of PAHs.

The PAHs analyzed by this TD-GC/MS system were: fluorene (Fl), phenanthrene (Phe), anthracene (Ant), fluoranthene (Ft), pyrene (Pyr), benzo[*a*]anthracene (BaA), chrysene (Chry), benzo[*b*]fluoranthene (BbFt), benzo[*k*]fluoranthene (BkFt), benzo[*a*]pyrene (BaP), indeno[1,2,3-*cd*]pyrene (IP), dibenzo[*a,h*]anthracene (DBaA), and benzo[*ghi*]perylene (BghiP). Among the 16 EPA-PAHs, naphthalene, acenaphthylene, and acenaphthene were not considered in this study since these compounds are mainly associated to the gas phase, and this may lead to erroneous values due to losses of these volatile analytes collected on filters.

Target PAHs were quantified by internal calibration based on a five-point calibration curve for each individual compound ranged from 2.5 to 50 ng μL^{-1} . PAHs calibration solutions were prepared diluting a certificated mixture containing the 16 EPA-PAHs (2000 $\mu\text{g mL}^{-1}$, SV Calibration Mix 5, Restek Corporation, USA) in methanol. The sample filters were spiked with 1 μL of a mixture of five deuterated internal standards including phenanthrene- d_{10} , pyrene- d_{10} , benzo[*a*]anthracene- d_{12} , benzo[*a*]pyrene- d_{10} , and benzo[*ghi*]perylene- d_{12} . The deuterated PAH internal standard solution was prepared by diluting a certified mixture (200 $\mu\text{g mL}^{-1}$, Perdeuterated Internal Standard—PAH-Mixture 6, Chiron AS, Norway) in methanol to a final concentration of 20 ng μL^{-1} . Methanol of HPLC grade (99.9%) was supplied by Lab-Scan Analytical Sciences (Gliwice, Poland).

2.4. Quality assurance and quality control (QA/QC)

The linearity of the method was determined by loading 2 portions of 1 cm^2 of the filters spiked with 1 μL of both the PAHs calibration solutions (ranging from 2.5 to 50 ng μL^{-1}) and the deuterated PAH internal standard solution (20 ng μL^{-1}). The obtained results showed good linearity values ($R^2 > 0.99$) for most of the compounds. The analytical precision of PAH determination was calculated by performing replicate measurements of blank filters ($n = 10$) spiked with 20 ng of each target PAH and 15 ng of each deuterated PAH, and it was expressed as relative standard deviation (RSD). The majority of results showed RSD values less than 10%.

The instrument detection (IDL) and quantitation limits (IQL) were calculated for each PAH in the lowest calibration standard (2.5 ng μL^{-1}), using a signal-to-noise ratio of 3 and 10, respectively. The IDLs and IQLs ranged from 0.01 ng (Ft, Pyr, BaA and BbFt) to 0.11 ng (DBahA), and from 0.02 ng (Ft and BaA) to 0.38 ng (DBahA), respectively. These values are similar to those reported by other authors (Gil-Moltó et al., 2009; Wang et al., 2015) measuring particle-bound PAHs by TD-GC/MS. The method detection limit (MDL) was calculated according to the EPA criteria (US-EPA, 2013) using the following equation:

$$\text{MDL} = t_{(n-1, 1-\alpha=0.99)} \cdot \text{SD} \quad (1)$$

where MDL is the method detection limit; $t_{(n-1, 1-\alpha=0.99)}$ is the student's *t*-value appropriate for a 99% confidence level and a standard deviation estimate with $n-1$ degrees of freedom; n is the number of replicates and SD is the standard deviation of the replicate analyses.

The method detection limit was determined by replicate measurements ($n = 10$) of blank filters spiked with the lowest level of the PAHs calibration solution (2.5 ng μL^{-1}), and considering a sample volume of 240 m^3 (8 h sampling at 30 $\text{m}^3 \text{h}^{-1}$). The method detection limit values ranged from $8.04 \cdot 10^{-4}$ to $6.97 \cdot 10^{-3}$ ng m^{-3} . Detailed results are reported in Table A.2 (appendix A: supplementary information).

Laboratory method blanks were analyzed in each batch in order to evaluate possible contaminations. Target analytes levels were less than 10% of the concentrations in the samples for each batch.

2.5. TD-GC/MS validation

The performance of the method when applied to atmospheric PM samples was determined using and Standard Reference Material (SRM) 1649b urban dust, obtained from the National Institute of Standards and Technology (NIST, Gaithersburg, MD, USA). The accuracy, repeatability and recovery of the method were calculated by adding known amounts (10.4 ± 0.1 mg) of the SRM 1649b to a one-eighth section of blank filters ($n = 10$), which were rolled and put

into the desorption tubes. Silanized glass wool (Supelco Inc., Bellefonte, USA) was introduced at the end, and at the head of the desorption tubes in order to prevent system contamination. Prior to use, glass wool plugs and filters were heated at 350 °C for 24 h to remove trace organic compounds. Before the analysis, filters were spiked with 1 μL of the deuterated PAH internal standard solution (20 ng μL^{-1}).

Table A.3 (appendix A: supplementary information) lists the results of the comparison between the calculated concentrations and the certificate values obtained for each PAH. The TD-GC/MS method had a good precision with RSD values of $11.62 \pm 4.27\%$ on average. The accuracy of the TD-GC/MS method ranged from -19% to 25%, while the average recovery efficiency was $96 \pm 13\%$. These performance parameters of the TD-GC/MS method accomplish the quality objectives for ambient air PAHs stated by the ISO 12884:2000 (ISO, 2000).

2.6. Data analysis

Statistically significant differences between the results were evaluated on the analysis of variance method (ANOVA, 95% confidence intervals test). Pearson correlation analysis was applied for checking potential relations between PAH concentrations and meteorological parameters and air regulated pollutants concentrations. These univariate statistics methods were performed using SPSS statistical software version 17.0 (SPSS, Inc., Chicago, IL, USA).

Multivariate analysis including Principal Component Analysis (PCA) and Multiple Linear Regression analysis (MLR) were applied using the PLS toolbox 7.82 (Eigenvector Research, Inc., USA) under Matlab version R2010 (The MathWorks, MA, USA). PCA and MLR were performed on autoscaled data, meaning that all variables were mean centered and scaled to unit variance. Additionally, Kaiser Meyer Olkin (KMO) tests were performed in order to ensure the suitability of the samples for PCA, showing values close to 1, which reflected the suitability of the different datasets to be used in PCA.

3. Results and discussion

3.1. Diurnal ambient concentrations of particle-bound PAHs in PM_{10}

The average diurnal period and monthly concentrations of individual and total PAHs ($\sum 13$ PAHs), as well as the contribution of PAH-ring groups to the PM_{10} fraction for each month ($n = 5$) of the sampling campaign, are shown in Table 1.

Over the sampling campaign, the diurnal period average concentration of individual PAHs ranged from 0.01 ± 0.01 to 2.75 ± 1.89 ng m^{-3} , whereas for total PAHs ($\sum 13$ PAHs) was between 1.18 ± 0.27 and 9.78 ± 5.35 ng m^{-3} . These results show a great variability in the PAHs concentrations, especially for the high molecular weight PAHs (5–6 rings) (RSD: 71.4–165.4%; median: 108.1% for the whole sampling period). Moreover, a different pattern was observed during the sampling campaign according to the diurnal sampling periods. Thus, in July, September and October most of the PAHs had their highest individual concentrations during the morning periods, ranging from 0.03 ± 0.01 to 0.77 ± 0.74 ng m^{-3} . In contrast, in November and December, the highest individual PAH levels occurred in the afternoon hours ranging from 0.06 ± 0.09 to 2.75 ± 1.89 ng m^{-3} . These results highlight a great range in the diurnal atmospheric PAH levels, showing a significant diurnal variation ($p < 0.05$) in October.

Specifically, the diurnal average BaP concentration ranged from 0.06 ± 0.03 ng m^{-3} (July, summer period) to 0.70 ± 0.28 ng m^{-3} (December, winter period); 0.21 ± 0.24 ng m^{-3} on average. This PAH presented higher concentration levels in the morning or

Table 1

Diurnal period (n = 7) and monthly (n = 21) average concentrations (ng m⁻³) of individual, total PAHs (Σ 13 PAHs) and contribution (in %) of PAH-ring groups to the PM₁₀ fraction during the sampling period. Standard deviation in brackets.

PAH	Period	July	September	October	November	December	Jul.–Dec.
Fl	M	0.09 (0.07)	0.14 (0.07)	0.05 (0.02)	0.05 (0.02)	0.13 (0.07)	0.09 (0.06)
	A	0.07 (0.04)	0.08 (0.04)	0.04 (0.01)	0.11 (0.08)	0.12 (0.08)	0.08 (0.06)
	N	0.12 (0.12)	0.09 (0.02)	0.04 (0.02)	0.09 (0.08)	0.11 (0.05)	0.09 (0.07)
	Mean	0.10 (0.08)	0.10 (0.05)	0.04 (0.01)	0.08 (0.07)	0.12 (0.07)	0.09 (0.06)
Phe	M	0.21 (0.07)	0.20 (0.06)	0.27 (0.11)	0.15 (0.04)	0.39 (0.17)	0.25 (0.13)
	A	0.14 (0.04)	0.14 (0.04)	0.21 (0.04)	0.27 (0.17)	0.44 (0.24)	0.24 (0.17)
	N	0.16 (0.05)	0.14 (0.04)	0.17 (0.07)	0.14 (0.13)	0.33 (0.06)	0.19 (0.10)
	Mean	0.17 (0.06)	0.16 (0.05)	0.22 (0.09)	0.19 (0.14)	0.39 (0.17)	0.22 (0.14)
Ant	M	0.03 (0.01)	0.04 (0.01)	0.06 (0.02)	0.06 (0.04)	0.08 (0.04)	0.05 (0.03)
	A	0.02 (0.01)	0.03 (0.01)	0.05 (0.02)	0.13 (0.10)	0.09 (0.05)	0.06 (0.06)
	N	0.02 (0.01)	0.03 (0.01)	0.04 (0.01)	0.07 (0.10)	0.10 (0.03)	0.05 (0.05)
	Mean	0.03 (0.01)	0.03 (0.01)	0.05 (0.02)	0.09 (0.09)	0.09 (0.04)	0.06 (0.05)
Ft	M	0.22 (0.09)	0.21 (0.08)	0.33 (0.14)	0.28 (0.13)	0.70 (0.30)	0.35 (0.24)
	A	0.15 (0.07)	0.19 (0.06)	0.34 (0.10)	0.43 (0.22)	0.94 (0.39)	0.40 (0.34)
	N	0.13 (0.04)	0.16 (0.07)	0.20 (0.07)	0.17 (0.15)	0.61 (0.13)	0.25 (0.20)
	Mean	0.17 (0.08)	0.19 (0.07)	0.29 (0.12)	0.30 (0.19)	0.74 (0.31)	0.34 (0.27)
Pyr	M	0.23 (0.09)	0.24 (0.09)	0.38 (0.16)	0.29 (0.15)	0.72 (0.27)	0.37 (0.24)
	A	0.14 (0.06)	0.21 (0.08)	0.39 (0.10)	0.43 (0.17)	0.97 (0.40)	0.42 (0.34)
	N	0.13 (0.04)	0.18 (0.08)	0.20 (0.67)	0.15 (0.13)	0.59 (0.12)	0.24 (0.19)
	Mean	0.17 (0.08)	0.21 (0.08)	0.32 (0.14)	0.29 (0.18)	0.76 (0.31)	0.35 (0.27)
BaA	M	0.08 (0.04)	0.13 (0.06)	0.32 (0.21)	0.08 (0.06)	0.47 (0.22)	0.22 (0.21)
	A	0.04 (0.01)	0.06 (0.02)	0.13 (0.03)	0.21 (0.15)	0.78 (0.45)	0.24 (0.33)
	N	0.06 (0.03)	0.12 (0.15)	0.14 (0.06)	0.07 (0.08)	0.69 (0.21)	0.21 (0.26)
	Mean	0.06 (0.04)	0.10 (0.10)	0.20 (0.15)	0.12 (0.12)	0.64 (0.32)	0.22 (0.27)
Chry	M	0.18 (0.10)	0.19 (0.11)	0.45 (0.32)	0.17 (0.07)	0.53 (0.19)	0.31 (0.23)
	A	0.11 (0.30)	0.10 (0.04)	0.15 (0.08)	0.34 (0.24)	0.82 (0.40)	0.29 (0.33)
	N	0.12 (0.04)	0.24 (0.31)	0.21 (0.08)	0.14 (0.09)	0.75 (0.22)	0.28 (0.28)
	Mean	0.14 (0.07)	0.18 (0.19)	0.27 (0.23)	0.22 (0.17)	0.69 (0.29)	0.30 (0.28)
BbFt	M	0.23 (0.14)	0.26 (0.11)	0.77 (0.74)	0.24 (0.17)	1.60 (0.49)	0.64 (0.68)
	A	0.12 (0.03)	0.13 (0.05)	0.33 (0.19)	0.78 (0.80)	2.75 (1.89)	0.78 (1.29)
	N	0.20 (0.12)	0.22 (0.21)	0.34 (0.17)	0.29 (0.27)	2.08 (0.87)	0.59 (0.81)
	Mean	0.19 (0.11)	0.20 (0.15)	0.48 (0.48)	0.45 (0.54)	2.12 (1.23)	0.69 (0.95)
BkFt	M	0.12 (0.09)	0.10 (0.03)	0.24 (0.23)	0.10 (0.07)	0.45 (0.12)	0.21 (0.18)
	A	0.08 (0.04)	0.07 (0.02)	0.13 (0.06)	0.49 (0.59)	0.69 (0.40)	0.28 (0.38)
	N	0.13 (0.08)	0.08 (0.05)	0.12 (0.05)	0.16 (0.15)	0.55 (0.16)	0.20 (0.20)
	Mean	0.11 (0.07)	0.08 (0.04)	0.16 (0.14)	0.26 (0.39)	0.56 (0.26)	0.23 (0.27)
BaP	M	0.10 (0.06)	0.12 (0.04)	0.34 (0.26)	0.09 (0.06)	0.44 (0.20)	0.22 (0.21)
	A	0.06 (0.03)	0.07 (0.02)	0.13 (0.03)	0.16 (0.09)	0.60 (0.35)	0.20 (0.25)
	N	0.09 (0.06)	0.11 (0.07)	0.16 (0.07)	0.08 (0.06)	0.70 (0.28)	0.22 (0.26)
	Mean	0.09 (0.05)	0.10 (0.05)	0.21 (0.17)	0.11 (0.08)	0.57 (0.29)	0.22 (0.24)
DBaH	M	0.04 (0.02)	0.06 (0.02)	0.14 (0.09)	0.01 (0.01)	0.21 (0.17)	0.10 (0.11)
	A	0.04 (0.03)	0.08 (0.07)	0.12 (0.09)	0.06 (0.09)	0.26 (0.20)	0.11 (0.13)
	N	0.05 (0.05)	0.07 (0.04)	0.10 (0.06)	0.02 (0.02)	0.26 (0.12)	0.10 (0.10)
	Mean	0.05 (0.03)	0.07 (0.05)	0.12 (0.08)	0.03 (0.06)	0.24 (0.16)	0.10 (0.11)
IP	M	0.11 (0.05)	0.12 (0.03)	0.30 (0.20)	0.05 (0.05)	0.54 (0.23)	0.23 (0.23)
	A	0.07 (0.02)	0.09 (0.03)	0.14 (0.02)	0.15 (0.17)	0.69 (0.52)	0.22 (0.32)
	N	0.14 (0.11)	0.12 (0.07)	0.17 (0.06)	0.06 (0.07)	0.81 (0.39)	0.25 (0.32)
	Mean	0.11 (0.08)	0.11 (0.05)	0.20 (0.14)	0.09 (0.12)	0.67 (0.38)	0.24 (0.11)
BghiP	M	0.17 (0.06)	0.18 (0.05)	0.32 (0.15)	0.11 (0.08)	0.55 (0.19)	0.28 (0.20)
	A	0.12 (0.03)	0.13 (0.05)	0.20 (0.03)	0.32 (0.36)	0.63 (0.28)	0.27 (0.27)
	N	0.16 (0.07)	0.16 (0.09)	0.20 (0.06)	0.10 (0.05)	0.66 (0.21)	0.25 (0.22)
	Mean	0.15 (0.06)	0.16 (0.07)	0.24 (0.11)	0.18 (0.23)	0.61 (0.22)	0.27 (0.23)
Σ 13 PAHs	M	1.82 (0.74)	1.97 (0.65)	3.97 (2.42)	1.67 (0.97)	6.80 (2.08)	3.18 (2.51)
	A	1.18 (0.27)	1.38 (0.29)	2.38 (0.46)	3.91 (2.94)	9.78 (5.35)	3.61 (4.01)
	N	1.53 (0.58)	1.71 (1.11)	2.08 (0.74)	1.54 (1.20)	8.24 (2.34)	2.91 (2.84)
	Mean	1.53 (0.61)	1.69 (0.77)	2.81 (1.64)	2.44 (2.14)	8.19 (3.53)	3.29 (3.15)
3 rings %	M	19 (5)	18 (4)	11 (4)	17 (6)	9 (2)	15 (6)
	A	20 (2)	18 (5)	13 (1)	15 (5)	7 (2)	15 (6)
	N	20 (8)	17 (6)	12 (1)	20 (8)	7 (1)	15 (8)
	Mean	20 (6)	18 (5)	12 (3)	17 (6)	8 (2)	15 (6)
4 rings %	M	39 (6)	36 (7)	39 (6)	51 (7)	35 (4)	40 (8)
	A	38 (8)	41 (7)	43 (6)	43 (11)	38 (4)	41 (8)
	N	30 (5)	38 (9)	37 (4)	36 (7)	33 (3)	35 (6)
	Mean	36 (7)	39 (7)	40 (6)	43 (10)	35 (4)	39 (8)
5–6 rings %	M	42 (8)	45 (6)	50 (10)	31 (10)	56 (6)	46 (11)
	A	43 (10)	41 (9)	44 (7)	42 (15)	55 (5)	45 (10)
	N	50 (11)	44 (10)	51 (4)	44 (13)	61 (4)	50 (10)
	Mean	46 (10)	43 (8)	48 (8)	40 (13)	57 (5)	47 (11)

Note: diurnal periods correspond to morning (M): 04:00–12:00 h, afternoon (A): 12:00–20:00 h and night (N): 20:00–04:00 h UTC.

afternoon periods (except in December), probably following a traffic emission pattern. These values were always below the target

value established by the European legislation (1 ng m⁻³, annual mean) (EUD, 2005). Moreover, the observed BaP concentrations

were also comparable to those reported previously in similar urban environments in Spain: Zaragoza: $0.089 \pm 0.34 \text{ ng m}^{-3}$ (warm period) and $0.48 \pm 0.48 \text{ ng m}^{-3}$ (cold period) (Callén et al., 2011), and Barcelona: $0.29 \pm 0.34 \text{ ng m}^{-3}$ (annual average) (Reche et al., 2012); and higher than the values measured in less populated and traffic affected cities: Ciudad Real: $0.014 \pm 0.007 \text{ ng m}^{-3}$ (autumn) and $0.035 \pm 0.050 \text{ ng m}^{-3}$ (winter) (Villanueva et al., 2015).

These results also clearly showed that the contribution to the total PAHs of the more volatile compounds measured in this study (i.e. 3 ring PAHs: Fl, Phe and Ant) was significantly low (7 ± 1 – $20 \pm 8\%$), but quite constant during the diurnal sampling periods (15% on average). This is likely due to their predominant presence in the gaseous phase (Kameda et al., 2011), according to which, their concentration in the particulate phase was lower in July and September, when higher temperatures ($9 \text{ }^\circ\text{C}$ higher than the average temperature in December) promote their volatilization. On the contrary, the high molecular weight PAHs (5–6 rings) and middle molecular weight PAHs (4 ring) accounted for the 31 ± 10 – $61 \pm 4\%$ and 30 ± 5 – $51 \pm 7\%$ of the total PAH content, respectively. In this sense, high molecular and middle molecular weight PAHs followed a different diurnal pattern, in which high molecular weight PAHs presented their maximum contributions levels at night, when the contribution of the middle molecular weight PAHs was minimum. This different pattern is probably related to their atmospheric reactivity (Xu et al., 2013), and changes in the sources and meteorological conditions.

Among these PAHs, BbFt was the major contributor to total PAHs in PM_{10} (6–36%; median: 13%), compound that is considered as a typical marker of diesel emissions (Harrison et al., 1996). High contributions of BbFt have been also observed in other urban areas characterized by high traffic density (Hassan and Khoder, 2012; He et al., 2014). Subsequently, the most abundant PAHs were, by descending order, Pyr (6–26%; median: 11%), Ft (6–23%; median: 11%) and Chry (2–24%; median: 9%). Indeed, a high presence of BbFt, Pyr, Ft and Chry in the PM_{10} fraction has been also reported in urban areas affected by vehicular, combustion and stationary emission sources (Aldabe et al., 2012; Callén et al., 2013). This seems to indicate the presence of multiple sources influencing this urban area, and therefore, this will be studied in more detail in section 3.2. Finally, PAHs diurnal variations due to the sampling period were significant ($p < 0.05$), showing overall values around 80% higher in December (winter) than those obtained in July and September (summer) (monthly average concentrations in Table 1). Furthermore, some of the PAHs reached their maximum concentration levels during the night period. This has also been observed in other studies (Zhu et al., 2014; Alam et al., 2015) that suggest that diurnal variations of particle-bound PAHs concentrations can be caused by anthropogenic factors (different emission contributions) as well as meteorological conditions. Therefore, the impact of meteorological conditions on the diurnal PAHs concentrations will be discussed in section 3.3.1, whereas their influence in combination with other air regulated pollutants will be studied in section 3.3.2.

3.2. PAH source assessment

3.2.1. Diagnostic ratios analysis

Diagnostic ratios reported in the literature (Yunker et al., 2002; Varea et al., 2011; Wu et al., 2014) have been extensively used to identify the main emissions sources of PAHs in urban environments (Table A.4, appendix A: supplementary information). In this regard, source identification can be improved using various ratios and performing their relative comparison (Ravindra et al., 2008). Thus, cross plots of several ratios and their cut-off values for various

sources are illustrated according to the months (Fig. 2A and B) and diurnal periods (Fig. 2C and D). The PAH diagnostic ratios calculated include Ant/(Ant + Phe); Ft/(Ft + Pyr); BaA/BaA + Chry and IP/IP + BghiP, whose values are detailed in Table A.5 (appendix A: supplementary information).

As illustrated in Fig. 2, the binary ratios calculated enabled us to discriminate between pyrogenic and petrogenic sources in the urban area. These results (Ant/(Ant + Phe) > 0.1 , Ft/(Ft + Pyr) > 0.4 , IP/(IP + BghiP) and BaA/(BaA + Chry) > 0.2) clearly indicated the predominance of pyrogenic sources (Yunker et al., 2002). Moreover, these cross plots also allowed us to distinguish between different pyrogenic forms that pointed out a mixed contribution from petroleum combustion as well as coal/biomass burning. In particular, the average value of the Ft/(Ft + Pyr) ratio obtained in this study was 0.49 ± 0.03 , which indicated the predominance of vehicular emissions (Varea et al., 2011) over other pyrogenic PAH sources (average Ant/(Ant + Phe) value = 0.19 ± 0.07) (Table A.5). Interestingly, Ft/(Ft + Pyr) values tended to be higher than 0.5 during the afternoon and night periods, which suggests a coal/biomass combustion source (Fig. 2C). In contrast, most of the morning periods were covered in the petroleum combustion area, pointing out the prevalence of vehicle exhaust emissions in that period. This mixed contribution was especially evident during November, which showed a different pattern highlighted by the highest values of the Ant/(Ant + Phe) and Ft/(Ft + Pyr) ratios (Fig. 2A). A different trend was also confirmed by the results obtained for the BaA/(BaA + Chry) (average = 0.38 ± 0.12) and IP/(IP + BghiP) ratios (average = 0.41 ± 0.10), whose values differentiated in a similar way November from the other months (Fig. 2B). Even more, these values also suggested that December was more influenced by coal/biomass combustion sources, not showing a clear differentiation between the different diurnal periods. A possible reason is that the different isomer ratios reflects PAH contributions from different sources. This was corroborated by the one-way ANOVA analysis that revealed significant ($p > 0.05$) differences between all the ratios, but a similarity ($p > 0.05$) between the BaA/(BaA + Chry) and IP/(IP + BghiP) ratios.

Complementary, BaA/BaP, BbFt/BkFt, BaP/BghiP and BghiP/IP ratios were calculated (Table A.5) in order to distinguish between gasoline and diesel exhausts on vehicular emissions. The average values obtained: 1.02 ± 0.51 (BaA/BaP); 2.57 ± 0.95 (BbFt/BkFt); 0.72 ± 0.25 (BaP/BghiP); 1.77 ± 1.57 (BghiP/IP), suggested that the main contribution of traffic emissions could be due to diesel vehicles (Slezakova et al., 2010; Callén et al., 2011; Oliveira et al., 2011; Sisovic et al., 2012). Nevertheless, these diagnostic ratios only indicate potential sources without providing the distribution of PAHs for each source. Thus, a principal component analysis was also carried out in an attempt to identify PAHs profiles according to the different diurnal sampling periods.

3.2.2. Principal component analysis

The PCA for each diurnal period resulted in two Principal Components (PCs) with eigenvalues > 1 , explaining 84.73% (morning), 90.06% (afternoon), and 88.02% (night) of the total variance for the urban site. Fig. 3 shows the loadings (Fig. 3A) and scores plots (Fig. 3B) of principal component 1 (PC1) versus principal component 2 (PC2) for all samples separated by diurnal period.

PC1 was characterized by high loadings of 4–6 rings PAHs, i.e. BaA, Chry, BbFt, BkFt, BaP, IP, DBaA and BghiP, all of which are characteristic of vehicular exhausts (He et al., 2014), and also 3–4 rings PAHs (depending on the diurnal period) such as Ant, Pyr, Ft and Phe, mainly associated with coal combustion profiles (Mastral et al., 1996; Simcik et al., 1999). Thus, this PC1 could be attributed to coal combustion and traffic sources.

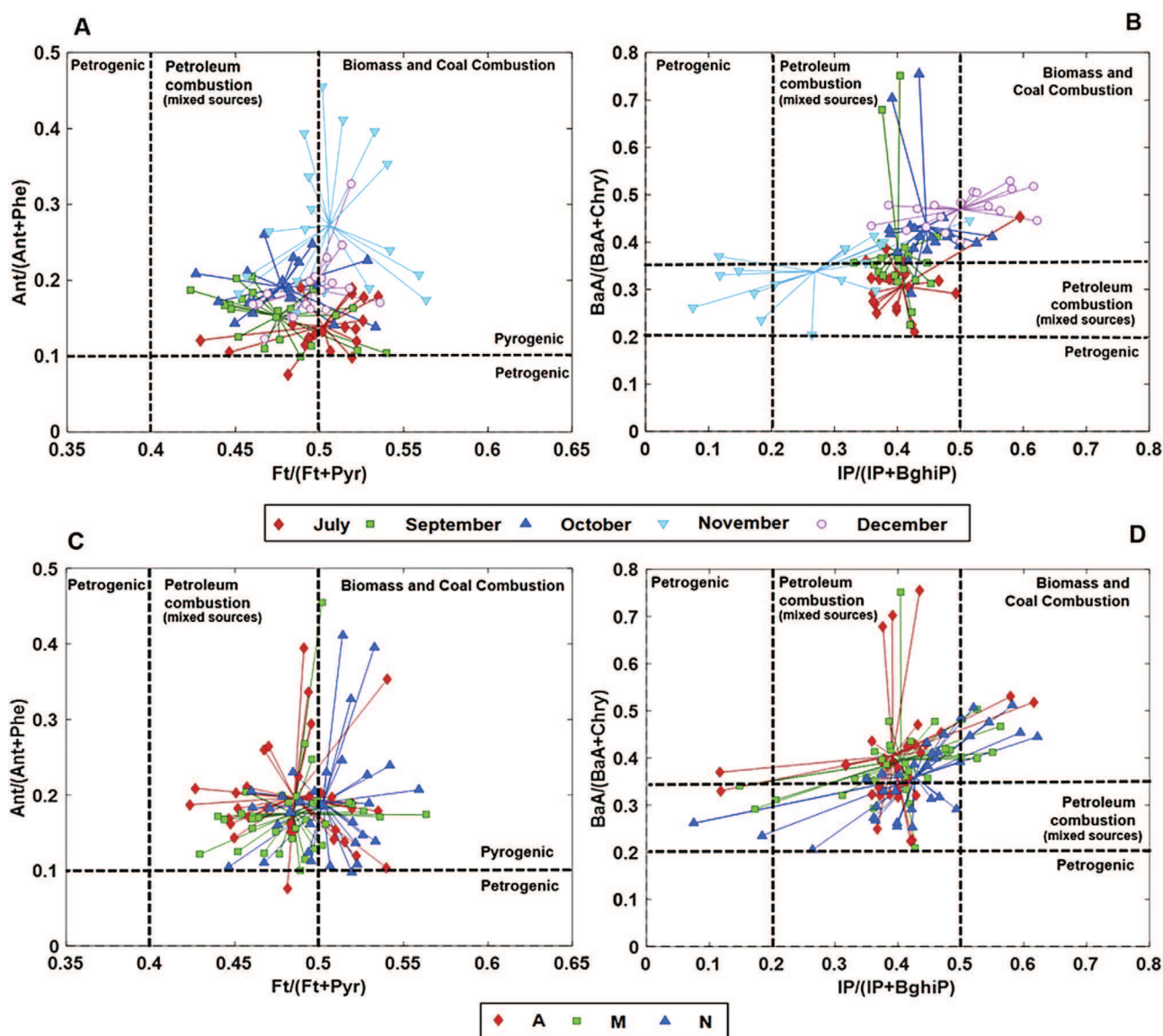


Fig. 2. Cross plots for the ratios $Ft/(Ft + Pyr)$ vs $Ant/(Ant + Phe)$ according to the (A) month and (C) diurnal period, and $IP/(IP + BghiP)$ vs $BaA/(BaA + Chry)$ according to the (B) month and (D) diurnal period.

In contrast, PC2 was strongly related to fluorene (FI), which is usually associated with coke combustion (Khalili et al., 1995; Simcik et al., 1999). Additionally, this PC2 was also moderately loaded on Phe, and depending on the diurnal period, was also loaded on Ant, Ft, Pyr and BkFt (Fig. 3A). Thus, PC2 also seems to be characterized for separating high molecular weight PAHs (5–6 rings) from middle and low molecular weight PAHs (3–4 rings) (Fig. 3). For instance, anthracene, which has been identified in coal combustion and coke production (Guo et al., 2003; Akyüz and Cabuk, 2008.), seemed to be more correlated to coke tracers (FI) during the afternoon, and coal markers during the morning and night time. A different trend during the day was also reflected by other PAHs. In the morning, fluoranthene and pyrene were associated with phenanthrene and anthracene, all of which are predominant in coal combustion profiles (Mastral et al., 1996; Simcik et al., 1999), whereas in the afternoon they were linked to traffic related sources, probably originated from soot collected from diesel engines (Ravindra et al., 2008). In a similar way, benzo[k]fluoranthene seemed to be related to traffic sources in the morning, whereas in the afternoon it was

associated with phenanthrene and coal combustion sources. Interestingly, it was during the night when these compounds tended to change this pattern. All of this indicated that PC2 was predominantly sourced from coke combustion emissions, and in some way, it might also reflect the pattern of some PAHs associated with coal combustion sources. This corroborates the results obtained in the diagnostic ratio analysis, but here, it is further differentiated a diurnal pattern of source contributions.

Additionally, the scores plots also pointed out possible PAHs trends. Even though, traffic related sources were prevalent, December, which was always the most polluted period (these samples have the highest weight in the PC1, Fig. 3), was also highly affected by coal combustion sources. Meanwhile, October mornings and November afternoon and night periods also reflected the influence of coal combustion sources, whereas, July and September did not show this pattern. Further, percentage contributions of these different PAH sources were subsequently quantified by regressing the PC1 and PC2 factors scores (independent variables) against the scores of the total PAH concentrations

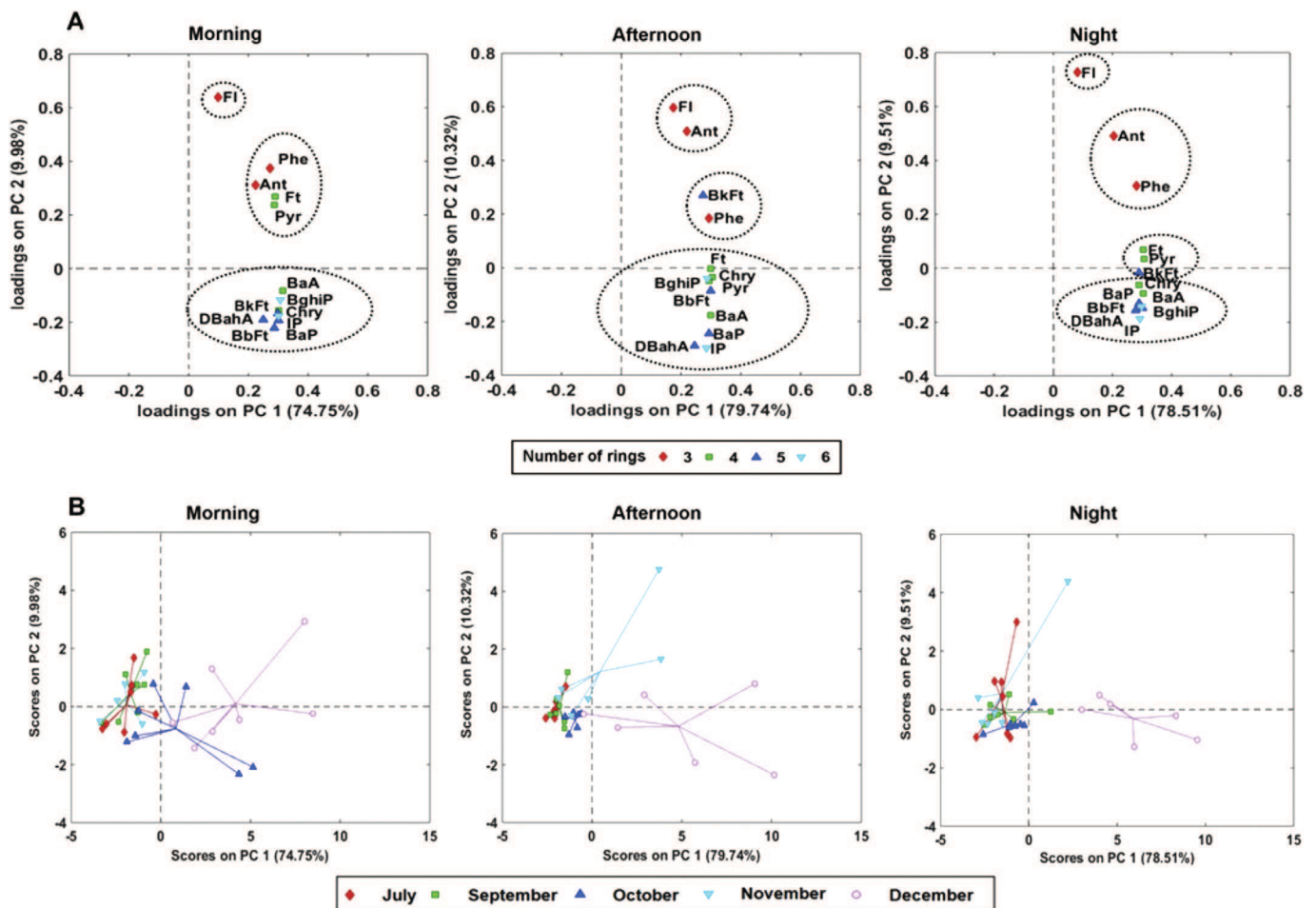


Fig. 3. PCA (A) loadings and (B) scores plots applied to the concentrations of 13 PAHs according to the diurnal sampling period.

(\sum 13 PAHs, dependent variable) in accordance with (Hussain et al., 2015). This resulted in $R^2 = 0.993$, $R^2 = 0.989$, $R^2 = 0.993$ ($p < 0.05$) for the morning, afternoon and night period, respectively. In this sense, mean source contributions were found to be 68.74% (PC1) and 31.26% (PC2) (morning), 65.68% (PC1) and 34.32% (PC2) (afternoon), 78.94% (PC1) and 21.06% (PC2) (night). Thus, the main difference in the source contributions was found to be in the night period, as it has been discussed above.

3.3. Influence parameters

3.3.1. Effect of meteorology

Pearson correlation coefficients between PAHs concentrations and the meteorological variables were calculated in Table A.6 (appendix A: supplementary information), in order to elucidate the most influential meteorological factors depending on the diurnal period. The significant meteorological parameters ($p < 0.05$ – 0.01 , Table A.6) were wind speed, temperature, and atmospheric pressure, whereas solar irradiation had not a significant influence for most of these PAHs. Rainfall and humidity had no clear influence on PAHs variation probably due to the lack of precipitations and the narrow humidity range during the sampling period (see Table A.1). These findings have been also observed in other studies (Barrado et al., 2012; Augusto et al., 2013; Callén et al., 2014).

Then, three factors (wind speed, temperature and atmospheric pressure) were selected to elucidate their influence on the diurnal

atmospheric concentrations of individual PAHs by means of multiple linear regression analysis (Sofuoglu et al., 2004), as follows:

$$C_i = m_1U + m_2T + m_3A + b \quad (2)$$

where C_i is the individual PAH concentration; U is the wind speed (m s^{-1}); T is the temperature ($^{\circ}\text{C}$); A is the atmospheric pressure (mbar); m_1 , m_2 , m_3 and b are the corresponding regression parameters and R^2 is the coefficient of determination for the corresponding sampling interval (M (morning), A (afternoon) and N (night)). These results are summarized in Table 2. These three meteorological parameters together accounted from 12% (Fl, Ant) to 62% (Ft, Pyr) of the variability in the diurnal atmospheric PAH concentrations, similar to other reported values (Liu et al., 2015). Remarkably, this correlation changed from the morning: $31 \pm 10\%$, and afternoon: $36 \pm 12\%$, to the night $48 \pm 14\%$ (average \pm standard deviation), when the maximum values were reached.

Significant ($p < 0.05$ – 0.01) high regression coefficients (m_2) of atmospheric temperature indicated that this was the most important factor affecting the accumulation and dilution of PAHs in PM_{10} at this urban site along the day, and particularly, during the night and morning periods. At night, lower temperatures generally result in temperature inversion under lower solar irradiation (Wu et al., 2014), whereas in the morning, higher temperatures increase their atmospheric degradation pathways as well as their participation in the gas phase (He et al., 2014). Furthermore, significant ($p < 0.05$ – 0.01) positive correlations and moderate regression

Table 2

Regression parameters for multiple linear regression analysis according to the diurnal period (n = 35 samples per diurnal period).

PAHs	Period	m ₁ (U)	m ₂ (T)	m ₃ (A)	R ²
Fl	M	-0.34	0.20	0.42	0.24
	A	-0.02	-0.04	0.34	0.13
	N	-0.13	0.21	0.33	0.12
Phe	M	-0.30	-0.28	0.15	0.17
	A	-0.32	-0.25	0.26	0.36
	N	-0.42	-0.45	0.27	0.41
Ant	M	0.09	-0.26	0.10	0.12
	A	0.01	-0.46	0.07	0.23
	N	-0.30	-0.32	0.39	0.34
Ft	M	-0.25	-0.49	0.26	0.41
	A	-0.41	-0.27	0.35	0.54
	N	-0.35	-0.62	0.33	0.62
Pyr	M	-0.25	-0.50	0.26	0.42
	A	-0.45	-0.27	0.36	0.59
	N	-0.37	-0.61	0.33	0.62
BaA	M	-0.20	-0.59	0.02	0.34
	A	-0.34	-0.29	0.28	0.43
	N	-0.24	-0.65	0.27	0.58
Chry	M	-0.15	-0.49	-0.02	0.22
	A	-0.24	-0.41	0.24	0.45
	N	-0.23	-0.54	0.27	0.44
BbFt	M	-0.21	-0.63	0.09	0.43
	A	-0.30	-0.26	0.30	0.38
	N	-0.21	-0.67	0.23	0.58
BkFt	M	-0.21	-0.58	0.06	0.36
	A	-0.10	-0.48	0.07	0.32
	N	-0.23	-0.63	0.23	0.53
BaP	M	-0.15	-0.57	-0.07	0.28
	A	-0.32	-0.28	0.24	0.38
	N	-0.19	-0.67	0.18	0.54
IP	M	-0.17	-0.63	-0.01	0.38
	A	-0.32	-0.26	0.14	0.30
	N	-0.20	-0.65	0.15	0.49
DBaA	M	-0.08	-0.47	0.05	0.23
	A	-0.41	-0.14	0.04	0.26
	N	-0.24	-0.65	0.05	0.43
BghiP	M	-0.19	-0.64	0.00	0.38
	A	-0.22	-0.47	0.02	0.39
	N	-0.25	-0.65	0.18	0.52

Note: diurnal periods correspond to morning (M): 04:00–12:00 h, afternoon (A): 12:00–20:00 h and night (N): 20:00–04:00 h UTC.

coefficients (m₃) were found between the atmospheric pressure and ambient particle-bound PAHs concentrations during the night and afternoon periods. This is related to the increase in the air atmospheric pressure which enhances the bound of these compounds to the particulate phase. In particular, it is interesting to note that the highest particle PAHs concentrations found in December were measured under a “blocking anticyclonic episode”, when higher atmospheric pressures due to lower temperatures and inversion phenomena resulted in a lower dispersion of these pollutants. In contrast, wind speed had an important role ($p < 0.05$ – 0.01) in atmospheric dispersion and dilution of PAHs, especially during the afternoon period (m₁). This was associated with the sea breeze cycles along the Bilbao estuary. During the summer (July and September), these intra-daily cycles generate a strong NW wind (from sea to land) which enhances the dispersion of pollutants, reaching its maximum value in the afternoon and disappearing during the night. This local dispersion mechanism changes in autumn, during which the wind is more persistent showing little diurnal variations (Millán et al., 1987; Acero et al., 2013).

3.3.2. Regulated atmospheric pollutants and meteorology

Here, a PCA including the individual PAHs, atmospheric pollutants and meteorological parameters (27 variables) was carried out,

aiming at better understanding the PAHs diurnal pattern. This PCA resulted in five PCs with eigenvalues >1 for all the diurnal periods, explaining 82.78% (morning), 86.90% (afternoon), and 85.05% (night) of the total variance. These results are illustrated in Fig. 4, which shows the loadings and scores plots of PC1 versus PC2 for all samples according to the month and separated by diurnal period: morning (Fig. 4A), afternoon (Fig. 4B), and night (Fig. 4C). Additionally, Pearson correlation coefficients between total PAHs concentrations ($\sum 13$ PAHs) and the air regulated pollutants concentrations were calculated in Table 3 in order to complement these results.

PC1 (Fig. 4) was dominated for all sampling periods by high

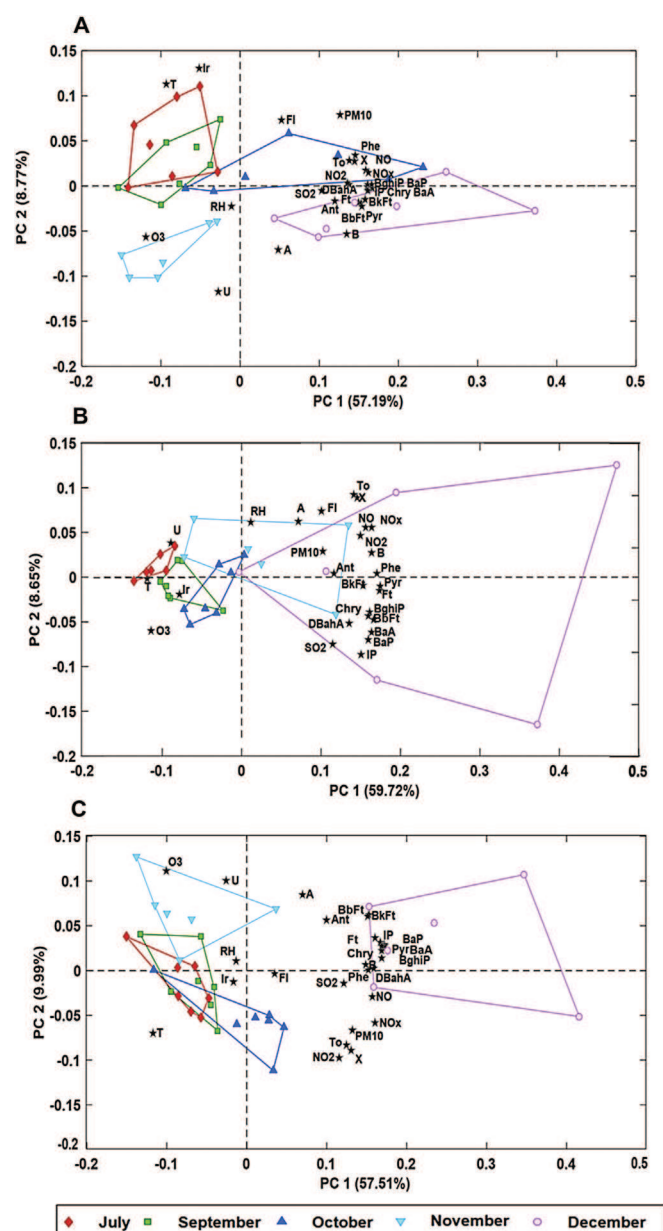


Fig. 4. Scores and loadings biplots according to the diurnal period: (A) Morning, (B) Afternoon and (C) Night. Acronyms: wind speed (U), temperature (T), atmospheric pressure (A), solar irradiation (Ir), relative humidity (RH), benzene (B), o-xylene (X), toluene (To), fluorene (Fl), phenanthrene (Phe), anthracene (Ant), fluoranthene (Ft), pyrene (Pyr), benzo[a]anthracene (BaA), chrysene (Chry), benzo[b]fluoranthene (BbFt), benzo[k]fluoranthene (BkFt), benzo[a]pyrene (BaP), indeno[1,2,3-cd]pyrene (IP), dibenzo[a,h]anthracene (DBaA), and benzo[ghi]perylene (BghiP).

loading values of temperature, PAHs and air regulated pollutants concentrations. Specifically, PC1 is positively loaded on PAHs and other atmospheric pollutants (except ozone), which may evidence that these pollutants were coming from common emission sources. As an exception, fluorene is mainly described by PC3 in the morning and night periods, highlighting a different apportionment from coke combustion emissions (section 3.2.2).

Nitrogen oxides concentration (used as traffic markers) and particulate PAHs showed a significant positive correlation during the daytime period, higher during the morning and decreasing until the night time (Table 3). This trend is likely related to a traffic emission pattern influenced by local atmospheric mechanisms (breezes), and evidenced by the negative significant loading of wind speed in PC1 during the afternoon period. Among the nitrogen oxides, Fig. 4 shows a daytime correlation predominance with NO, which is directly emitted from vehicles. Meanwhile, NO₂ especially in the night periods (Fig. 4C) seemed to be highly contributed from the photochemical conversion of NO to NO₂, which was reflected by the negative correlation of NO₂ with O₃ (Pearson correlation coefficients = −0.54 (morning), −0.64 (afternoon) and −0.74 (night)). In urban environments, sulfur dioxide (SO₂) is generally emitted from domestic central heating and from industrial plants (coal combustion) (Tham et al., 2008), whereas volatile organic compounds, specifically benzene (B), toluene (To) and o-xylene (X), are used as markers of vehicle exhaust pollution (Chang et al., 2009). Fig. 4.A and B shows that toluene and o-xylene compounds were strongly correlated with PAHs concentrations during the rush traffic hours (morning and afternoon periods). In contrast, SO₂ and benzene showed higher correlations during the afternoon and night periods (Table 3), likely due to the influence of industrial plants of the surroundings (Uria-Tellaetxe et al., 2016).

On the other hand, PC1 was negatively loaded on temperature and ozone. This is in agreement with the previous results (section 3.3.1), which demonstrated that there was a strong dependence of particle-bound PAHs concentrations on atmospheric temperature. In the same way, ozone concentration was one of the main controlling factors of PAHs pollution levels, except during the night time (minimum correlation values in Table 3), due to the absence of photochemical oxidation reactions induced by solar irradiation. Ozone concentrations reached its highest levels during the afternoon (Table A.1), as a consequence of photochemical reactions through the photolysis of NO₂, favored by temperature and solar irradiation (Agudelo-Castaneda et al., 2014). These daily maximum values measured in the afternoon hours also suggested that the source of primary pollutants was located close to the monitoring site (Kovač-Andrić et al., 2013).

The second factor (PC2), was dominated by wind speed (U) and solar irradiation (Ir) in the morning period, and atmospheric pressure (A) during the morning and night periods. The negative relation of PAH levels with wind speed suggested again the predominance of local sources. During the sampling period, the prevailing winds (Table A.1) were: NW (23.9%) and ESE (23.5%) for the morning; NW (21.9%) and WNW (40.6%) for the afternoon; and ESE (39.4%) and WNW (15.2%) for the night time. Higher PAHs

concentrations stood out to the ESE direction, due to mountain/valley breezes, which especially occurred in stable atmosphere situations during the night and morning hours. The ESE direction, which corresponds to the upstream valleys, pointed out again the influence of local industries located in the area, which can contribute to higher PAHs levels. In contrast, solar irradiation particularly during the morning, could be related to higher rates of ozone formation, which favors the degradation processes of PAHs in the atmosphere. The effect of atmospheric pressure has been already discussed in section 3.3.1.

The rest of PCs, which accounted for less than the 20% of the variance, mainly corresponded to humidity conditions; irradiance and atmospheric pressure during the afternoon periods, and wind speed during the night period. The influence of the relative humidity was related to the washout effect of rain that contributed to reduce PAHs levels in the atmosphere especially in November. Moreover, these PCA results (Fig. 4) clarified that the reaction with O₃, favored by temperature and solar irradiation, seemed to be the most important atmospheric photo-degradation process responsible of the lowest concentrations observed in July and September (summer period). Regarding November, October and December, local dispersion mechanisms as well as source apportionment variations played a key role in diurnal PAH concentrations.

4. Conclusions

In this study, TD-GC/MS was employed to investigate the diurnal variability of 13 PM₁₀-bound EPA-PAHs in one of the most populated urban areas of Spain (Bilbao city). The good performance of this method allowed us to use short-term sampling times (8 h diurnal periods corresponding to morning, afternoon and night time) for elucidating the potential controlling factors of diurnal PAHs levels.

Short-term data analysis pointed out different diurnal patterns, where the highest PAHs levels were found in the morning (July, September and October) and afternoon periods (November and December). BbFt, Pyr, Ft and Chry were the major contributors to total PAHs in PM₁₀, which suggested the presence of multiple sources such as traffic and industrial activities influencing this urban area. PAHs diurnal variations due to the sampling period were significant and highlighted the effect of meteorological conditions on the diurnal PAHs concentrations.

Results obtained from binary diagnostic ratios and PCA indicated the prevalence of pyrogenic sources coming from a mixed contribution from traffic and coal/coke combustion sources. The values of the diagnostic ratios obtained for the morning periods indicated the prevalence of traffic emissions, for which the main contribution could be due to diesel vehicles. In contrast, other diurnal periods seemed to be more influenced by coal/biomass combustion sources. Furthermore, the PCA differentiated a diurnal pattern of source contributions, where particulate PAHs followed a different trend along the day according to the variations in the emission sources, which was more evident during the night period. This is probably linked to the fact that it was during the night when

Table 3
Pearson correlation coefficients of total particulate PAHs concentrations (Σ 13 PAHs) with regulated air pollutants according to the diurnal period (n = 35 per diurnal period).

PAH	Period	NO	NO ₂	NO _x	O ₃	SO ₂	Benzene (B)	O-xylene (X)	Toluene (To)
Σ 13 PAHs	M	0.84**	0.71**	0.85**	−0.63**	0.53**	0.70**	0.71**	0.66**
	A	0.76**	0.69**	0.78**	−0.55**	0.66**	0.82**	0.64**	0.61**
	N	0.78**	0.50**	0.77**	−0.44*	0.61**	0.78**	0.54**	0.52**

**Significant correlation significant at the 0.01 level (2 tailed).

*Significant correlation significant at the 0.05 level (2 tailed).

Note: diurnal periods correspond to morning (M): 04:00–12:00 h, afternoon (A): 12:00–20:00 h, and night (N): 20:00–04:00 h UTC.

the combined effects of significant meteorological parameters played a crucial role in the atmospheric dispersion/accumulation of particle-bound PAHs. The most influential meteorological factors were, in decreasing order, temperature, wind speed and atmospheric pressure. These results suggested that the diurnal PAHs concentrations were likely influenced by the atmospheric temperature as the most significant factor controlling their degradation and accumulation during the morning and night periods. Meanwhile, wind speed was an important controlling factor in the afternoon periods related to land-sea breeze cycles, and atmospheric pressure inhibited PAHs dispersion, both vertically and horizontally, in the atmosphere during the afternoon and night time.

Finally, PCA of the diurnal levels of particle-bound PAHs, regulated atmospheric pollutants and meteorological parameters showed that the diurnal PAHs variations were mainly influenced by variations in the emission sources, atmospheric oxidants such as ozone, and temperature conditions. While wind dispersion and other meteorological parameters contributed in same extend to these observed concentrations.

The results gathered here may throw light on the characterization of PAHs diurnal patterns in urban areas and suggest that 24 h-sampling may largely mask the intra-day concentration differences, which can be detectable using higher temporal resolutions.

Acknowledgements

The authors gratefully thank the University of the Basque Country (UPV/EHU, UFI 11/47) and the Spanish Ministry of Science and Innovation (MICINN) for financing the project PROMESHAP (CTM 2010-20607). Iñaki Elorduy wants to thank MICINN for his doctoral grant, and Saioa Elcoroaristizabal also wants to thank UPV/EHU for the grant received from the program “*Contratación de Doctores Recientes*”.

Appendix A. Supplementary data

Supplementary data related to this article can be found at <http://dx.doi.org/10.1016/j.atmosenv.2016.05.012>.

References

- Acero, J.A., Arrizabalaga, J., Kupski, S., Katzschner, L., 2013. Deriving an urban climate map in coastal areas with complex terrain in the Basque Country (Spain). *Urban Clim.* 4, 35–60.
- Agudelo-Castaneda, D.M., Teixeira, E.C., Pereira, F.N., 2014. Time-series analysis of surface ozone and nitrogen oxides concentrations in an urban area at Brazil. *Atmos. Pollut. Res.* 5, 411–420.
- Akyüz, M., Cabuk, H., 2008. Particle-associated polycyclic aromatic hydrocarbons in the atmospheric environment of Zonguldak. *Turk. Sci. Total Environ.* 405, 62–70.
- Alam, M.S., Keyte, I.J., Yin, J., Stark, C., Jones, A.M., Harrison, R.M., 2015. Diurnal variability of polycyclic aromatic compound (PAC) concentrations: relationship with meteorological conditions and inferred sources. *Atmos. Environ.* 122, 427–438.
- Alam, M.S., Delgado Saborit, J.M., Stark, C.P., Harrison, R.M., 2014. Investigating PAH relative reactivity using congener profiles, quinone measurements and back trajectories. *Atmos. Chem. Phys.* 14, 2467–2477.
- Aldabe, J., Santamaría, C., Elustondo, D., Parra, A., Foan, L., Simon, V., Santamaría, J.M., 2012. Polycyclic aromatic hydrocarbons (PAHs) sampled in aerosol phase at different sites of the western Pyrenees in Navarra (Spain). *Environ. Eng. Manag. J.* 11 (6), 1049–1058.
- Augusto, S., Pereira, M.J., Maguas, C., Branquinho, C., 2013. A step towards the use of biomonitors as estimators of atmospheric PAHs for regulatory purposes. *Chemosphere* 92, 626–632.
- Bates, M., Bruno, P., Caputi, M., Caselli, M., de Gennaro, G., Tutino, M., 2008. Analysis of polycyclic aromatic hydrocarbons (PAHs) in airborne particles by direct sample introduction thermal desorption GC/MS. *Atmos. Environ.* 42, 6144–6151.
- Barrado, A.I., García, S., Barrado, E., Perez, R.M., 2012. PM_{2.5}-bound PAHs and hydroxy-PAHs in atmospheric aerosol samples: correlations with season and with physical and chemical factors. *Atmos. Environ.* 49, 224–232.
- Callén, M.S., López, J.M., Mastral, A.M., 2011. Characterization of PM₁₀-bound polycyclic aromatic hydrocarbons in the ambient air of Spanish urban and rural areas. *J. Environ. Monit.* 13, 319–327.
- Callén, M.S., López, J.M., Iturmendi, A., Mastral, A.M., 2013. Nature and sources of particle associated polycyclic aromatic hydrocarbons (PAHs) in the atmospheric environment of an urban area. *Environ. Pollut.* 183, 166–174.
- Callén, M.S., Iturmendi, A., López, J.M., 2014. Source apportionment of atmospheric PM_{2.5}-bound polycyclic aromatic hydrocarbons by a PMF receptor model. Assessment of potential risk for human health. *Environ. Pollut.* 195, 167–177.
- Chang, C.C., Wang, J.L., Candice Lung, S.C., Liu, S.C., Shiu, C.J., 2009. Source characterization of ozone precursors by complementary approaches of vehicular indicator and principal component analysis. *Atmos. Environ.* 43, 1771–1778.
- Council of the European Union, 2004. Council Decision 2004/259/EC of 19 February 2004 concerning the conclusion, on behalf of the European community, of the 1988 protocol to the 1979 convention on long range transboundary air pollution on persistent organic pollutants. *Off. J. Eur. Union* L81, 37–71. http://eur-lex.europa.eu/legal-content/EN/TXT/?uri=uriserv:OJ.L_.2004.081.01.0035.01.ENG (Last accessed: May 2015).
- Delhomme, O., Millet, M., 2012. Characterisation of particulate polycyclic aromatic hydrocarbons in the east of France urban areas. *Environ. Sci. Pollut. Res.* 19, 1791–1799.
- Elcoroaristizabal, S., de Juan, A., García, J.A., Elorduy, I., Durana, N., Alonso, L., 2014. Chemometric determination of PAHs in aerosol samples by fluorescence spectroscopy and second-order data analysis algorithms. *J. Chemom.* 28, 260–271.
- EUD (European Union Directive), 2005. Directive 2004/107/EC of the European parliament and of the council of 15 December 2004 relating to arsenic, cadmium, mercury, nickel and polycyclic aromatic hydrocarbons in ambient air. *Off. J. Eur. Union* L23, 3–17. <http://eur-lex.europa.eu/legal-content/EN/TXT/?uri=CELEX:32004L0107> (Last accessed: May 2015).
- Finlayson-Pitts, B.J., Pitts Jr., J.N., 2000. *Chemistry of the Upper and Lower Atmosphere—theory, Experiments, and Applications*. Academic Press, San Diego, CA, USA.
- Gil-Moltó, J., Varea, M., Galindo, N., Crespo, J., 2009. Application of an automatic thermal desorption–gas chromatography–mass spectrometry system for the analysis of polycyclic aromatic hydrocarbons in airborne particulate matter. *J. Chromatogr. A* 1216, 1285–1289.
- Grandesso, E., Perez Ballesta, P., Kowalewski, K., 2013. Thermal desorption GC–MS as a tool to provide PAH certified standard reference material on particulate matter quartz filters. *Talanta* 105, 101–108.
- Guo, H., Lee, S.C., Ho, K.F., Wang, X.M., Zou, S.C., 2003. Particle-associated polycyclic aromatic hydrocarbons in urban air of Hong Kong. *Atmos. Environ.* 37, 5307–5317.
- Guzmán-Torres, D., Eiguren-Fernández, A., Cicero-Fernández, P., Maubert-Franco, M., Retama-Hernández, A., Ramos Villegas, R., Miguel, H.A., 2009. Effects of meteorology on diurnal and nocturnal levels of priority polycyclic aromatic hydrocarbons and elemental and organic carbon in PM₁₀ at a source and a receptor area in Mexico city. *Atmos. Environ.* 43, 2693–2699.
- Harrison, R.M., Smith, D.J.T., Luhana, L., 1996. Source apportionment of atmospheric polycyclic aromatic hydrocarbons collected from an urban location in Birmingham, U.K. *Environ. Sci. Technol.* 30, 825–832.
- Hassan, S.K., Khoder, M.I., 2012. Gas-particle concentration, distribution, and health risk assessment of polycyclic aromatic hydrocarbons at a traffic area of Giza, Egypt. *Environ. Monit. Assess.* 184 (6), 3593–3612.
- He, J.B., Fan, S.X., Meng, Q.Z., Sun, Y., Zhang, J., Zu, F., 2014. Polycyclic aromatic hydrocarbons (PAHs) associated with fine particulate matters in Nanjing, China: distributions, sources and meteorological influences. *Atmos. Environ.* 89, 207–215.
- Hussain, T., Singh, B.P., Anward, F., 2015. Development of specific marker for PCR diagnostic of late blight of potato caused by *Phytophthora infestans* using RAPD based SCAR methodology. *J. Saudi Soc. Agric. Sci.* <http://dx.doi.org/10.1016/j.jssas.2015.10.001>.
- IARC (International Agency for Research on Cancer), 1983. *Monographs on the Evaluation of the Carcinogenic Risk of Chemicals to Humans*, vol. 32. IARC, Lyon, France, p. 33. <http://monographs.iarc.fr/ENG/Monographs/vol1-42/mono32.pdf> (Last accessed: May 2015).
- ISO (International Organization for Standardization), 2000. *Ambient Air. Determination of Total (Gas and Particle-phase) PAHs. Collection on Sorbent-backed Filters with GC/MS Analyses*. ISO 12884:2000.
- Jamhari, A.A., Sahani, M., Latif, M.T., Chan, K.M., Tan, H.S., Khan, M.F., Mohd Tahir, N., 2014. Concentration and source identification of polycyclic aromatic hydrocarbons (PAHs) in PM₁₀ of urban, industrial and semi-urban areas in Malaysia. *Atmos. Environ.* 86, 16–27.
- Jeon, S.J., Meuzelaar, H.L.C., Sheya, S.A.N., Lightly, J.S., Jarman, W.M., Kasteler, C., Sarofim, A.F., Simoneit, B.R., 2001. Exploratory studies of PM₁₀ receptor and source profiling by GC/MS and principal component analysis of temporally and spatially resolved ambient samples. *J. Air Waste Manag. Assoc.* 51 (5), 766–784.
- Kameda, T., Akiyama, A., Toriba, A., Tang, N., Hayakawa, K., 2011. Atmospheric formation of hydroxynitropyrenes from a photochemical reaction of particle-associated 1-nitropyrene. *Environ. Sci. Technol.* 45, 3325–3332.
- Khalili, N.R., Scheff, P.A., Holsen, T.M., 1995. PAH source fingerprints for coke ovens, diesel and gasoline engines, highway tunnels and wood combustion emissions. *Atmos. Environ.* 29, 533–542.
- Kim, Y.H., Kim, K.H., 2015. A simple methodological validation of the gas/particle fractionation of polycyclic aromatic hydrocarbons in ambient air. *Sci. Rep.* 5, 11679. <http://dx.doi.org/10.1038/srep11679>.
- Kovač-Andrić, E., Radanović, T., Topalović, I., Marković, B., Sakač, N., 2013. Temporal

- variations in concentrations of ozone, nitrogen dioxide, and carbon monoxide at Osijek, Croatia. *Adv. Meteorol.* 2013, 1–7.
- Liu, J., Man, R., Ma, S., Li, J., Wu, Q., Peng, J., 2015. Atmospheric levels and health risk of polycyclic aromatic hydrocarbons (PAHs) bound to PM_{2.5} in Guangzhou, China. *Mar. Pollut. Bull.* 100 (1), 134–143.
- Liu, J.W., Li, J., Lin, T., Liu, D., Xu, Y., Chaemfa, C., Qi, S.H., Liu, F.B., Zhang, G., 2013. Diurnal and nocturnal variations of PAHs in the Lhasa atmosphere, Tibetan Plateau: implication for local sources and the impact of atmospheric degradation processing. *Atmos. Res.* 124, 34–43.
- Mastral, A.M., Callen, M.S., Murillo, R., 1996. Assessment of PAH emissions as a function of coal combustion variables. *Fuel* 75 (13), 1533–1536.
- Millán, M., Otamendi, E., Alonso, L., Ureta, I., 1987. Experimental characterization of atmospheric diffusion in complex terrain with land–sea interactions. *JAPCA* 37, 807–811.
- Morville, S., Delhomme, O., Millet, M., 2011. Seasonal and diurnal variations of atmospheric PAH concentrations between rural, suburban and urban areas. *Atmos. Pollut. Res.* 2, 366–373.
- OFR (Office of the Federal Registration), 1982. Appendix A: priority pollutants. *Fed. Reg.* 47, 52309.
- Oliveira, C., Martins, N., Tavares, J., Pio, C., Cerqueira, M., Matos, M., Silva, H., Oliveira, C., Camões, F., 2011. Size distribution of polycyclic aromatic hydrocarbons in a roadway tunnel in Lisbon, Portugal. *Chemosphere* 83, 1588–1596.
- Poster, D.L., Schantz, M.M., Sander, L.C., 2006. Analysis of polycyclic aromatic hydrocarbons (PAHs) in environmental samples: a critical review of gas chromatographic (GC) methods. *Anal. Bioanal. Chem.* 386, 859–881.
- Ravindra, K., Sokhi, R., Grieten, R.V., 2008. Atmospheric polycyclic aromatic hydrocarbons: source attribution, emission factors and regulation. *Atmos. Environ.* 42, 2895–2921.
- Reche, C., Moreno, T., Amato, F., Viana, M., Van Drooge, B.L., Chuang, H.C., Bérubé, K., Jones, T., Alastuey, A., Querol, X., 2012. A multidisciplinary approach to characterize exposure risk and toxicological effects of PM₁₀ and PM_{2.5} samples in urban environments. *Ecotoxicol. Environ. Saf.* 78, 327–335.
- Ringuet, J., Albinet, A., Leoz-Garziandia, E., Budzinski, H., Villenave, E., 2012a. Diurnal/nocturnal concentrations and sources of particulate-bound PAHs, OPAHs and NPAHs at traffic and suburban sites in the region of Paris (France). *Sci. Total Environ.* 437, 297–305.
- Ringuet, J., Albinet, A., Leoz-Garziandia, E., Budzinski, H., Villenave, E., 2012b. Reactivity of polycyclic aromatic compounds (PAHs, NPAHs and OPAHs) adsorbed on natural aerosol particles exposed to atmospheric oxidants. *Atmos. Environ.* 61, 15–22.
- Sharma, H., Jai, V.K., Khan, Z.H., 2007. Characterization and source identification of polycyclic aromatic hydrocarbons (PAHs) in the urban environment of Delhi. *Chemosphere* 66, 302–310.
- Sheu, H.L., Lee, W.J., Lin, S.J., Fang, G.C., Chang, H.C., You, W.C., 1997. Particle-bound PAH content in ambient air. *Environ. Pollut.* 96, 369–382.
- Simcik, M.F., Eisenreich, S.J., Liou, P.J., 1999. Source apportionment and source/sink relationships of PAHs in the coastal atmosphere of Chicago and Lake Michigan. *Atmos. Environ.* 33, 5071–5079.
- Sisovic, A., Pehncic, G., Jakovljevic, I., Silovic Hujic, M., Vadic, V., Beslic, I., 2012. Polycyclic aromatic hydrocarbons at different crossroads in Zagreb, Croatia. *B. Environ. Contam. Toxicol.* 88, 438–442.
- Slezakova, K., Castro, D., Pereira, M.C., Moralis, S., Delerue-Matos, C., Alvim-Ferraz, M.C., 2010. Influence of traffic emissions on the carcinogenic polycyclic aromatic hydrocarbons in outdoor breathable particles. *J. Air Waste Manag.* 60 (4), 393–401.
- Sofuoğlu, A., Cetin, E., Bozacioglu, S.S., Sener, G.D., Odabasi, M., 2004. Short-term variation in ambient concentrations and gas/particle partitioning of organochlorine pesticides in Izmir, Turkey. *Atmos. Environ.* 38, 4483–4493.
- Sogri, K., 2007. Monitoring of environmental exposure to polycyclic aromatic hydrocarbons: a review. *Environ. Chem. Lett.* 5, 169–195.
- Tham, Y.W.F., Takeda, K., Sakugawa, H., 2008. Exploring the correlation of particulate PAHs, sulfur dioxide, nitrogen dioxide and ozone, a preliminary study. *Water Air Soil Poll.* 194, 5–12.
- UNECE (United Nations Economic Commission for Europe), 1979. Convention on Long-range Trans-boundary Air Pollution. United Nations Economic Commission for Europe, Geneva. http://www.unece.org/env/lrtap/lrtap_h1.html (Last accessed: May 2015).
- US-EPA, July 1, 2013. Guidelines Establishing Test Procedures for the Analysis of Pollutants (Part 136, Appendix B. Definition and Procedure for the Determination of the Method Detection Limit-Revision 1.11). U.S. Code of Federal Regulations, Washington, DC, pp. 344–347. Title 40. <http://www.gpo.gov/fdsys/pkg/CFR-2013-title40-vol24/pdf/CFR-2013-title40-vol24-part136.pdf> (Last accessed: March 2016).
- Uria-Tellaetxe, I., Navazo, M., de Blas, M., Durana, N., Alonso, L., Iza, J., 2016. Gas-phase naphthalene concentration data recovery in ambient air and its relevance as a tracer of sources of volatile organic compounds. *Atmos. Environ.* 131, 279–288.
- Van Drooge, B.L., Nikolova, I., Pérez Ballesta, P., 2009. Thermal desorption gas chromatography-mass spectrometry as an enhanced method for the quantification of polycyclic aromatic hydrocarbons from ambient air particulate matter. *J. Chromatogr. A* 1216, 4030–4039.
- Varea, M., Galindo, N., Gil-Moltó, J., Pastor, C., Crespo, J., 2011. Particle-bound polycyclic aromatic hydrocarbons in an urban, industrial and rural area in the western Mediterranean. *J. Environ. Monit.* 13, 2471–2476.
- Villanueva, F., Tapia, A., Cabañas, B., Martínez, E., Albaladejo, J., 2015. Characterization of particulate polycyclic aromatic hydrocarbons in an urban atmosphere of central-southern Spain. *Environ. Sci. Pollut. Res. Int.* 22 (23), 18814–18823.
- Villar-Vidal, M., Lertxundi, A., Martínez Lopez de Dicastillo, M.D., Alvarez, J.I., SantaMarina, L., Ayerdi, M., Basterrechea, M., Ibarluzea, J., 2014. Air polycyclic aromatic hydrocarbons (PAHs) associated with PM_{2.5} in a North Cantabric coast urban environment. *Chemosphere* 99, 233–238.
- Wang, J., Ho, S.S.H., Cao, J., Huang, R., Zhou, J., Zhao, Y., Xu, H., Liu, S., Wang, G., Shen, Z., Han, Y., 2015. Characteristics and major sources of carbonaceous aerosols in PM_{2.5} from Sanya, China. *Sci. Total Environ.* 530–531, 110–119.
- Wu, Y., Yang, L., Zheng, X., Zhang, S.J., Song, S.J., Li, J.Q., Hao, J.M., 2014. Characterization and source apportionment of particulate PAHs in the roadside environment in Beijing. *Sci. Total Environ.* 470–471, 76–83.
- Xu, H.M., Tao, J., Ho, S.S.H., Ho, K.F., Cao, J.J., Li, N., Chow, J.C., Wang, G.H., Han, Y.M., Zhang, R.J., Watson, J.G., Zhang, J.Q., 2013. Characteristics of fine particulate non-polar organic compounds in Guangzhou during the 16th Asian Games: effectiveness of air pollution controls. *Atmos. Environ.* 76, 94–101.
- Yunker, M.B., Macdonald, R.W., Vingarzan, R., Mitchell, R.H., Goyette, D., Sylvestre, S., 2002. PAHs in the Fraser River basin: a critical appraisal of PAH ratios as indicators of PAH source and composition. *Org. Geochem.* 33, 489–515.
- Zhu, Y., Yang, L., Yuan, Q., Yan, C., Dong, C., Meng, C., Sui, X., Yao, L., Yang, F., Lu, Y., Wang, W., 2014. Airborne particulate polycyclic aromatic hydrocarbon (PAH) pollution in a background site in the North China Plain: concentration, size distribution, toxicity and sources. *Sci. Total Environ.* 466–467, 357–368.